NASA CR-161,304

3 1176 00139 0153

Report 32967F
August 1979

NASA-CR-161304
19790023171

DUAL-FUEL, DUAL-THROAT ENGINE PRELIMINARY ANALYSIS

Final Report

By

C. J. O'Brien

AEROJET LIQUID ROCKET COMPANY

Prepared for

NATIONAL AERONAUTICS AND SPACE ADMINISTRATION

NASA-Marshall Space Flight Center

Contract NAS8-32967

1 Report No	2 Government Accession No	3 Recipient's Catalog No
32967F		

4 Title and Subtitle	5 Report Date
Dual-Fuel, Dual-Throat Engine Preliminary Analysis, Final Report	August 1979
	6 Performing Organization Code
7 Author(s)	8. Performing Organization Report No
C. J. O'Brien	
9 Performing Organization Name and Address	10 Work Unit No
Aerojet Liquid Rocket Company Post Office Box 13222 Sacramento, California 95813	11 Contract or Grant No NAS8-32967
	13 Type of Report and Period Covered Contractor Report, Final
12 Sponsoring Agency Name and Address National Aeronautics and Space Administration Washington, D.C. 20546	14 Sponsoring Agency Code

15 Supplementary Notes

Project Manager, F. W. Braam, Propulsion Division
NASA-Marshall Space Flight Center
Marshall Space Flight Center, Alabama 35812

16 Abstract

The dual-fuel, dual-throat engine provides a means to obtain a large area ratio adjustment within a single thrust chamber assembly without the need for extendible nozzles. A propulsion system analysis of the engine for launch vehicle applications was conducted. Basic dual throat engine characterization data were obtained to allow vehicle optimization studies to be conducted. A preliminary baseline engine system was defined.

Dual throat engine performance, envelope and weight parametric data were generated over the parametric range of thrust from 890 to 8896 KN (200K to 2M lb-force), chamber pressure from 6.89×10^6 to 3.45×10^7 N/m^2 (1000 to 5000 psia), thrust ratio from 1.2 to 5, and mixture ratio for the two propellant combinations: LO_2/RP-1 + LH_2 and LO_2/LCH_4 + LH_2.

The results of the study indicate that the dual-fuel, dual-throat engine is a viable SSTO candidate.

17 Key Words (Suggested by Author(s))	18 Distribution Statement
Dual Throat Aerodynamics Dual Throat Performance Liquid Rocket Thrust Chamber LO_2/LH_2/Hydrocarbon Tripropellant Engine	Unclassified - Unlimited

19 Security Classif (of this report)	20 Security Classif (of this page)	21 No of Pages	22 Price*
Unclassified	Unclassified	235	

N79-31342#

This Page Intentionally Left Blank

FOREWORD

The work described herein was performed at the Aerojet Liquid Rocket Company under NASA Contract NAS 8-32967 with Mr. Fred W. Braam, NASA-Marshall Space Flight Center, as Project Manager. The ALRC Program Managers were Mr. Larry B. Bassham and Mr. Jeff W. Salmon and the Project Engineer was Mr. Charles J. O'Brien.

The technical period of performance for the study was from 1 August 1978 to 31 May 1979.

The author acknowledges the efforts of the following ALRC engineering personnel who contributed significantly to this report:

R. L. Ewen	(Heat Transfer)
G. R. Cunnington	(Heat Transfer)
R. B. Lundgreen	(Performance)
R. Salkeld	(Vehicle System)
N. P. Smith	(Turbomachinery)
G. R. Janser	(Materials)
A. V. Lundback	(Controls)
P. E. Brown	(Structures)
R. J. Sak	(Engine Layout)

I also wish to thank Mr. Rudi Beichel, ALRC Senior Scientist, for his comments and assistance throughout the study effort.

This Page Intentionally Left Blank

TABLE OF CONTENTS

TABLE OF CONTENTS (cont.)

TABLE OF CONTENTS (cont.)

LIST OF TABLES

LIST OF TABLES (cont.)

LIST OF FIGURES

LIST OF FIGURES (cont.)

LIST OF FIGURES (cont.)

LIST OF FIGURES (cont.)

LIST OF FIGURES (cont.)

NOMENCLATURE

Term	Definition
Mode I - Parallel Burn	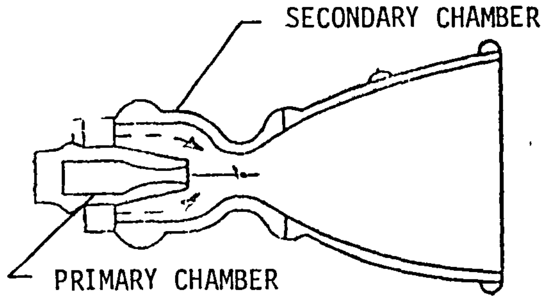 ---► HIGH SECONDARY FLOW (PCS ∿ 2800 PSIA) ——► HIGH PRIMARY FLOW (PCP ∿ 4000 PSIA)
Mode II - Operation	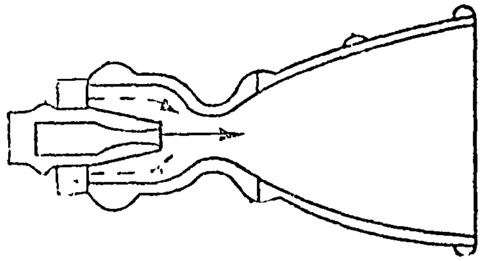 ——► HIGH PRIMARY FLOW (PCP ∿ 4000 PSIA) ---► LOW BLEED FLOW (PCS ∿ 200 PSIA)
Mode I - Series Burn	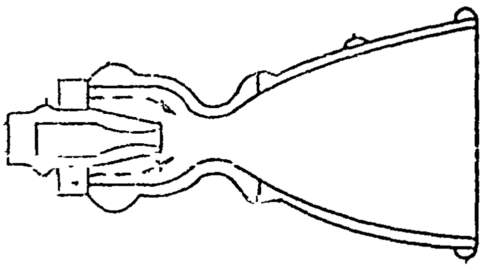 ---► HIGH SECONDARY FLOW (PCS ∿ 2800 PSIA) ZERO PRIMARY FLOW

NOMENCLATURE (cont.)

Term	Definition
Primary Flow	LO_2/LH_2 combustion products
Secondary Flow	LO_2/Hydrocarbon (RP-1 or LCH_4) combustion products
Bleed Flow	Gas generator or preburner tap-off flow
Thrust Ratio, F_I/F_{II}	$\frac{\text{Engine vacuum thrust Mode I}}{\text{Engine vacuum thrust in Mode II}}$
Stream-Tube Thrust Split (mode I-Parallel Burn, Sea Level)	$\frac{\text{\% one dimensional thrust contribution of } LO_2 \text{ hydrocarbon stream}}{\text{\% one dimensional thrust contribution of } LO_2/LH_2 \text{ stream}}$

SECTION I

SUMMARY

A. STUDY OBJECTIVES AND SCOPE

The major objectives of this study program were to: (1) conduct a propulsion system analysis of the dual-fuel, dual-throat engine for launch vehicle application, (2) obtain basic engine parametric data to allow vehicle optimization studies to be conducted, and (3) define a preliminary baseline engine system.

To accomplish the objectives, the three task study program, summarized on Figure 1, was conducted. Various engine cycle candidates were examined and their regions of operation (chamber pressure, thrust level, etc.) were established. Thrust chamber heat transfer and structural analyses were performed for baseline and scaled engines. In order to make use of the available design data from previous studies, a preliminary baseline engine was established. Parametric scaling studies were conducted around this design point.

Engine performance, envelope and weight parametric data were generated over the parametric range of thrust from 890 to 8896 KN (200K to 2M lb-force), chamber pressure from 6.89×10^6 to 3.45×10^7 N/m^2 (1000 to 5000 psia), thrust ratio from 1.2 to 5, and mixture ratio for two propellant combinations LO_2/RP-1 + LH_2 and LO_2/LCH_4 + LH_2.

A preliminary definition of a dual-throat baseline engine system was obtained based on the parametric data and on a simplified vehicle applications analysis.

Throughout the entire study effort, basic data gaps and areas requiring technology work were identified.

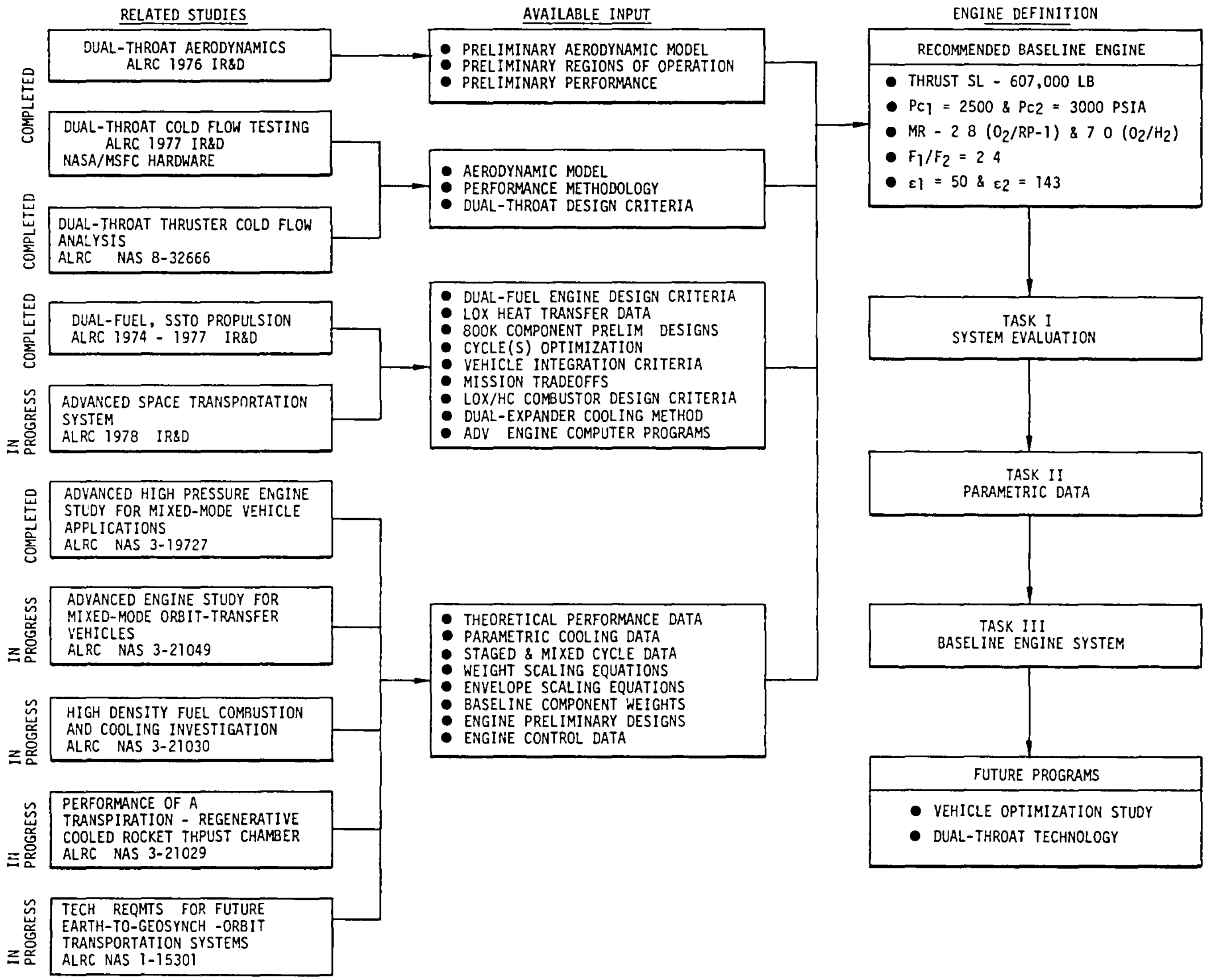

Figure 1. Dual-Fuel, Dual-Throat Engine Preliminary Analysis Program Summary

I, Summary (cont.)

B. RESULTS AND CONCLUSIONS

High engine performance is achieved by the dual throat system at both sea level and vacuum conditions with a small weight penalty. Application of the engine to a single-stage-to-orbit (SSTO) mission would provide competitive vehicle performance with that provided by the baseline propulsion system evaluated in Reference 1 (combination of $Pc = 2.76 \times 10^7$ N/m^2 or 4000 psia advanced SSME and LO_2/RP-1 engines).

SECTION II

INTRODUCTION

A. BACKGROUND

Propulsion systems for future vehicles such as the single-stage-to-orbit (SSTO) and heavy lift launch vehicle (HLLV) may embrace such capabilities as mixed-mode operation and in-flight changes in area for altitude compensation. These vehicles benefit from mixed-mode operation through reduced vehicle volume by taking advantage of high bulk density propellants in one mode and low density but higher performance propellants in the other mode. Area ratio change during flight provides an increase in performance as ambient pressure drops with altitude.

The SSTO and HLLV concepts promise large improvement in delivered payload and cost-effectiveness. The practicality of these concepts was enhanced by discovery (Salkeld, R., Reference 2) and investigation of the mixed-mode vehicle concept on several NASA contracts (NAS 1-13916, NAS 1-13944, NAS 9-14710, NAS 8-32169, and NAS 3-19727, References 1, 3, 4, 5 and 6, respectively). Advanced high pressure bipropellant engine and tripropellant engine (TPE) concepts have emerged from the studies. These propulsion systems meet the unique requirement of high performance density demanded by the SSTO and HLLV concepts, and thus offer a means to achieve an economical space transportation system.

One of the major propulsion system candidates that was not evaluated in the previous parametric studies is the dual-throat concept, proposed earlier by NASA/MSFC to obtain a large area ratio adjustment within a single thrust chamber assembly, without the need for extendible nozzles. The concept is readily adaptable to TPE applications. Dual-fuel, dual-throat engines combine both mixed-mode and variable area ratio capabilities in a single design. The dual-throat combustors allow use of two propellant combinations and the two separate nozzle throats and a fixed nozzle exit allow a shift in area ratio without resorting to translating nozzle mechanisms.

B. PURPOSE AND SCOPE

The feasibility of the dual throat concept when utilized for a tripropellant dual mode engine is dependent upon the weight for two nozzles, the performance during Mode II (LO_2/LH_2) operation, and the performance during Mode I (LO_2/LH_2/Hydrocarbon) operation. A substantial data base from dual throat aerodynamic analysis and cold flow testing was available from ALRC in-house studies, and an aerodynamic model and performance methodology were available from the Dual-Throat Thruster Cold Flow Analysis program (Ref. 7). It is the purpose of this study to conduct a propulsion system analysis that will allow the assessment of the potential of the tripropellant dual throat engine.

Dual throat engine design, performance, weight, envelope, and operational characteristics were evaluated for a variety of candidate power cycles. The selected engine cycle was chosen partly on the basis of a simplified vehicle trajectory analysis.

C. GENERAL REQUIREMENTS

For purposes of this study, the engine design points cover the parametric ranges given in Table I. Both parallel burn and series burn conditions are assumed as requirements for the engine during Mode I operation. However, emphasis is placed on the parallel burn operation in Mode I to take advantage of the unique features of tripropellant engine cycles. Mode II operation is assumed to involve only the high specific impulse propellant combination (LO_2/LH_2).

TABLE I

DUAL THROAT ENGINE DESIGN CONDITIONS

Propellant Combinations	$LO_2/RP\text{-}1$ + LO_2/LH_2	LO_2/LCH_4 + LO_2/LH_2
Mixture Ratio	2 to 3.5 + 5 to 7	3 to 4.5 + 5 to 7
Thrust	200K to 2M lb_F	
Chamber Pressure	1000 to 5000 psia	
Area Ratio	20 to 500	
Thrust Ratio (Mode 1/Mode 2)	1.2 to 5.0	

II, Introduction (cont.)

D. APPROACH

To accomplish the program objectives, an effort involving three technical tasks was conducted. Tasks accomplished are:

1. Task I - System Evaluation

   Generate fundamental engine cycle candidates potentially applicable to dual-fuel dual-throat engines and identify the areas needing technological investigation (Figure 2).

2. Task II - Parametric Data

   Generate engine system performance, envelope, and weight parametric data (Figure 3).

3. Task III - Baseline Engine System

   Prepare a preliminary definition of the dual-fuel dual-throat baseline engine (Figure 4).

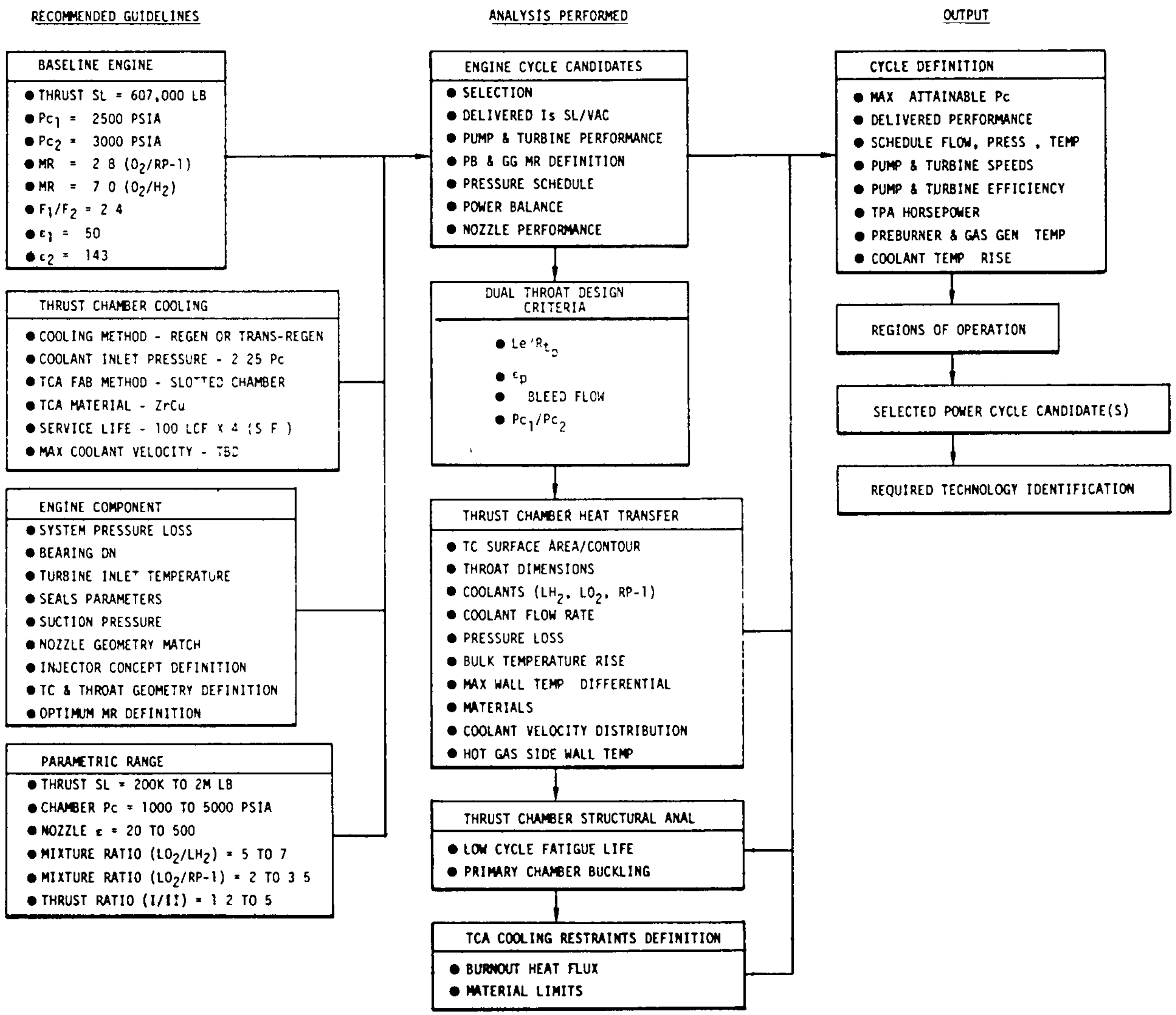

Figure 2. Task I - System Evaluation

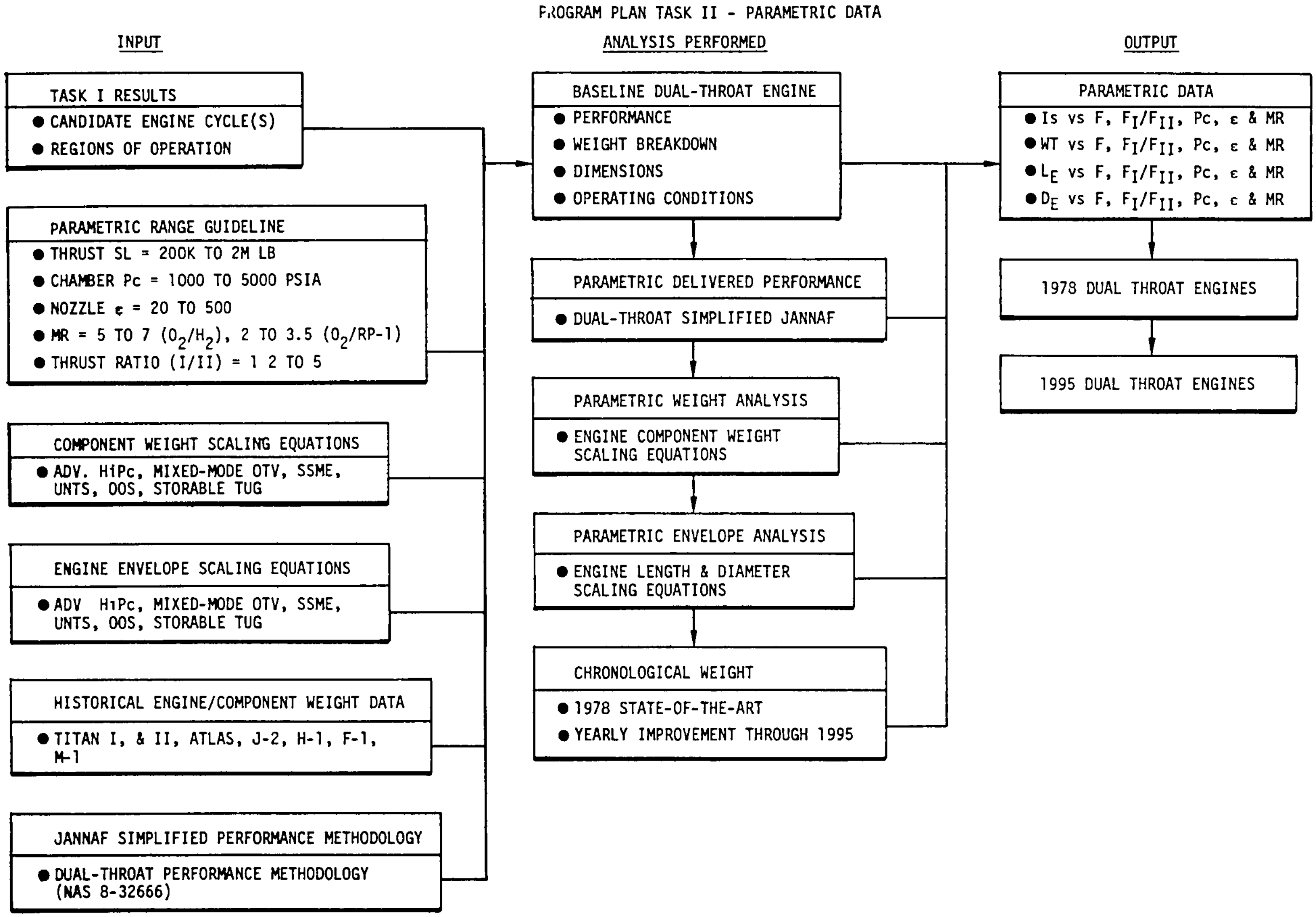

Figure 3. Task II - Parametric Data

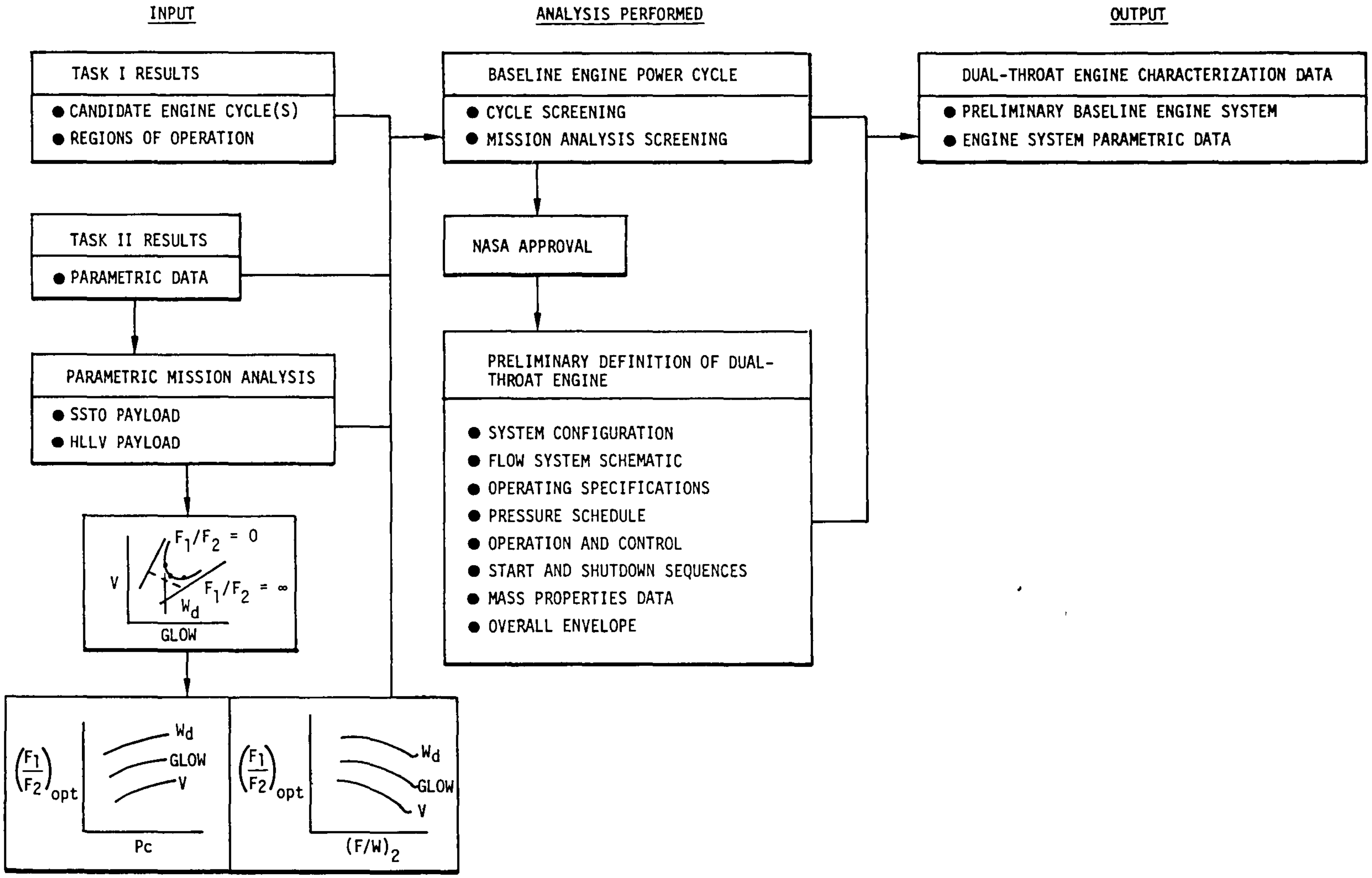

Figure 4. Task III - Baseline Engine System

SECTION III

SYSTEM EVALUATION

A. OBJECTIVES AND GUIDELINES

Fundamental engine cycle candidates potentially applicable to dual-fuel, dual-throat engines were generated in this task. Output from the task (see Figure 2) includes: (1) the determination of the regions of operation best suited to the various candidate power cycles in terms of chamber pressure, mixture ratio, thrust range and thrust ratio, (2) the selection of a power cycle candidate(s) for use in a baseline engine system definition and (3) the identification of areas needing technological investigation.

Recommended guidelines for the conduction of the parametric cycle and heat transfer analyses are based, with some modification, on those utilized on Contract NAS 3-19727 (Ref. 6). These are listed in Table II.

B. ENGINE CYCLE CANDIDATES

Power cycle candidates were evaluated by a two step process. In the initial step a preliminary baseline engine specification was established for a selected staged combustion cycle. Engine flowrates were generated and a pressure schedule was established for this baseline system. Heat transfer, structural and materials analyses were then conducted over the parametric range of variables utilizing the baseline engine as a reference.

In the second step, coolant channel pressure drop data were used to generate a more realistic pressure schedule for the various cycle candidates.

The results of the power cycle evaluation are summarized in this section.

TABLE II

GUIDELINES FOR PARAMETRIC STUDY

PARAMETER	
NPSH at Engine Inlet, m (ft)	LOX: 5(16)
	LH_2: 31(100)
	RP-1: 20(65)
	LCH_4: 7(23)
Coolant Inlet Temperature, °K (°R)	LOX: 111(200)
	LH_2: 61(110)
	RP-1: 311(560)
	LCH_4: 144(259)
Coolant Inlet Pressure	$\leq$ 2.25 Pc
Chamber Wall Thickness, cm (in.)	$\geq$ 0.064 (0.025)
Chamber Service Free Life, cycles	$\geq$ 100
Injector Pressure Loss ($\Delta P/P_{upstream}$)	Liquid: $\leq$ 15% Gas: $\leq$ 8%
Valve Pressure Loss ($\Delta P/P_{upstream}$)	Shutoff: $\leq$ 1% Liquid Control: $\leq$ 5% Gas Control: $\leq$ 10%
Main Pump Suction Specific Speed	$\approx$ 20,000
Turbine Inlet Temperature °K (°R)	Oxidizer Rich: $\geq$ 922 (1660) Fuel Rich: LOX/RP-1: $\geq$ 867 (1560) LOX/LH_2: $\geq$1033 (1860)

Dual throat engine cycles consist of either a closed loop or an open loop system, as depicted in Figure 5. The basic components of the cycles are: (1) turbopumps (2 x LO_2, HDF (RP-1 or LCH_4) and LH_2, (2) preburners (0 to 4), and (3) gas generators (0 to 2). The matrix of power cycles evaluated in this study are shown in Figure 6. Parameters utilized in the rating of the various cycles are summarized in Figure 7.

1. Baseline Engine Specification

The preliminary baseline dual throat engine was selected to provide a 60% LO_2/RP-1 and a 40% LO_2/LH_2 sea level thrust contribution (stream-tube thrust split) to Mode 1 operation. This percentage during Mode 1 operation was found to be optimum in recent studies at NASA/LaRC utilizing similar tripropellant engines (Ref. 8). The engine thrust level was selected to be 2669 KN or 600,000 (600K lb) because extensive preliminary design criteria and scaling relationships exist for components and engine subsystems at the 2700 KN (607K lb) thrust level (Ref. 6).

The preliminary baseline engine specification is given in Table III. The specification is based on the following assumptions:

(1) The primary chamber pressure must be 1.43 times the secondary chamber pressure to achieve supersonic flow in the primary throat during Mode I parallel burn.

(2) The stream tube thrust efficiencies are 97% and 98%, respectively, for the LO_2/RP-1 and LO_2/LH_2 streams.

(3) The steam tube area ratios are selected for a small amount of overexpansion at sea level and to achieve equal static pressures.

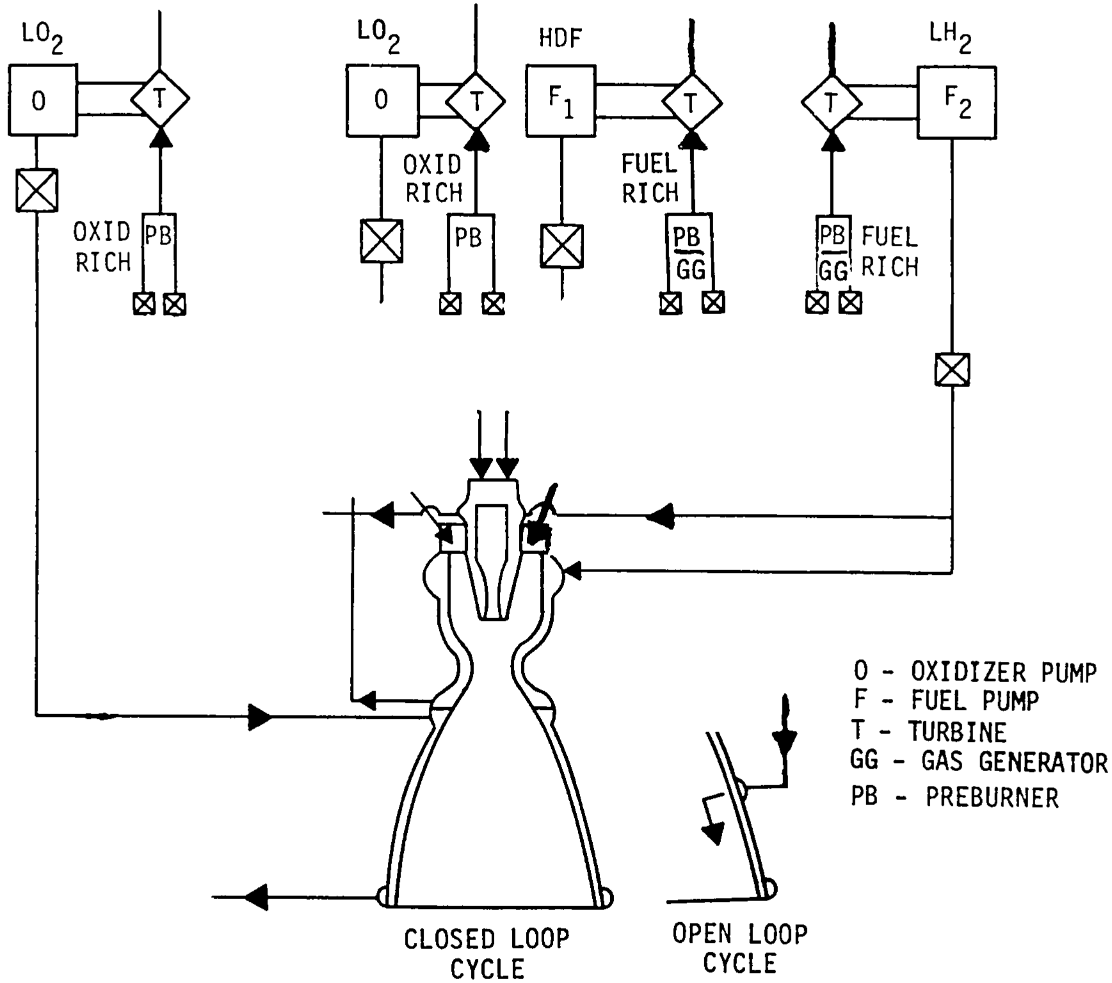

Figure 5. Dual Throat Engine Cycle Components

ENGINE CYCLE	CYCLE CLASSIF.	H-RICH PREBURN./ GAS GEN.	O/H OXID.-RICH PREBURNER	HC-RICH PREBURN./ GAS GEN.	O/HC OXID.-RICH PREBURNER	RATING*
EXPANDER (H_2)	CLOSED LOOP					N/A
EXPANDER BLEED (H_2)	OPEN LOOP					N/A
GAS GENERATOR I						8
GAS GENERATOR II						1/2
STG. COMB. I	CLOSED LOOP					6
STG. COMB. II						1/2
STG COMB. III						9
STG. COMB. IV						5
EXP. BLEED/ STG. COMB.	OPEN LOOP					8
GAS GEN./ STG. COMB.						10

CODE: [dotted box] COMPONENTS UTILIZED

*SEE TABLE IX.

Figure 6. Power Cycle Matrix for Dual Throat Engine

PARAMETER	ENGINE CYCLE			EFFECT
	SC	GG	EB	
PUMP DISCHARGE PRESSURE	HIGH	LOWER	LOWER	TPA CYCLE LIFE
ENGINE PERFORMANCE	HIGH	LOWER	LOWER	PAYLOAD CAPABILITY
TANK MIXTURE RATIO	OPTIMUM	NOT OPTIMUM	NOT OPTIMUM	PAYLOAD CAPABILITY
TURBINE TEMPERATURE	HIGH	LOWER	LOWEST	TPA CYCLE LIFE COOLING SYSTEM COMPLEXITY POWER REQUIREMENT
LO_2/HC FUEL-RICH TURBINE	COKING	COKING	NONE	TPA/INJECTOR CYCLE LIFE PURGE SYSTEM REQUIREMENT LOW PERFORMANCE
LO_2/H_2 FUEL-RICH TURBINE	LOW P_2/P_1	HIGH P_2/P_1	NONE	STAGED TURBINE HIGH PERFORMANCE
INTER-PROPELLANT SEAL REQUIREMENT FOR TPA	NO/YES	YES	YES	TPA CYCLE LIFE & PERFORMANCE

INDICATES DESIREABLE CONDITION

Figure 7. Engine Cycle Rating Parameters

TABLE III

PRELIMINARY BASELINE DUAL-FUEL DUAL-THROAT ENGINE SPECIFICATION

SI UNITS

	STREAM TUBES		F_1/F_2 = 2.41	
	60% x 1 LO_2/RP-1	40% x 1 LO_2/LH_2	MODE 1 LO_2/RP-1 & LH_2	MODE 2 LO_2/LH_2
Thrust, SL, KN	1601	1068	2669	-
Thrust, VAC, KN	1867	1219	3087	1280
Mixture Ratio	2.8	7.0	3.607	7.0 (TCA)
Chamber Pressure, N/m^2	1.45×10^7	2.07×10^7	-	2.07×10^7
Area Ratio	(40)*	(50)*	43.1	139
ODE Is, SL, sec	308.8	395.9	-	-
ODE Is, VAC, sec	360.1	452.2	-	470.3
Is Efficiency, %	97	98	-	97**
Is, SL, Delivered, sec	299.5	388.0	329.6	-
Is, VAC, Delivered, sec	349.3	443.2	381.2	456.2
Total Flow Rate, Kg/s	545	281	826	286**
Fuel Flow Rate, Kg/s	143	35	179	39**
Oxidizer Flow Rate, Kg/s	402	246	647	246
c*, M/s	1799	2255	-	2255
Throat Area, cm^2	677	306	983	306
Throat Diameter, cm	-	20	35	20
Exit Area, cm^2	27056	15295	42377	42377
Exit Diameter, cm	-	-	232	232
Exit Pressure, N/m^2	3.7×10^4	3.7×10^4	3.7×10^4	9.7×10^3

*Optimum LO_2/LH_2 ε_{SL} = 23 LO_2/RP-1 ε_{SL} = 19

**Assumed 1% Is loss and 2% bleed flow

TABLE III (Cont.)

ENGLISH UNITS

	STREAM TUBES		F_1/F_2 = 2.41	
	60% x 1 LO_2/RP-1	40% x 1 LO_2/LH_2	MODE 1 LO_2/RP-1 & LH_2	MODE 2 LO_2/LH_2
Thrust, SL, lb	360,000	240,000	600,000	-
Thrust, VAC, lb	419,806	274,144	693,950	287,825
Mixture Ratio	2.8	7.0	3.607	7.0 (TCA)
Chamber Pressure, psia	2,100	3,000	2100/3000	3,000
Area Ratio	(40)*	(50)*	43.1	139
ODE Is, SL, sec	308.8	395.9	-	-
ODE Is, VAC, sec	360.1	452.2	-	470.3
Is Efficiency, %	97	98	-	97**
Is, SL, Delivered, sec	299.5	388.0	329.6	-
Is, VAC, Delivered, sec	349.3	443.2	381.2	456.2
Total Flow Rate, lb/s	1,201.86	618.56	1,820.42	630.93**
Fuel Flow Rate,lb/s	316.28	77.32	393.60	89.69**
Oxidizer Flow Rate, lb/s	885.58	541.24	1,426.82	541.24
c*, ft/s	5,901	7,399	-	7.399
Throat Area, in^2	104.97	47.42	152.4	47.42
Throat Diameter, in.	-	7.77	13.93	7.77
Exit Area, $in.^2$	(4,198.7)	(2,370.8)	6,569.5	6,569.5
Exit Diameter, in.	-	-	91.46	91.46
Exit Pressure, psia	5.4	5.4	5.4	1.4

*Optimum LO_2/LH_2 ε_{SL} = 23 LO_2/RP-1 ε_{SL} = 19

**Assumed 1% Is loss and 2% bleed flow

(4) The Mode II engine efficiency is assumed to be 97% to allow for bleed flow correction.

(5) The amount of bleed flow is assumed to be 2%.

Assumptions 1, 4 and 5 are based on cold flow results previously obtained (Ref. 7). While the resultant performance differs slightly from that given in Section IV,B, the method gives sufficient accuracy for the generation of parametric cycle data.

2. Staged Combustion Cycles

The four staged combustion cycles shown in Figures 8 through 11 were analyzed for the baseline engine condition. No cycles were analyzed that utlized only oxidizer-rich preburners. This was because of the lower efficiency of the oxidizer-rich turbine drive fluid, and because of the desire to eliminate interpropellant seals in the turbomachinery design.

The flow circuits for the single preburner staged combustion cycle will be traced to illustrate the operation of this typical cycle during both modes. Flow from the LO_2 pump, shown in Figure 8 attached to the HDF (high density fuel, i.e., RP-1 or LCH_4) pump by a common shaft, passes through a control valve to the secondary injector during Mode I operation only. Fuel from the HDF pump flows through a control valve to the secondary injector during Mode I only. Flow from the other LO_2 pump passes through a control valve to the nozzle coolant jacket, out of the coolant jacket to the primary injector with a small portion going to the preburner. The LH_2 fuel flows from the pump through a control valve and splits to flow into two combustion chamber coolant jackets. The coolant jacket outlet flows are combined and fed to the preburner. The fuel-rich preburner gas drives the turbines (shown in series in this schematic) and flow in Mode I to the primary injector.

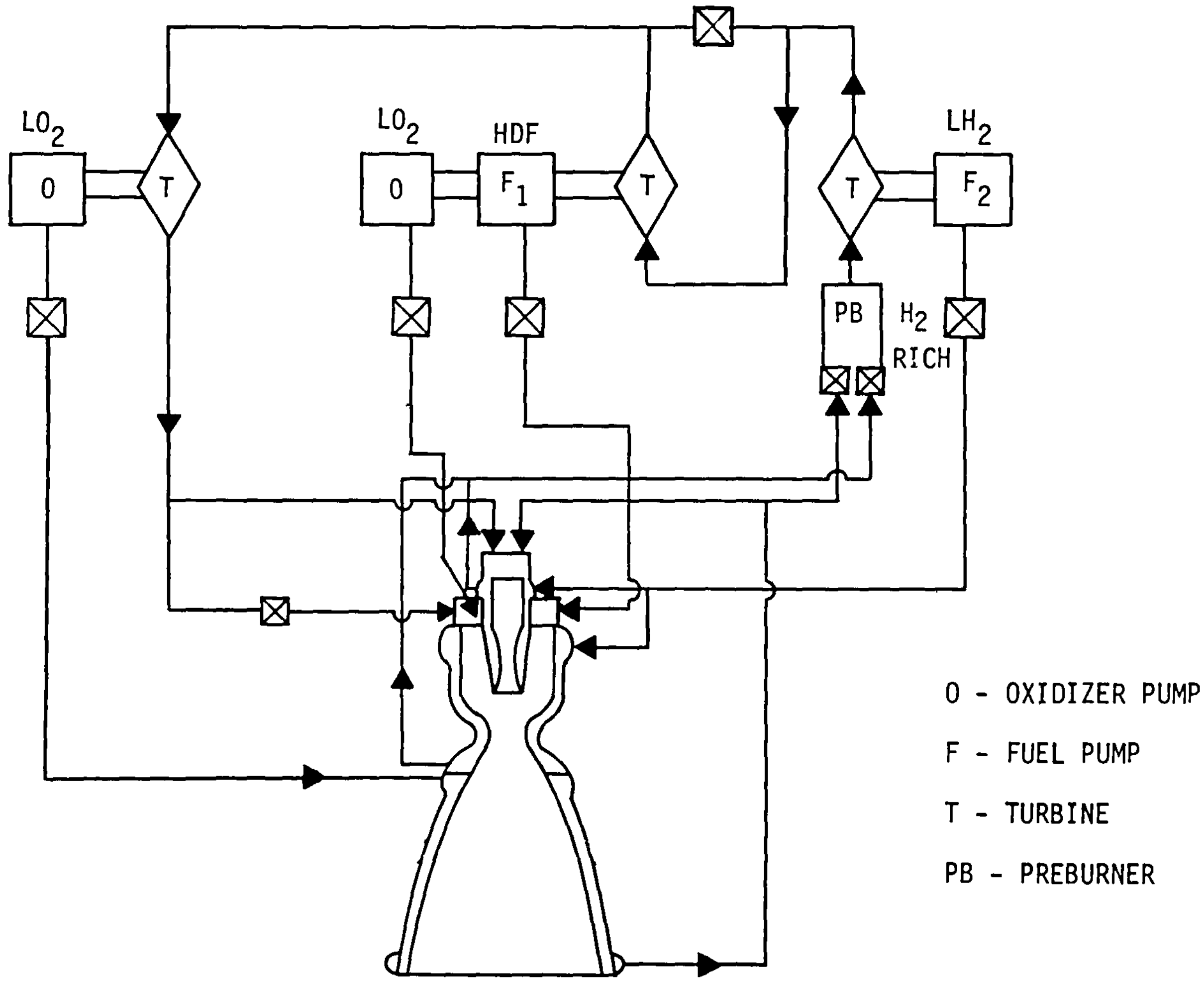

Figure 8. Dual-Fuel, Dual-Throat Engine Staged Combustion Cycle I (Single Preburner)

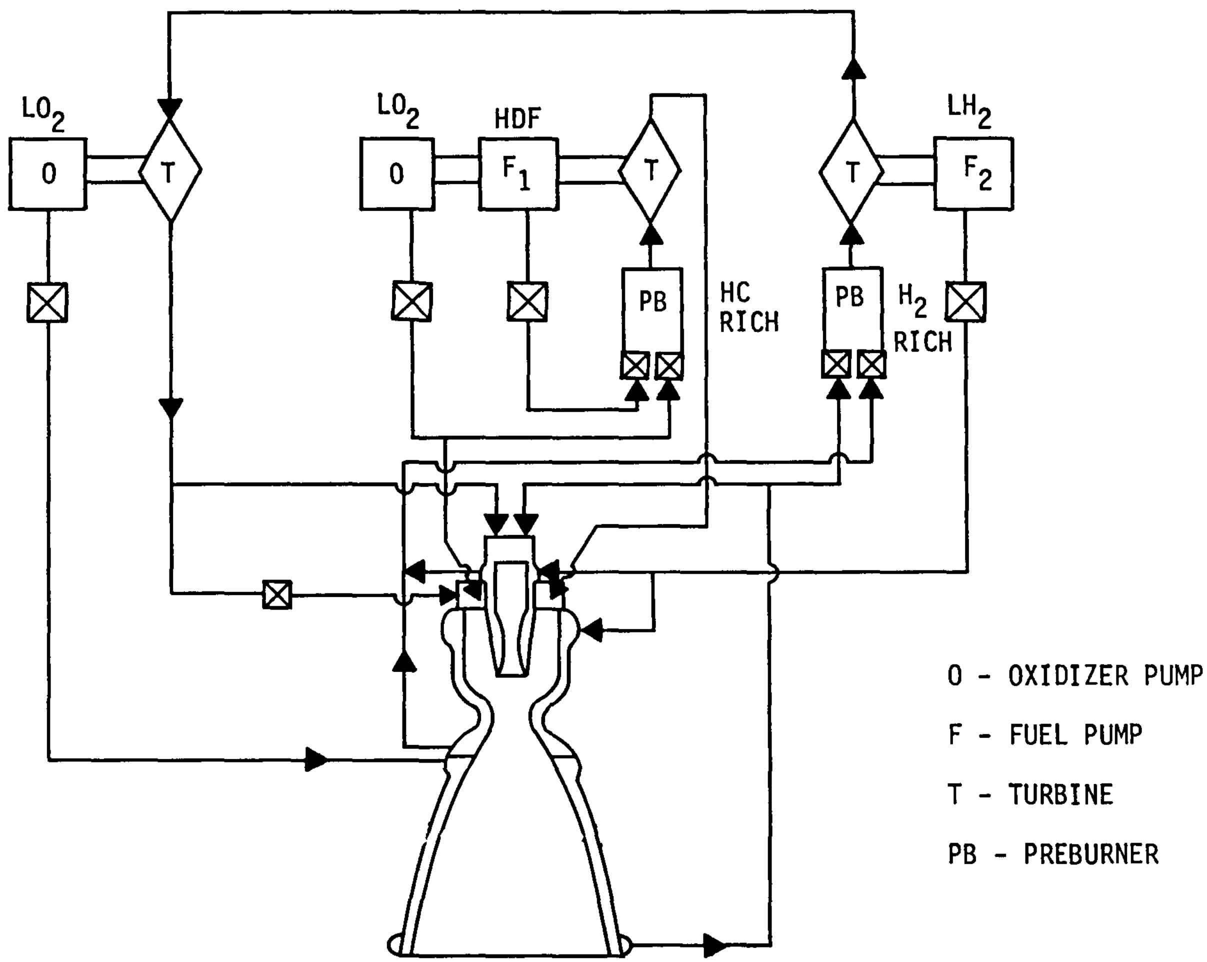

Figure 9. Dual-Fuel, Dual-Throat Engine Staged Combustion Cycle II (Two Preburner)

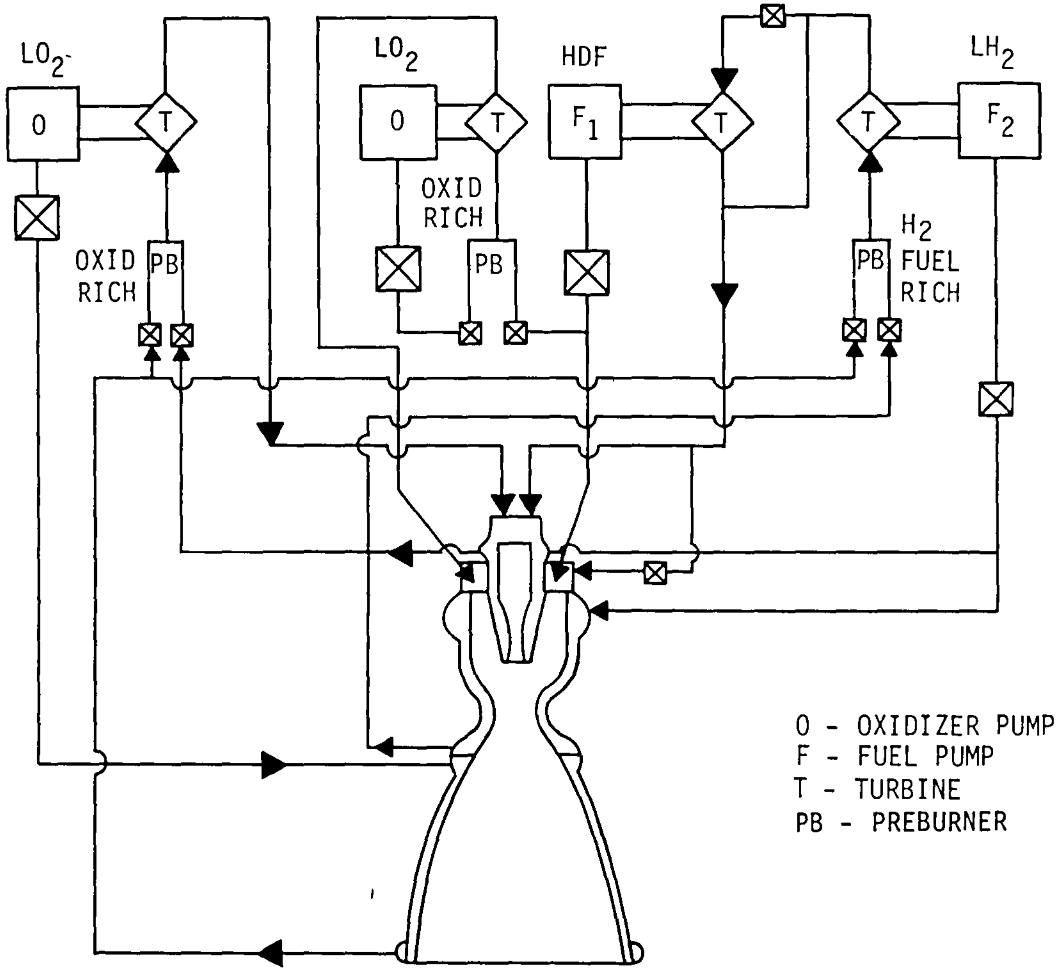

Figure 10. Dual-Fuel, Dual-Throat Engine Staged Combustion Cycle III (Three Preburner)

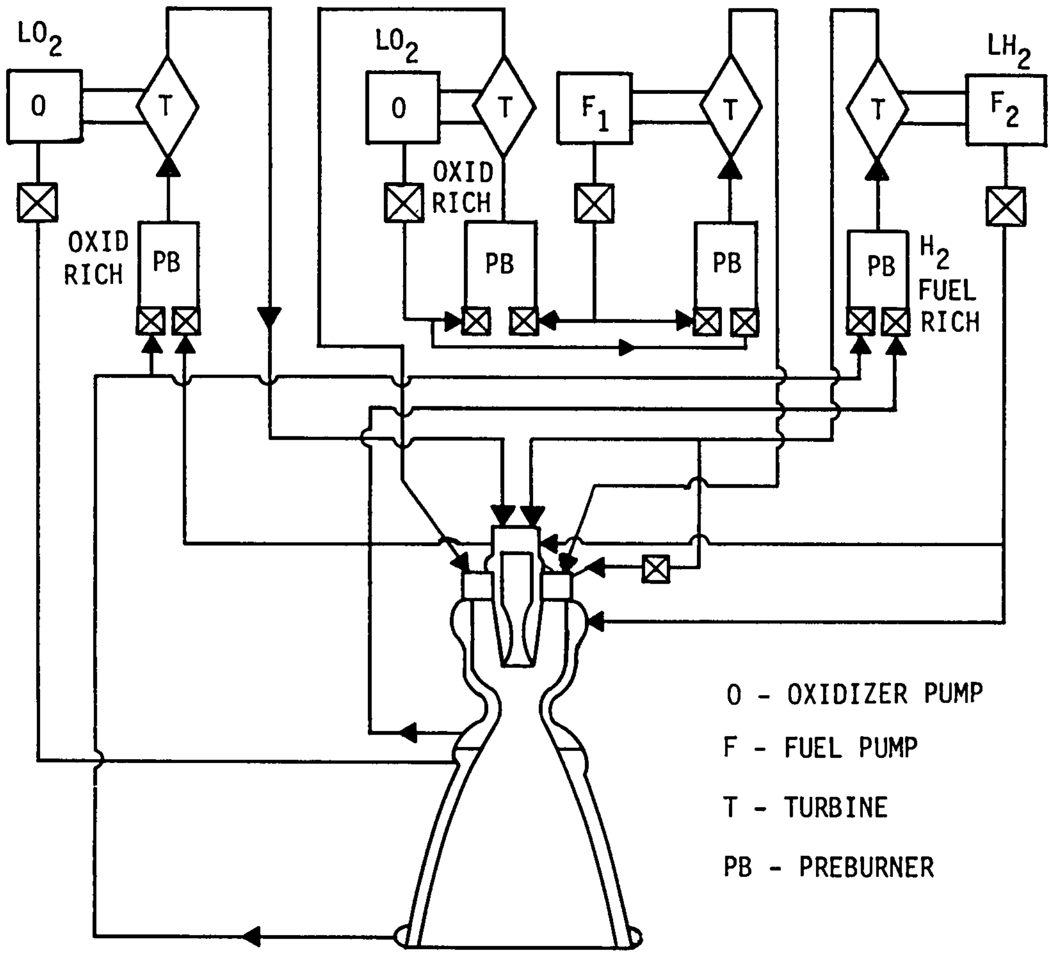

Figure 11. Dual-Fuel, Dual-Throat Engine Staged Combustion Cycle IV (Four Preburner)

For Mode II operation, a small portion (2 to 4% of the total engine flow) is used as bleed flow in the secondary chamber. The bleed flow positions the primary chamber exhaust plume on the secondary throat to obtain efficient nozzle performance as described in Reference 7. Since the common shaft LO_2 and HDF pumps are not required for Mode II operation, the turbine exhaust gas from the LH_2 pump bypasses their turbine as shown in Figure 8.

The flow circuits for the other staged combustion cycles are similar to the single preburner cycle, except that separately driven turbines and additional preburners are utilized.

A typical pressure schedule obtained from the power balance of the three preburner cycle (Cycle III, Figure 10) is given in Table IV. The pressure drop assumptions for valves, lines and injectors are listed in the table. The valve losses are more conservative than those given in Table II, but the trends in the parametric data remain the same. The coolant pressure drops are obtained from the heat transfer analysis reported in Section III,C.

A typical summary of the LH_2 pump discharge pressure and LH_2 coolant pressure drop as a function of primary chamber pressure is given in Figure 12 for the three-preburner staged combustion cycle. Stream-tube thrust split was varied from 80% (LO_2/RP-1)/20% (LO_2/LH_2) to 20% (LO_2/RP-1)/80% (LO_2/LH_2). This range covers the thrust ratio (F_I/F_{II}) range from approximately 1.2 to 5.0 as shown in Figure 13.

If it is assumed that the practical upper limit pump discharge pressure (state-of-the-art in 1990) for LH_2 is 6.89×10^7 N/m^2 (10,000 psia), then the primary chamber pressure is limited to 2.69, 2.55, 2.34 and 2.28×10^7 N/m^2 (3900, 3700, 3400, and 3300 psia), respectively, for

TABLE IV

DUAL THROAT LOX/RP-1 + LH_2 (60/40)
STAGED COMBUSTION CYCLE III PRESSURE SCHEDULE

SI UNITS

F = 2669 KN PCS = 1 95 x 10^7 PCP = 2 07 x 10^7 N/M^2

PRESSURE	PRIMARY CHAMBER		SECONDARY CHAMBER	
	LH_2	LO_2 2 1	HDF 1 2	LO_2
P_D (N/M^2)	4 52 x 10^7	4 41 x 10^7/4 39 x 10^7	2 12 x 10^7/2 48 x 10^7	2 68 x 10^7
ΔP Shutoff Valve	10%	10%	10%	10%
ΔP Line	0 5%	0 5%	0 5%	0 5%
P_{JI}	4 05 x 10^7	3 95 x 10^7/3 93 x 10^7	-	-
ΔP Coolant	4 70 x 10^6	7 58 x 10^5	-	-
P_{JO}	3 57 x 10^7	3 87 x 10^7/3 85 x 10^7	-	-
ΔP Line	0 5%	0 5%	-	-
ΔP Control	10%	10%	10%	10%
P_{PBI}	3 20 x 10^7	3 47 x 10^7/3 45 x 10^7	1 70 x 10^7/1 99 x 10^7	2 16 x 10^7
ΔP_{INJ}	8%	15%	8%	15%
P_{PBC}	2 95 x 10^7	2 95 x 10^7/2 93 x 10^7	1 83 x 10^7	1 83 x 10^7
$P_{TI}(1)$	2 95 x 10^7	2 93 x 10^7	-	1 83 x 10^7
$P_{TO}(1)$		2 26 x 10^7	-	1 58 x 10^7
$P_{TI}(2)$		-	-	-
$P_{TO}(2)$	2 26 x 10^7	-	-	-
ΔP Line	0 5%	0 5%	-	0 5%
P_{INJ}	2 25 x 10^7	2 25 x 10^7	1 70 x 10^7	1 57 x 10^7
ΔP_{INJ}	8%	8%	15%	8%
Pc	2 07 x 10^7	2 07 x 10^7	1 45 x 10^7	1 45 x 10^7
Horsepower (W)	2 89 x 10^7	1 15 x 10^7	-	1 15 x 10^7
Flowrates (Kg/s)	35 1	245 5	143 5	401 7
Flow Split	33 1/2 0	23 8/221 7	1 345/8 9	-
Preburner Flowrates	56 9	223 7	-	410 6
MR_{PB}	0 72	110	-	45
T_{PB}(°K)	1033	922	-	922
MW_{PB}	3 467	30 1	-	31 9
γ_{PB}	1 360	1 312	-	1 31
ρ (Kg/m^3)	70 5	1137	-	1137
η_p	0 80	0 82	0 82	0 82
η_T	0 80	0 80	0 80	0 80

TABLE IV (Con t)

ENGLISH UNITS

F = 600K lb_f PCS = 2100   PCP = 3000 PSIA

PRESSURE	PRIMARY CHAMBER		SECONDARY CHAMBER	
	LH_2	LO_2 2 1	HDF 1 2	LO_2
P_D (psia)	6550	6390/6360	3070/3590	3880
ΔP Shutoff Valve	10%	10%	10%	10%
ΔP Line	0 5%	0 5	0 5%	0 5%
P_{JI}	5867	5722/5698	-	-
ΔP Coolant	682	110	-	-
P_{JO}	5185	5612/5588	-	-
ΔP Line	0 5%	0 5%	-	-
ΔP Control	10%	10%	10%	10%
P_{PBI}	4643	5026/5004	2470/2892	3130
ΔP_{INJ}	8%	15%	8%	15%
P_{PBC}	4272	4272/4254	2660	2660
$P_{TI}^{(1)}$	4272	4254	-	2660
$P_{TO}^{(1)}$		3277	-	2294
$P_{TI}^{(2)}$		-	-	-
$P_{TO}^{(2)}$	3277	-	-	-
ΔP Line	0 5%	0 5%	-	0 5%
P_{INJ}	3261	3261	2470	2283
ΔP_{INJ}	8%	8%	15%	8%
Pc	3000	3000	2100	2100
Horsepower (HP)	38,700	15,460	-	15,400
Flowrates (lb/s)	77 32	541 24	316 28	885 58
Flow split	72 88/4 44	52 47/488 77	296 69/19 68	-
Preburner Flowrates	125 35	493 21	-	905 26
MR_{PB}	0 72	110	-	45
T_{PB}(°R)	1860	1660	-	1660
MW_{PB}	3 467	30 1	-	31 9
γ_{PB}	1 360	1 312	-	1 31
ρ(lb/ft^3)	4 4	71	-	71
η_p	0 80	0 82	0 82	0 82
η_T	0 80	0 80	0 80	0 80

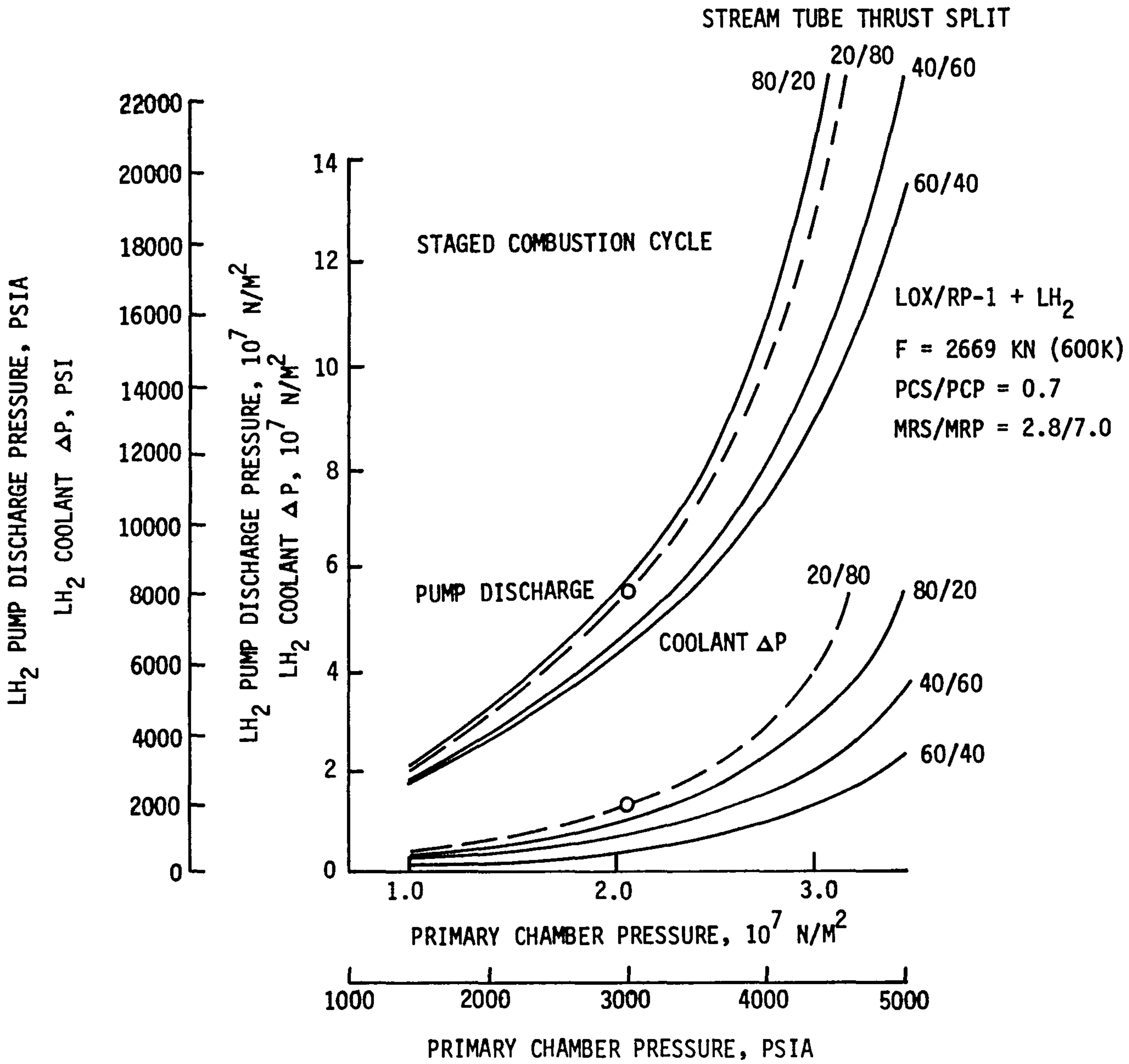

Figure 12. Dual Throat Engine Cycle Power Balance Summary
Staged Combustion Cycle III (Three Preburner)

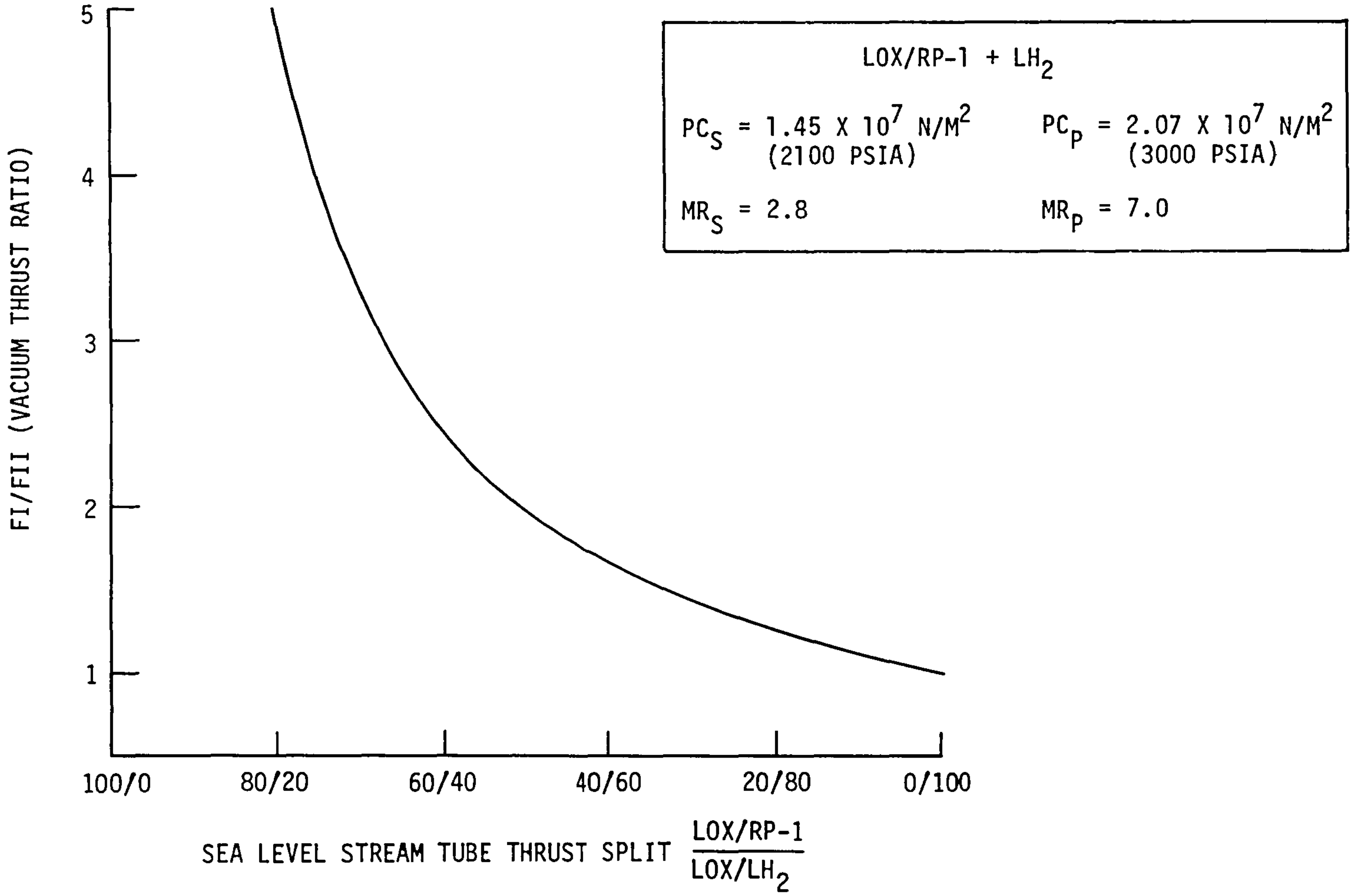

Figure 13. Dual Throat Engine Vacuum Thrust Ratio Versus Sea Level Stream-Tube Thrust Split

stream-tube thrust split values of 60/40, 40/60, 20/80, and 80/20. The primary reason for this limitation is seen to be the coolant pressure drop at the higher chamber pressures for the all-regeneratively cooled system.

The variation of pump discharge pressure with mixture ratio is given in Figure 14 for the three-preburner staged combustion cycle. It is seen that the variation is slight for all pumps (hydrogen, PD_H, oxygen, PD_O; and RP-1, PD_{RP-1}). The variation in LH_2 coolant pressure drop is also seen to be slight.

The variation of pump discharge pressure with engine thrust is also slight, as shown in Figure 15. The noticeable change in PD_H is primarily due to the increase in coolant pressure drop with the larger engines (greater surface area).

A power balance summary for the four staged combustion cycles is given in Table V. In order to achieve a workable cycle power balance, Cycle I is seen to require the highest LH_2 pump discharge pressure when compared to the other cycles which utilize additional preburners to drive the pumps. Cycle II, because of the poor quality working fluid of the RP-1 fuel-rich preburner gases, requires the highest RP-1 pump discharge pressure. Cycles III and IV differ slightly in pump discharge requirements despite the fact that cycle IV utilizes an additional RP-1 fuel-rich preburner.

When the features of the four staged combustion cycles are compared, along with the pump discharge pressures, Cycle III appears to be the best cycle for a reusable, long-life application. Cycle III requires no interpropellant seals between the turbomachinery components and involves no hydrocarbon coking in the turbines. It makes maximum use of the chemical energy of the propellants, without the need for high turbine temperatures

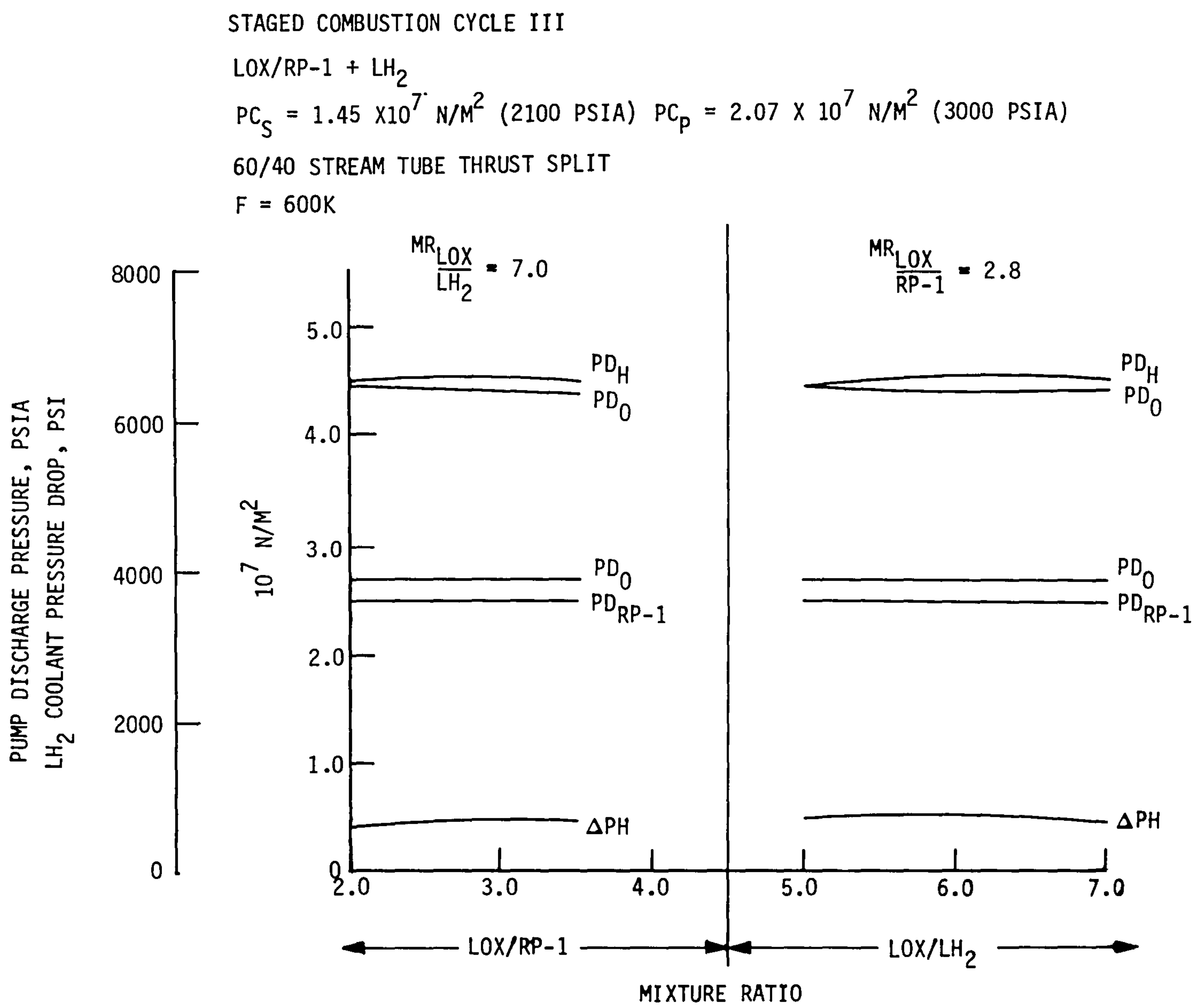

Figure 14. Discharge Pressure vs Mixture Ratio

LOX/RP-1 + LH_2

$PC_S = 1.45 \times 10^7$ N/M² (2100 PSIA) $PC_P = 2.07 \times 10^7$ N/M² (3000 PSIA)

$MR_S = 2.8$ $MR_P = 7.0$

60/40 STREAM TUBE THRUST SPLIT

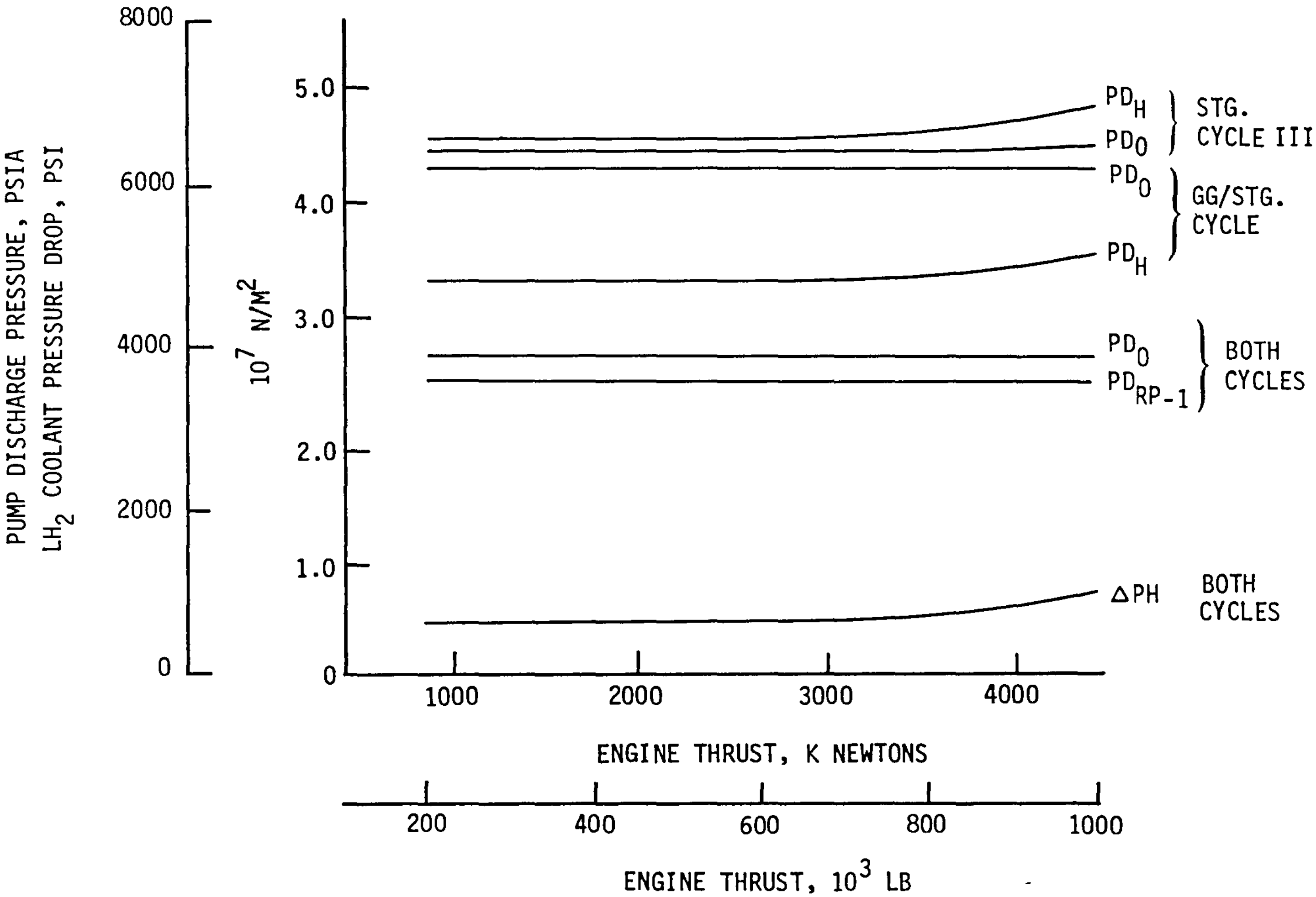

Figure 15. Discharge Pressure Versus Engine Thrust

TABLE V

POWER BALANCE SUMMARY FOR STAGED COMBUSTION CYCLES

F = 2669 KN (600K) PCS = 1.45×10^7 N/M^2 (2100 psia) PCP = 2.07×10^7 N/M^2 (3000 psia)

STREAM-TUBE THRUST SPLIT = 60/40

Pump Discharge Pressure 10^7 N/M^2 (psia)	Cycle I	II	III	IV
PDH	5.16 (7490)	4.56 (6610)	4.52 (6550)	4.50 (6520)
PDO	5.10 (7400)	4.45 (6460)	4.41 (6390)	4.38 (6350)
PDHC (RP-1)	1.90 (2760)	4.24 (6150)	2.48 (3590)	2.61 (3780)
PDO	1.76 (2550)	3.92 (5680)	2.68 (3880)	2.83 (4100)
Engine Features				
Interpropellant Seal(s)	Yes	Yes	No	No
Hydrocarbon Coking	No	Yes	No	Yes
Fuel-Rich Preburner(s)	Yes (1)	Yes (2)	Yes (1)	Yes (2)
Oxid.-Rich Preburner(s)	No	No	Yes (2)	Yes (2)
ΔIs Mode I* (sec)	0	-4	0	-4

*Incomplete Combustion of Coke Assumed to Lower Performance ~1%

and working fluids that can leave a coke deposit on the turbine and main injector.

Transpiration cooling of the primary throat section was investigated for the primary chamber pressure of 3.45×10^7 N/m^2 (5,000 psia). The results of the trans-regen analysis are given in Table VI. Maintaining the coolant pressure drop at 1.03×10^7 N/m^2 (1500 psia) is seen to lower the pump discharge pressure from 1.34 to 1.11×10^8 N/m^2 (19,400 to 16,070 psia). The performance remains essentially the same during Mode I because of the excellent properties of heated hydrogen as a working fluid, but drops 1.5 seconds in specific impulse during Mode II. The LO_2/LH_2 stream-tube mixture ratio is seen to shift from a value of 7.0 to 6.1 because of the added amount of transpiration coolant.

In Figure 16, the trans-regen point is superimposed on the curves previously shown in Figure 12. Extrapolation of this data point allows the estimation of the pump discharge pressure required at lower primary chamber pressures.

Similar power balance calculations were made for a LO_2/LCH_4 + LH_2 dual throat engine. The results from this study are summarized in Figures 17 and 18. It is seen that the use of methane instead of RP-1 fuel requires a slight increase in hydrogen pump discharge pressure (staged combustion Cycle III) for an increase in sea level specific impulse of 1.8 to 2.3 percent (6 to 8 seconds).

3. <u>Gas Generator Cycles</u>

Two gas generator cycle dual throat engines were evaluated, as depicted in Figures 19 and 20. Only fuel-rich gas generators were con-

TABLE VI

TRANS-REGEN COOLING LOWERS PUMP DISCHARGE PRESSURE

PCS/PCP = 2.41/3.45 x 10^7 N/M^2 (3500/5000 PSIA)

F = 2669 KN (600K lb) (60/40)

STAGED COMBUSTION CYCLE (III)

			COOLANT					
	FI/F II	PDH 10^8 N/M^2 (PSIA)	ΔP 10^7 N/M^2 (PSI)	$\dot{W}$ Kg/S (LB/S)	ΔISI	ΔISII	MR I	MR II
Regen Cooled	2.43	1.34 (19400)	2.41 (3500)	0	0	0	2.8/7.0	7.0
Trans.-Regen.	2.51	1.11 (16070)	1.03 (1500)	5.22 (11.5*)	+0.2	-1.5	2.8/6.06	6.06

*0.66% MODE I FLOWRATE

1.90% MODE II FLOWRATE

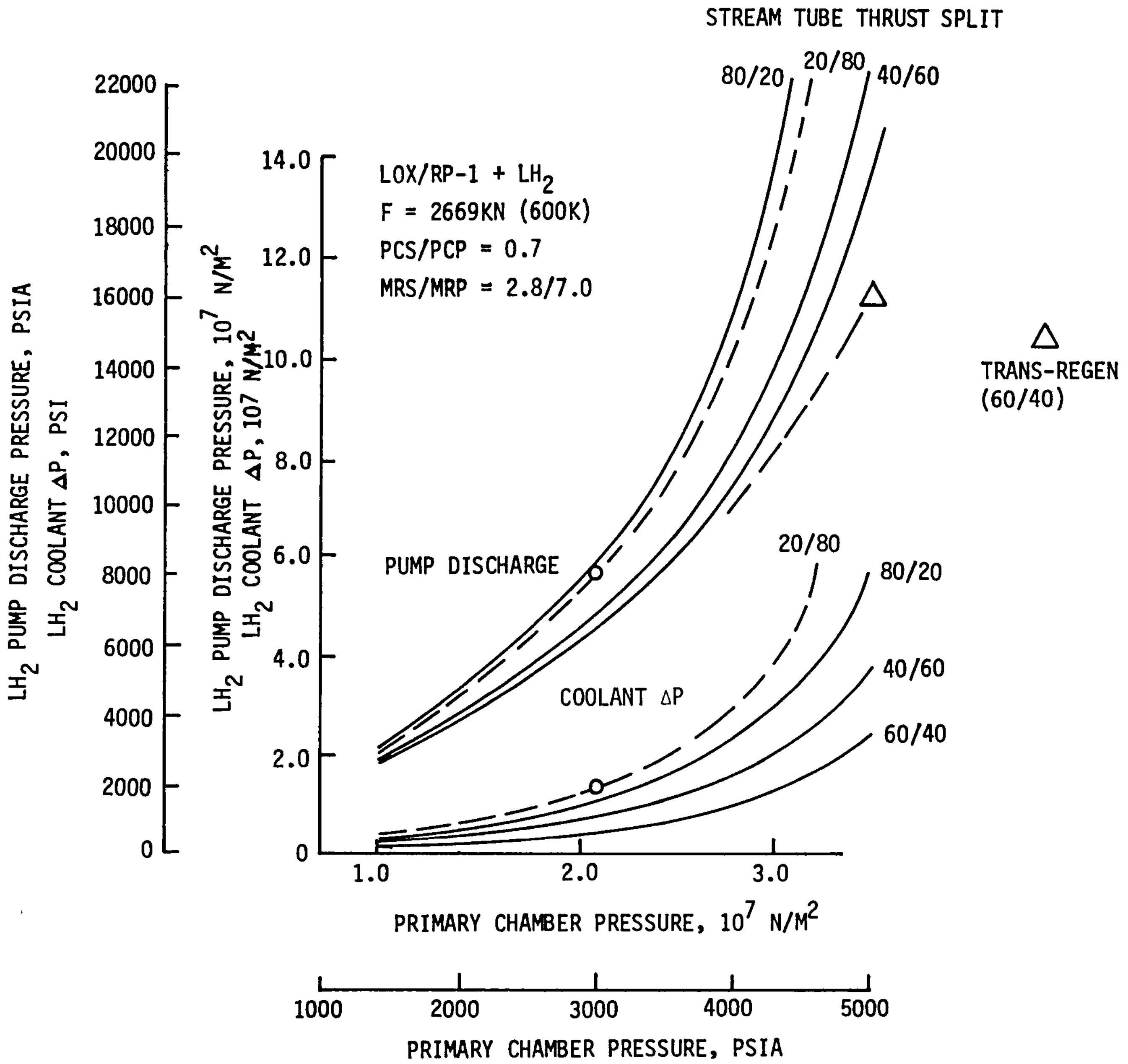

Figure 16. Effect of Trans-Regen Cooling on Cycle Power Balance Staged Combustion Cycle III (Three Preburner)

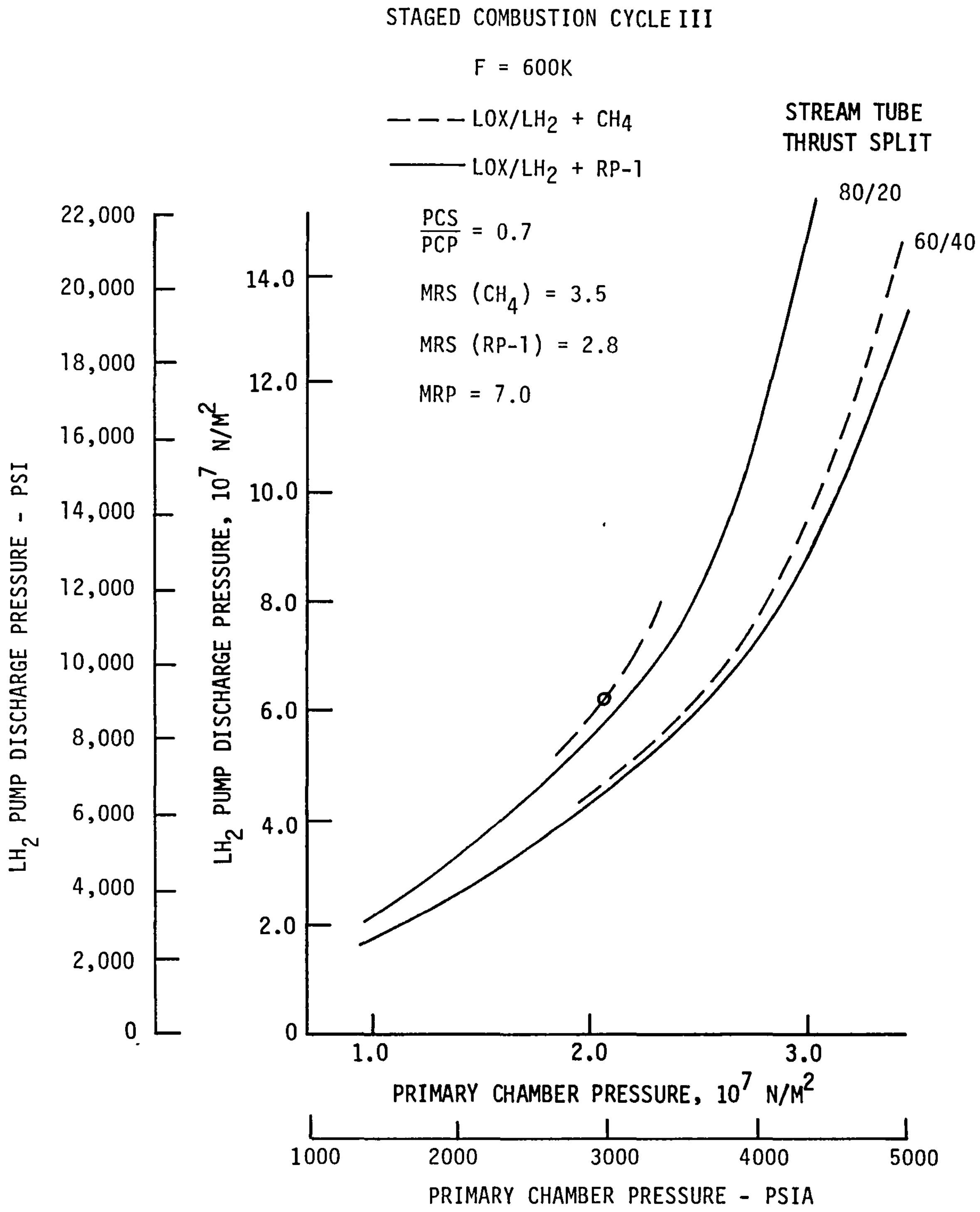

Figure 17. Comparison of LH_2 Pump Discharge Pressure for RP-1 & CH_4 Dual Throat Engines

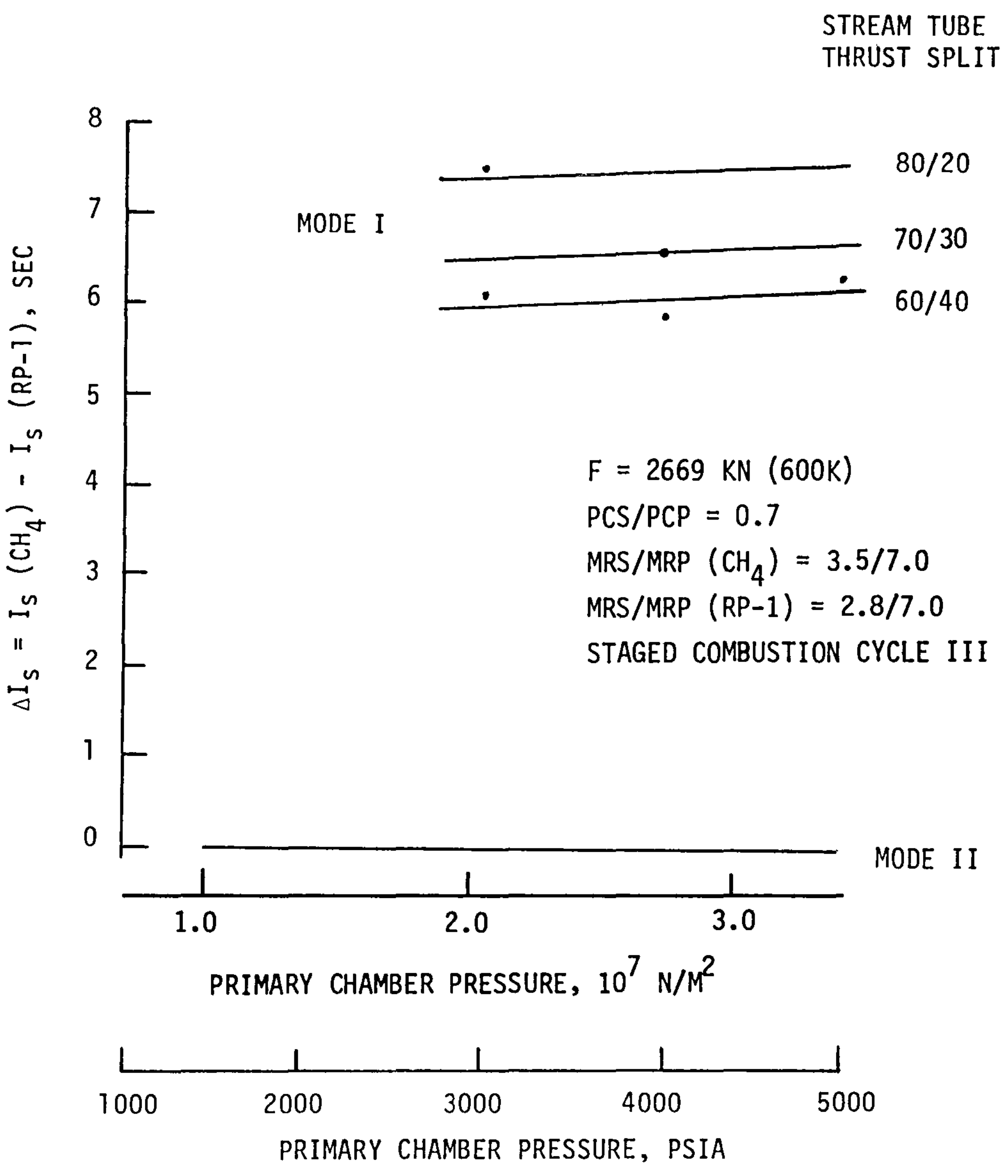

Figure 18. Performance Difference Between LOX/LH_2 + RP-1 & LOX/LH_2 + CH_4 Dual Throat Engines

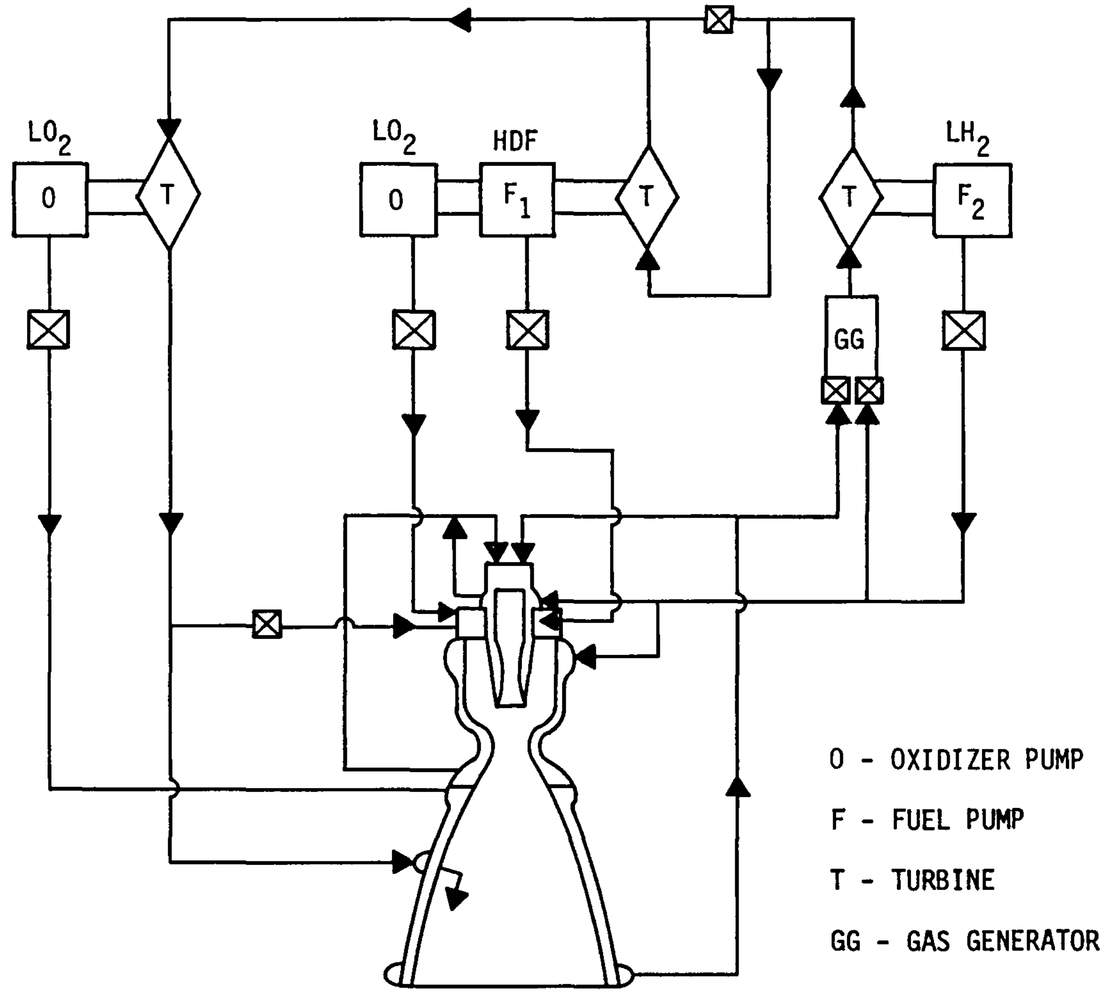

Figure 19. Dual-Fuel, Dual-Throat Engine Gas Generator Cycle I

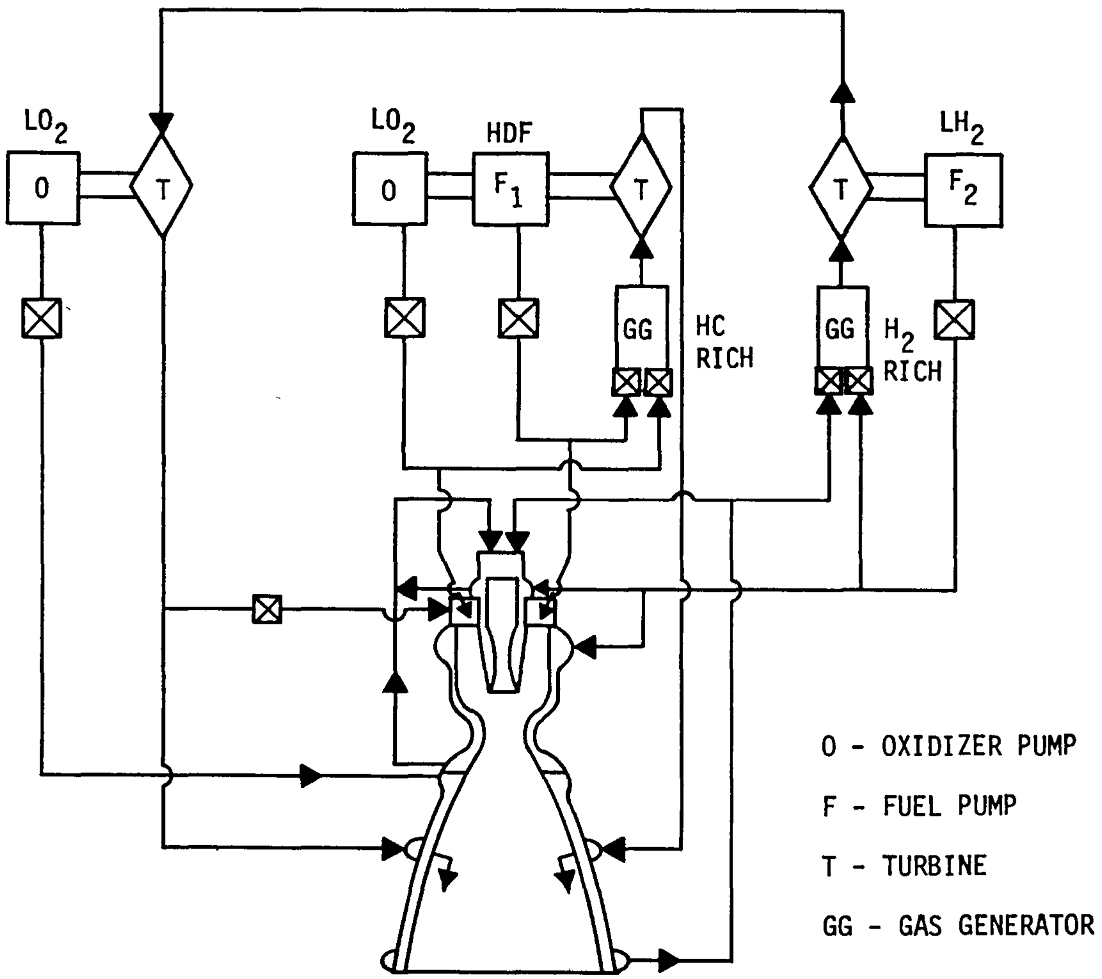

Figure 20. Dual-Fuel, Dual-Throat Engine Gas Generator (Dual) Cycle II

sidered. The flow circuits are similar to those described for the staged combustion cycles except that the turbine exhaust gas is dumped into the nozzle, as shown in the figures. During Mode II, all or a portion of the gas generator turbine exhaust is used as bleed flow in the secondary chamber.

The pump discharge pressures obtained from the cycle power balance calculations are given in Table VII for both gas generator cycles. Also shown in the table are the engine features, including the gas generator flow rates during both modes of operation, the LO_2/LH_2 mixture ratio in Mode II, and the loss in performance during Mode I (compared to the staged combustion cycle performance). Gas generator Cycle II is seen to be a poor performer because of the hydrocarbon coking and the requirement for such a large hydrocarbon-rich flow rate to achieve a power balance. Gas generator Cycle I is seen to be an excellent candidate for the baseline pressure conditions, but becomes somewhat power limited at higher pressures because of the complete dependence upon hydrogen as a working fluid. Both cycles require interpropellant seals.

4. Expander and Expander Bleed Cycles

It was not possible to obtain a power balance for the baseline dual throat engine utilizing an expander cycle. Expander cycles are commonly balanced for engines with chamber pressures of the order of 6.89×10^6 N/m^2 (1000 psia).

It was also not possible to obtain a practical power balance for an expander bleed cycle at baseline engine conditions because of the low temperature of the hydrogen coolant. A redesign of the coolant channels and/or a redistribution of coolant flow to obtain higher hydrogen temperatures should allow a balance, but at the expense of dumping a large amount of hydrogen fuel.

TABLE VII

POWER BALANCE SUMMARY FOR GAS GENERATOR CYCLES

F = 2669 KN (600K)   PCS = 1.45×10^7 N/M^2 (2100)   PCP = 2.07×10^7 N/M^2 (3000 PSIA)

STREAM-TUBE THRUST SPLIT = 60/40

	CYCLE	
Pump Discharge Pressure (psia)	I	II
PDH	3.05 (4420)	3.05 (4420)
PDO	3.10 (4500)	3.10 (4500)
PDHC (RP-1)	1.90 (2760)	2.77 (4020)
PDO	1.76 (2550)	3.00 (4350)
Engine Features		
Interpropellant Seal(s)	Yes	Yes
Hydrocarbon Coking	No	Yes
GG Flow Rate, Mode I Kg/S (lb/sec)	12.2 (26.8)	49.0 (108)
GG Flow Rate, Mode II Kg/S (lb/sec)	8.1 (17.8)	8.1 (17.8)
ΔIs Loss, Mode I* (sec)	-0.7	-11
Mixture Ratio, Mode II	6.3	6.3

*Difference between staged combustion cycle performance
(Note: Mode II loss is the same as staged combustion cycle also requires bleed flow)

These "pure" cycles were, therefore, not considered further in the study. A mixed cycle incorporating both expander bleed and staged combustion components was considered as a candidate, however.

5. Expander Bleed/Staged Combustion Mixed Cycle

The expander bleed/staged combustion cycle shown in Figure 21 was analyzed for the dual-fuel, dual-throat engine. The cycle consists of two oxidizer-rich preburners (LO_2/HDF and LO_2/LH_2) and uses the hot hydrogen from the coolant jacket to power both fuel turbines during Mode I and only the LH_2 turbine during Mode II. The LO_2/HDF preburner and turbine operate only during Mode I. The schematic indicates that all of the hydrogen is used as coolant, but the best version of this cycle involves heating only a small portion of the coolant to a high temperature, and utilizing this portion as the turbine drive fluid. The remaining (lower temperature) coolant is burned in the main injector and the preburner.

The power balance summary and the engine features for this cycle are given in Table VIII. The cycle is a major candidate, its principal disadvantage being the large shift in mixture ratio from 7.0 to 5.7 in Mode II operation. The fairly large amount of dump flow rate also induces a performance loss in Mode II that is greater than that incurred for the staged combustion cycle with its smaller amount of bleed flow.

6. Gas Generator/Staged Combustion Mixed Cycle

The schematic of the dual-fuel, dual-throat engine gas generator/staged combustion mixed cycle is shown in Figure 22. The basic engine operation is as follows. LO_2, for the secondary chamber operation in Mode I, flows to the oxidizer-rich preburner. The turbine exhaust from this preburner flows to the oxidizer manifold of the secondary injector. HDF (RP-1 or LCH_4) flows to the secondary injector during Mode I operation. A small amount of the HDF is burned in the oxidizer-rich preburner as shown in the schematic. LO_2, for the primary chamber operation in both modes, is

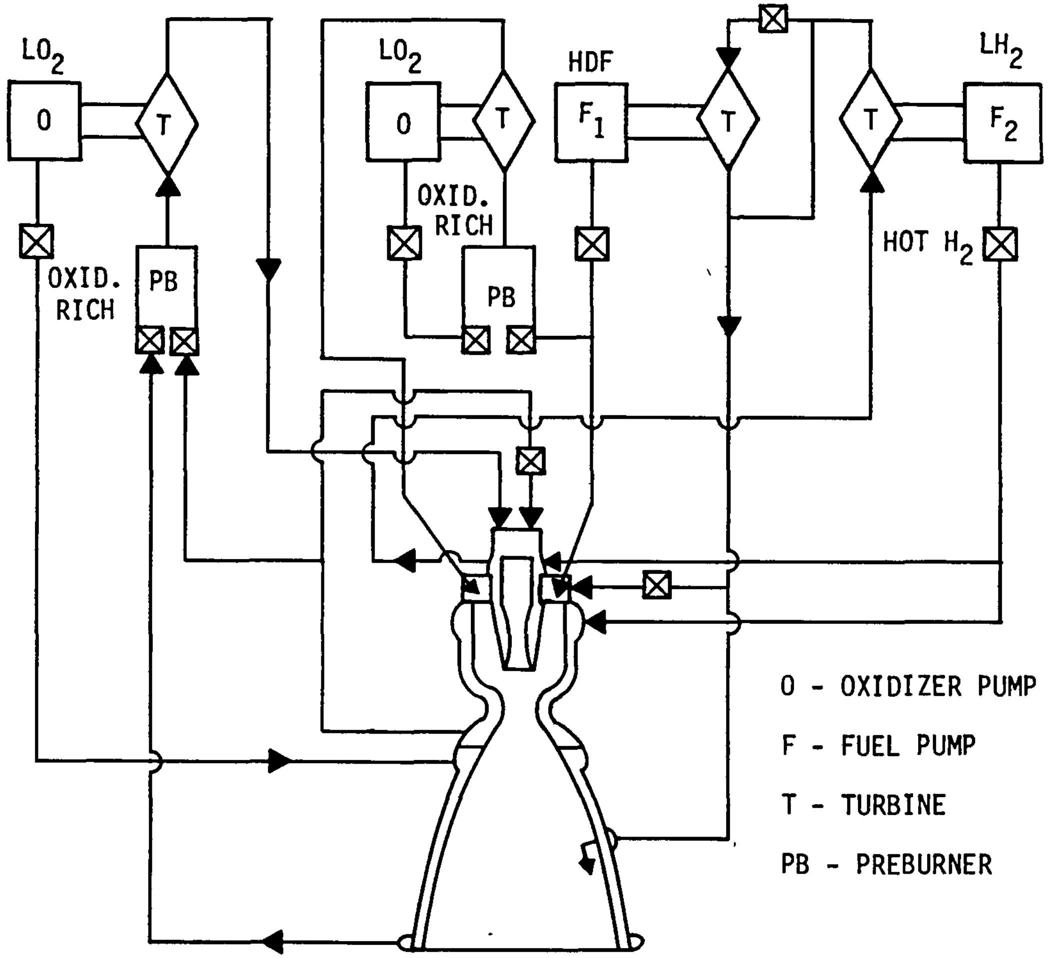

Figure 21. Dual-Fuel, Dual-Throat Engine Expander Bleed/Staged Combustion Mixed Cycle

TABLE VIII

POWER BALANCE SUMMARY FOR EXPANDER BLEED/STAGED COMBUSTION CYCLE

F = 2669 KN (600K)   PCS = 1.45×10^7 N/M^2 (2100)   PCP = 2.07×10^7 N/M^2 (3000 psia)

STREAM-TUBE THRUST SPLIT = 60/40

Pump Discharge Pressure 10^7 N/M^2 (psia)	
PDH	3.85 (5590)
PDO	3.83 (5550)
PDHC (RP-1)	2.48 (3590)
PDO	2.68 (3890)
Engine Features	
Interpropellant Seal(s)	No
Hydrocarbon Coking	No
Dump Flow Rate, Mode I Kg/s (lb/sec)	10.6 (23.4)
Mixture Ratio, Mode II	5.7
ΔIs Loss, Mode I* (sec)	-0.2

*Difference between staged combustion cycle performance

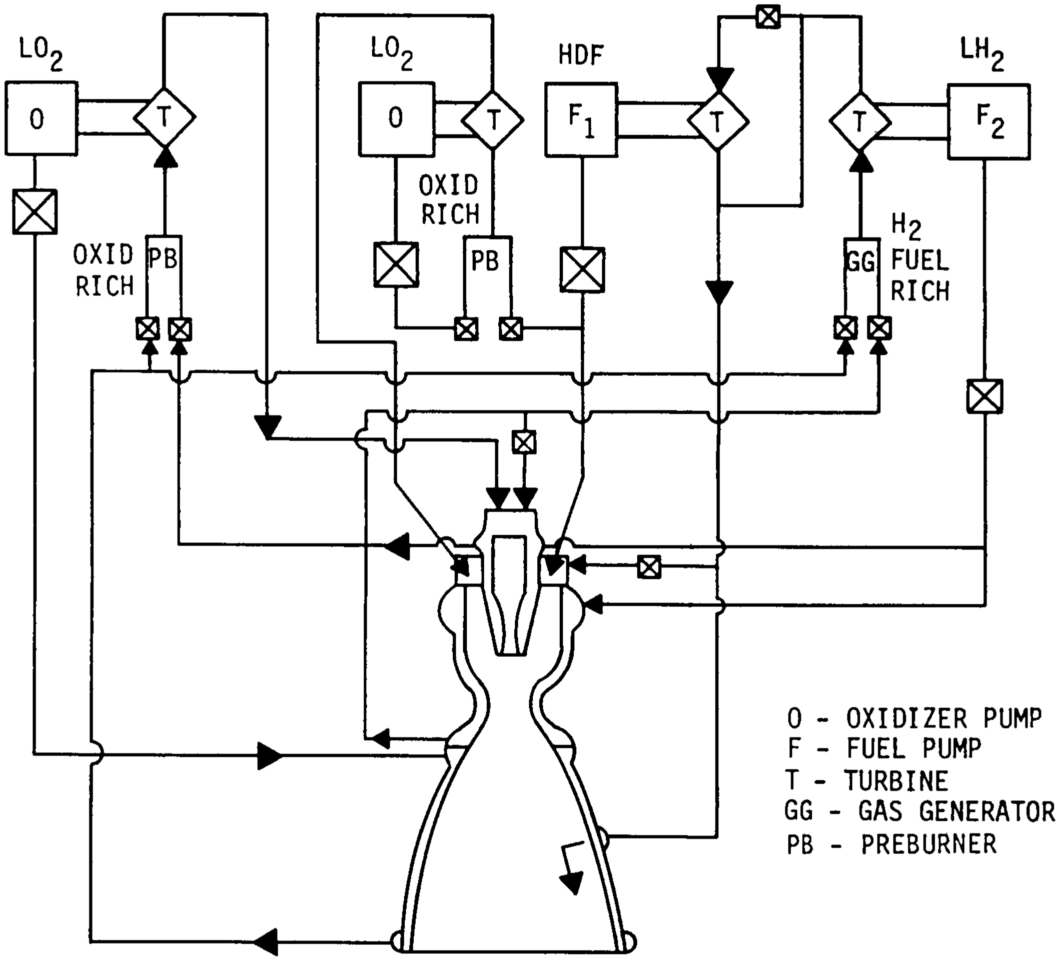

Figure 22. Dual-Fuel, Dual-Throat Engine Gas Generator/Staged Combustion Mixed Cycle

utilized to cool the nozzle prior to its being burned in the oxidizer-rich and fuel-rich preburners. The exhaust from the oxidizer-rich preburner turbine enters the primary chamber injector oxidizer manifold. LH_2 is utilized as coolant for the high heat flux regions of both chambers, as shown in the schematic. The coolant jacket outlet flow is split between the main injector, the oxidizer-rich preburner and the fuel-rich preburner. In Mode I the fuel-rich preburner turbine exhaust is dumped in the nozzle, while in Mode II the fuel-rich exhaust is used as bleed flow in the secondary chamber.

Parametric power balance data for the gas generator/staged combustion mixed cycle are shown in Figure 23. If the practical upper limit pump discharge pressure (state-of-the-art in 1990) is assumed to be 6.89 x 10^7 N/m^2 (10,000 psia), the primary chamber pressure will be limited to 3.31, 3.10 and 2.83 x 10^7 N/m^2 (4800, 4500 and 4100 psia), respectively, for stream-tube thrust split values of 60/40, 40/60 and 80/20. These values should be compared with those quoted for the staged combustion cycle depicted in Figure 10.

Pump discharge pressures and coolant pressure drop are given in Figure 15 as a function of engine thrust from 890 to 4448 KN (200K to 1M pounds). It is seen that there is only a small variation in these parameters with engine thrust level.

The variation in engine mixture ratio (LO_2/LH_2 circuit only) resulting from use of the mixed cycle is shown in Figure 24. This variation could have an impact on vehicle performance because of the increase in the low density hydrogen requirement.

The loss in specific impulse due to the gas generator component of the engine cycle is shown in Figure 25 for Mode I operation. The loss as a

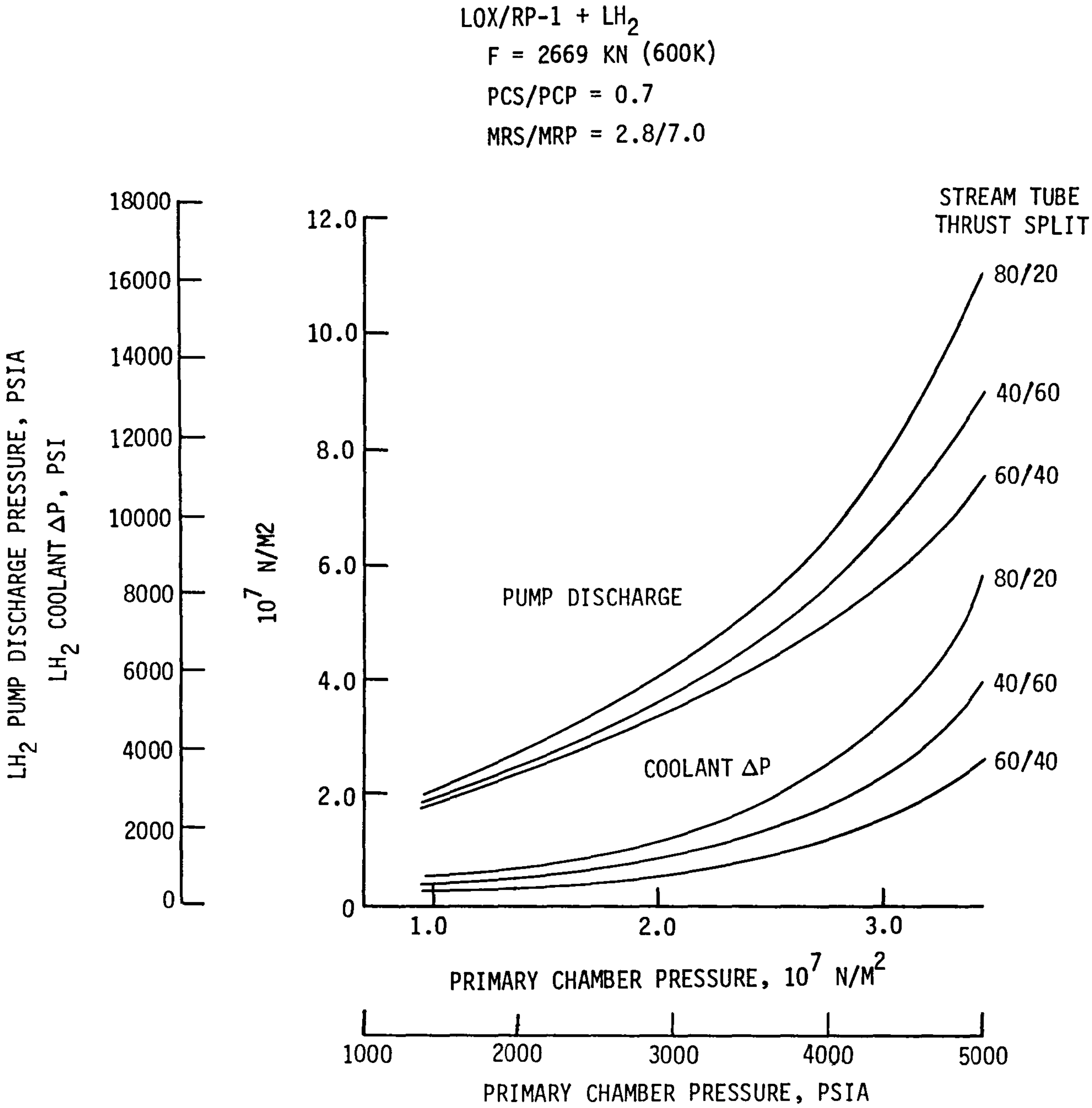

Figure 23. Dual Throat Engine Cycle Power Balance, Gas Generator/ Staged Combustion Mixed Cycle

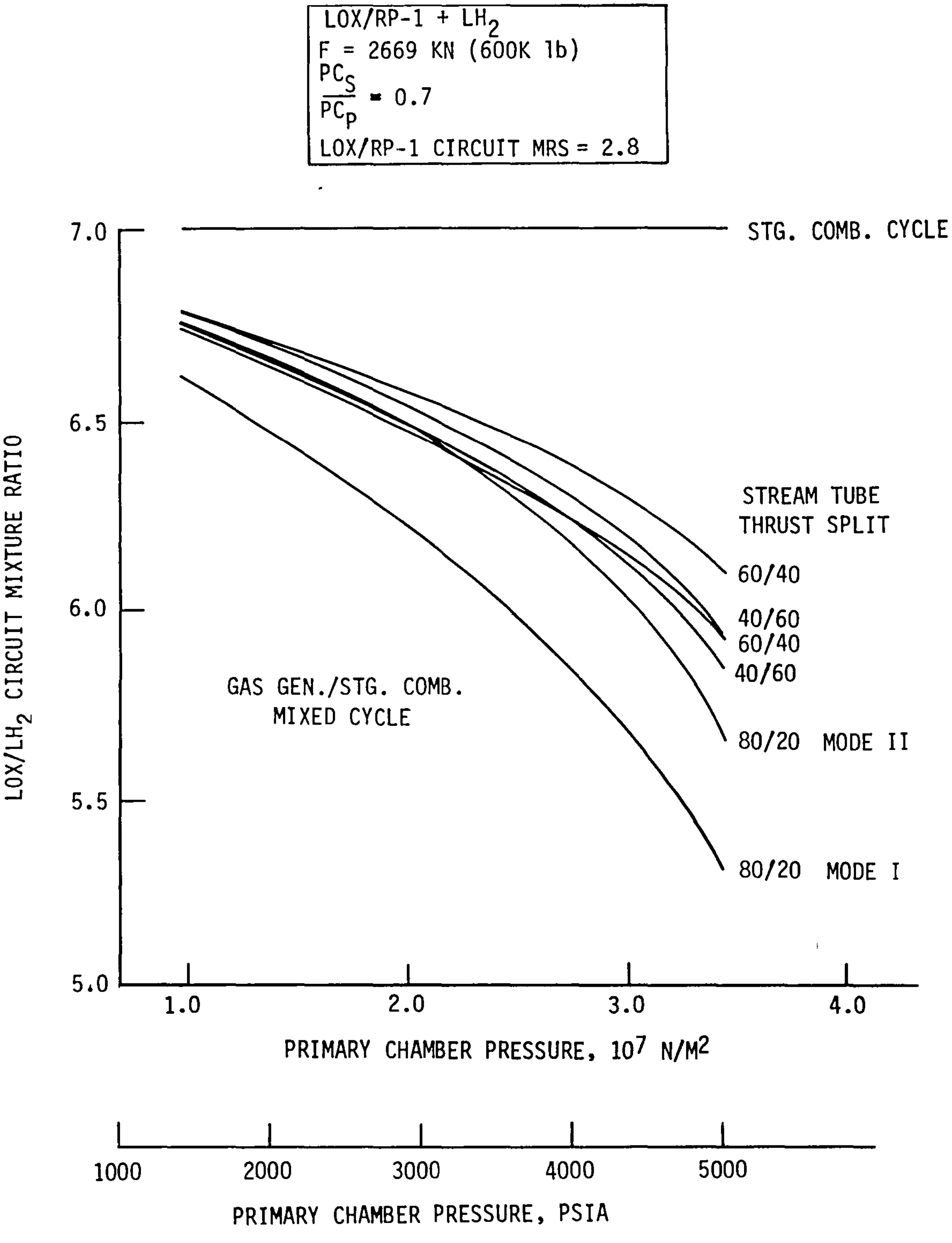

Figure 24. Dual-Throat Engine Mixture Ratio Variation

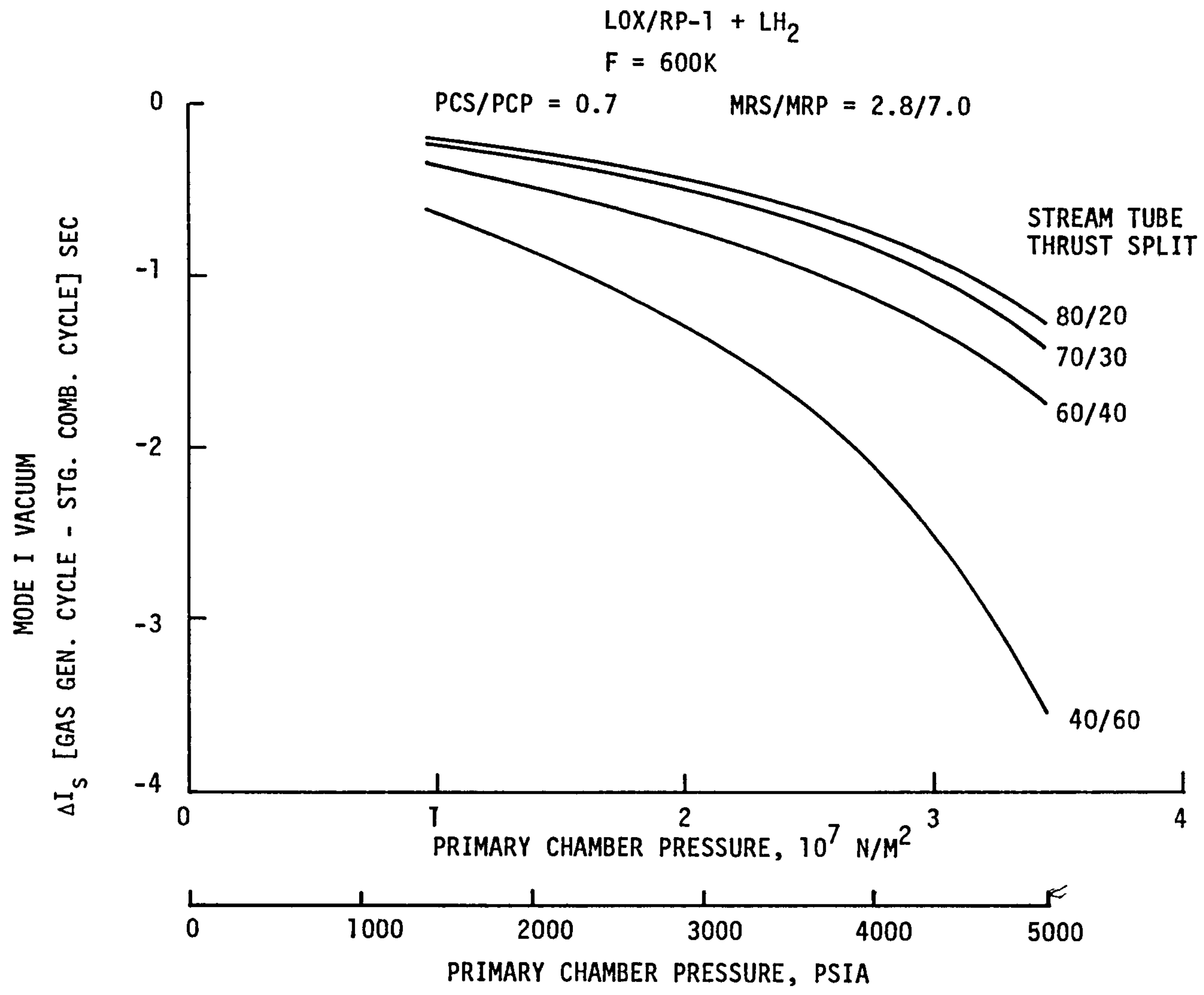

Figure 25. Dual Throat Engine Cycle Performance Comparison

function of primary chamber presssure does not appear that significant. The loss in Mode II operation can be less than that shown for Mode I, because of the bleed flow requirement for the staged combustion cycle in Mode II.

7. Engine Cycle Selection

The engine cycle selected for the dual throat engine is the gas generator/staged combustion cycle. The rationale for the selection is given in Table IX and Figure 26. In addition, the selection included an increase in chamber pressures to PCS = 1.93×10^7 N/m^2 (2800) and PCP = 2.76×10^7 N/m^2 (4000 psia), and a change in stream-tube thrust split to 70% LO_2/RP-1 : 30% LO_2/LH_2. The increase in chamber pressures and the change in stream-tube thrust split were predominantly the result of the mission application analysis discussed in Section IV,E. The high density fuel RP-1 was selected over LCH_4, but a definitive application/cost study is required before NASA can choose between these and LC_3H_8 fuels.

C. THRUST CHAMBER HEAT TRANSFER

Parametric analyses were conducted for parallel hydrogen-cooled chamber circuits and an oxygen-cooled secondary nozzle tube bundle to investigate the effects of thrust, stream-tube thrust-split, chamber pressure, and mixture ratio on coolant pressure drop requirements. Minimum pressure drop values are obtained for a stream-tube thrust split near the baseline (60/40). To achieve a practical pressure drop at a primary chamber pressure of 3.45×10^7 N/m^2 (5000 psia), transpiration cooling of the primary throat was ncessary. The results of the heat transfer analysis briefly summarized, and specific details of the effort are presented for chamber and nozzle cooling.

TABLE IX

DUAL THROAT ENGINE CYCLE SELECTION

	Pump Discharge** Pressure (psia)				Inter-Propellant Seal(s)	Hydrocarbon Coking	ΔIs Mode I (sec)	ΔIs* Mode II (sec)	Mixture Ratio Mode II	Engine Weight (lb)	Rating Points Subtracted From Maximum of 10	Rating
	LH_2	LO_2	RP-1	LO_2								
Gas Generator I	4420 + 1/2	4500 + 1/2	2760 + 1/2	2550 + 1/2	Yes -3	No	-0 7 -1/2	-4 5	6 3 -1	5547 + 1/2	10 -2 =	8
Gas Generator II	4420 + 1/2	4500 + 1/2	4020 - 1/2	4350 - 1/2	Yes -3	Yes -3	-11 -3	-4 5	6 3 -1	5588 + 1/2	10 - 9 1/2 =	1/2
Stg Combustion I	7490 -1	7400 -1	2760 + 1/2	2550 + 1/2	Yes -3	No	0	-4 7	7 0	5991	10 -4 =	6
Stg Combustion II	6610 -1/2	6460 -1/2	6150 -1/2	5680 -1/2	Yes -3	Yes -3	-4 -1	-4 7	7 0	6330 -1/2	10 -9 1/2 =	1/2
Stg Combustion III	6550 -1/2	6390 -1/2	3590	3880	No	No	0	-4 7	7 0	6168	10 -1 =	9
Stg Combustion IV	6520 -1/2	6350 -1/2	3780	4100	No	Yes -3	-4 -1	-4 7	7 0	6222	10 -5 =	5
Expander Bleed/ Stg Combustion	5590 -1/2	5550	3590	3880	No	No	-0 2 -1/2	-3 1 +1	5 7 - 2 1/2	5795 + 1/2	10 -2 =	8
Gas Generator/ Stg Combustion	5000	5550	3590	3880	No	No	-0 4 -1/2	-2 6 +1	6 6 -1	5771 + 1/2	10 -0 =	10
Reference	5000	5500	3600	3900	No	No	0	-4 7	7 0	6168	-	10

*1% Is loss assumed for staged combustion cycles plus 2% bleed flow requirement

**PCS/PCP = 2100/3000 psia

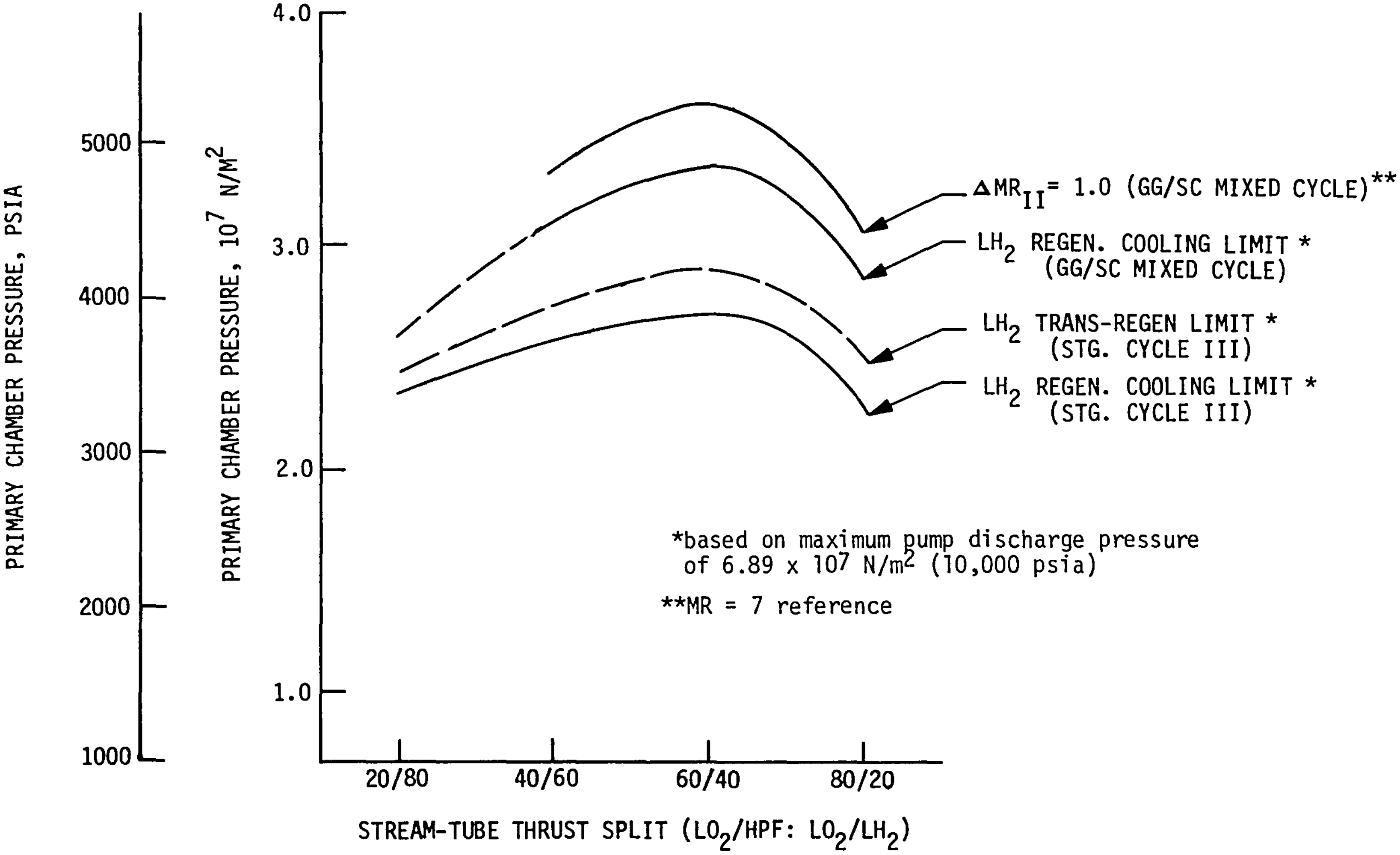

Figure 26. Dual Throat Engine Cycle Parameter Variation

1. Summary of Results

The engine cooling studies were divided into two parts: hydrogen cooling of the primary and secondary chambers using rectangular channels in zirconium-copper liners with electroformed nickel closures, and oxygen cooling of the secondary nozzle using two-pass Inconel 718 tube bundles. Table X and Figure 27 show the regeneratively cooled chamber geometry for the preliminary baseline engine, which develops 2700 KN (607,000 lbF) thrust with 60 percent of the stream-tube thrust from the LOX/RP-1 propellants; primary and secondary chamber pressures are 2.07 and 1.45 x 10^7 N/m^2 (3000 and 2100 psia), respectively. The conical nozzle was utilized to facilitate the parametric analysis. Two parallel hydrogen flow circuits are used for chamber cooling. One circuit cools the outer contour, with the coolant inlet at area ratio 8:1 in the secondary nozzle and the outlet at the secondary injector. The primary circuit cools the inner surface of the secondary chamber in series with the primary chamber, with the inlet at the secondary injector and the outlet at the primary injector. In all cases the flow fraction between circuits was determined such that the required pressure drops were balanced with no bypass flow (see Figure 28 and Table XI).

A coolant pressure drop of 4.72 x 10^6 N/m^2 (685 psi) is required to provide a life of 100 cycles for the baseline chamber, with 36 percent of the hydrogen flow in the primary circuit. Coolant bulk temperature rises are 165°K (297°F) in the primary circuit and 280°K (504°F) in the secondary. Substitution of methane for RP-1 in the combustion zone had a negligible effect. Scaling of the baseline engine to other thrust levels, stream-tube thrust split values, and chamber pressures is presented along with the effect of changing the primary and secondary mixture ratios in Figures 29 through 36. It was found that the minimum pressure drop requirement is for a stream-tube thrust split near the baseline value.

TABLE X

PRELIMINARY BASELINE CHAMBER DESIGN

OUTER CHAMBER CONTOUR AND HEAT TRANSFER RESULTS

(See Figure 50 for nomenclature)

IOP = 3 OUTER CHAMBER CONTOUR:

Z(1)	Z(2)	Z(3)	Z(4)	Z(5)	Z(6)	Z(7)	Z(8)	Z(9)	Z(10)	Z(11)	Z(12)	Z(13)	Z(14)	Z(15)
16.05	16.29	16.53	18.44	20.22	22.05	23.88	25.79	27.57	28.53	38.52	48.50	58.49	68.48	78.46
R(1)	R(2)	R(3)	R(4)	R(5)	R(6)	R(7)	R(8)	R(9)	R(10)	R(11)	R(12)	R(13)	R(14)	R(15)
11.48	11.48	11.48	11.23	10.49	9.43	8.38	7.64	7.39	7.51	10.19	12.87	15.54	18.22	20.89
S(1)	S(2)	S(3)	S(4)	S(5)	S(6)	S(7)	S(8)	S(9)	S(10)	S(11)	S(12)	S(13)	S(14)	S(15)
16.05	16.29	16.53	18.46	20.40	22.51	24.62	26.55	28.49	29.46	39.79	50.13	60.47	70.81	81.15

PCP = 3000. PCS = 2100. THRUST = 607000. STREAM TUBE THRUST SPLIT = 60/40

STA	P	TB	LAND	WIDTH	DEPTH	MACH	TBS	TINT	TWL2	TWGC	QAO3	QAI2
1	5994.	111.	.158	.079	.395	.015	157.	159.	411.	463.	6.4	3.9
2	5987.	178.	.128	.079	.395	.021	210.	212.	529.	594.	8.3	4.7
3	5976.	240.	.098	.079	.395	.027	263.	265.	687.	770.	10.9	5.6
4	5967.	305.	.067	.079	.395	.032	319.	319.	900.	1016.	15.1	7.7
5	5711.	383.	.060	.056	.280	.073	394.	395.	925.	1059.	23.6	14.1
6	5688.	485.	.041	.044	.220	.133	492.	492.	1131.	1306.	40.4	25.4
7	5658.	496.	.040	.044	.220	.136	499.	500.	1032.	1213.	40.9	30.0
8	5620.	517.	.041	.046	.230	.127	522.	522.	1111.	1287.	40.5	28.3
9	5569.	539.	.049	.046	.230	.131	545.	545.	1044.	1195.	34.5	25.0
10	5510.	560.	.061	.046	.230	.136	571.	572.	1021.	1137.	27.2	18.3
11	5450.	58[illegible].	.073	.046	.230	.140	594.	594.	978.	1079.	23.1	16.4
12	5392.	597.	.082	.046	.230	.145	619.	620.	1024.	1115.	21.7	13.8
13	5333.	615.	.084	.046	.230	.149	636.	637.	1019.	1105.	20.5	13.2
14	5326.	617.	.084	.046	.230	.149	633.	634.	978.	1070.	20.7	15.2
15	5318.	619.	.084	.046	.230	.150	636.	636.	981.	1073.	20.7	15.3

NO. CHANNELS = 554. DELTAT = 508. DELTAP = 681. COOLANT FLOW = 48.06

TABLE X (Cont.)

PRELIMINARY BASELINE CHAMBER DESIGN

INNER ANNULUS AND PRIMARY CHAMBER CONTOUR AND HEAT TRANSFER RESULTS

IOP = 4

INNER ANNULUS CONTOUR:

Z(1)	Z(2)	Z(3)	Z(4)	Z(5)	Z(6)	Z(7)	Z(8)	Z(9)	Z(10)	Z(11)	Z(12)	Z(13)	Z(14)	Z(15)
16.05	16.72	17.39	18.07	18.74	.00	.00	.00	.00	.00	.00	.00	.00	.00	.00
R(1)	R(2)	R(3)	R(4)	R(5)	R(6)	R(7)	R(8)	R(9)	R(10)	R(11)	R(12)	R(13)	R(14)	R(15)
7.07	6.80	6.54	6.27	6.01	.00	.00	.00	.00	.00	.00	.00	.00	.00	.00
S(1)	S(2)	S(3)	S(4)	S(5)	S(6)	S(7)	S(8)	S(9)	S(10)	S(11)	S(12)	S(13)	S(14)	S(15)
16.05	16.77	17.49	18.22	18.94	.00	.00	.00	.00	.00	.00	.00	.00	.00	.00

PHI = 21.5

PCP = 3000. PCS = 2100. THRUST = 607000. SPLIT = 60/40

STA	P	TH	LAND	WIDTH	DEPTH	MACH	TBS	TINT	TWL2	TWGC	QAU3	QAI2
1	5949.	111.	.193	.046	.230	.045	263.	267.	735.	831.	21.6	16.6
2	5940.	120.	.193	.046	.230	.047	267.	271.	735.	832.	21.6	16.6
3	5934.	120.	.193	.046	.230	.047	266.	271.	733.	830.	21.5	16.6
4	5927.	120.	.188	.046	.230	.047	270.	275.	766.	867.	22.7	17.0
5	5920.	120.	.172	.046	.230	.047	261.	265.	785.	889.	24.0	17.3

NO. CHANNELS = 301. DELTAT = 9. DELTAP = 79. COOLANT FLOW = 27.03

IOP = 2

INNER CHAMBER CONTOUR:

Z(1)	Z(2)	Z(3)	Z(4)	Z(5)	Z(6)	Z(7)	Z(8)	Z(9)	Z(10)	Z(11)	Z(12)	Z(13)	Z(14)	Z(15)
.00	1.08	2.16	4.14	5.99	6.59	7.18	8.18	9.10	9.43	11.29	13.16	15.02	16.88	18.74
R(1)	R(2)	R(3)	R(4)	R(5)	R(6)	R(7)	R(8)	R(9)	R(10)	R(11)	R(12)	R(13)	R(14)	R(15)
6.07	6.07	6.07	5.80	5.04	4.69	4.35	3.97	3.84	3.87	4.19	4.52	4.85	5.18	5.51
S(1)	S(2)	S(3)	S(4)	S(5)	S(6)	S(7)	S(8)	S(9)	S(10)	S(11)	S(12)	S(13)	S(14)	S(15)
.00	1.08	2.16	4.17	6.17	6.86	7.55	8.55	9.56	9.89	11.78	13.67	15.56	17.45	19.34

PCP = 3000. PCS = 2100. THRUST = 607000. SPLIT = 60/40

STA	P	TB	LAND	WIDTH	DEPTH	MACH	TBS	TINT	TWL2	TWGC	QAU3	QAI2
1	5898.	120.	.060	.065	.276	.030	172.	174.	1186.	1355.	32.2	15.5
2	5872.	155.	.052	.065	.202	.050	207.	210.	1162.	1371.	38.1	20.8
3	5823.	185.	.045	.065	.152	.078	234.	238.	1129.	1381.	44.0	26.8
4	5735.	213.	.040	.063	.124	.114	256.	260.	1095.	1390.	49.9	32.9
5	5636.	239.	.040	.055	.130	.140	272.	275.	1114.	1397.	55.9	36.8
6	5517.	264.	.041	.047	.144	.162	287.	289.	1142.	1402.	62.0	40.1
7	5583.	269.	.040	.047	.198	.118	277.	277.	1123.	1398.	63.1	44.9
8	5509.	284.	.043	.047	.169	.146	298.	299.	1117.	1406.	65.7	48.1
9	5485.	300.	.052	.047	.182	.141	318.	319.	1139.	1415.	62.3	45.9
10	5429.	310.	.059	.047	.167	.160	348.	350.	1187.	1427.	56.4	37.5
11	5463.	321.	.067	.047	.217	.125	350.	352.	1222.	1428.	49.7	31.0
12	5422.	350.	.084	.047	.235	.122	375.	376.	1025.	1206.	40.5	30.8
13	5370.	378.	.090	.047	.235	.129	404.	405.	1002.	1174.	37.6	29.7
14	5340.	393.	.090	.047	.235	.132	427.	429.	1097.	1257.	37.2	25.7
15	5310.	408.	.090	.047	.235	.136	442.	444.	1107.	1268.	37.1	25.8

NO. CHANNELS = 279. DELTAT = 288. DELTAP = 609. COOLANT FLOW = 27.03

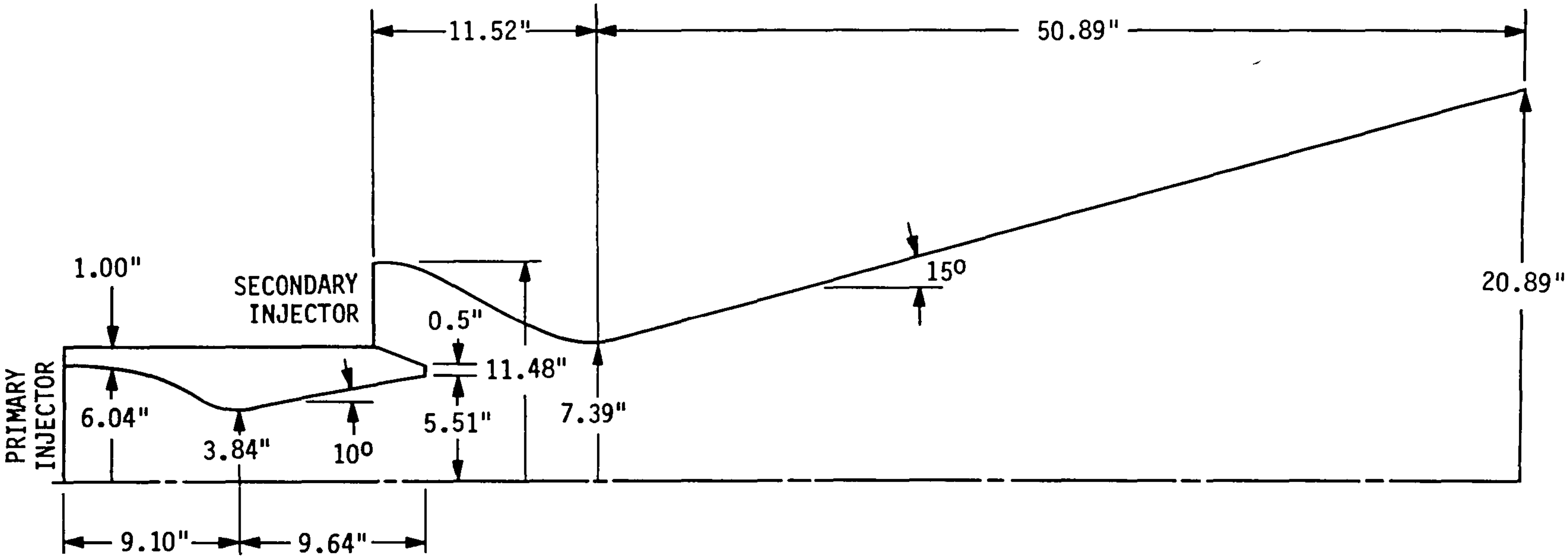

Figure 27. Dual Fuel Dual Throat Preliminary Baseline Engine Geometry

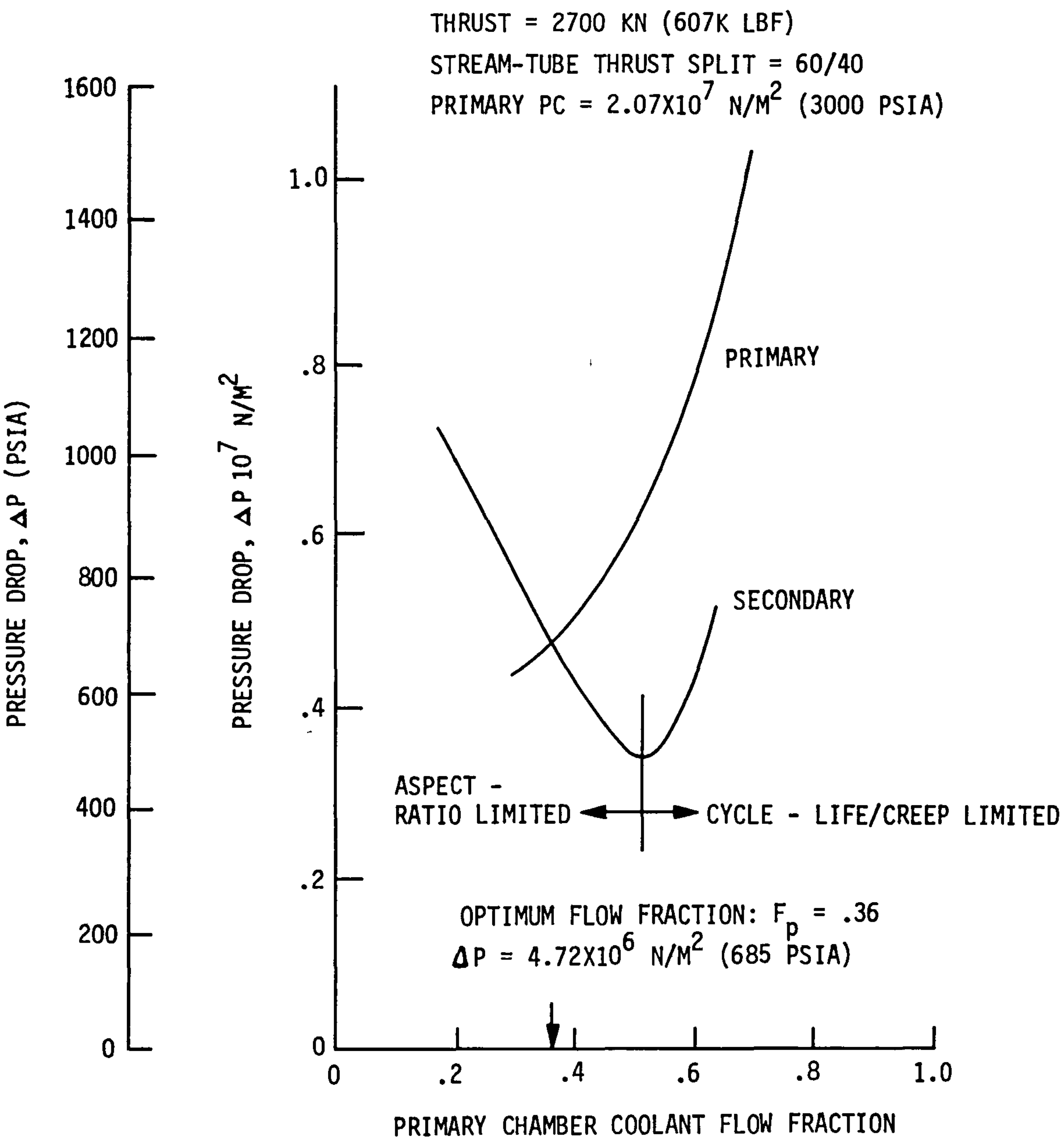

Figure 28. Pressure Drop vs Flow Fraction

TABLE XI

DUAL THROAT PRIMARY FLOW FRACTION OPTIMIZATION

Thrust KN (10^3 lb)	Stream Tube Thrust Split	Primary Pc 10^7 N/M^2 (psia)	Primary Flow Fraction	
890 (200)	60/40	2.07 (3000)	0.53	
2700 (607	80/20		0.31	
	60/40		0.36	Baseline (Preliminary)
	40/60		0.45	
	60/40	0.97 (1400)	0.50	
		3.45 (5000)	0.57	No Transpiration
		3.45 (5000)	0.355	Regen + 0.165 Transpiration (ΔP = 1500 psi)
4448 (1,000)	60/40	2.07 (3000)	0.41	

MIXTURE RATIO STUDY FOR BASELINE CONFIGURATION

Primary O/F	Secondary O/F	Primary Flow Fraction	
5	2.8	0.33	
6		0.32	
7		0.36	Preliminary Baseline
	2.0	0.22	
	3.5	0.36	

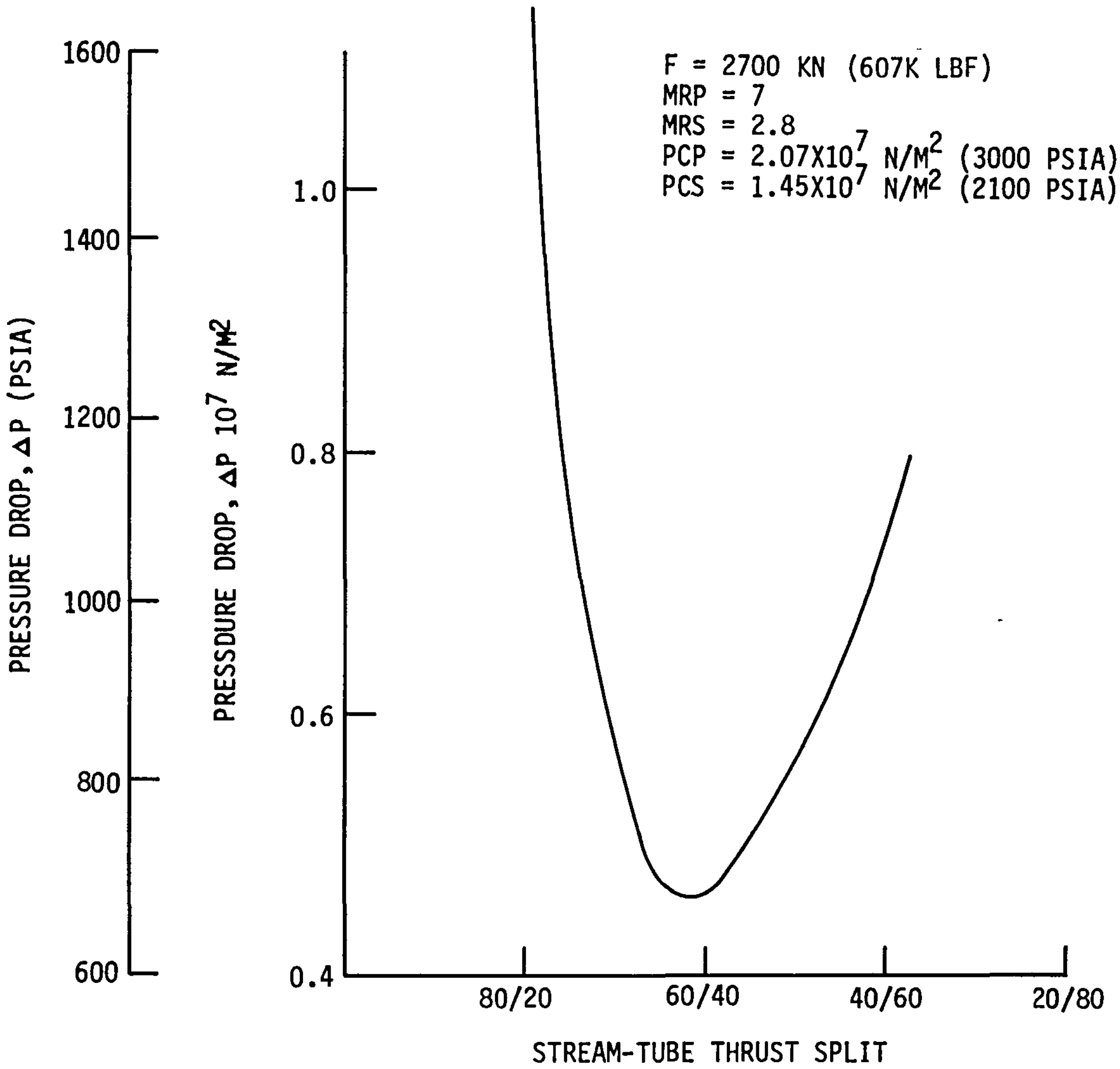

Figure 29. Pressure Drop vs Stream-Tube Thrust Split

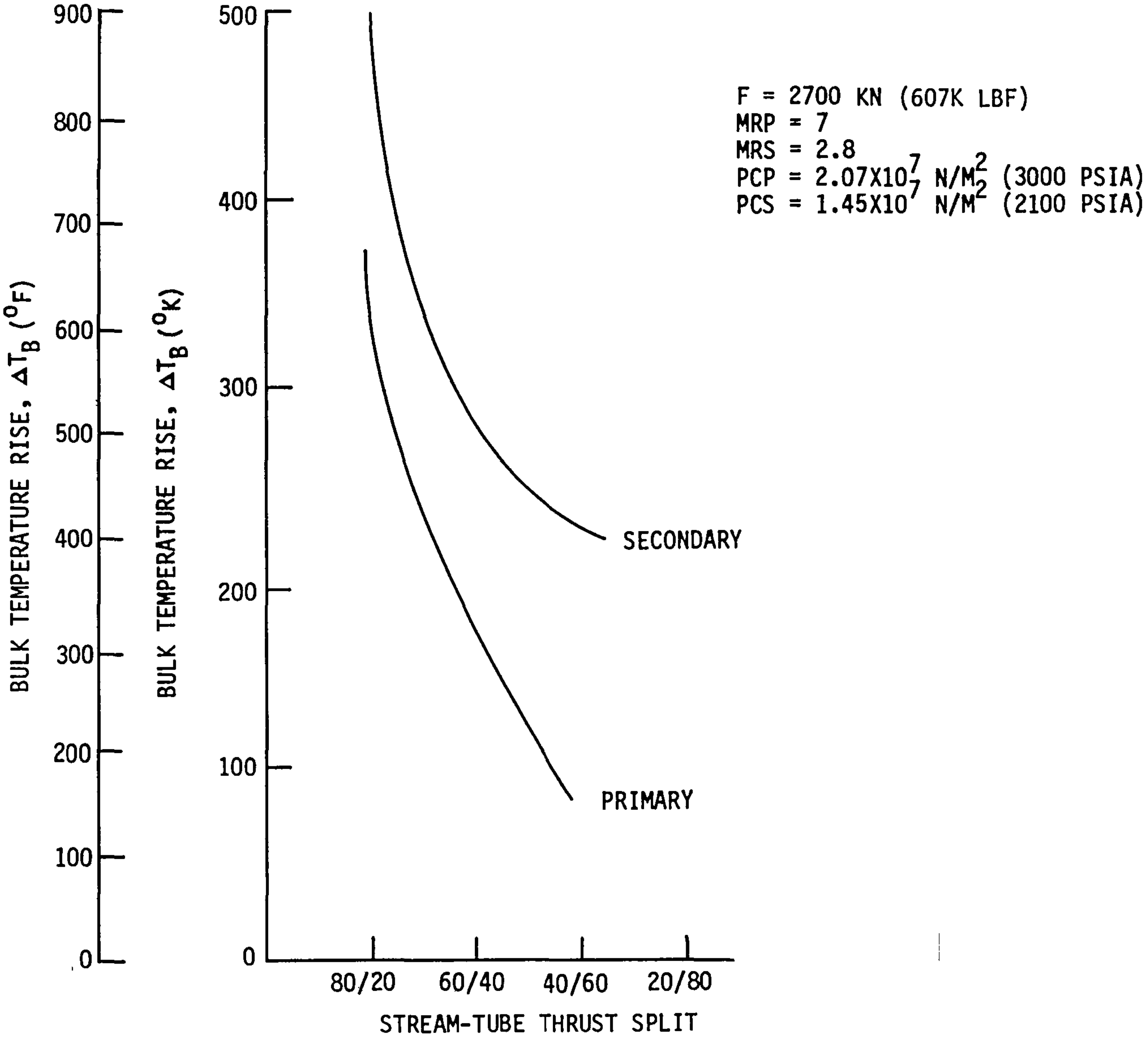

Figure 30. Coolant Bulk Temperature Rise vs Stream-Tube Thrust Split

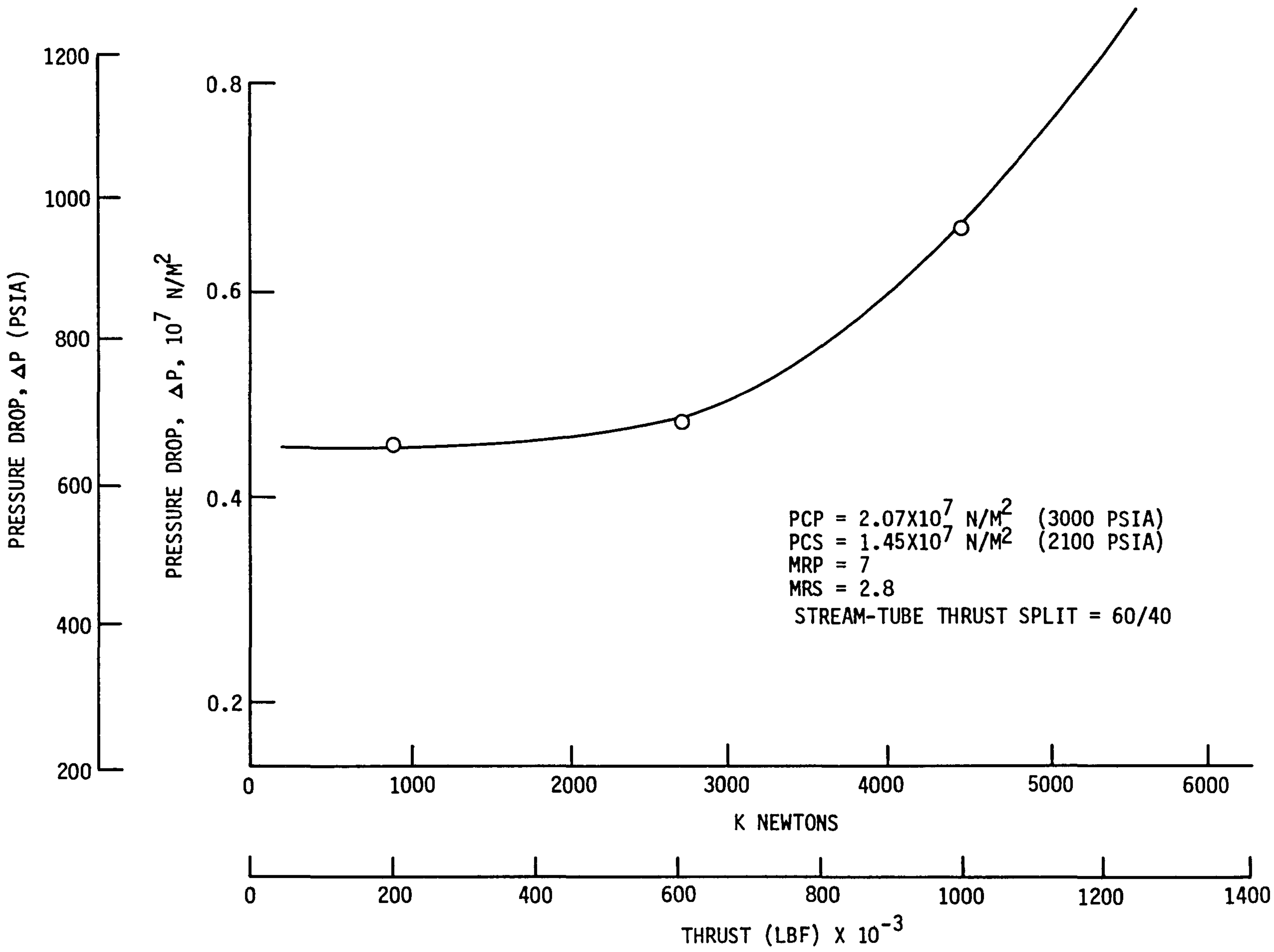

Figure 31. Pressure Drop vs Thrust

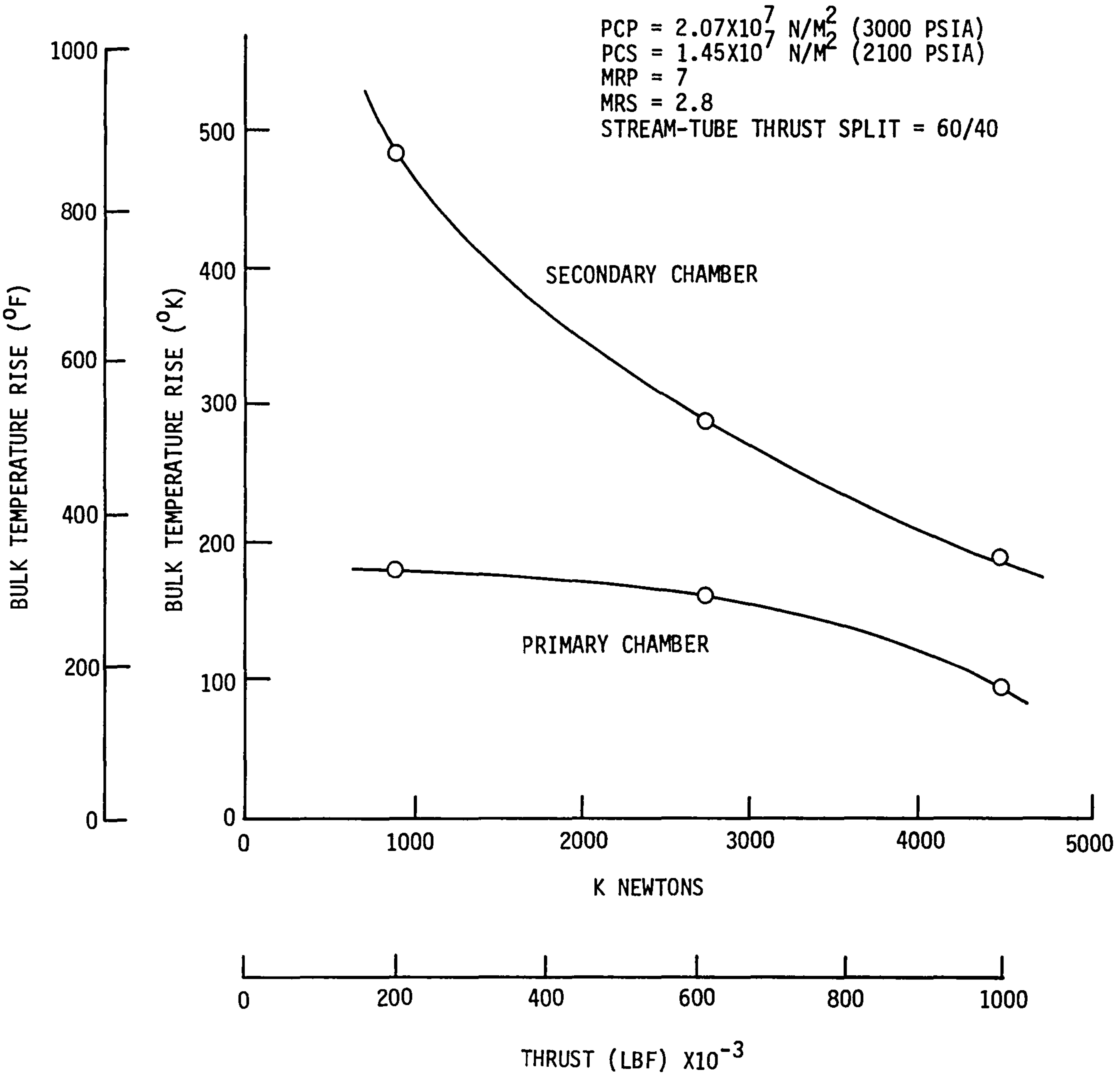

Figure 32. Coolant Bulk Temperature Rise vs Thrust

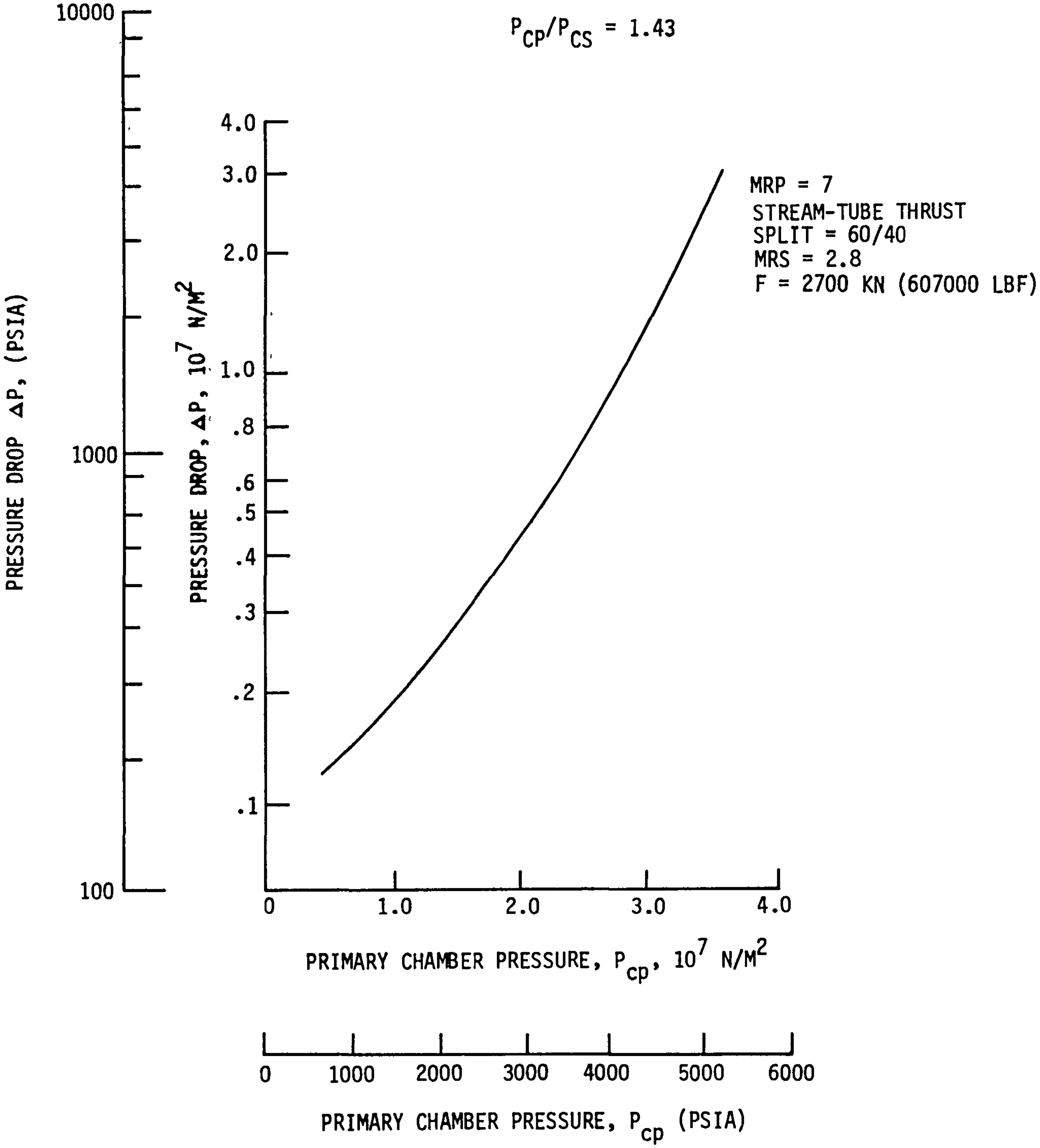

Figure 33. Pressure Drop vs Primary Chamber Pressure

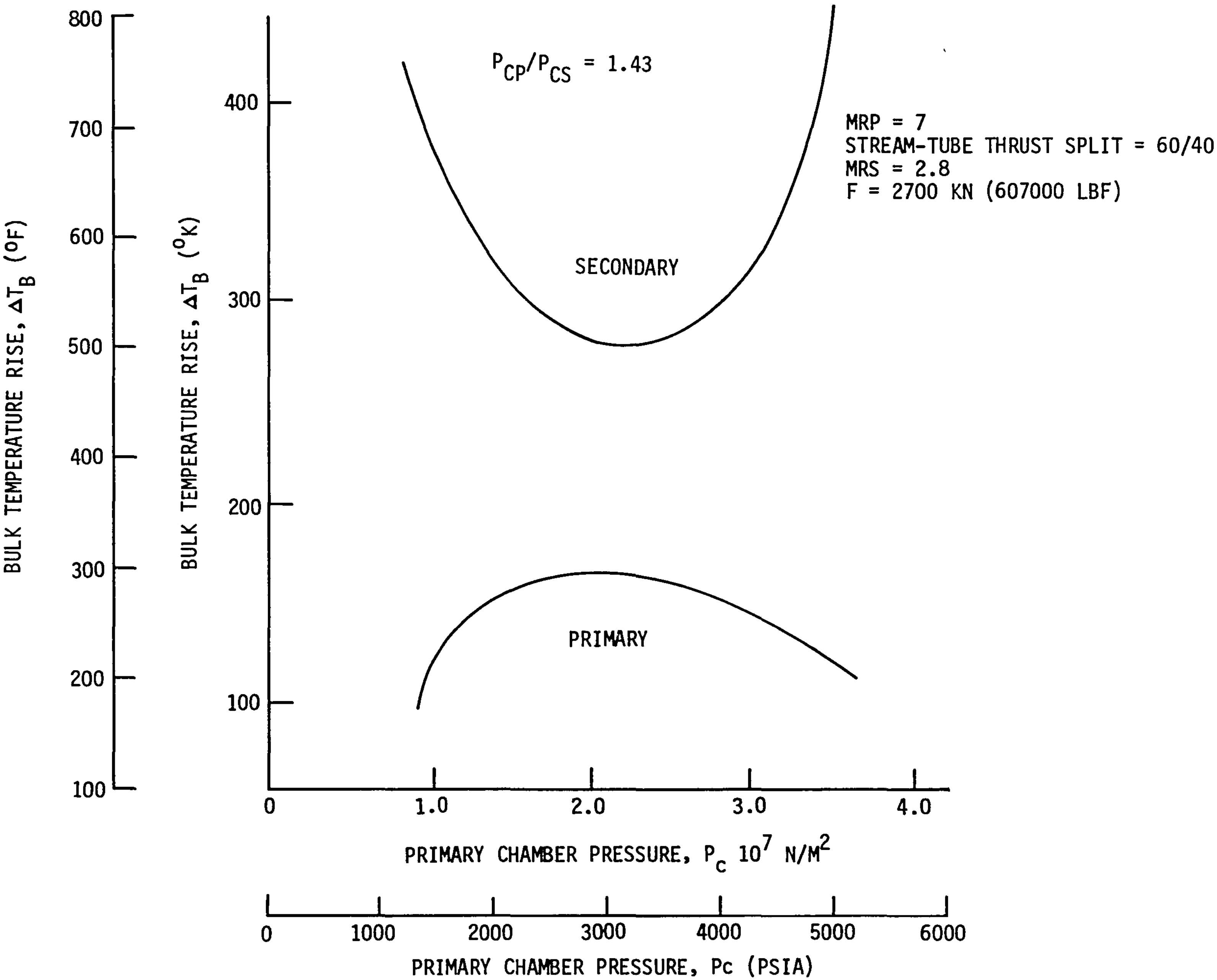

Figure 34. Coolant Bulk Temperature Rise vs Primary Chamber Pressure

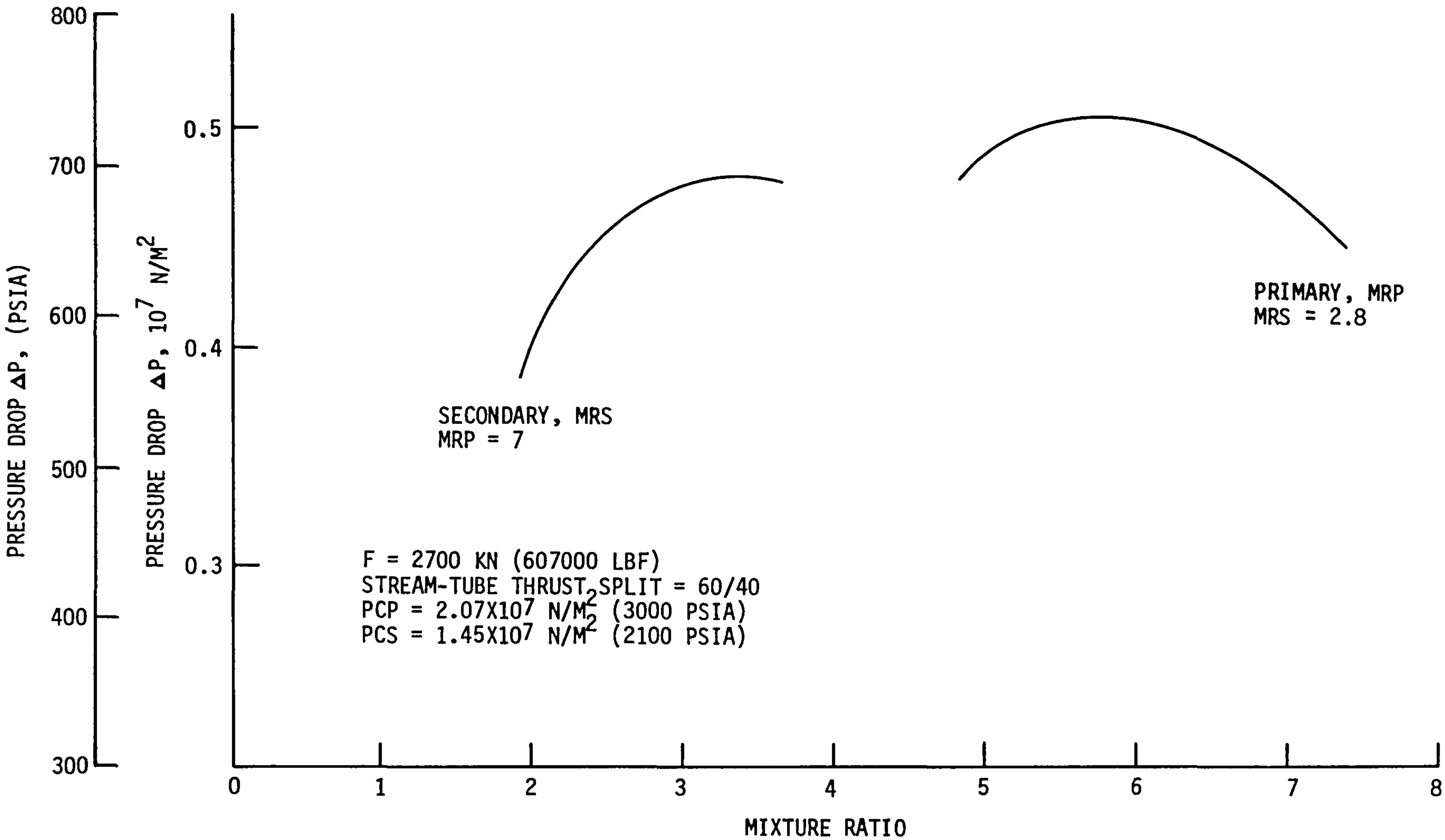

Figure 35. Pressure Drop vs Mixture Ratio for Primary and Secondary Chambers

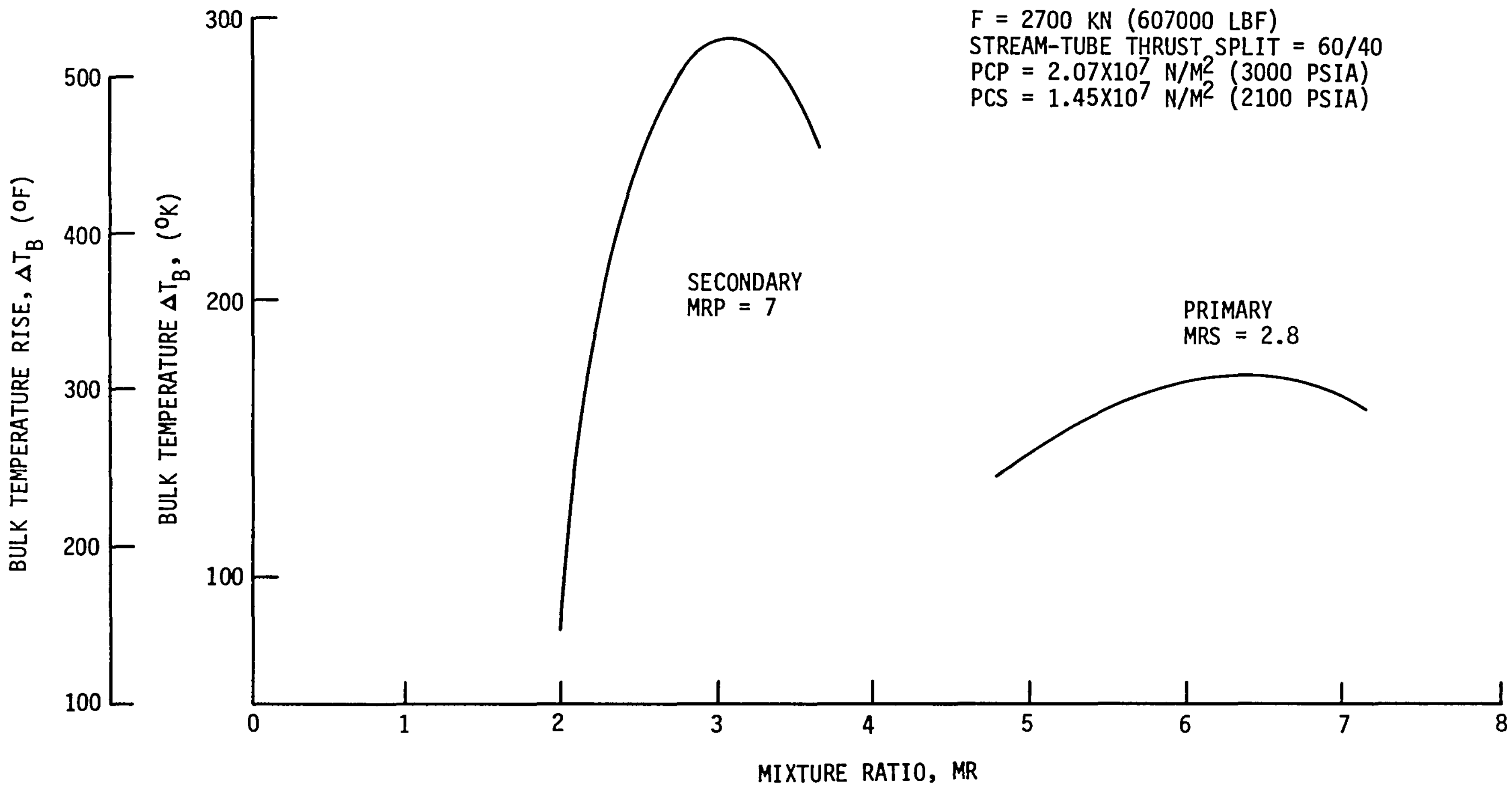

Figure 36. Coolant Bulk Temperature Rise vs Mixture Ratio

Scaling the baseline engine to a thrust of 8896 KN (2 x 10^6 lbF) was not possible because of the high pressure drops resulting from the increased channel lengths and the flow area constraint resulting from the imposition of a channel aspect ratio limit; bypassing part of the hydrogen flow to alleviate this problem was not investigated. A hydrogen pressure drop of 2.41 x 10^7 N/m^2 (3500 psi) was calculated for a primary chamber pressure of 3.45 x 10^7 N/m^2 (5000 psia). (The secondary chamber pressure was 70 percent of the primary chamber pressure in all cases.) In order to reduce this requirement, transpiration cooling of the throat region of the primary chamber was investigated. A regenerative-cooling pressure drop of 1.03 x 10^7 N/m^2 (1500 psi) can be obtained by using 16.5 percent of the hydrogen for transpiration cooling (cf. Figures 37 through 39).

The secondary nozzle (Figure 40 and Table XII) was cooled with the primary chamber oxidizer flow from area ratio 8:1 to 43:1. A pressure drop of 6 x 10^5 N/m^2 (87 psi) is required for the baseline engine, with a bulk temperature rise of 116°K (209°F) as shown in Table XIII. Scaling of the baseline nozzle to other thrust levels, stream-tube thrust splits, and chamber pressures was also accomplished as summarized in Figures 41 through 43. As in the case of the chamber, the minimum coolant pressure drop occurs for a stream-tube thrust split near the baseline value.

2. <u>Chamber Regenerative Cooling</u>

Chamber design studies were conducted using a special regenerative cooling program with the dual throat chamber geometry built in. Geometric and flow scaling from the baseline configuration to other thrust levels, stream-tube thrust splits and chamber pressures was provided. Baseline gas-side heat transfer coefficients and heat loads are input by axial position on each surface to the dual-throat program, which includes scaling

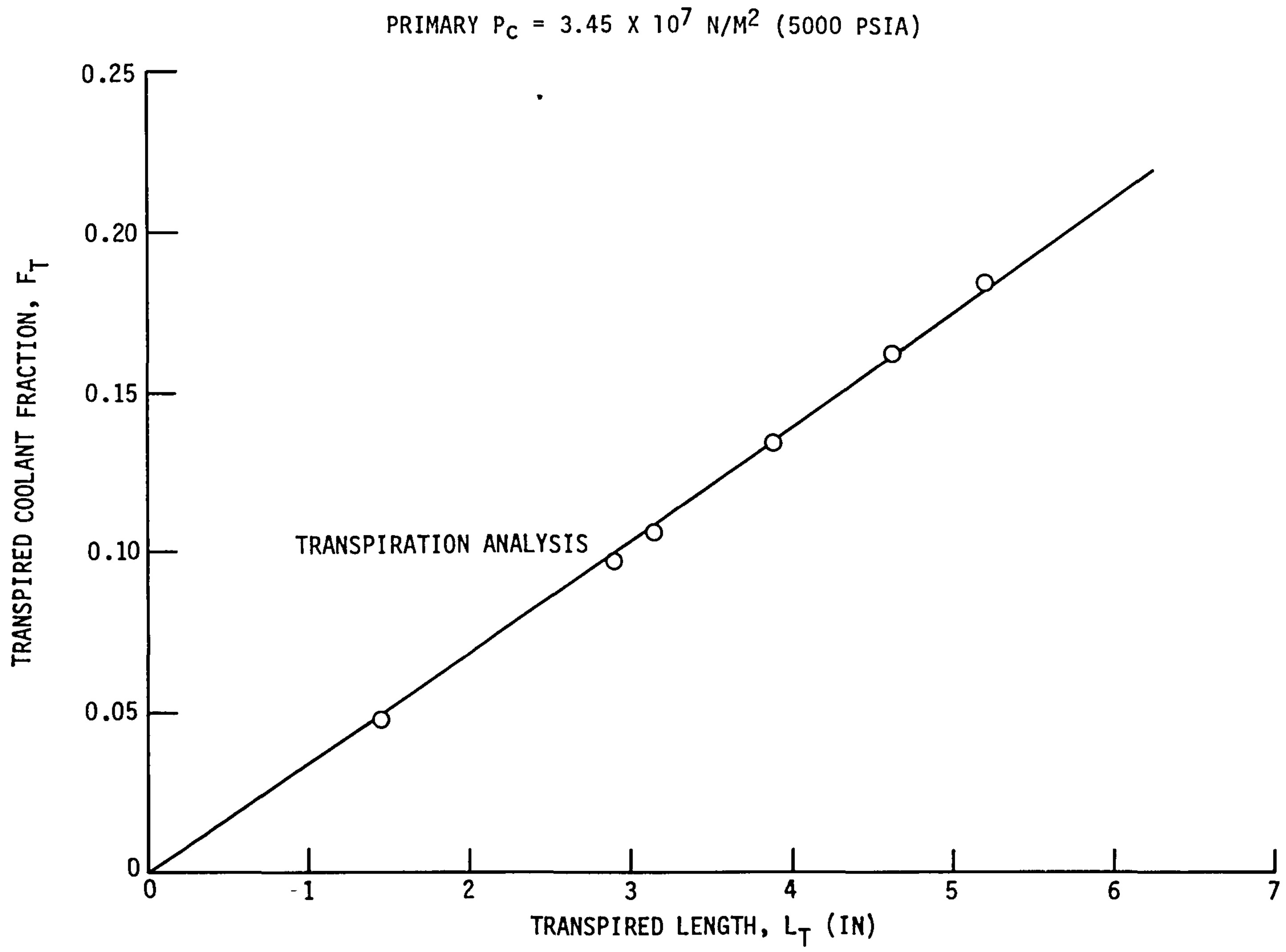

Figure 37. Trans-Regen Analysis

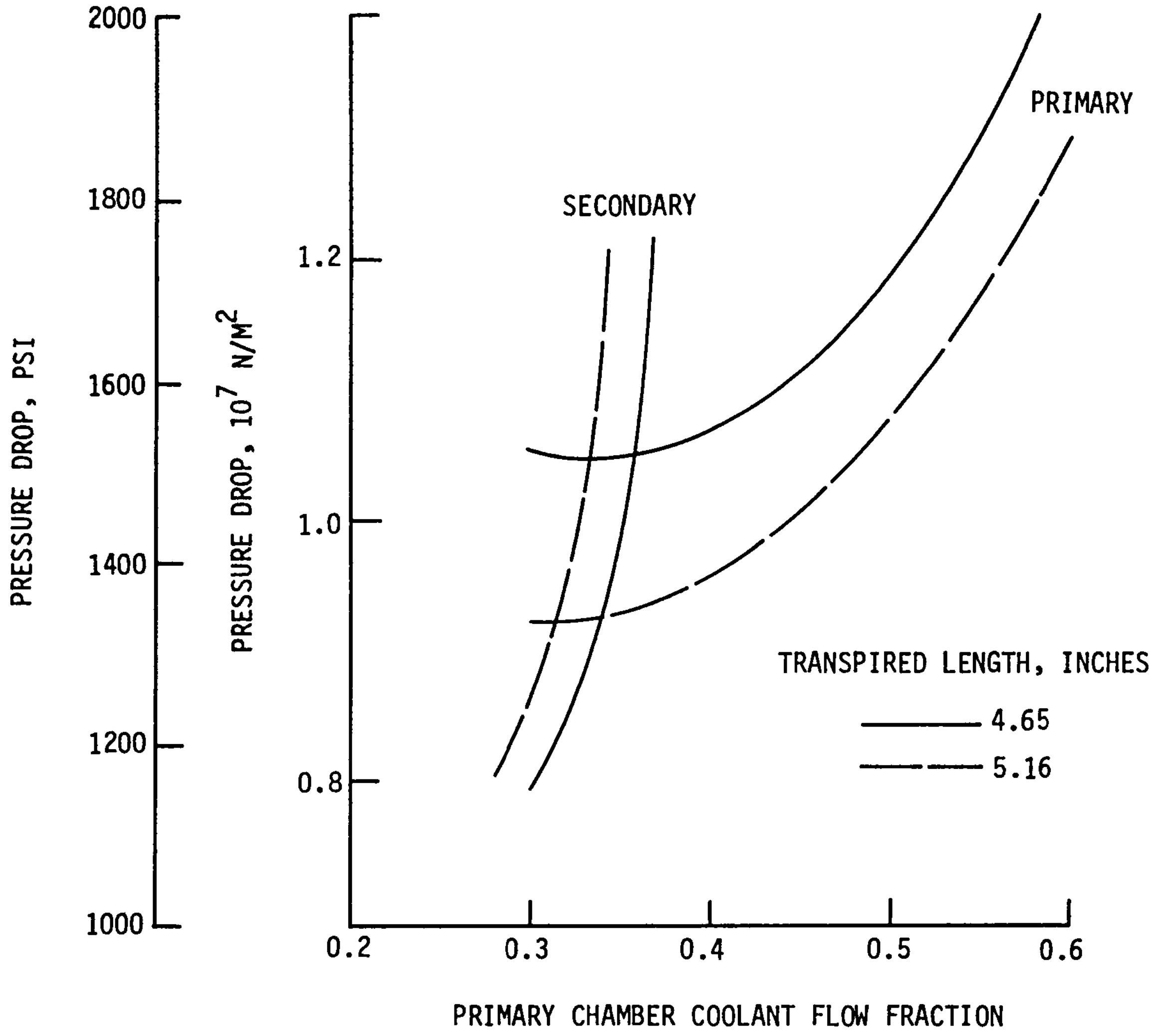

Figure 38. Regenerative Cooling Analysis for a Primary Chamber Pressure of 3.45×10^7 N/M^2 (5000 PSIA)

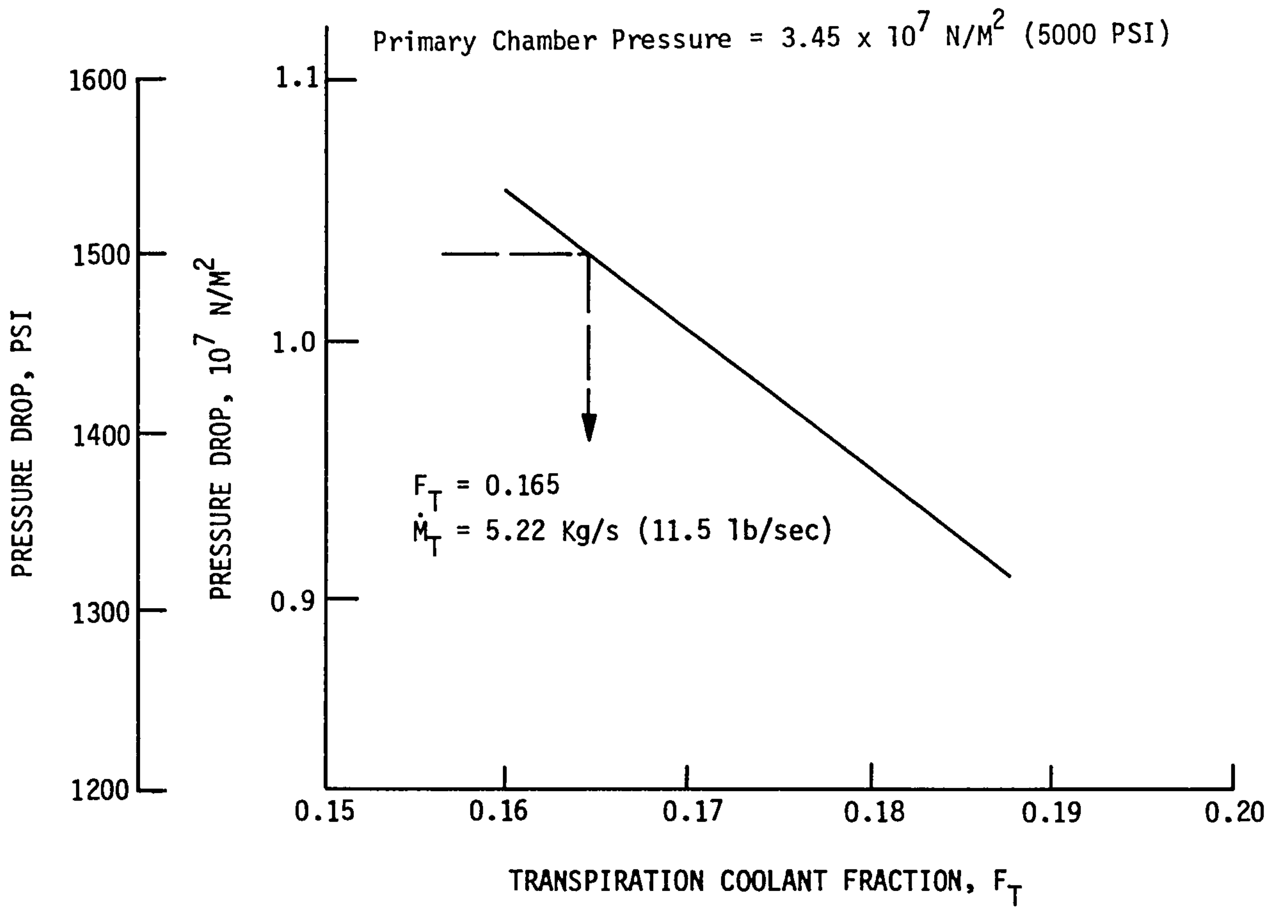

Figure 39. Effect of Transpiration Coolant Flow on Regenerative Cooling Pressure Drop

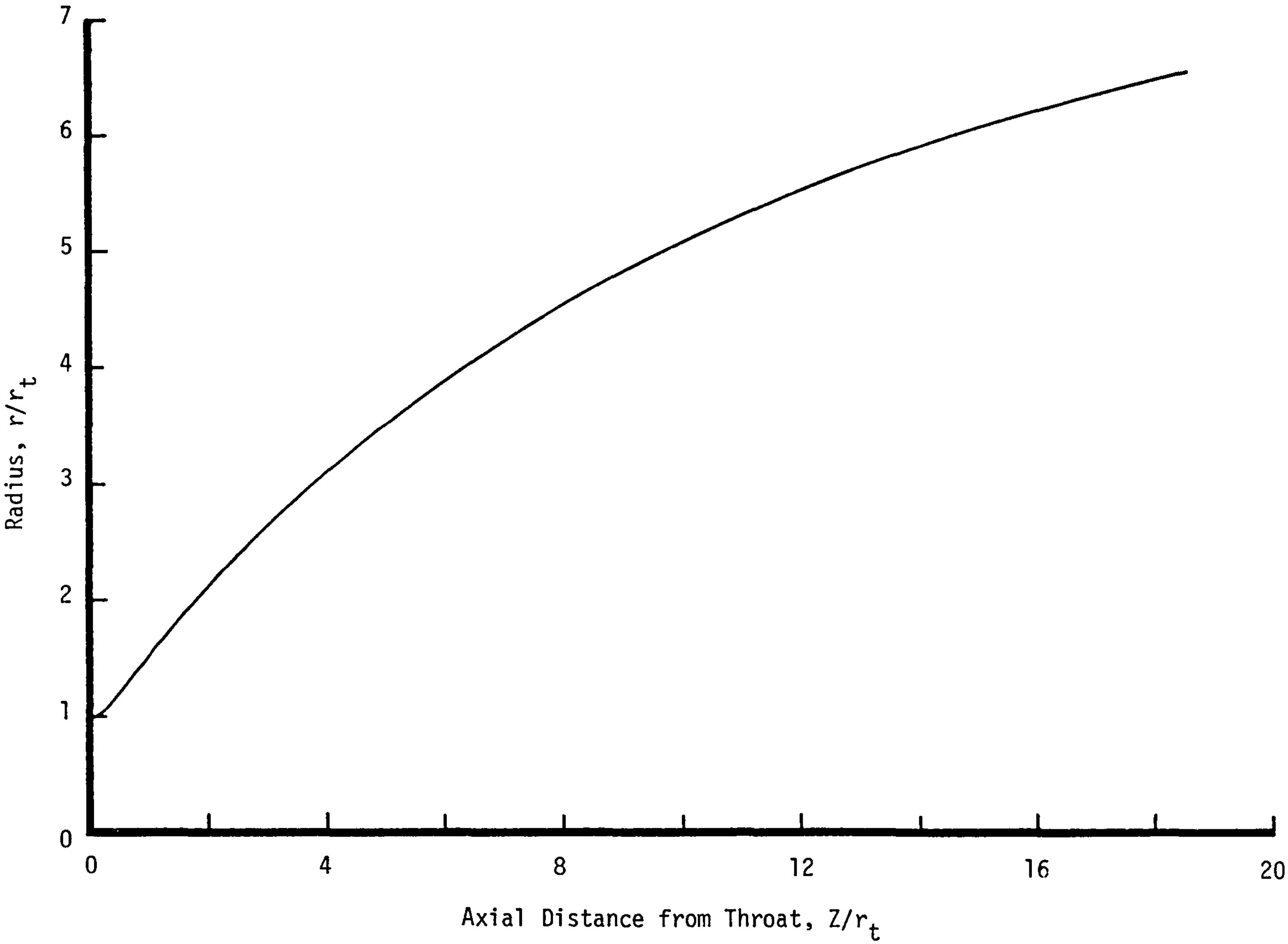

Figure 40. Nozzle Contour for Oxygen-Cooled Tube Bundle Design Studies

TABLE XII

NOZZLE TUBE BUNDLE SUMMARY

LOX/RP-1 Stream Tube Thrust, %	Thrust KN (10^3 lbf)	Primary Pc 10^7 N/M^2 (psia)	No. Tubes	Tube Wall mm (in.)	Pressure Drop 10^6 N/M^2 (psi)	Bulk Rise °K, (°F)
60	890 (200)	2.07 (3000)	248	.61 (.024)	.54 (78)	126 (226)
	2700 (607)		268	.99 (.039)	.60 (87)	116 (209)
	8896 (2,000)		336	1.45 (.057)	.97 (140)	106 (190)
40	2700 (607)		204	1.24 (.049)	.71 (103)	74 (134)
80			486	.56 (.022)	.92 (134)	257 (463)
60		2.76 (4000)	300	.89 (.035)	1.49 (216)	118 (212)
		3.45 (5000)	346	.76 (.030)	3.63 (527)	119 (214)

TABLE XIII

PRELIMINARY BASELINE ENGINE TUBE BUNDLE STUDY

THE COOLANT IS OXYGEN (PRUPO) FLOWING IN ROUND OR FLATTENED

MR= 2.80 PC= 2100. PSIA TC=6856. R WGSTAR=1850.70 LB/SEC PIN=5662. PSIA TIN= 200. R

FLOW SUMMARY TABLE

STATION NO	POS	FLOW RATE	* * * * * * * * LIQUID			* * * * * * *	FILM COEFFICIENTS			WALL TEMPERATURES			* * HEAT TRANSFER * *			
			PRESSURE	TEMP	VELOCITY	MACH NO.	LAND	GAS	LIQUID	LIQUID	METAL	GAS	Q/AI	Q/AO	QSUM	Q/QBO
	IN.	LBM/SEC	PSIA	DEG F	FT/SEC		BTU/IN2-SEC-R			DEGREE F			BTU/IN2-SEC		BTU	--
-	INLET	-	5662.0	-259.7	0.0											
1	25.34	525.70	5624.0	-259.8	57.7	.019	.190-01	.852-03	.204-01	-10.5	926.9	926.9	5.10	4.29	.0000	.000
2	29.37	525.70	5629.3	-253.5	47.3	.016	.102-01	.724-03	.873-02	229.5	962.1	962.1	4.21	3.60	.1235+04	.000
3	39.06	525.70	5634.2	-240.0	33.5	.012	.733-02	.551-03	.574-02	311.5	870.4	870.4	3.17	2.78	.3892+04	.000
4	49.61	525.70	5636.1	-227.1	25.5	.009	.567-02	.434-03	.414-02	369.6	810.0	810.0	2.47	2.20	.6456+04	.000
5	61.84	525.70	5636.9	-214.0	20.3	.008	.454-02	.347-03	.316-02	406.7	759.8	759.8	1.96	1.77	.9099+04	.000
6	76.00	525.70	5637.2	-200.4	16.7	.007	.371-02	.281-03	.249-02	435.4	721.9	721.9	1.58	1.44	.1183+05	.000
7	92.93	525.70	5637.4	-185.9	14.1	.006	.313-02	.230-03	.205-02	441.4	677.6	677.6	1.29	1.18	.1473+05	.000
8	113.15	525.70	5637.4	-170.3	12.3	.005	.269-02	.189-03	.172-02	444.7	640.9	640.9	1.06	.98	.1781+05	.000
9	137.72	525.70	5637.3	-153.6	11.0	.005	.230-02	.157-03	.143-02	456.5	619.4	619.4	.87	.81	.2113+05	.000
10	138.04	525.70	5637.3	-153.4	11.0	.005	.231-02	.156-03	.143-02	456.6	619.1	619.1	.87	.81	.2117+05	.000
11	138.04	525.70	5636.9	-153.4	11.0	.005	.231-02	.156-03	.143-02	456.6	619.1	619.1	.87	.81	.2117+05	.000
12	137.72	525.70	5636.9	-153.2	11.0	.005	.232-02	.157-03	.143-02	457.5	620.3	620.3	.87	.81	.2121+05	.000
13	113.15	525.70	5636.3	-137.1	13.4	.006	.265-02	.188-03	.152-02	542.5	726.3	726.3	1.03	.96	.2449+05	.000
14	92.93	525.70	5635.4	-122.5	16.5	.008	.314-02	.227-03	.169-02	610.7	822.2	822.2	1.24	1.14	.2748+05	.000
15	76.00	525.70	5634.0	-108.8	21.0	.011	.383-02	.278-03	.200-02	646.3	897.0	897.0	1.51	1.38	.3026+05	.000
16	61.84	525.70	5631.7	-96.0	27.2	.015	.474-02	.343-03	.247-02	657.8	960.5	960.5	1.86	1.68	.3286+05	.000
17	49.61	525.70	5627.5	-83.5	36.5	.021	.616-02	.428-03	.324-02	640.5	1015.6	1015.6	2.34	2.09	.3536+05	.000
18	39.06	525.70	5619.1	-71.3	51.0	.030	.835-02	.544-03	.449-02	597.4	1072.3	1072.3	3.00	2.63	.3779+05	.000
19	29.37	525.70	5598.2	-58.6	77.1	.046	.119-01	.716-03	.696-02	518.1	1146.0	1146.0	4.01	3.43	.4032+05	.000
20	25.34	525.70	5577.9	-52.8	96.7	.058	.147-01	.838-03	.885-02	481.5	1210.6	1210.6	4.73	3.98	.4148+05	.000
-	EXIT	-	5577.9	-52.3	0.0											

STATION NO POS	AREA RATIO	* * * *TEMPERATURES* * * *			* * *PRESSURE LOSSES* * *		
		GAS RECOVERY	GAS FILM	COOLANT FILM	FRICT DROP	DYNAM DROP	TURN LOSS

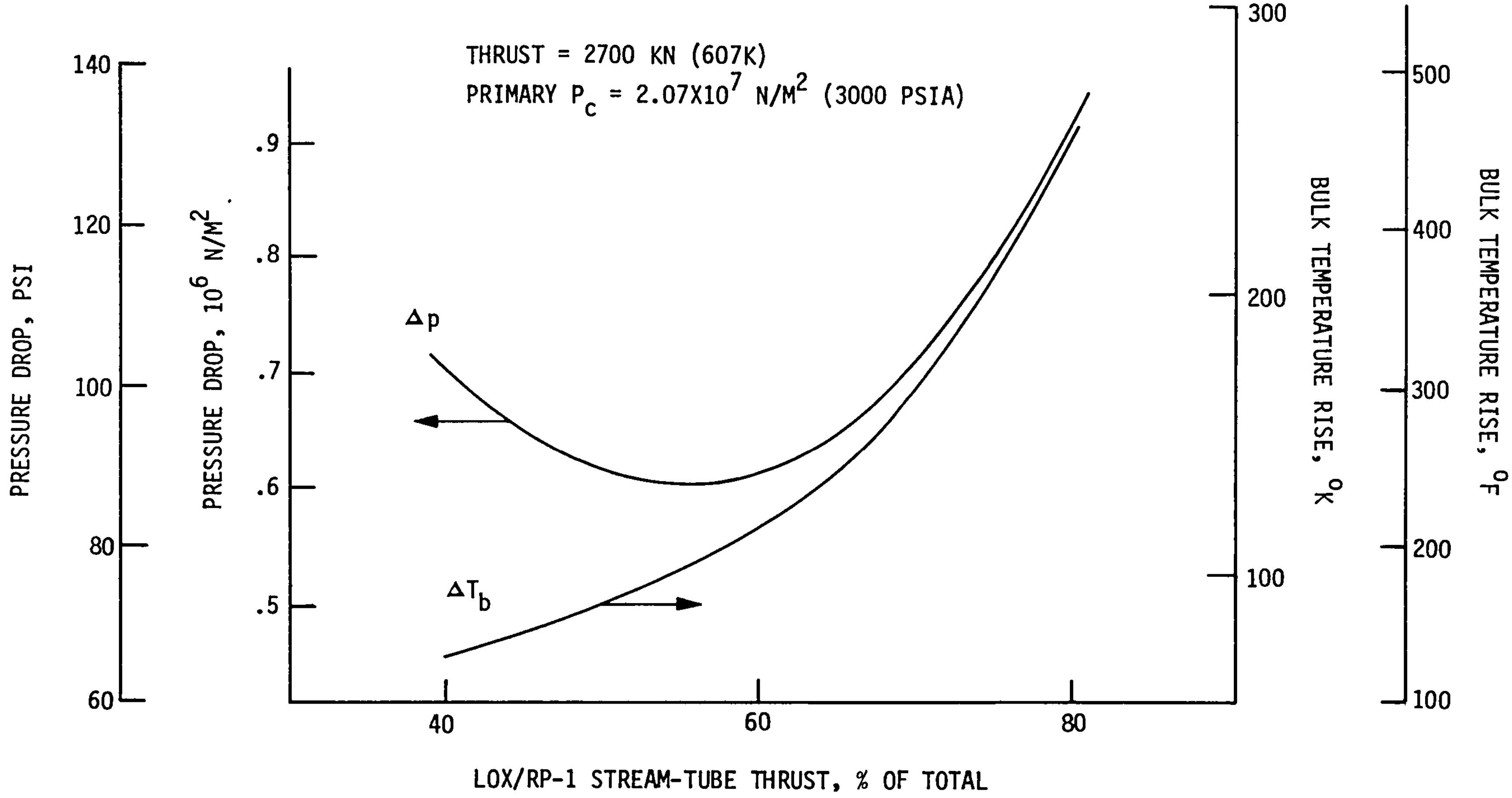

Figure 41. Effect of Stream-Tube Thrust Split on Oxygen-Cooled Nozzle

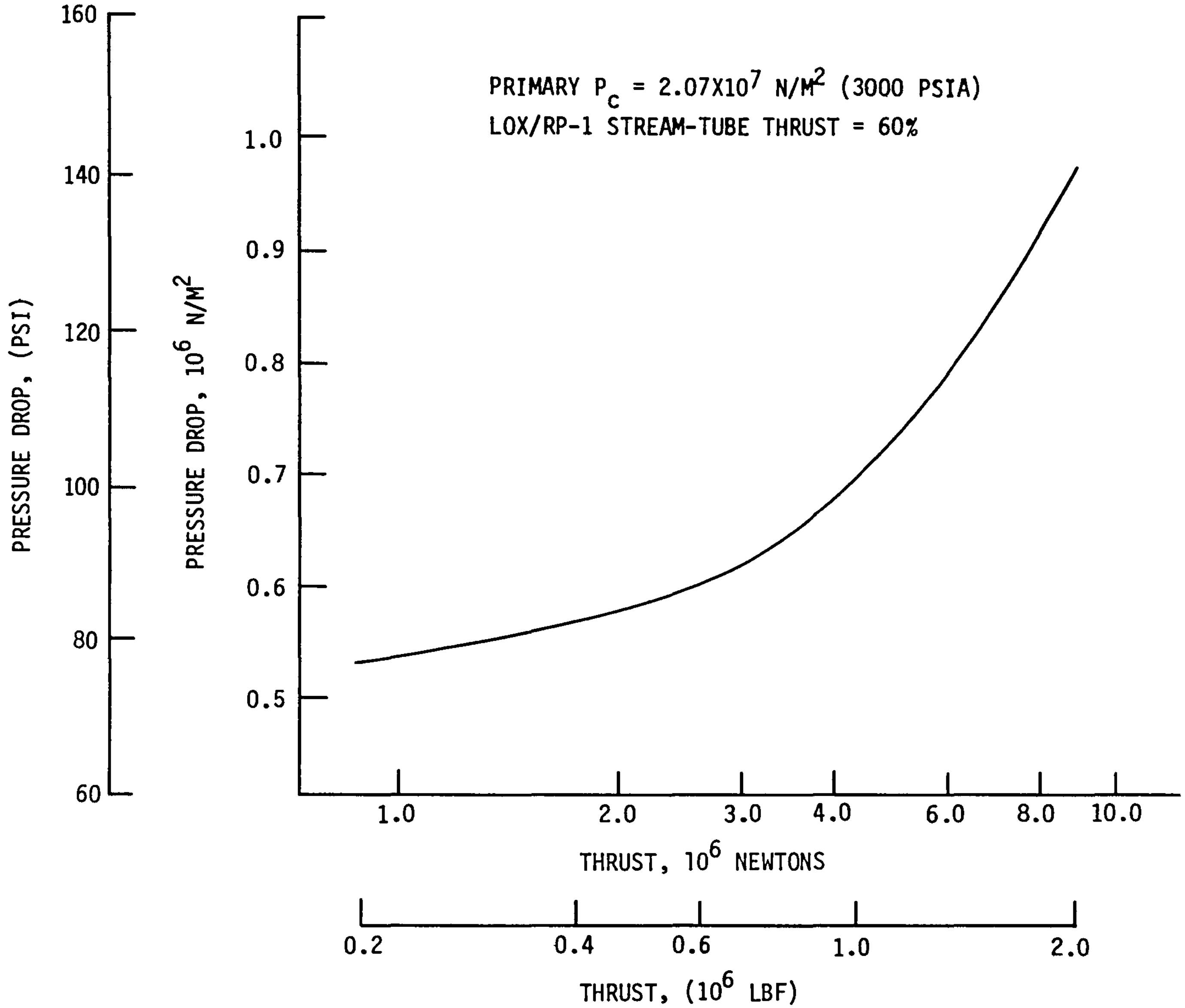

Figure 42. Nozzle Pressure Drop vs Thrust

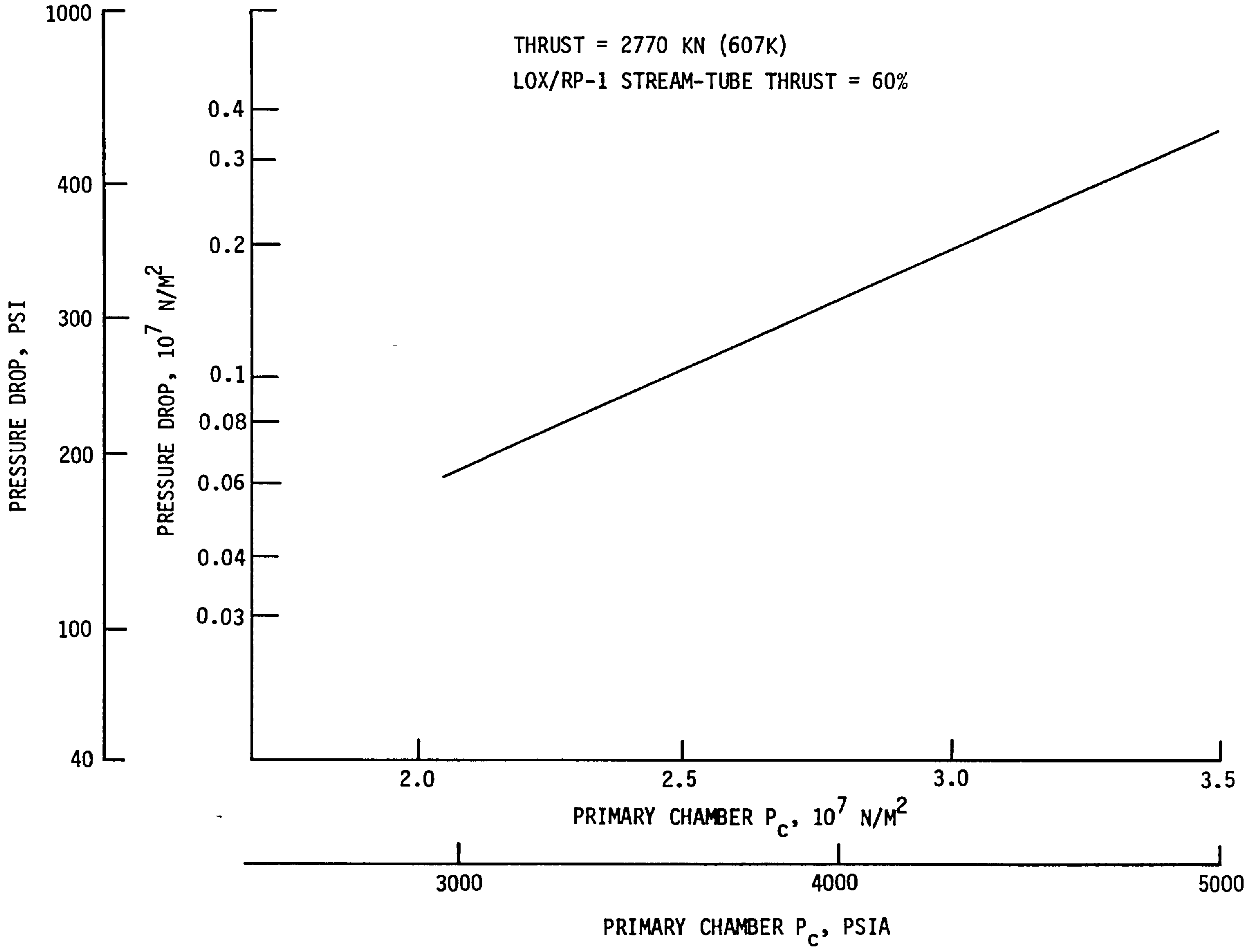

Figure 43. Nozzle Pressure Drop vs Primary Chamber Pressure

relationships to vary these quantities with thrust, stream-tube thrust split and chamber pressure. The baseline inputs were determined from the ALRC standard regenerative cooling program for gas-side wall temperatures approximating those allowed by the cycle life and creep criteria described later. Since the dual throat program defines the coolant channel depths based on these criteria, the discrepancy between input boundary conditions and calculated wall temperatures is usually small. Baseline heat transfer coefficients were calculated as follows:

$$St_f = 0.026\ C_g\ Re_f^{-0.2}\ Pr_f^{-0.6}$$

with properties evaluated at the average of the wall and recovery temperatures. Figure 44 shows the C_g profile for the baseline primary chamber; a similar profile was used for the secondary chamber. The Hess and Kunz correlation, Ref. (9), was used to calculate coolant heat transfer coefficients for hydrogen. Curvature effects were accounted for as follows:

$$\frac{h_{curve}}{h_{straight}} = \left[Re_b \left(\frac{d_e}{R_c}\right)^2 \right]^{\pm 0.05}$$

in which R_c is the radius of curvature and d_e is the hydraulic diameter.

Fabrication considerations resulted in the selection of 1.02 mm (0.040 in.) as the minimum land width and minimum channel width; in addition, a maximum channel aspect ratio (depth/width) of 5:1 was imposed. The channel aspect ratio limit had a significant impact on many of the designs, as will be seen in the discussion of results. A gas-side wall thickness of 0.64 mm (0.025 in.) was used in the high heat flux regions, except in the case of a primary chamber pressure of 3.45×10^7 N/m^2 (5000 psia), in which case it was necessary to use a 0.76 mm (0.030 in.) wall to provide adequate strength with a 1.02 mm (0.040 in.) channel. The wall thickness was increased in the

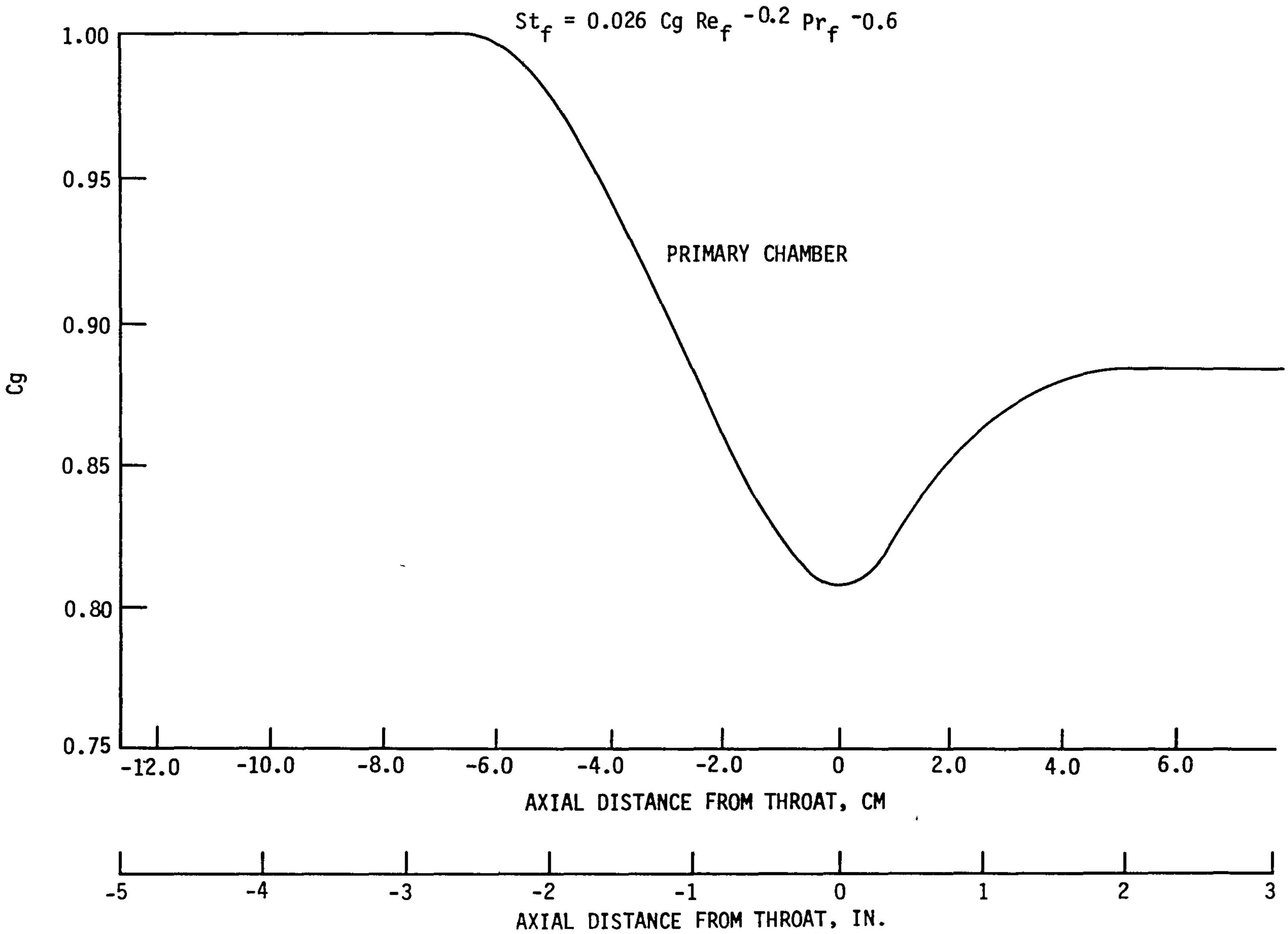

Figure 44. Gas-Side Heat Transfer Correlation Coefficient

nozzles in order to allow wider channels and increased flow areas. The maximum wall thickness in the primary nozzle was 0.89 mm (0.035 in.) for chamber pressures $\leq 2.07 \times 10^7$ N/m^2 (3000 psia) and 1.14 mm (0.045 in.) for 3.45×10^7 N/m^2 (5000 psia); the maximum wall thickness in the secondary nozzle was 1.27 mm (0.050 in.) in all cases.

Maximum allowable channel widths were initially defined by the gas-side wall strength criteria of Figure 45, considering cold startup (cold walls, no chamber pressure and coolant inlet pressure throughout the channel) as well as steady state operation. Since the criteria of Figure 45 made it difficult to maintain secondary chamber throat channel widths above 1.02 mm (0.040 in.), some yielding was allowed during steady state operation for primary chamber pressures $\geq 2.07 \times 10^7$ N/m^2 (3000 psia). This allowed channel width/wall thickness ratios at high temperatures 16 percent higher than those of Figure 45. In general, cold startup dictated the maximum allowable wall thickness in the primary chamber and the annular part of the secondary chamber.

Channel widths were generally set at the maximum allowed by the above structural criteria for the wall in order to maximize the flow area obtainable within the channel aspect ratio limit of 5:1. The throat land widths were set at the minimum of 1.02 mm (0.040 in.) in order to improve cooling capability and maximize the number of coolant channels. Figures 46 and 47 give the channel and land width profiles for the baseline primary and secondary chambers, respectively.

Maximum gas-side wall temperatures were determined from the cycle life/creep criteria given in Figure 48. In this figure the difference between the maximum gas-side temperature and the average nickel closeout temperature is plotted as a function of closeout temperature. For closeout

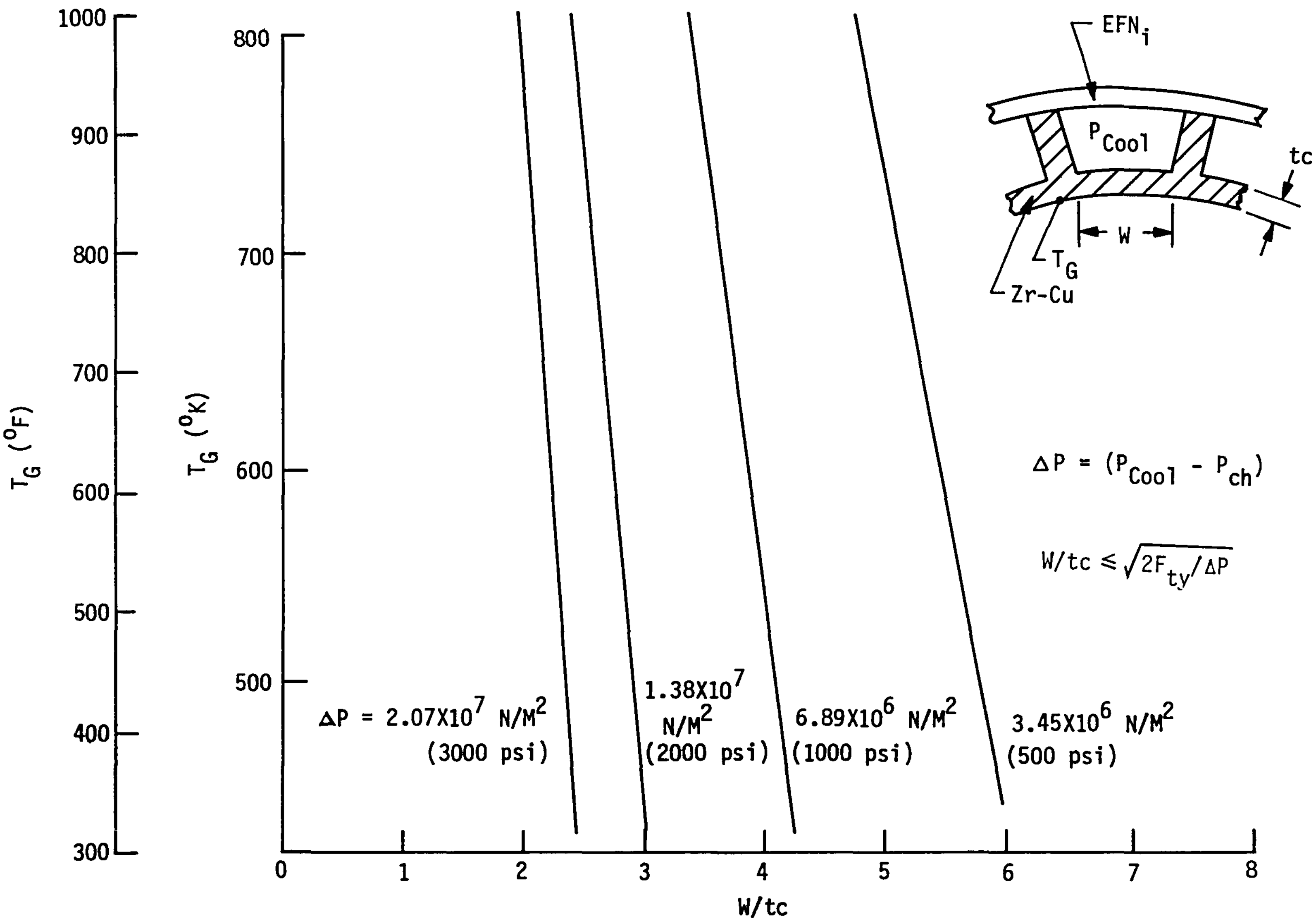

Figure 45. Zr-Cu Chamber Wall Strength Criteria

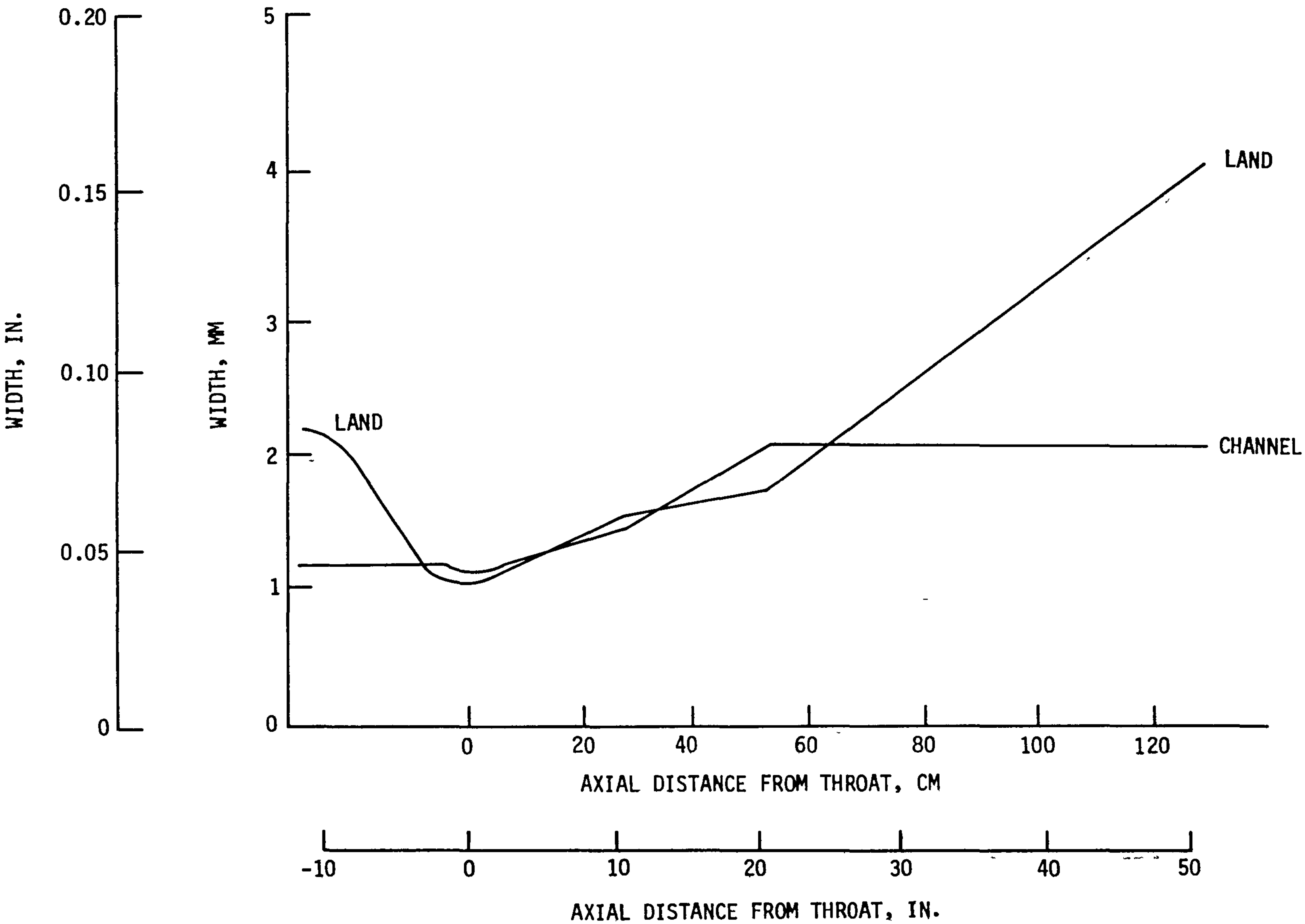

Figure 46. Land and Channel Widths Preliminary Baseline Secondary Chamber

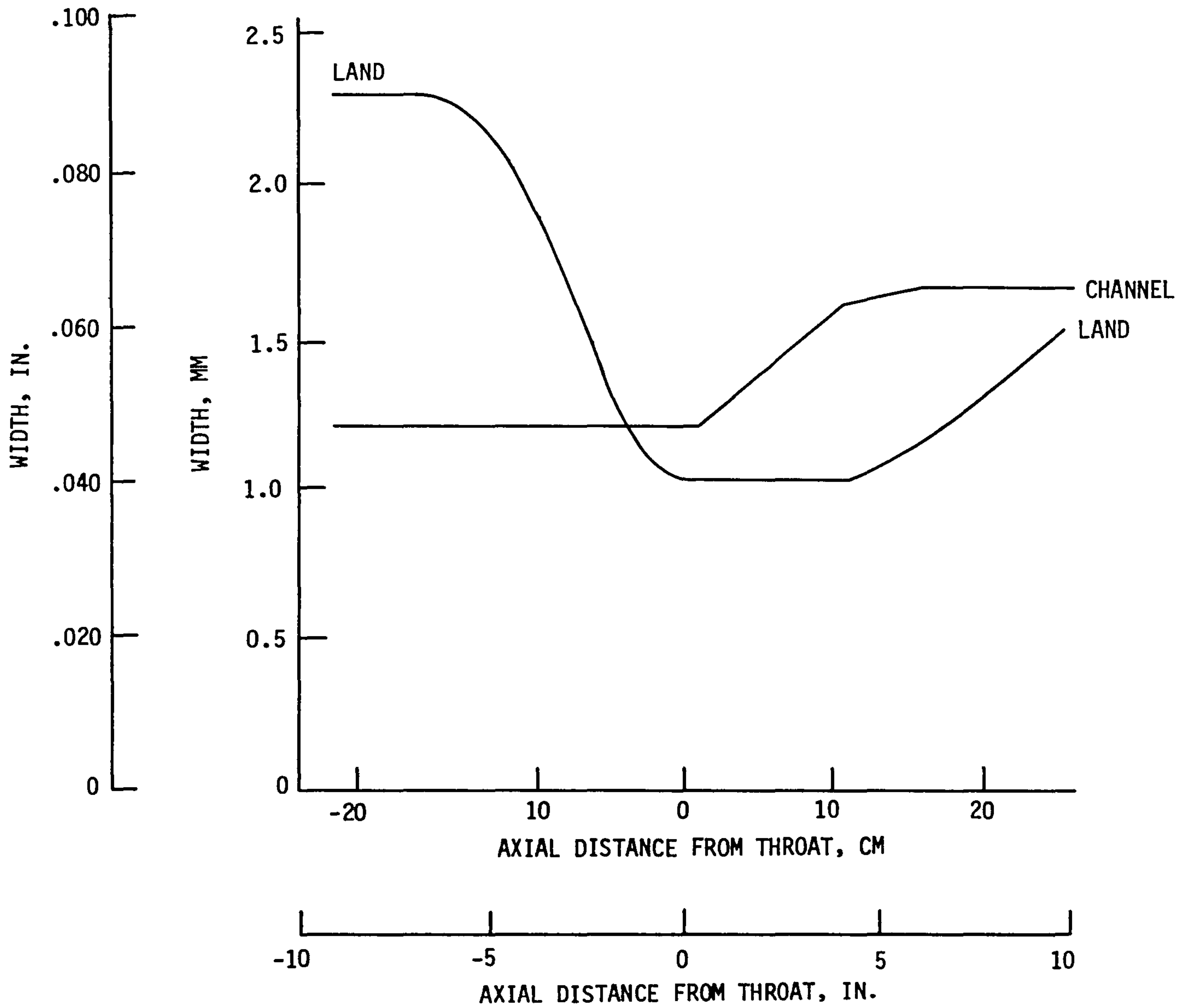

Figure 47. Land and Channel Widths Preliminary Baseline Primary Chamber

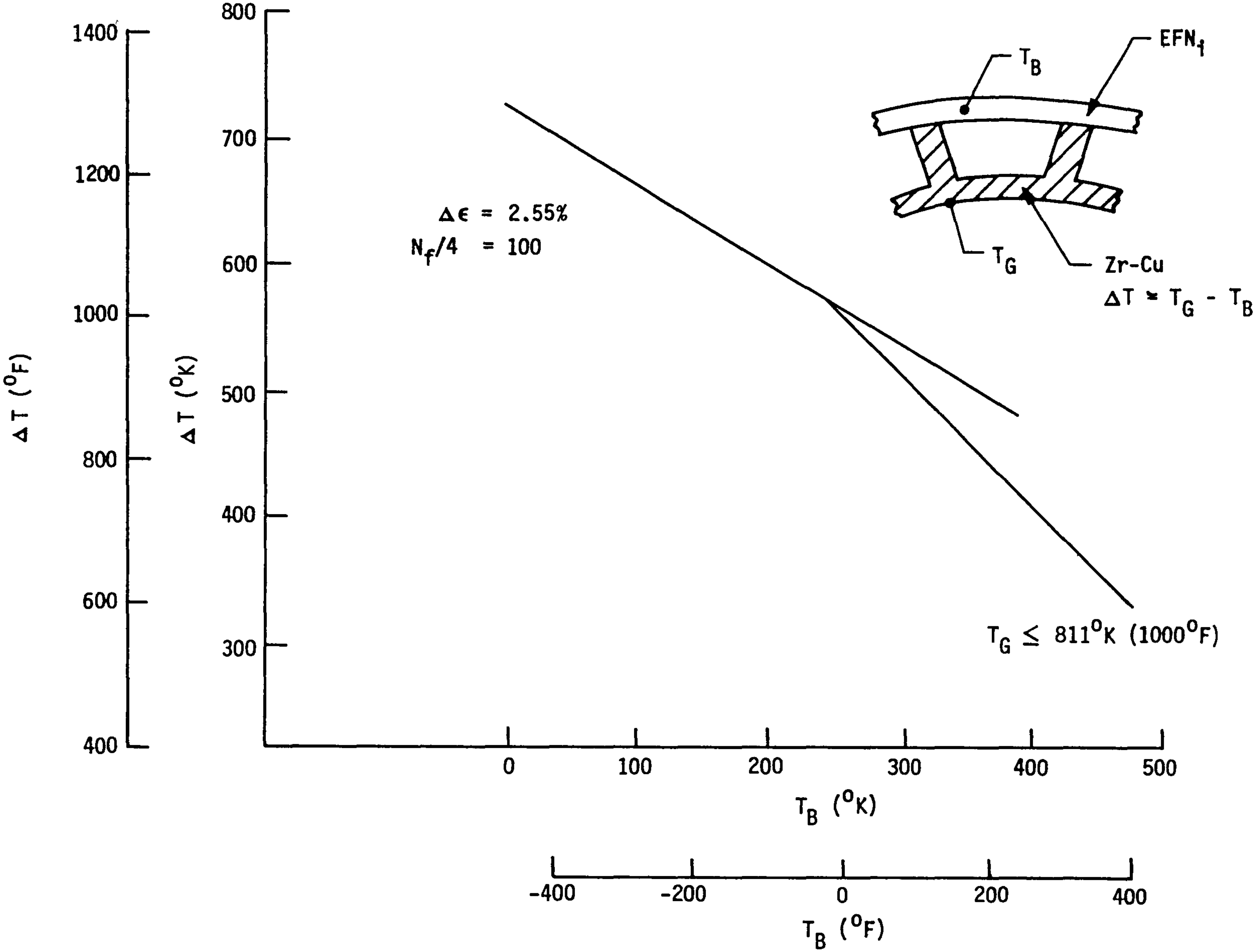

Figure 48. Cycle Life/Creep Wall Temperature Criteria

temperatures less than 239°K (-30°F), a cycle life of 100 cycles determines the allowable gas-side temperature. For closeout temperatures above 239°K (-30°F), creep limits the maximum gas-side wall temperature to 811°K (1000°F). The two line segments shown in Figure 48 are input to the computer program, and the maximum gas-side wall temperature limitation automatically determines the local channel depth provided the resultant depth/width ratio is within the limit of 5:1. Figure 49 gives the resultant channel depth profile for the baseline primary chamber. The alternate increases and decreases between the throat and a point about 7.6 cm (3 in.) upstream of the throat are caused by the combined effects of variations in heat flux, land width and channel curvature. The channel aspect ratio limited the depth in the first 10.4 cm (4.1 in.) of the chamber. Reducing the throat region channel width from the current 1.2 mm (0.047 in.), thereby increasing the number of channels, could reduce the extent of overcooling in this 10.4 cm (4.1 in.) section. This type of channel optimization was not investigated in the present contract, although initial studies with 1.02 mm (0.040 in.) wide channels in the throat resulted in overcooling the throat region due to the channel aspect ratio limit. All channel depths in the baseline secondary circuit were defined by the aspect ratio limit.

All chamber designs were based on balancing the pressure drop of the two circuits by selection of the coolant flow fraction between circuits. Figure 28 shows the individual circuit pressure drop characteristics for the baseline design point as a function of the fraction of the hydrogen flow used to cool the primary circuit. These curves generally exhibit a minimum point as shown in Figure 28 for the secondary circuit. Pressure drops are higher at low circuit flows, in this case corresponding to a high primary circuit flow, since the channel depths are reduced (high L/de) and the high bulk temperature rise requires higher mass velocities for wall temperature control. At high circuit flows the channel aspect ratio limit results in

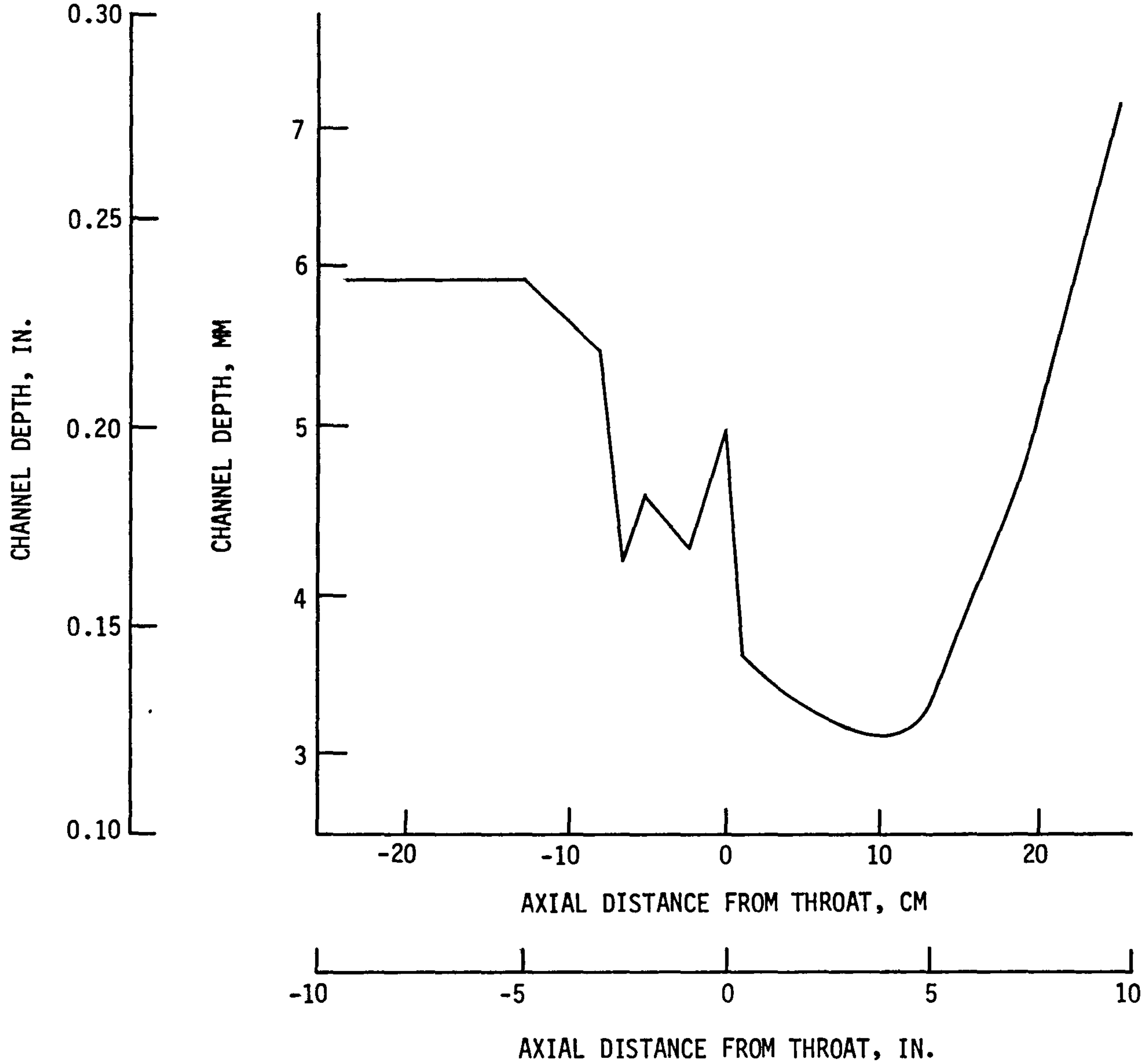

Figure 49. Channel Depth Profile Preliminary Baseline Primary Chamber

overcooling and the fixed coolant flow area results in the pressure drop increasing with flow rate. For the baseline design, equal circuit pressure drops of 685 psi are obtained with 36 percent of the hydrogen flowing in the primary circuit and the balance in the secondary circuit. It is apparent that bypassing part of the hydrogen flow, which would shift the secondary circuit curve in Figure 28 to the left, would result in a somewhat lower pressure drop. However, all results reported herein are based on no bypass flow. Table X provides the dual throat regenerative cooling program output for the baseline design, and Figure 50 gives some of the nomenclature asociated with Table X. Note that the geometry tables follow the combustion gas flow starting at the injectors, while the heat transfer tables follow the coolant flow.

The baseline design point was also investigated with methane replacing RP-1. Combustion product temperatures and properties with methane are very similar to those with RP-1. As a result, virtually identical flow fractions and chamber pressure drops were obtained with these fuels. A shorter, 30° secondary nozzle was also investigated, resulting in a 1.4 x 10^5 N/m^2 (20 psi) pressure drop reduction compared to the reference 15° nozzle; in this case the primary circuit coolant flow was 32.5 percent of the total hydrogen flow.

Figures 29 and 30 show the effect of Mode 1 propellant thrust split on chamber pressure drop and coolant bulk temperature rise, respectively. The pressure drop curve exhibits a minimum near the baseline 60/40 stream-tube thrust split. As the stream-tube thrust split varies, the available hydrogen flow varies; therefore, the shape of the pressure drop characteristic is explained by the same flow effects observed in Figure 28 as the flow fraction was varied in an individual circuit. In the same way, the increased hydrogen flow associated with lower LOX/RP-1 stream-tube thrusts results in the decreased bulk temperature rise of Figure 30.

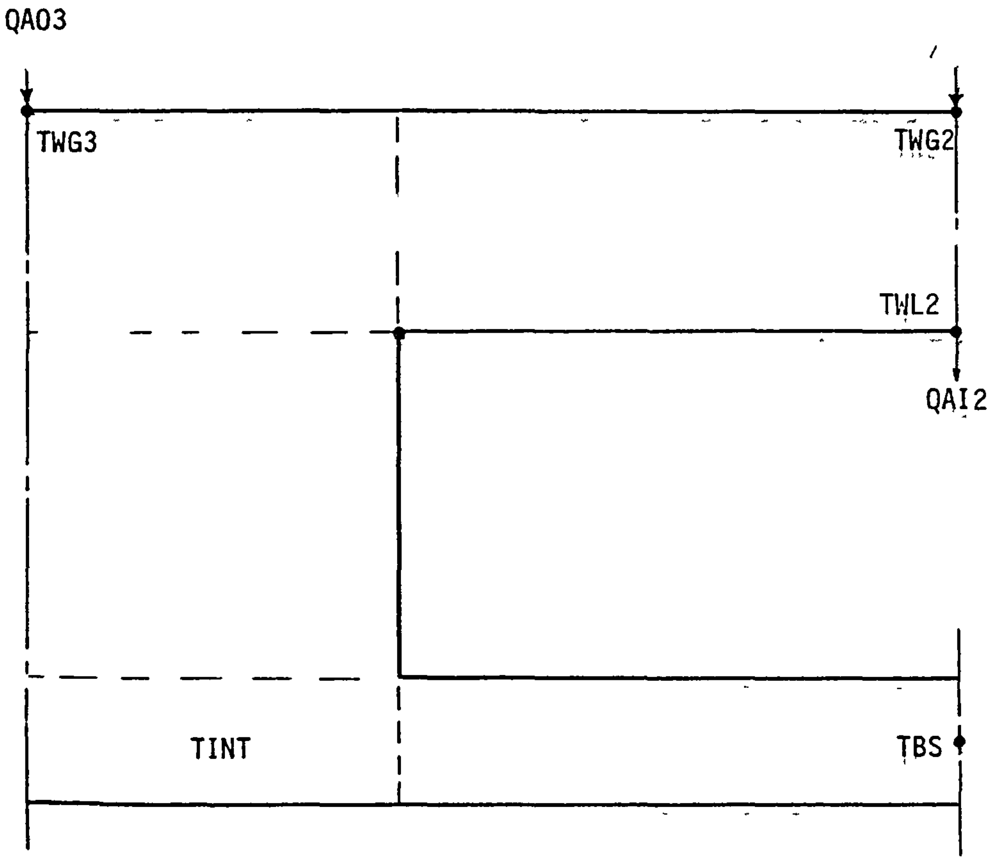

TWGC IS THE MAXIMUM OF TWG2 AND TWG3

Figure 50. Location of Various Heat Transfer Output Parameters

Figures 31 and 32 show the effect of total engine thrust on chamber pressure drop and bulk temperature rise, respectively. The trends shown are the same as for conventional thrust chambers. Increasing thrust increases the channel length, while the channel aspect ratio limit restricts the flow area increase desired to accommodate the higher flow rates. Even without the aspect ratio limit the hydraulic diameter increase with thrust would be small. These considerations explain the significant increase in pressure drop at the higher thrust levels. It was not possible to achieve converged computer solutions at 8896 KN (2×10^6 lbF) thrust due to the very high pressure drops.

Figures 33 and 34 give the effect of chamber pressure on pressure drop and bulk temperature rise, respectively. In all cases the secondary chamber pressure was 70 percent of the primary pressure. Presure drop increases with chamber pressure due to the higher heat fluxes, reaching 2.4×10^7 N/m^2 (3500 psi) at a primary chamber pressure of 3.45×10^7 N/m^2 (5000 psia). The bulk temperature rise characteristics of Figure 34 are influenced by the circuit flow fractions. The primary circuit flow fraction was smallest at the baseline primary chamber pressure of 2.07×10^7 N/m^2 (3000 psia), resulting in a maximum primary circuit bulk rise and a minimum secondary circuit bulk rise at this pressure.

Figure 35 shows the effects of primary and secondary mixture ratio variations on chamber pressure drop. For LO_2/RP-1 combustion the stoichiometric mixture ratio is 3.4. For mixture ratios less than this the heat flux is reduced, so that the cooling requirements are reduced. For LO_2/LH_2 combustion the stoichiometric mixture ratio is 8. However, at lower mixture ratios more free hydrogen is available, which enhances the gas-side heat transfer coefficient and offsets the reduced combustion gas temperature. Figure 36 shows coolant bulk temperature rise versus mixture ratio for the circuit in which the mixture ratio varies. These curves reflect the above heat flux variations plus the effects of hydrogen flow variations as the primary mixture ratio changes. In addition, a significant shift in the circuit flow fraction reduced the secondary circuit bulk temperature rise for a secondary chamber mixture ratio of 2.0.

3. Chamber Combined Transpiration-Regenerative Cooling

The high coolant pressure drop noted above for a primary chamber pressure of 3.45×10^7 N/m^2 (5000 psia) is unacceptable from an engine power balance standpoint. Therefore, a combination of transpiration and regenerative cooling was investigated. Individual circuit pressure drop vs. hydrogen flow fraction characteristics indicated it was the primary circuit which was responsible for the high pressure drop; the minimum pressure drop for this circuit was 2.28×10^7 N/m^2 (3300 psi) compared to just over 6.89×10^6 N/m^2 (1000 psi) for the secondary circuit. Since a coolant pressure drop of 1.03×10^7 N/m^2 (1500 psi) was desired for a realistic engine power balance, transpiration cooling of the secondary throat region was not necessary; at this pressure drop, 48 percent of the hydrogen flow is required for the secondary circuit. The balance of the hydrogen flow was split between a transpiration-cooled primary circuit identical to that considered previously except that it bypasses the transpiration-cooled throat section.

Parametric studies for various lengths of the transpiration-cooled section were conducted in order to split the available hydrogen flow between this section and the primary regenerative cooling circuit. In all cases the aft end of the transpiration section was 7.9 cm (3.1 in.) downstream of the throat at an area ratio of 1.40. Figure 37 gives the transpiration flow requirements as a function of the contour length in the transpiration section. This section was assumed to be made of 0.20 mm (8 mil) stainless steel platelets with 0.10 mm (4 mil) coolant channels normal to the chamber axis; local coolant flows were selected to limit the maximum platelet temperature to 1222°K (1740°F). Regenerative cooling requirements were analyzed for two transpiration section lengths, as shown in Figure 38 as a function of the primary circuit coolant flow fraction. Primary circuit pressure drops include a throat bypass loss based on velocity head loss coefficients of 0.5 at the nozzle section outlet and 0.1 at the chamber section inlet. The shift in the secondary circuit characteristics with increased transpiration section length reflects the reduced coolant flow available for the primary circuit. Balancing the primary and secondary circuit pressure drops from Figure 38 yields the final result of this analysis, i.e., the required regenerative cooling pressure drop as a function of the transpiration coolant flow as shown in Figure 39. The desired pressure drop of 1.03 x 10^7 N/m^2 (1500 psi) requires that 16.5 percent of the hydrogen be used for transpiration cooling.

4. Secondary Nozzle Coolng

Two-pass, oxygen-cooled tube bundles were investigated for cooling the secondary nozzle from area ratio of 8:1 to 43:1; the contour assumed for this study is shown in Figure 40. Round Inconel 718 tubes with a uniform wall thickness were utilized, with the wall temperature limited to 922°K (1200°F). This temperature limit provides a life of approximately 250 cycles. Tube wall thicknesses were based on the strength criterion of Figure 51. This criterion was applied in a conservative manner by imposing the coolant inlet pressure at area ratio 43:1 and assuming a 922°K (1200°F) wall temperature at this location. Using the primary chamber oxidizer flow as the coolant flow, the number of tubes was varied to obtain maximum wall temperature of 922°K (1200°F). This temperature occurred at the coolant outlet in all cases.

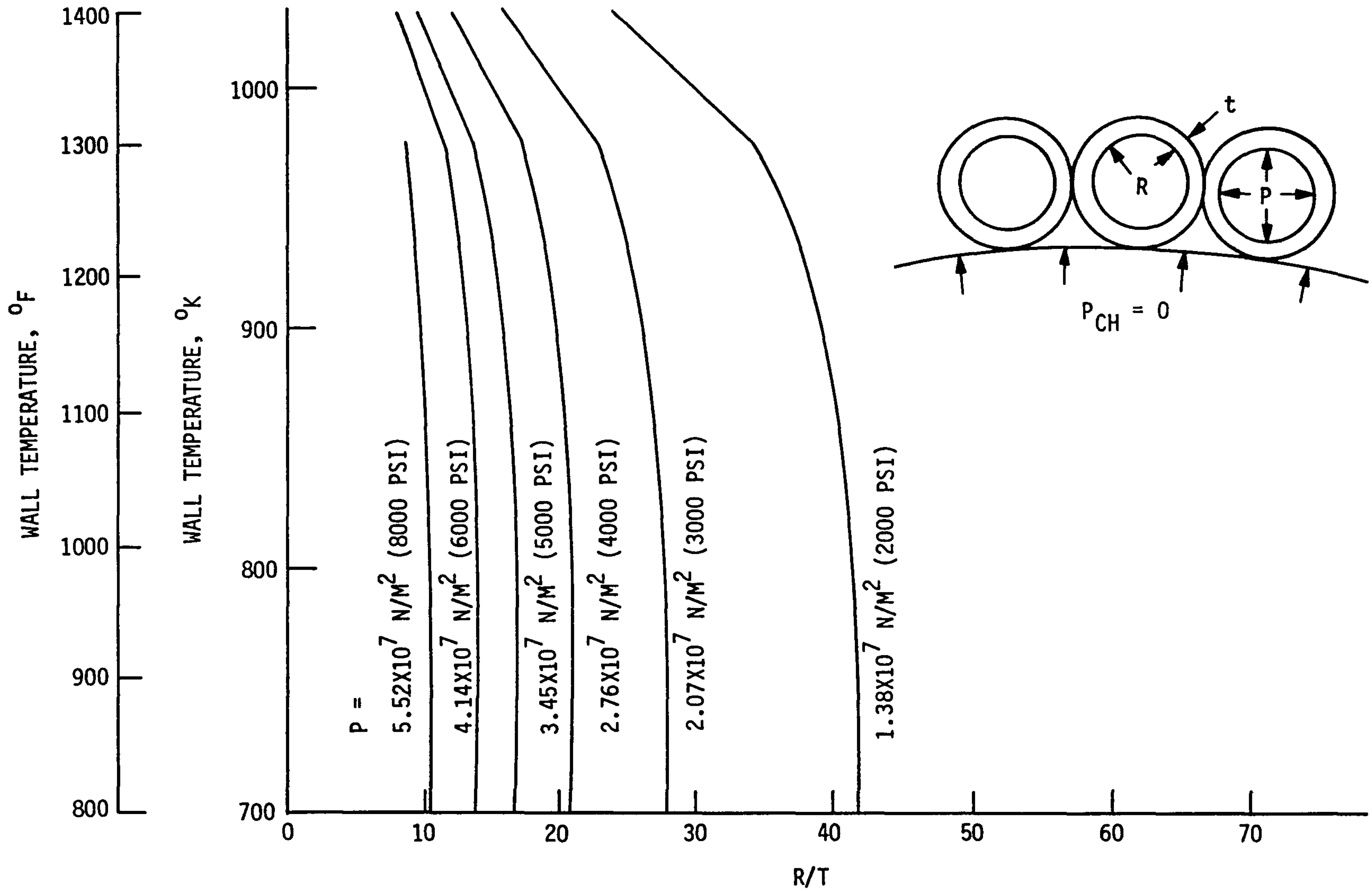

Figure 51. Inconel 718 Maximum Allowable R/t

Oxygen heat transfer coefficients were calculated from the ALRC correlation of Ref. (10):

$$Nu_b = 0.0025\ Re_b\ Pr_b^{0.4} \left(\frac{\rho_b}{\rho_w}\right)^{-0.5} \left(\frac{K_b}{K_w}\right)^{0.5} \left(\frac{\bar{C}_p}{C_{p_b}}\right)^{0.667} \left(\frac{P}{P_{cr}}\right)^{-0.2} \left(1 + \frac{2}{L/d_e}\right)$$

All tube bundle designs are summarized in Table XII, and a sample computer output for the baseline engine is given in Table XIII. Figure 41 shows the effect of stream-tube thrust split on coolant pressure drop and bulk temperature rise. As the LOX/RP-1 stream-tube thrust increases from nominal, the coolant flow available decreases, resulting in a larger bulk temperature rise, smaller tubes (greater L/d_e) and a corresponding increase in pressure drop. At lower stream-tube thrust splits with higher coolant flow rates, larger tubes result in thicker walls which require higher coolant mass velocities and, therefore, slightly higher pressure drops than the nominal 60/40 stream-tube thrust split. Figures 42 and 43 show the increase in coolant pressure drop required with increasing thrust and chamber pressure, respectively; bulk temperature rise variations with these parameters are small. Pressure drop increases with thrust because of increased tube length and wall thickness.

D. THRUST CHAMBER STRUCTURAL ANALYSIS

A preliminary structural and low cycle fatigue evaluation of the baseline dual-fuel, dual-throat engine concept was performed. The low cycle fatigue life of the structure was predicted to exceed the service life requirements of the design.

1. Summary of Results

Structural and low cycle fatigue analyses were conducted to demonstrate the feasibility of the baseline engine slotted zirconium-copper liner and electroformed nickel jacket geometry.

Two locations in each of the primary and secondary thrust chambers (throat and cylindrical region) were selected for detailed elastic/plastic analyses with thermal and thermal plus mechanical loading conditions. Results of these analyses indicate the design concept is feasible.

Low cycle fatigue life for the baseline engine configuration is based on iterative elastic/plastic plane strain predictions obtained from computer analyses. Predicted total strain and corresponding cyclic life are summarized in Table XIV.

TABLE XIV

PREEDICTED TOTAL STRAIN AND CYCLIC LIFE

Component	T_G °K (°F)	T_B °K (°F)	Minimum EFNi Wall Thickness mm (in.)	ε_T(%)	N_f Cycles
Primary Chamber					
Throat	777 (938)	154 (-183)	2.8 (0.11)	2.14	130
Cylinder	698 (797)	237 (-33)	8.9 (0.35)	2.37	105
Secondary Chamber					
Throat	674 (753)	278 (40)	4.1 (0.16)	1.58	225
Cylnder	594 (610)	354 (178)	12.7 (0.5)	1.35	300

Strain concentration factors, K_ε, from these results are shown in Figure 52 for comparison with factors from previous studies. The large scatter is thought to result from constraints imposed by the relatively thick nickel jacket liner required to sustain pressure induced hoop membrane forces.

On the basis of the preliminary analysis results the predicted cyclic life of the baseline engine design concept is limited to 105 cycles

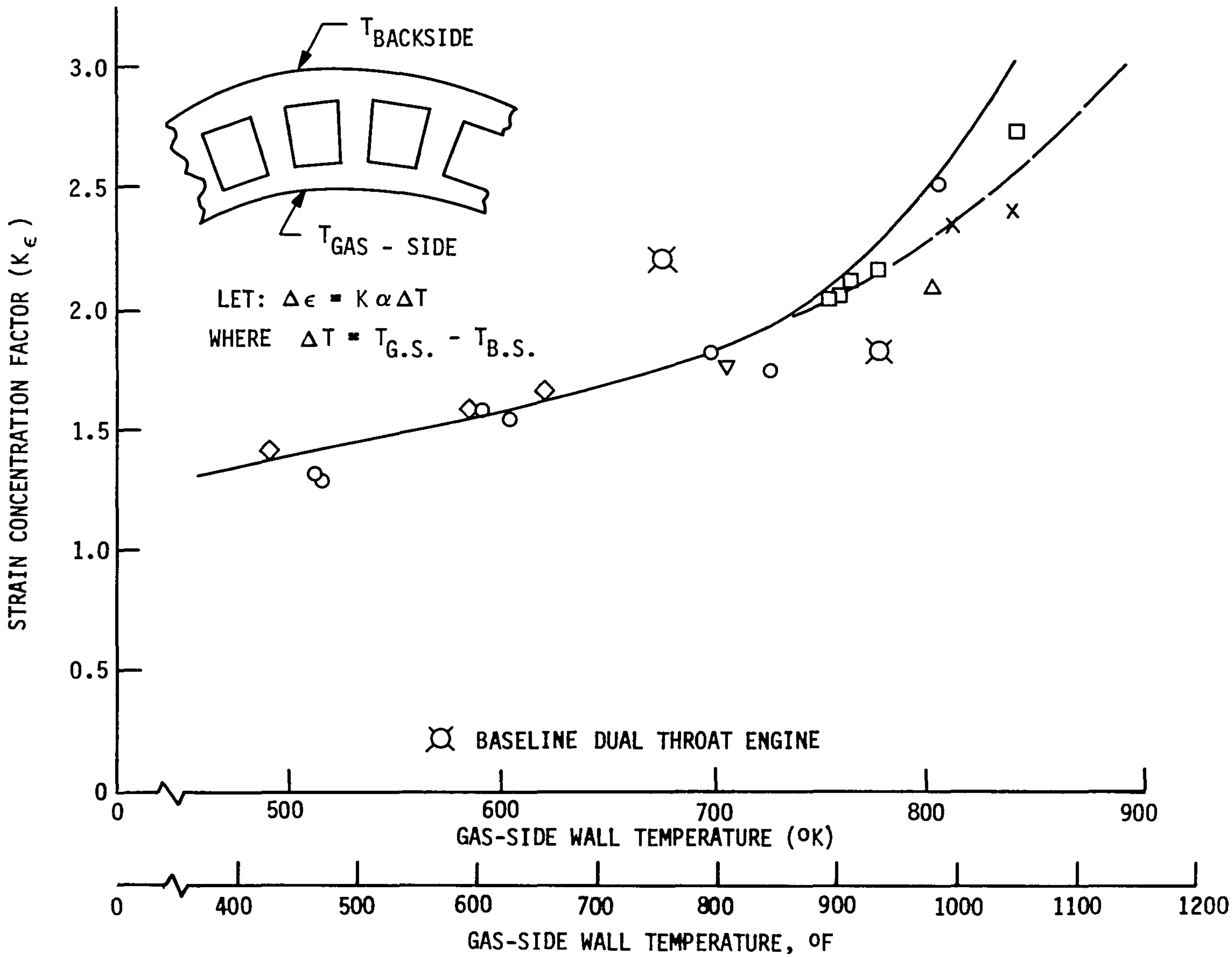

Figure 52. Predicted Strain Concentration Factor vs Gas-Side Wall Temperature

calculated for the cylindrical section of the primary thrust chamber.

The stress and strain distribution in the copper liner indicates the need for increasing the copper thickness from the present 0.64 mm (0.025 inch) to a minimum 0.76-0.89 mm (0.030-0.035 inch) range. Thickness of electroform nickel required to sustain pressure loads becomes substantial in the cylindrical sections. Evaluation of alternate design options should lead to a less severe stress and strain distribution.

2. Design Criteria

a. Static Strength

The following factors of safety are utilized with limit loads and pressure loads:

- 1.0 on yield strength
- 1.5 on ultimate strength

Limit loads are defined as combinations of:

- Pressure load
- Static force loads
- Shock/dynamic loads

Thermal loads are self-limiting and are not subject to safety factors other than those used for life predictions.

b. Fatigue Life

Typical zirconium copper design allowable fatigue curves utilized in the analysis are shown in Figures 53 and 54. Where multi-axial stresses occur, effective stresses are calculated using the Mises-Hencky constant energy of distortion theory and are used with the fatigue curves. For low cycle fatigue strength the following factors are used.

Factor on Cycles	Data Basis
4.	Figures 53 and 54 10 Hour Hold
10.	Figures 53 and 54 0.1 N_f @ t = 0 curve

c. Geometry

The high heat flux region of the chamber uses slotted zirconium copper for the liner and electroformed nickel for the outer jacket. The slotted zirconium copper dimension limits are as follows:

- Minimum Slot Width = 1.02 mm (0.04 in.)
- Minimum Load Width = 1.02 mm (0.04 in.)
- Minimum Wall Thickness = 0.64 mm (0.025 in.)

d. Service Life

Service life criteria are:

- Life = 100 Cycles (Times Safety Factor of 4)
- Duration = 10 Hours Accumulated Operation

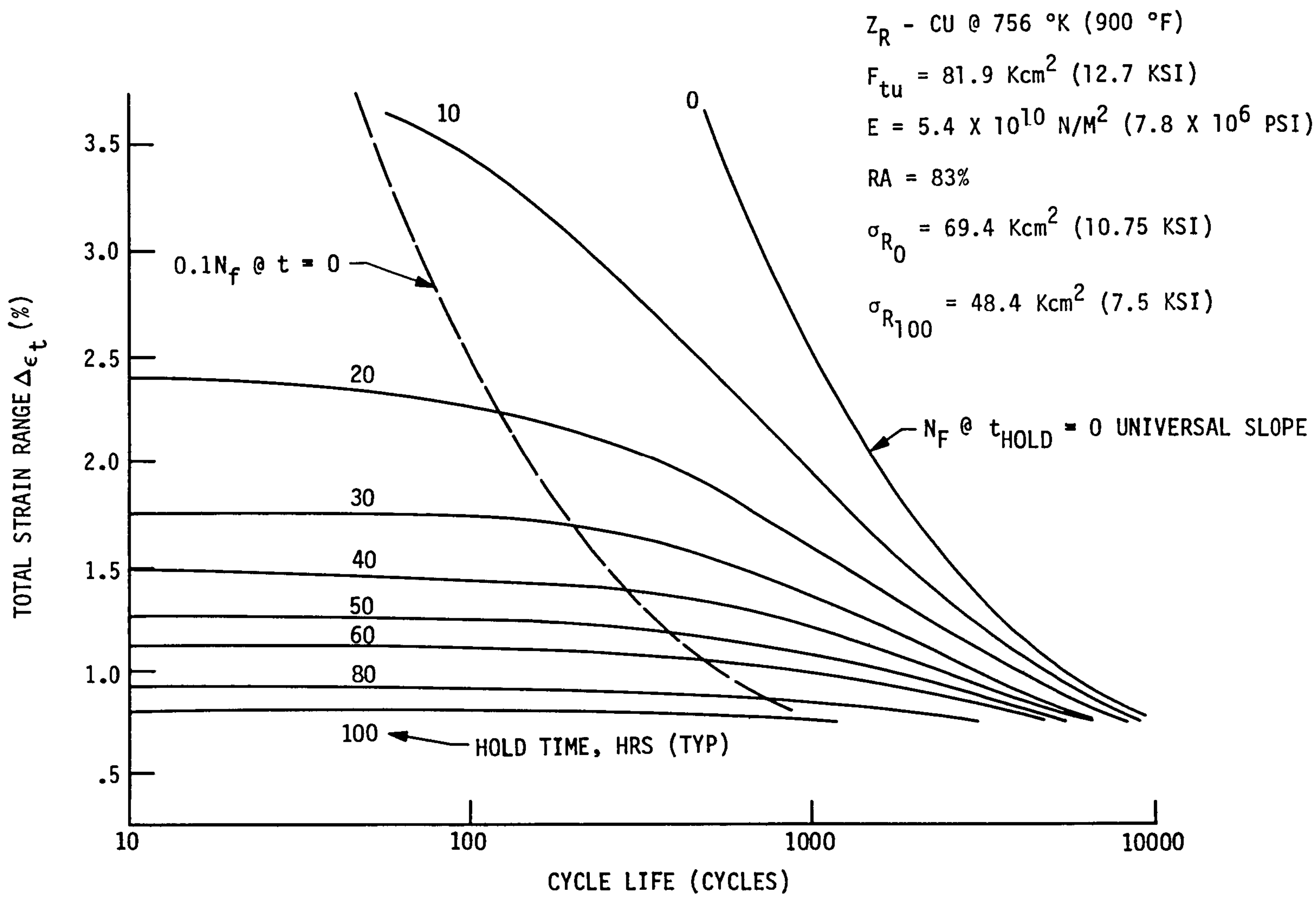

Figure 53. Total Strain Range vs. Cycle Life

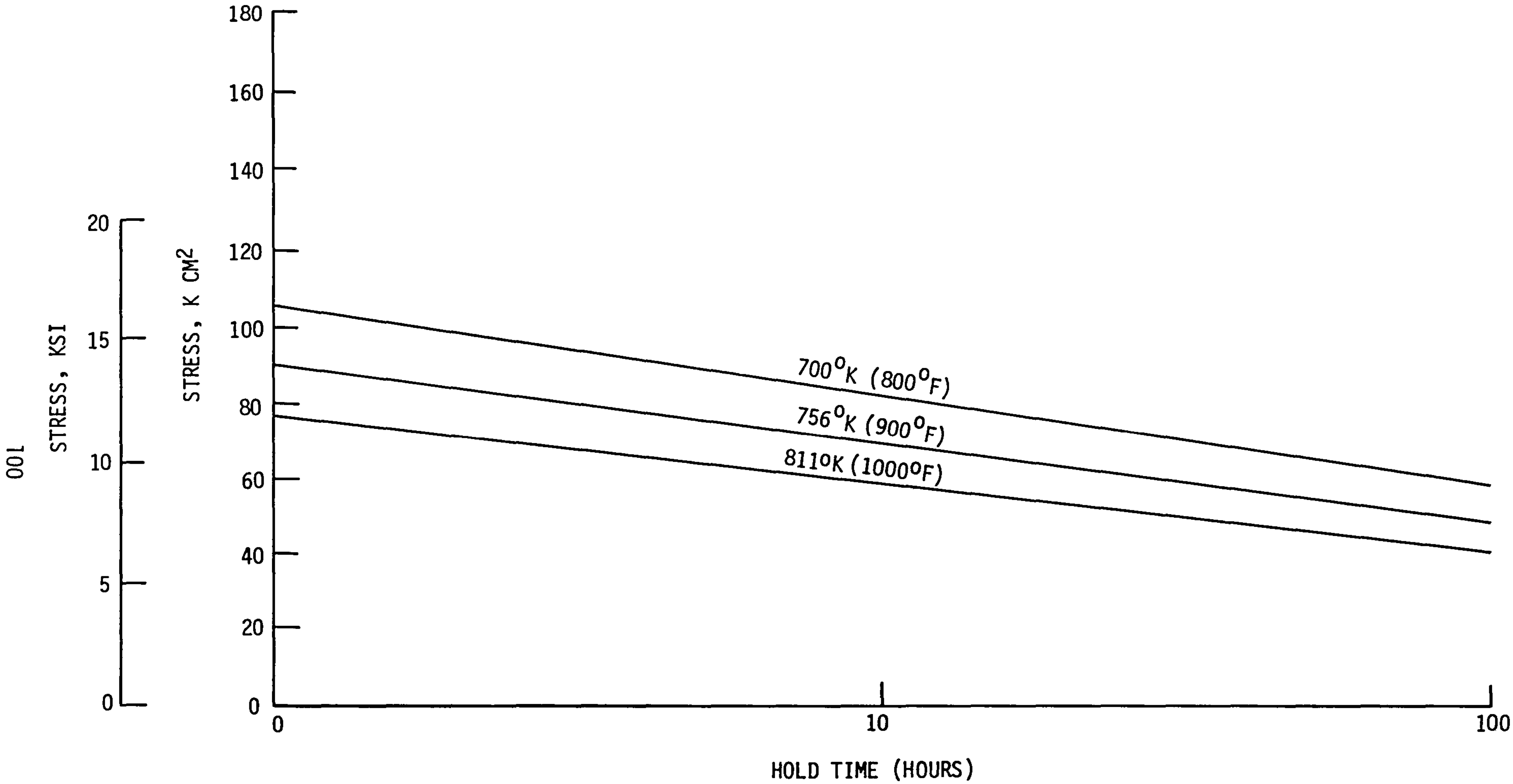

Figure 54. Stress Rupture Properties Zirconium Copper

e. Temperatures

The gas-side wall is limited by service life and material properties to 1000°F maximum.

f. Presure

The chamber pressures for the analysis are:

- 2.07×10^7 N/m^2 (3000 psi) primary
- 1.45×10^7 N/m^2 (2100 psi) secondary

The coolant pressures for the analysis are:

- 3.85×10^7 N/m^2 (5583 psi) (throat), 3.68×10^7 N/m^2 (5340 psi) (cyl) (primary)
- 3.90×10^7 N/m^2 (5658 psi) (throat); 3.67×10^7 N/m^2 (5326 psi) (cyl) secondary

g. Material Properties

The basic thrust chamber construction utilizes slotted zirconium copper for the liner material and electrofomed nickel for the closeout material (jacket).

Zirconium copper properties used in the analysis are shown in Figure 55.

3. Analytical Method and Model Description

Strength of materials methods are used in the analysis of the slotted coolant channel and jacket design to first establish minimum

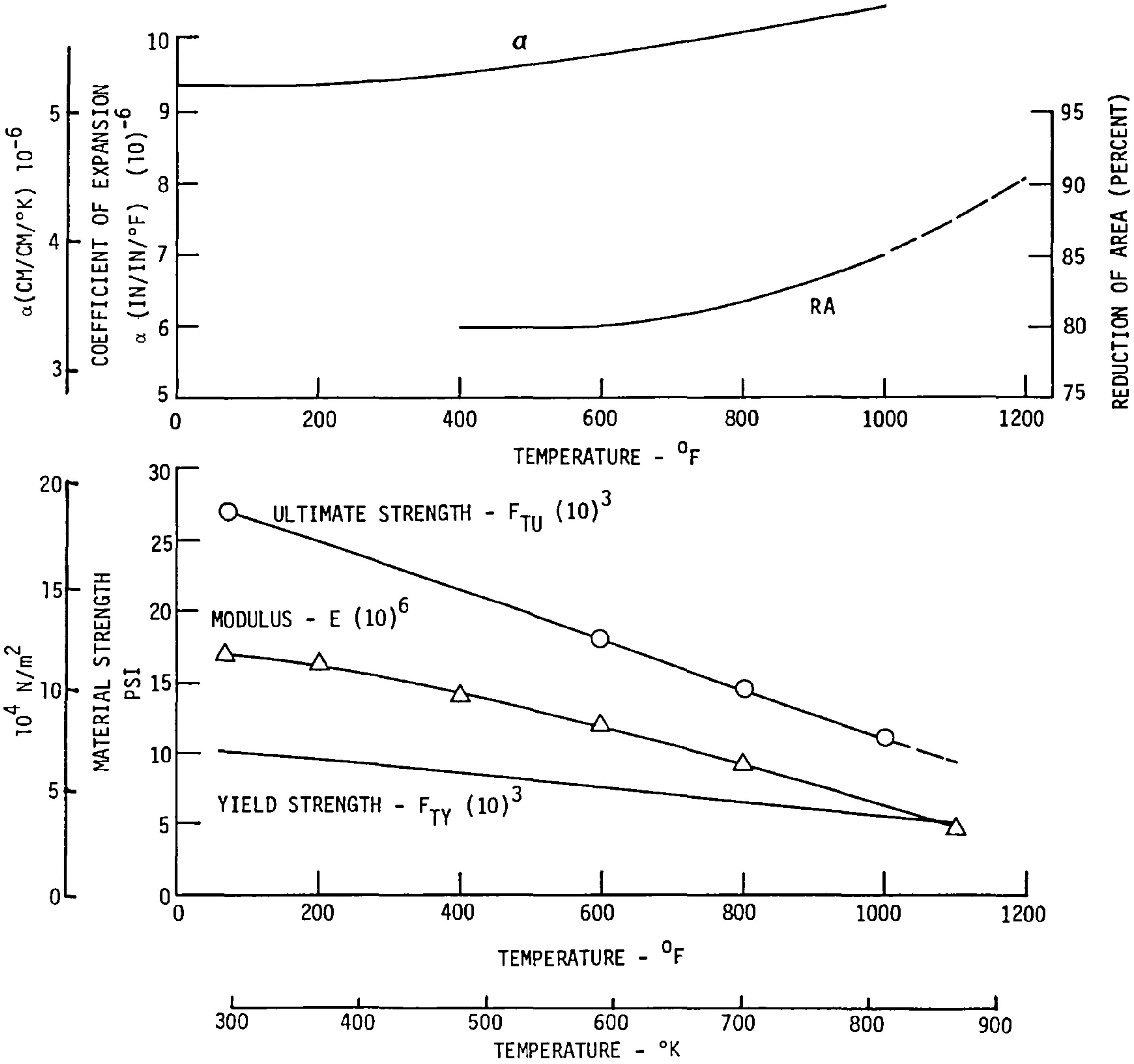

Figure 55. Mechanical Properties of Zirconium Copper

material thicknesses required to sustain the coolant and chamber pressure. These minimum thicknesses are based on the properties of the material at operating temperature.

An elastic/plastic plane strain analysis is then conducted using a detailed finite element model representation of a cross section of the thrust chamber wall. For this analysis thermal and thermal plus mechanical loads are applied to the model and a sufficient number of load iterations is performed to establish a converged solution. The AB5U finite element computer program is the principal tool employed for this analysis effort.

The finite element model is a cylindrical segment of the chamber wall bounded by two radials which form two cut boundary lines, with one radial bisecting a "land" and the other bisecting a coolant channel. Boundary conditions imposed along the cut lines allow only for movement along the radial lines to simulate a continuous ring effect. The included angle between the boundary radial is defined as $\theta = 360°/2N$, where N is the number of coolant channel slots. A typical finite element model of the wall cross section is presented in Figure 56.

4. Parametric Sizing Results

Initial sizing calculations were made to determine thrust chamber liner coolant channel geometry and EFNi jacket thickness needed to sustain the pressure loads and to establish the feasibility of the design to meet the desired low cycle fatigue objective. This is accomplished through the development of a family of design curves of allowable pressures and temperatures.

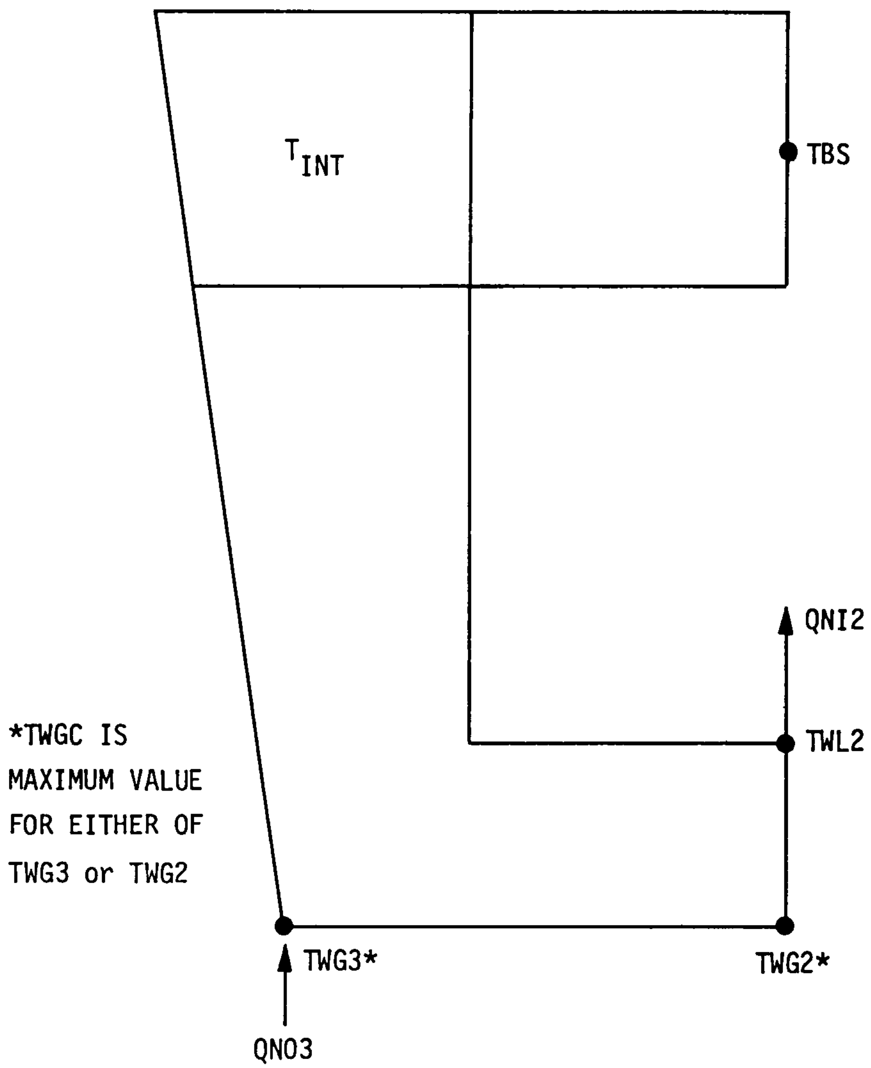

Figure 56. Typical Coolant Channel Configuration Used in Obtaining Thermal Profile for Cross Section

The zirconium copper liner coolant channel wall between lands can be visualized as a beam with built-in edge fixity (at the lands), subjected to a uniform pressure equal to the differential between coolant channel pressure and thrust chamber pressure.

The maximum bending moment for the beam shown in the adjacent sketch occurs at the built-in edges and is defined by:

$$M = \frac{\Delta P}{12} w^2$$

and the corresponding bending stress is

$$\sigma_b = \frac{6M}{t^2}$$

Substituting for M gives

$$\sigma_b = \frac{6}{t^2} \frac{\Delta P w^2}{12} = \frac{\Delta P}{2} \left(\frac{w}{t} \right)^2$$

For the beam to remain elastic, the bending stress must be less than or equal to the allowable tensile strength of the material at operating temperatures:

$$\sigma_b = \frac{\Delta P}{2} \left(\frac{w}{t} \right)^2 \leq F_{ty}$$

The aspect ratio of span to thickness can be determined from

$$\frac{w}{t} \leq \left(\frac{2F_{ty}}{\Delta P} \right)^{1/2}$$

Table XV summarizes aspect ratios determined for a range of pressures 0.35 to 5.52 x 10^7 N/m^2 (500 psi to 8000 psi) and gas side wall temperatures 478 to 811°K (400°F to 1000°F). Data from Table XV are plotted in Figure 57.

TABLE XV

SUMMARY OF COOLANT CHANNEL ASPECT RATIO (w/t_c)

$$\sigma = \frac{LP}{2}\left(\frac{W}{tc}\right)^2 \leq F_{Ty}$$

$$\therefore \frac{w}{tc} \leq \sqrt{\frac{2\,F_{Ty}}{\Delta P}}$$

T_G (°F)	400	500	600	700	800	900	1000
F_{Ty} (PSI)	8600	8100	7600	7100	6600	6100	5600
ΔP = 8000 PSI							
w/tc	1.458	1.414	1.369	1.323	1.275	1.225	1.172
ΔP = 6000 PSI							
w/tc	1.683	1.633	1.581	1.527	1.472	1.414	1.354
ΔP = 5000 PSI							
w/tc	1.844	1.789	1.732	1.673	1.612	1.549	1.483
ΔP = 4000 PSI							
w/tc	2.061	2.000	1.936	1.871	1.803	1.732	1.658
ΔP = 3000 PSI							
w/tc	2.38	2.309	2.236	2.160	2.081	2.000	1.915
ΔP = 2000 PSI							
w/tc	2.915	2.828	2.738	2.645	2.549	2.449	2.345
ΔP = 1000 PSI							
w/tc	4.122	3.999	3.872	3.741	3.605	3.464	3.316
ΔP = 500 PSI							
w/tc	5.86	5.69	5.51	5.32	5.13	4.93	4.73

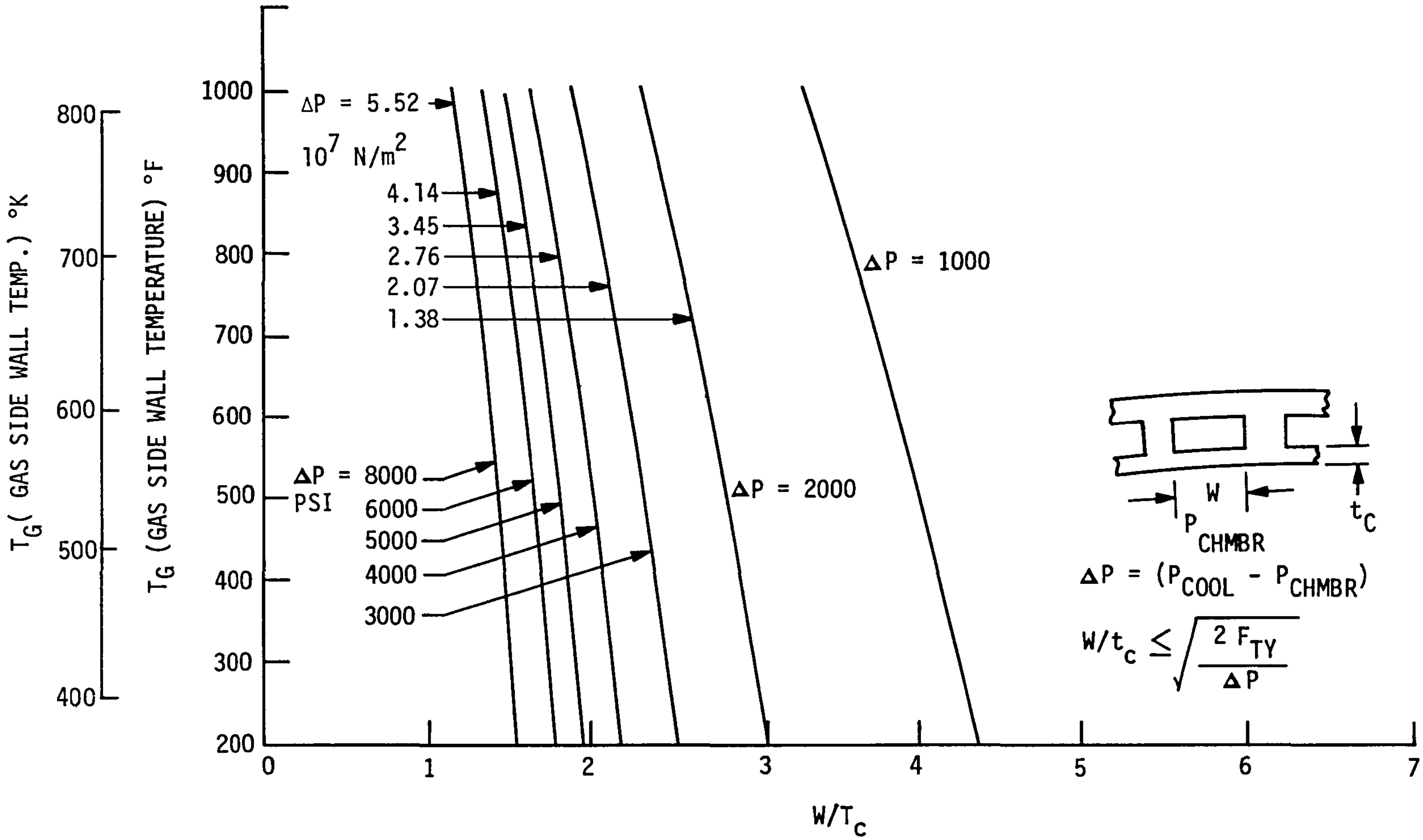

Figure 57. Aspect Ratio ZR-Cu Chamber Wall

5. Allowable Temperature Range

The allowable range of differential temperature ($\Delta T = T_g - T_b$) is established as a function of gas side and backside wall temperatures, total strain range, and cyclic life using the relationship.

$$T = \frac{\Delta\varepsilon}{(S.F.)(\alpha)(K_\varepsilon)}$$

Where:

$\Delta\varepsilon$ = Total Strain Range

S.F. = Applicable Design Safety Factor

α = Coefficient of Thermal Expansion

K_ε = Strain Concentration Factor (Figure 52).

Table XVI summarizes the allowable ΔT, and backside wall temperature T_b determined for a range of gas side wall temperatures 478 to 811°K (400°F to 1000°F) and strain ranges (1.0 to 2.55%). Data from Table XVI are plotted in Figure 58.

6. Low Cycle Fatigue Analysis

Low cycle fatigue analyses were conducted for coolant channel and jacket geometries selected for the baseline engine primary and secondary thrust chambers. The LCF evaluations were conducted on cross sections of the chamber wall taken from the throat and cylindrical regions.

Four iteration elastic/plastic computer analyses were performed for thermal and thermal plus mechanical loading. Results obtained from the computer analyses were used to plot curves of predicted strain versus effective stress for the four iteration ponts; where necessary, the curve

TABLE XVI

CYCLIC LIFE VERSUS STRAIN RANGE

F_{Ty} (PSI)	8600	8100	7600	7100	6600	6100	5600
T_G (°F)	400	500	600	700	800	900	1000
K_ε	1.35	1.45	1.56	1.69	1.83	2.05	2.36
α (IN/IN/°F)	$9.8(10)^{-6}$	$10.0(10)^{-6}$	$10.1(10)^{-6}$	$10.2(10)^{-6}$	$10.3(10)^{-6}$	$10.4(10)^{-6}$	$10.5(10)^{-6}$
$\Delta\varepsilon$ = 1.0% $N_f/4$ = 510 CYCLES							
ΔT	540	493	453	414	379	335	288
T_B	-140	7	147	286	421	565	712
$\Delta\varepsilon$ = 1.33% $N_f/4$ = 300 CYCLES							
ΔT	718	655	603	551	504	446	383
T_B	-318	-155	-3	149	296	454	617
$\Delta\varepsilon$ = 1.61% $N_f/4$ = 209 CYCLES							
ΔT	869	793	730	667	610	539	464
T_B	-469	-293	-130	33	190	361	536
$\Delta\varepsilon$ = 1.86% $N_f/4$ = 165 CYCLES							
ΔT	1004	916	843	771	705	623	536
T_B	-604	-416	-243	-71	95	277	464
$\Delta\varepsilon$ = 2.55% $N_f/4$ = 100 CYCLES							
ΔT	1927	1758	1618	1479	1353	1196	1029
T_B	-1527	-1258	-1018	-779	-552	-296	-29

NOTE

1. $\Delta T = \frac{\Delta\varepsilon}{1.4\,\alpha\,K_\varepsilon}$ (FOR $\Delta\varepsilon$ = 1.0, 1.33, 1.61, AND 1.86)

2. $\Delta T = \frac{\Delta\varepsilon}{\alpha\,K_\varepsilon}$ (FOR $\Delta\varepsilon$= 2.55%)

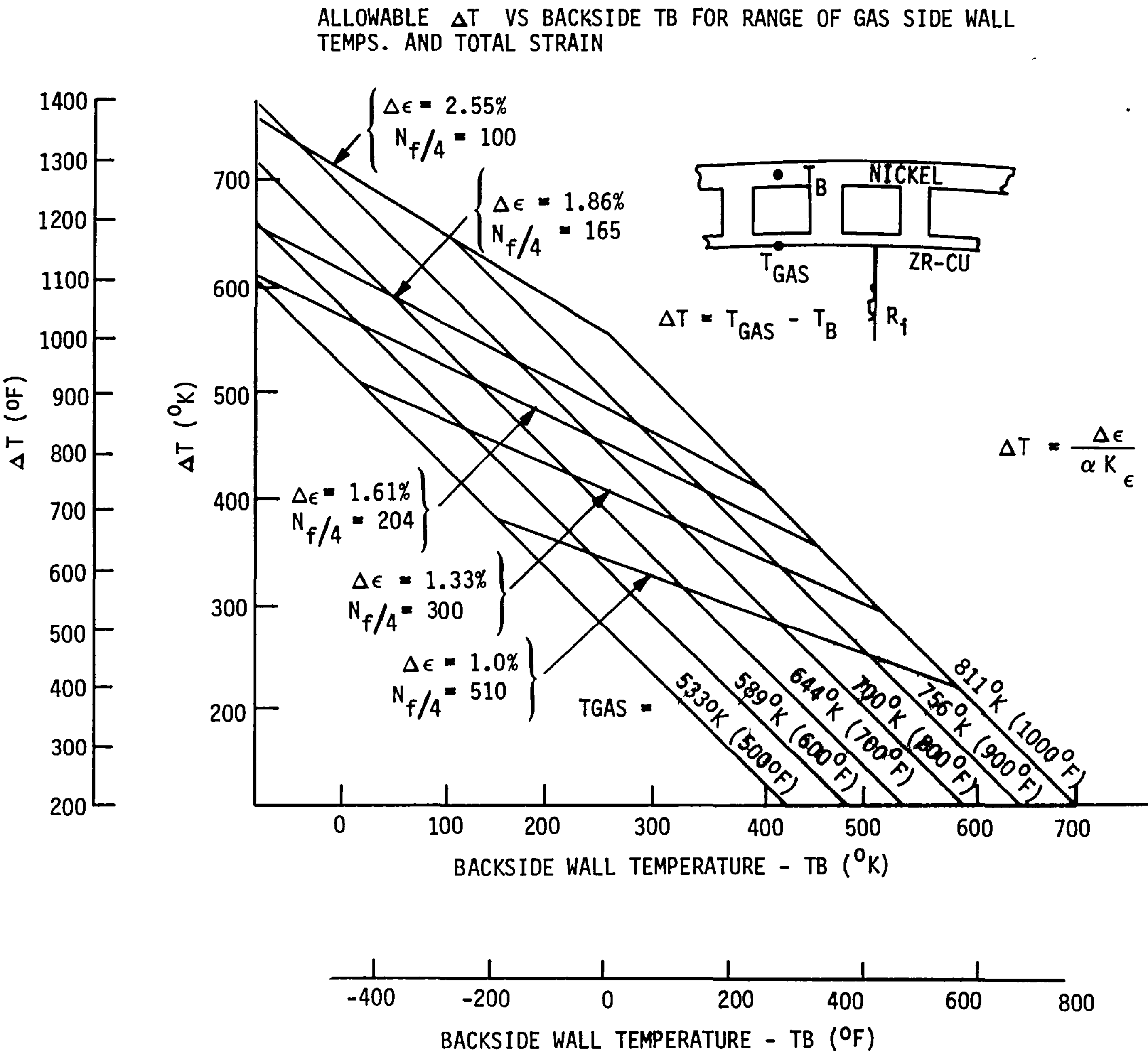

Figure 58. Allowable Temperature Differential

was extrapolated to intersect the secondary modulus slope. The corresponding strain is used to predict cyclic life. Figures 59 and 60 show the predicted strain ranges for selected elements for typical conditions analysed.

E. TECHOLOGY IDENTIFICATION

Areas requiring technological investigation for the dual throat engine are identified as including: (1) gas-gas injector performance, combustion stability, and design, (2) bleed flow system design evaluation to optimize non-isoenergetic flow, (3) maximum secondary/primary pressure ratio ($\geq$ 0.7) determination to insure stable engine operation, (4) series burn design evaluation to achieve higher secondary chamber pressure, (5) thrust chamber manufacturing methods for double wall cooling, (6) gas generator turbine exhaust nozzle and secondary chamber bleed dump performance determination, (7) start/shutdown transient analysis and determination for parallel flow operation, (8) trans-regen cooling and performance determination, (9) engine weight reduction through the application of advanced materials, (10) performance determination for LOX/hydrocarbon thrust chambers, where the hydrocarbon is RP-1, CH_4 or subcooled C_3H_8, (11) stoichiometric preburner (gas generator) demonstration, (12) microprocesor based controller demonstration for lightweight, precise engine control, (13) turbopump demonstration utilizing hydrostatic journal bearings for long life, (14) turbopump demonstration with a self-aligning thrust balancer (articulated, floating face seal), and (15) positive displacement pump demonstration of zero NPSH and variable flow.

A state-of-the-art assessment, justification, objectives and technical approach for each of the technologies are given in Table XVII.

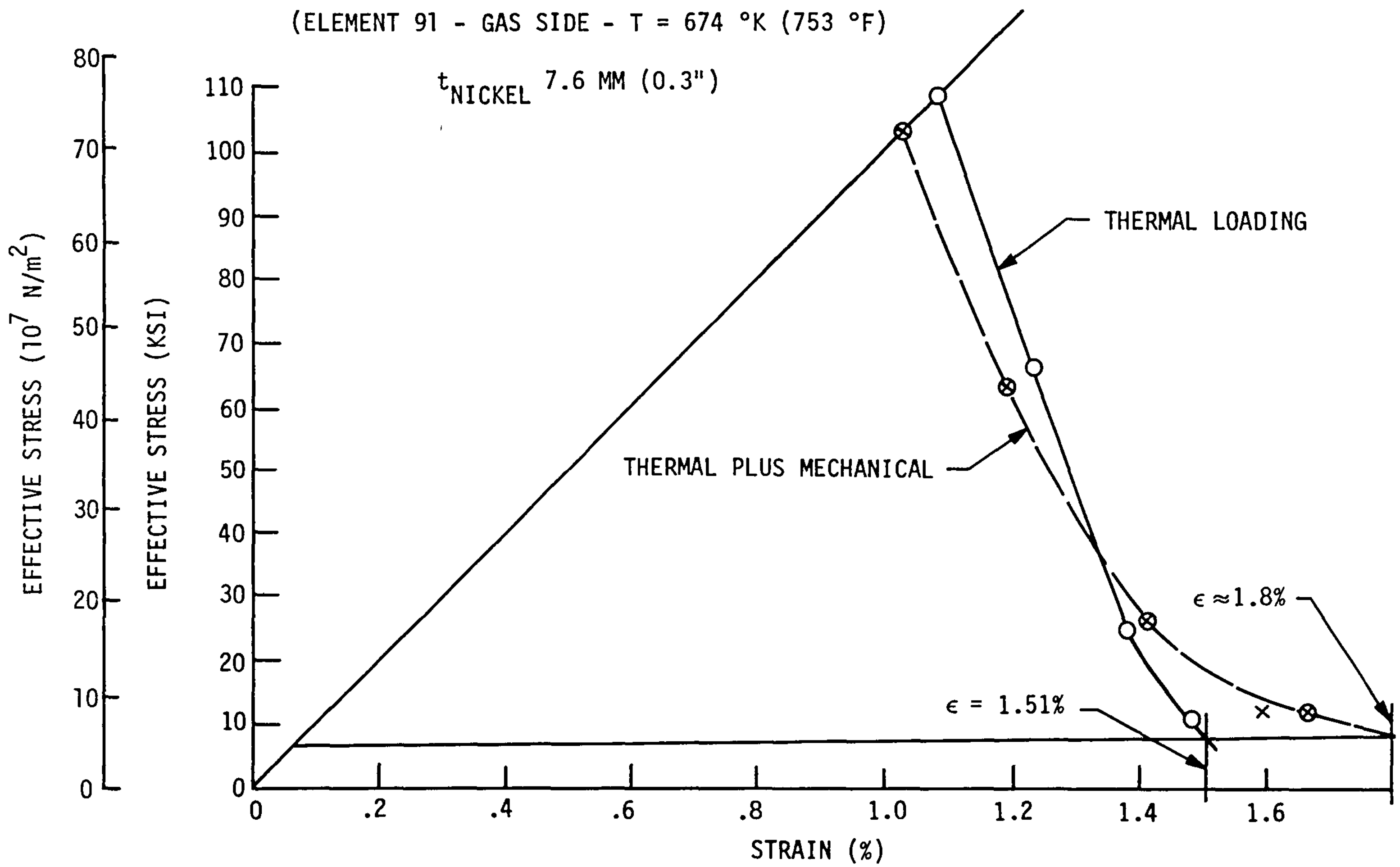

Figure 59. Predicted Strain (%) - Preliminary Baseline Outer Chamber Throat

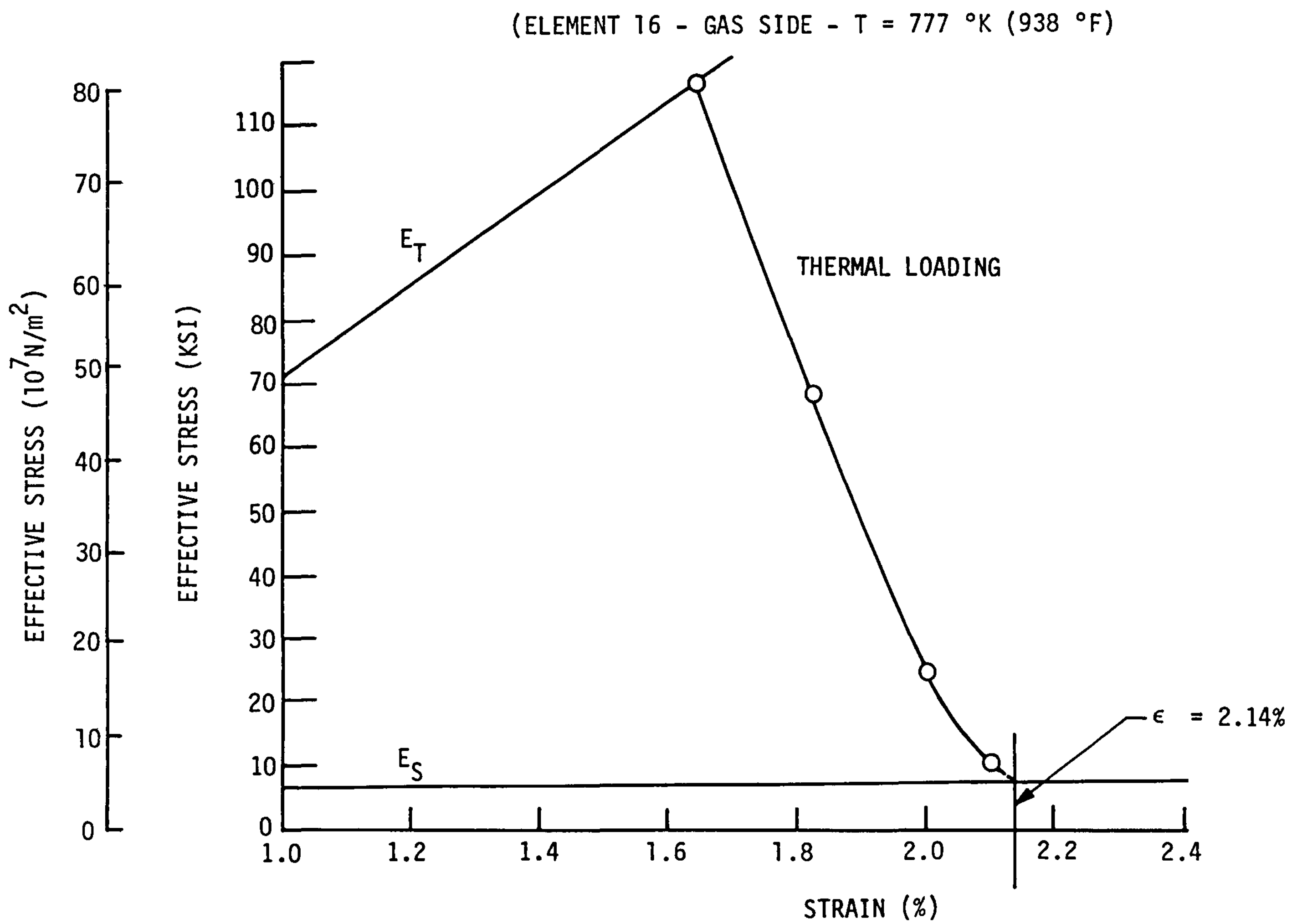

Figure 60. Predicted Strain - Preliminary Baseline Inner Chamber Throat

TABLE XVII

DUAL THROAT ENGINE REQUIRED TECHNOLOGY

TECHNOLOGY	STATE-OF-THE-ART ASSESSMENT	JUSTIFICATION	OBJECTIVE	TECHNICAL APPROACH
IA Gas-Gas Injector Performance (Staged Combustion Cycles)	NAS 3-15850 (ITA) NAS 3-14379 (Design/Test)	Design criteria for two 1000 °F (Oxidizer-rich & fuel-rich) gas streams not available at Hi Pc	Determine performance versus L', stability criteria	Single element & sub-scale testing & analytical model development
IB Hot Gas - Gas/Liquid Injector Performance (Mixed GG/SC Cycle)	AF 04(611) 10830 (ARES) AF 04(611) 10785 (H_2O_2/Al-43) Ramjets (Air/JP-4)	Design criteria for Oxid.-rich hot (1000°F) gas & lower temperature Gas/liquid fuel is limited	Determine performance versus L', stability criteria	Single element & sub-scale testing & analytical model development
II Bleed Flow System Design/Evaluation	NAS 8-32666 cold flow	Isoenergetic bleed flow required for minimum performance loss and minimum mixture ratio shift	Determine optimum design configuration for non-isoenergetic bleed flow during Mode II operation	Generate & evaluate design concepts in subscale hot fire tests
III Secondary/Primary Chamber Pressure ratio (≥ 0.7)	ALRC IR&D 8877-06 cold flow testing & analysis	High pressure in secondary chamber improves dual throat performance. Stability of engine system not known if subsonic primary is utilized	Determine combustion stability of dual throat over range of PCS/PCP ≥ 0.7	Evaluate designs for combustion stability in subscale hot fire tests
IV Series Burn Design Concept Evaluation	ALRC IR&D 8877-06 cold flow testing & analysis	High pressure in secondary chamber improves dual throat performance. Cooling requirements for series burn designs not available	Determine feasibility of series burn design concepts	Analyze series burn design concepts and select most promising cooling system design
V Double Wall Thrust Chamber Fabrication/Design		Design criteria for primary chamber double cooling jacket and nozzle lip not available	Determine optimum design configuration for primary chamber/nozzle walls	Generate & evaluate jacket designs capable of being fabricated. Analyze designs for heat transfer, structures, and fabrication methods
VI Gas Generator Turbine Exhaust Performance		Achievement of maximum gas generator exhaust performance improves engine performance	Determine optimum design configuration for GG nozzle dump and secondary chamber bleed flow dump	Generate & evaluate nozzle dump and bleed dump design concept
VII Parallel Flow Transient Analysis	ALRC IR&D 8877-06 cold flow testing	Start and shutdown procedures for the dual throat engine requires special analysis due to the staging of multiple combustors	Determine fool-proof operational control sequence	Analyze flow/ignition/combustion circuits for dual throat engine. Select optimum control system

TABLE XVII (Cont)

	TECHNOLOGY	STATE-OF-THE-ART ASSESSMENT	JUSTIFICATION	OBJECTIVE	TECHNICAL APPROACH
VIII	Trans-Regen Cooling/Performance	NAS 3-21029	Trans-regen performance criteria is not available for dual throat configuration Contribution of Trans-coolant as bleed flow during Mode II needs to be determined	Determine trans-regen performance contribution during Mode I and Mode II	Evaluate designs in subscale testing
IX	Engine Weight Reduction with Advanced Materials		Reusability of the dual throat engine allows the utilization of expensive advanced composite materials for both low and high temperature applications	Reduce dual throat engine weight by at least 20%	Design, fabricate and test select subscale components made of advanced composite materials
X	LOX/Hydrocarbon Engine Performance	NAS 3-21030	The dual throat design may enhance the efficiency of LOX/Hydrocarbon combustion due to the hot LOX/LH_2 core	Determine the efficiency of the dual throat engine in Mode I operation	Design, fabricate & test subscale dual throat engine using LOX/RP-1, LOX/CH_4 and LOX/C_3H_8
XI	Stoichiometric Preburner	Ariane first stage engine	Fuel-rich & Oxid -rich preburners operate at conditions close to flame-out and on the steep portion of the T vs MR curve A stoich preburner operates at no worse than design condition	Determine optimum design configuration for stoich preburner	Generate & evaluate designs in subscale hot fire tests with LOX/LH_2 and LOX/CH_4
XII.	Microprocessor - Based Engine Controller	ALRC IR&D 8878-06 design analysis	Microprocessor controller offers precise engine control for minimum weight & volume	Determine feasibility of microprocessor based dual fuel engine controller	Design & evaluate microprocessor controller for subscale dual throat engine testing
XIII	Hydrostatic Journal Bearing Turbopump	Rolling element bearings possess limited size, speed load capability, and short life	Long life turbopumps for High pressure engines require minimum rubbing contact	Demonstrate capability of subscale rotating machinery utilizing hydrostatic journal bearing	Design, fabricate and test turbomachinery with propellant lubricated hydrostatic journal bearing
XIV	Self-Aligning Thrust Balancer turbopump	Axial thrust balancers are limited in capacity and stability, and require a large flow	Long life turbopumps for high pressure engines must compensate for large variations in load	Demonstrate capability of subscale rotating machinery utilizing articulated thrust balancer	Design, fabricate and test turbomachinery with propellant actuated self-aligning thrust balancer
XV	Positive Displacement Pump	American Hydraulic Propulsion Systems, Inc	Positive displacement pumps offer minimum NPSH operation and variable flow capability	Demonstrate low NPSH operation and variable flow	Design, fabricate and test positive displacement pump with LH_2, CH_4

SECTION IV

PARAMETRIC DATA

A. OBJECTIVES AND GUIDELINES

Engine system performance, envelope, and weight parametric data were generated in this task for selected dual-fuel dual-throat engine power cycles. The system weight is based on 1978 state-of-the-art. Improvement in engine weight is predicted through 1995, depending upon the types of materials available in this time span.

The parametric data cover the ranges shown in Figure 3.

Parametric vehicle performance data generated on an ALRC in-house effort were used in assessing the merits of the various engine cycles. These data are summarized and included in this section,,

B. ENGINE PERFORMANCE

The dual throat performance methodology used for this analysis incorporates the same procedures described in the cold flow data final report (Ref. 7). This appraoch, used for both Modes I and II, is based upon the simplified JANNAF performance prediction procedures given in Ref. (11).

1. Methodology

The first step is to determine the one-dimensional equilibrium specific impulse (Isp_{ODE}) which is a function of propellant combination and mixture ratio (MR), nozzle area ratio (ε), chamber pressure (PC), and the propellant temperature (tank conditions). Isp_{ODE} data were obtained using the TDK Program (Ref. 12) and tabulated covering the range of conditions (Pc, MR, ε) for this analysis. These data are programmed in the form of subroutines in the performance analysis program as a function of the propellant combination (LOX/RP-1, LOX-H_2, or LOX-CH_4), mixture ratio, chamber pressure and area ratio.

The predicted delivered specific impulse (Isp_{Pred}) is obtained by calculating the efficiency from the known loss mechanisms that degrade the ideal (Isp_{ODE}) performance. For this analysis these loss mechanisms were divided into four categories; energy release efficiency (η_{ERE}), reaction kinetics efficiency (η_K), two-dimensional nozzle divergence efficiency (η_{2D}), and loss due to the thrust decrement within the boundary layer.

It should be noted that in calculating the predicted Isp for the dual throat engine which normally utilizes two flow streams (primary and secondary) the overall engine Isp_{ODE} is based upon a mass-average of the two stream tube Isp_{ODE} values. These streamtube Isp_{ODE} values are calculated based upon the conditions (MR, Pc, area ratio, and propellant combination) for each flow stream. For the Mode II analysis presesnted herein the bleed flow or secondary flow was assumed to be combustion products burned at the same conditions (MR and Pc) as in the primary chamber yielding the same Isp_{ODE} value for both streamtubes. The use of hydrogen only for the bleed flow does not appear feasible because it would result in significantly higher hydrogen propellant usage for the engine, which would adversely affect the vehicle tankage requirements.

The energy release efficiencies used for this analysis were established to be consistent with similar studies; i.e., η_{ERE} is 98% for LOX/RP-1 and LOX/CH_4 and 99% for LOX/H_2.

The kinetic efficiency was obtained by comparing the one-dimensional kinetics specific impulse (Isp_{ODK}) to the Isp_{ODE}

(η_K = Isp_{ODK}/Isp_{ODE}). The Isp_{ODK} values were also obtained through calculations using the ODK computer program.

The two-dimensional efficiency for Mode I was obtained from charts which give the η_{2D} for optimum Rao nozzles as described in Ref. (13) and (14). These charts were tabularized to facilitate their use in the performance program.

Because of the gap or free boundary region present in the Mode II nozzle profile, the above method for obtaining the Mode II η_{2D} is not complete. Several Mode II nozzle contours comprising the primary nozzle, the free expansion region and the secondary nozzle from the point of attachment were input into the TDK (Ref. 12) program to obtain a composite nozzle divergence efficiency. Subsequent comparisons revealed that the η_{2D} values obtained with the TDK program were approximately 0.5% lower than those obtained using the charts for the conventional Rao nozzles of the same area ratio. The TDK program was unable to complete many of the nozzle calculations because of the non-uniformity of some Mode II composite nozzles. In an attempt to deal with this potential error and to facilitate the performance calculation procedures for this analysis, the Mode II divergence efficiency was obtained by subtracting 0.5% from the η_{2D} value corresponding to an optimum Rao nozzle of the same area ratio.

The Mode I boundary layer loss was obtained using the BLPL computer program developed at ALRC which is an implementation of the turbulent boundary layer chart procedures given in Ref. (14).

The Mode II boundary layer loss was also obtained using the BLPL program but with some additional consideration to the aerodynamics associated with Mode II operation. The primary assumptions for this calculation is that the boundary thrust decrement is additive and proportional to the momentum thickness. The boundary layer loss was obtained using the BLPL program for a conventional Rao nozzle having an area ratio defined by the point of plume attachment and the primary throat. A ratio of the boundary layer momentum thickness (at the point of attachment given by the base flow aerodynamics program) to the momentum thickness (given by the BLPL program) was used to proportion the conventional nozzle boundary layer loss to approximate the actual thrust loss due to the plume shear layer. This loss was added to the boundary layer loss obtained for the nozzle from the attachment point to the secondary nozzle exit, yielding the total Mode II boundary layer loss.

Another condition inherent with the dual throat engine is the possibility of a normal shock in the primary nozzle during the Mode I parallel burn operation. Because of the relative high back pressure or secondary chamber pressure at the primary nozzle exit, the supersonic flow in the primary nozzle must pass through a normal shock to equalize the static pressures. While the existence of this normal shock does not represent a loss in engine performance, it does produce an additional pumping loss equal to the loss of stagnation presure across the shock. This reduced stagnation chamber pressure msut be used to properly size the primary flow component (stream tube) in the secondary throat area for the Mode I, parallel burn operation. A one-dimensional, normal shock approximation is used to account for this change in stagnation presure in order to more precisely predict the dual throat Mode I engine operating characteristics.

Another approach was investigated to arrive at an effective stagnation presure. This approach utilized the solution of the energy, continuity and momentum equations in the manner solved for an ejector. In this approach, there is a stagnation pressure loss in the primary stream and a stagnation pressure gain in the secondary (pumped) stream. Since the efficiency of the momentum exchange for the dual throat configuration is not known, this approach was not adopted. The true effective pressure for the system probably lies between the conservative value calculated using the shock relations and the optimistic value calculated for an efficient ejector.

2. Parametric Analysis Results

A total of 22 different cases were analyzed during this performance parameter study. The parameters evaluated in the analysis are: the primary nozzle area ratio, nozzle separation distance, thrust level, stream-tube thrust split, optimum expansion, chamber pressure, mixture ratio and propellant combination. These cases and the terminology are described in Figure 61 and Table XVIII. Table XIX is a listing of the intermediate values necessary to obtain the Mode II boundary layer loss as described earlier. Table XX is a summary of the Mode II performance parameters for each of the 22 cases analyzed. A trace of the computer generated plot of the baseline case engine (Case #1 Table XVIII) is given in Figure 62. Figures 63 through 78 are a summary of the major variables considered in this analysis.

The effects of the primary nozzle variations are plotted in Figures 63 and 64. A high degree of sensitivity exists between the primary nozzle area ratio and the percent bleed required to minimize the shock (see Figure 63). The primary nozzle area ratio only slightly affects the engine Isp efficiency (Figure 64). The same effects are evident for the nozzle separation variations plotted in Figures 65 and 66.

The variation in Isp efficiency and engine geometry with Mode I thrust is given in Figures 67 and 68.

The effects of the Mode I to Mode II vacuum thrust ratio on Isp

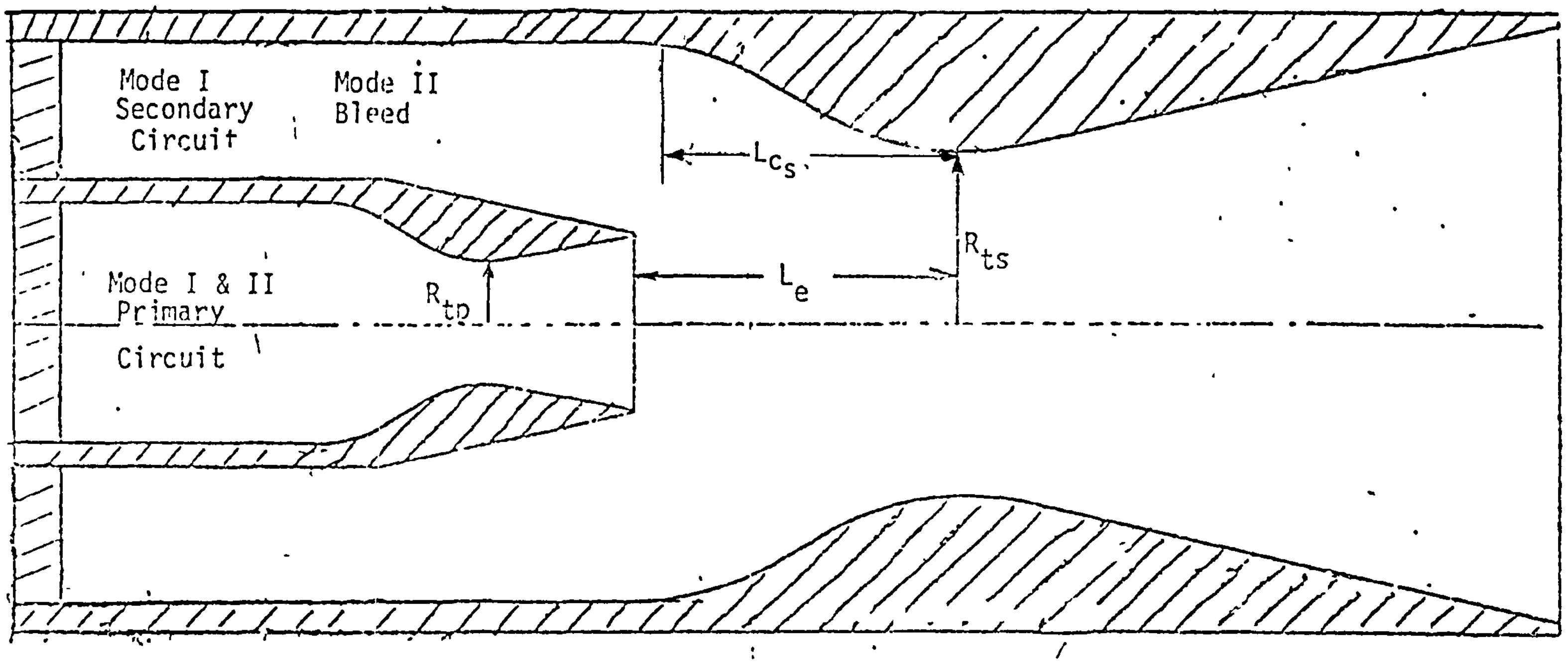

OPERATING MODES

MODES	PRIMARY	SECONDARY
I - SEA LEVEL SERIES BURN	0	100%
I - SEA LEVEL PARALLEL BURN	~20-30%	~70-80%
II - ALTITUDE	~90-100%	0-10%

Figure 61. Dual Throat Terminology

TABLE XVIII

DUAL THROAT PARAMETRIC PERFORMANCE CASES

MODE I (PARALLEL SERIES) & MODE II

CASE	F1SL	FRATIO	PCP	PCS	MRP	MRS	SECONDARY FUEL	COMMENTS
1	600K	2.4	3000	2100	7.0	2.8	RP1	Baseline
2	600K	2.4	3000	2100	7.0	2.8	RP1	Smaller ϵ_p
3	600K	2.4	3000	2100	7.0	2.8	RP1	Larger ϵ_p
4	600K	2.4	3000	2100	7.0	2.8	RP1	Smaller L_e
5	600K	2.4	3000	2100	7.0	2.8	RP1	Larger L_e
6	600K	2.4	3000	2100	7.0	2.8	RP1	Smaller ϵ_s
7	600K	2.4	3000	2100	7.0	2.8	RP1	Smaller ϵ_s
8	600K	2.4	1400	1000	7.0	2.8	RP1	
9	600K	2.4	5000	3500	7.0	2.8	RP1	
10	600K	1.2	3000	2100	7.0	2.8	RP1	
11	600K	5.0	3000	2100	7.0	2.8	RP1	
12	600K	2.4	3000	2100	5.0	2.8	RP1	
13	600K	2.4	3000	2100	6.0	2.8	RP1	
14	600K	2.4	3000	2100	7.0	2.0	RP1	
15	600K	2.4	3000	2100	7.0	3.5	RP1	
16	600K	2.4	3000	2100	7.0	3.5	CH_4	
17	600K	2.4	1400	1000	7.0	3.5	CH_4	
18	600K	2.4	5000	3500	7.0	3.5	CH_4	
19	600K	1.2	3000	2100	7.0	3.5	CH_4	
20	600K	5.0	3000	2100	7.0	3.5	CH_4	
21	200K	2.4	3000	2100	7.0	2.8	RP1	
22	2M	2.4	3000	2100	7.0	2.8	RP1	

F1SL = Mode 1 Sea Level Thrust, lbf
FRATIO = Mode 1 to Mode 2 Vacuum Thrust Ratio
PCP = Primary Chamber Pressure, psi
PCS = Secondary Chamber Pressure, psi
MRP = Primary Chamber Mixture Ratio
MRS = Secondary Chamber Mixture Ratio

TABLE XIX

DUAL THROAT MODE II BOUNDARY LAYER LOSS CALCULATION

CASE	ϵ_{II}	$\Delta BL_{(1)}$	MOMENTUM THICKNESS RATIO	$\Delta BL'_{(1)}$	$\Delta BL_{(2)}$	TOTAL ΔBL
1	165.3	.71	4.5	3.2	1.7	4.9
2	161.5	.68	5.2	3.5	1.7	5.2
3	169.8	.76	3.6	2.7	1.7	4.4
4	165.3	.71	3.2	2.3	1.7	4.0
5	165.3	.71	5.5	3.9	1.7	5.6
6	70.5	.73	4.5	3.3	1.3	4.6
7	95.6	.73	4.5	3.3	1.5	4.8
8	89.8	.76	2.5	1.9	1.4	3.3
9	250.9	.68	4.7	3.2	1.9	5.1
10	83.5	.30	9.8	2.9	1.6	4.5
11	346.1	1.15	2.4	2.7	2.0	4.7
12	155.4	.74	4.4	3.3	1.7	5.0
13	160.3	.73	4.4	3.2	1.7	4.9
14	163.8	.73	4.2	3.1	1.7	4.8
15	165.7	.71	4.5	3.2	1.7	4.9
16	168.8	.71	4.4	3.2	1.8	5.0
17	91.4	.76	3.9	3.0	1.4	4.4
18	256.4	.68	4.9	3.3	1.9	5.2
19	84.0	.30	9.8	2.9	1.6	4.5
20	356.0	1.15	2.4	2.7	2.0	4.7
21	165.2	.80	4.3	3.4	1.9	5.3
22	164.4	.63	4.7	3.0	1.6	4.6

$\Delta BL_{(1)}$ = Specific impulse loss up to plume attachment, seconds

Momentum Thickness Ratio = Shear layer momentum thickness divided by nozzle boundary layer momentum thickness corresponding to same area ratio as point of plume attachment.

$\Delta BL'_{(1)}$ = $BL_{(1)}$ x momentum thickness ratio, seconds

$\Delta BL_{(2)}$ = Specific impulse loss from secondary throat to secondary exit, seconds

Total ΔBL = Total Mode II boundary layer loss due to drag, seconds

TABLE XX

DUAL THROAT MODE II PERFORMANCE ANALYSIS

Propellants = O_2/H_2

Case	Pc	MR	ϵ_{II}	Isp_{ODE}	η_{2D}	ΔBL	Delivered Isp	Dual Throat Loss,%	ϵ_p	Le/Rt_p	% Bleed	Secondary Fuel
1	3000	7 0	165 3	472 8	9915	4 9	459 2	1 02	1 77	2 301	4 26	RP1
2	3000	7 0	161 5	472 5	9911	5 2	458 3	1 10	1 23	2 370	7 56	RP1
3	3000	7 0	169 8	473 2	9917	4 4	460 1	0 93	2 54	2 200	2 00	RP1
4	3000	7 0	165 3	472 8	9915	4 0	460 0	0 85	1 77	1 726	2 32	RP1
5	3000	7 0	165 3	472 8	9915	5 6	458 4	1 18	1 77	2 876	5 95	RP1
6	3000	7 0	70 5	458 4	9903	4 6	444 8	1 05	1 80	2 322	4 47	RP1
7	3000	7 0	95 6	464 3	9914	4 8	451 0	1 04	1 79	2 314	4 40	RP1
8	1400	7 0	89 8	462 0	9911	3 3	450 0	72	1 77	1 482	1 41	RP1
9	5000	7 0	250 9	479 1	9905	5 1	464 7	1 01	1 75	2 354	4 12	RP1
10	3000	7 0	83 5	461 6	9912	4 5	448 4	1 06	1 01	1 624	2 78	RP1
11	3000	7 0	346 1	482 6	9905	4 7	468 1	83	4 07	3 247	1 39	RP1
12	3000	5 0	155 4	474 9	9912	5 0	461 0	1 04	1 70	2 257	4 02	RP1
13	3000	6 0	160 3	475 5	9914	4 9	461 7	1 00	1 73	2 280	4 09	RP1
14	3000	7 0	163 8	472 7	9915	4 8	459 1	98	1 84	2 328	3 79	RP1
15	3000	7 0	165 7	472 9	9915	4 9	459 2	1 00	1 75	2 290	4 16	RP1
16	3000	7 0	168 8	473 1	9915	5 0	459 3	98	1 76	2 295	4 23	CH_4
17	1400	7 0	91 4	462 3	9912	4 4	449 2	97	1 78	2 228	3 69	CH_4
18	5000	7 0	256 4	479 3	9905	5 2	464 8	1 05	1 75	2 357	4 10	CH_4
19	3000	7 0	84 0	461 8	9913	4 5	448 7	1 03	1 01	1 622	2 78	CH_4
20	3000	7 0	356 0	482 9	9906	4 7	468 8	74	4 06	3 253	1 38	CH_4
21	3000	7 0	165 2	472 8	9916	5 3	458 1	1 05	1 77	2 467	4 76	RP1
22	3000	7 0	165 4	472 8	9914	4 6	459 4	1 02	1 76	2 200	3 69	RP1

Pc = Chamber Pressure, psi

MR = Mixture Ratio, O/F

ϵ_{II} = Mode II Area Ratio, Ae_s/At_p

Isp_{ODE} = ODE Specific Impulse, Seconds

η_{2D} = Nozzle Divergence Efficiency

ΔBL = Boundary Layer - Drag Performance Loss

Delivered Isp = Predicted Performance, Sec

Dual Throat Loss = Difference in Isp Efficiency Between Conventional and Dual Throat Mode II Nozzle

ϵ_p = Primary Nozzle Area Ratio, Ae_p/At_p

Le/Rt_p = Normalized Nozzle Separation Distance (Primary Exit to Secondary Throat Divided by Rt_p)

% Bleed = % of Total Mode II Flow Used for Bleed

$Isp_{Delivered} = Isp_{ODE} * \eta_K * \eta_{ERE} * \eta_{2D} - \Delta BL$

Where η_K = Kinetic Efficiency = 9999

η_{ERE} = Energy Release Efficiency = 99

η_{2D} = η_{2D} of Conventional Minus 5%

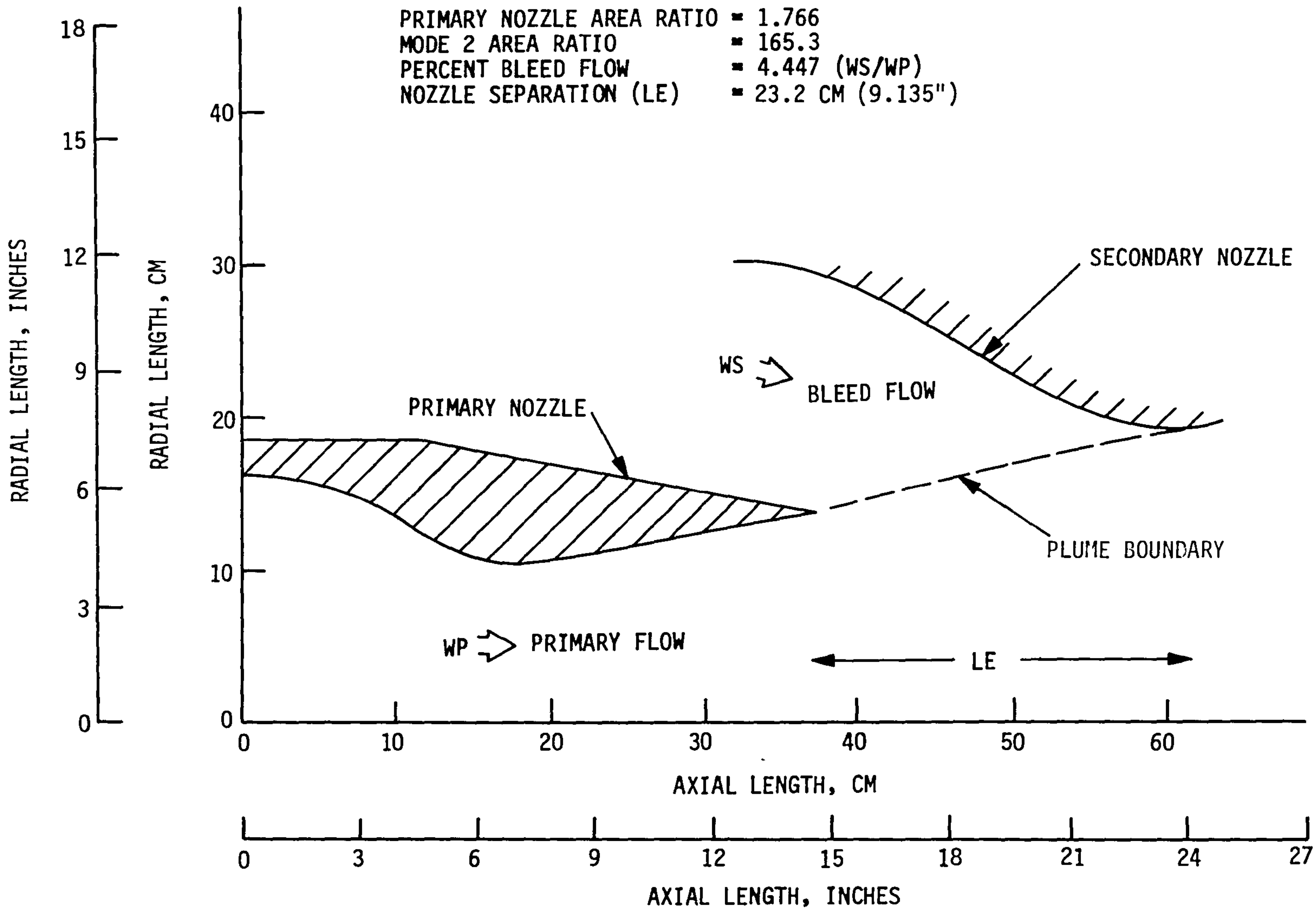

Figure 62. Dual Throat Preliminary Analysis - Case IA

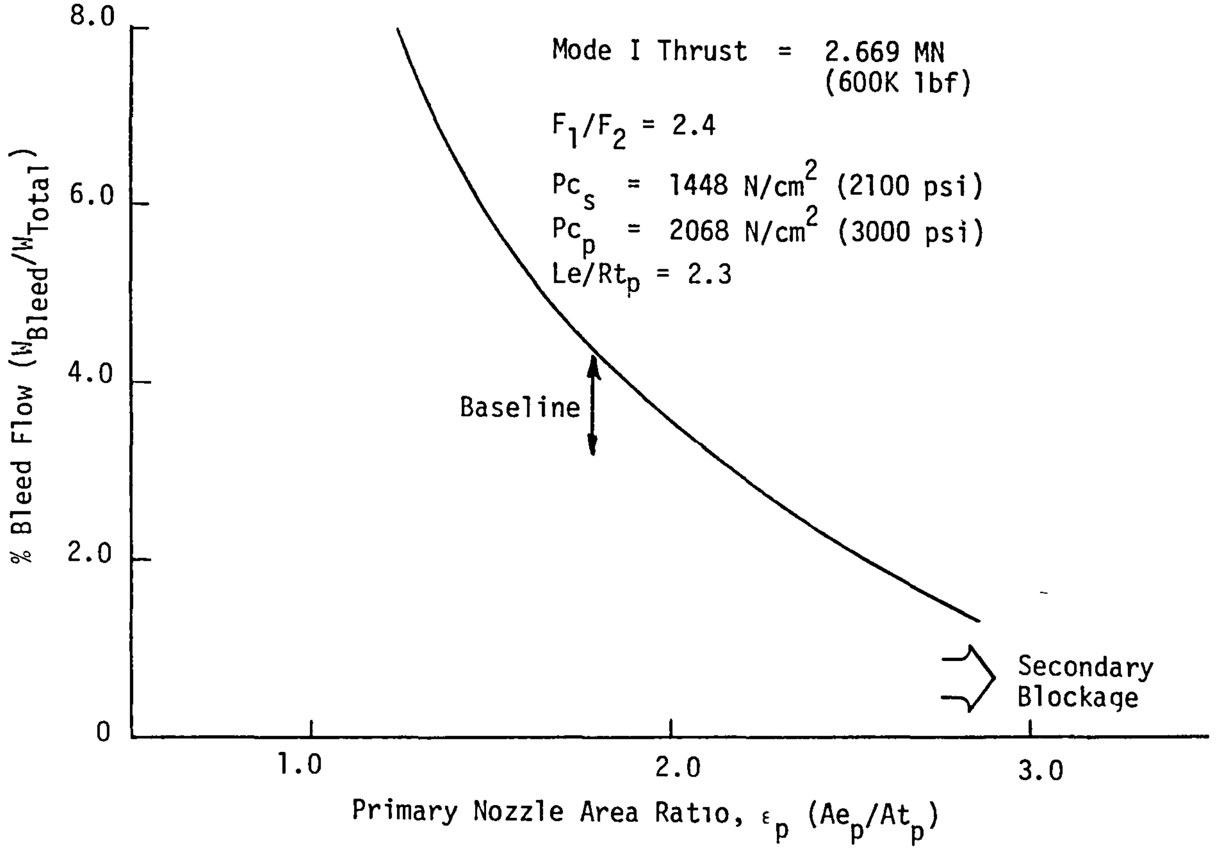

Figure 63. % Bleed Flow vs. Primary Nozzle Area Ratio

Mode I Thrust = 2.699 M N (600K lbf)

F_1/F_2 = 2.4

Pc_s = 1448 N/cm^2 (2100 psi); MR_s = 2.8 (RP1)

Pc_p = 2068 N/cm^2 (3000 psi); MR_p = 7.0 (H_2)

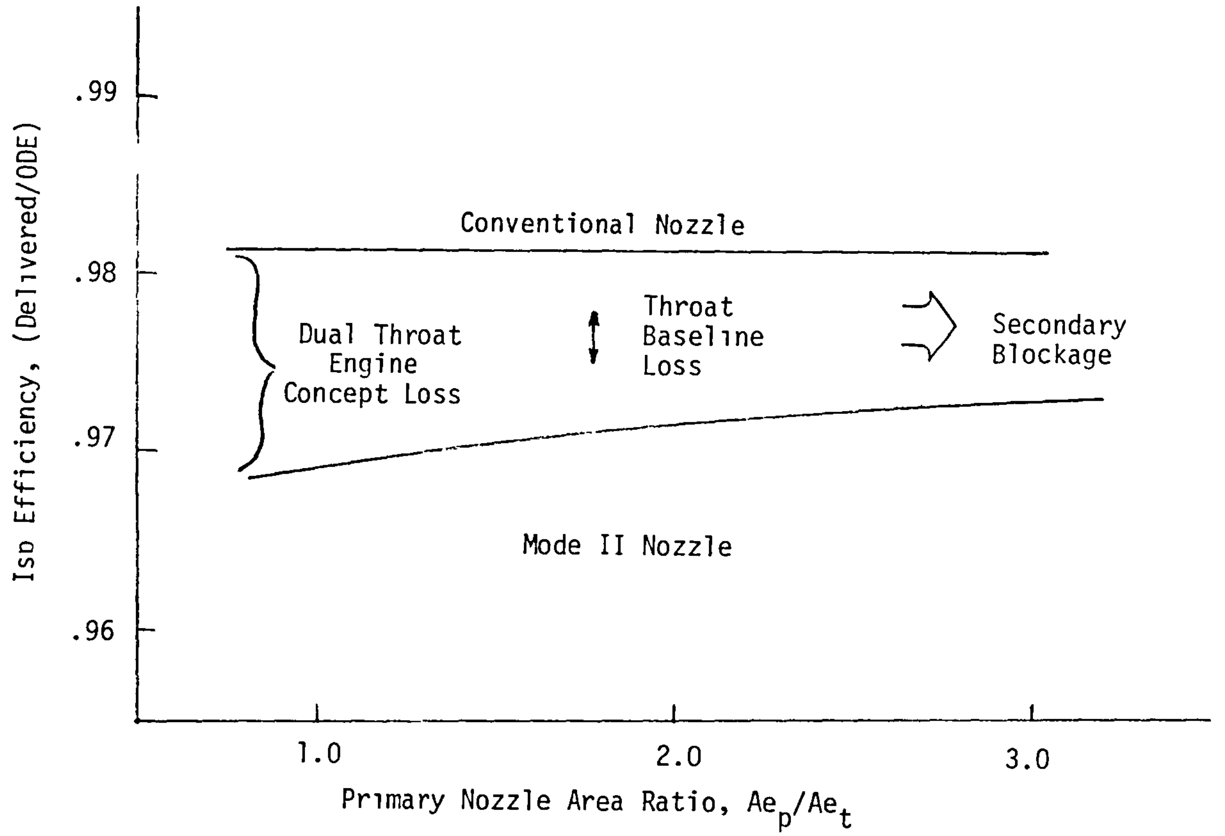

Figure 64. Mode II Isp Efficiency vs. Primary Nozzle Area Ratio

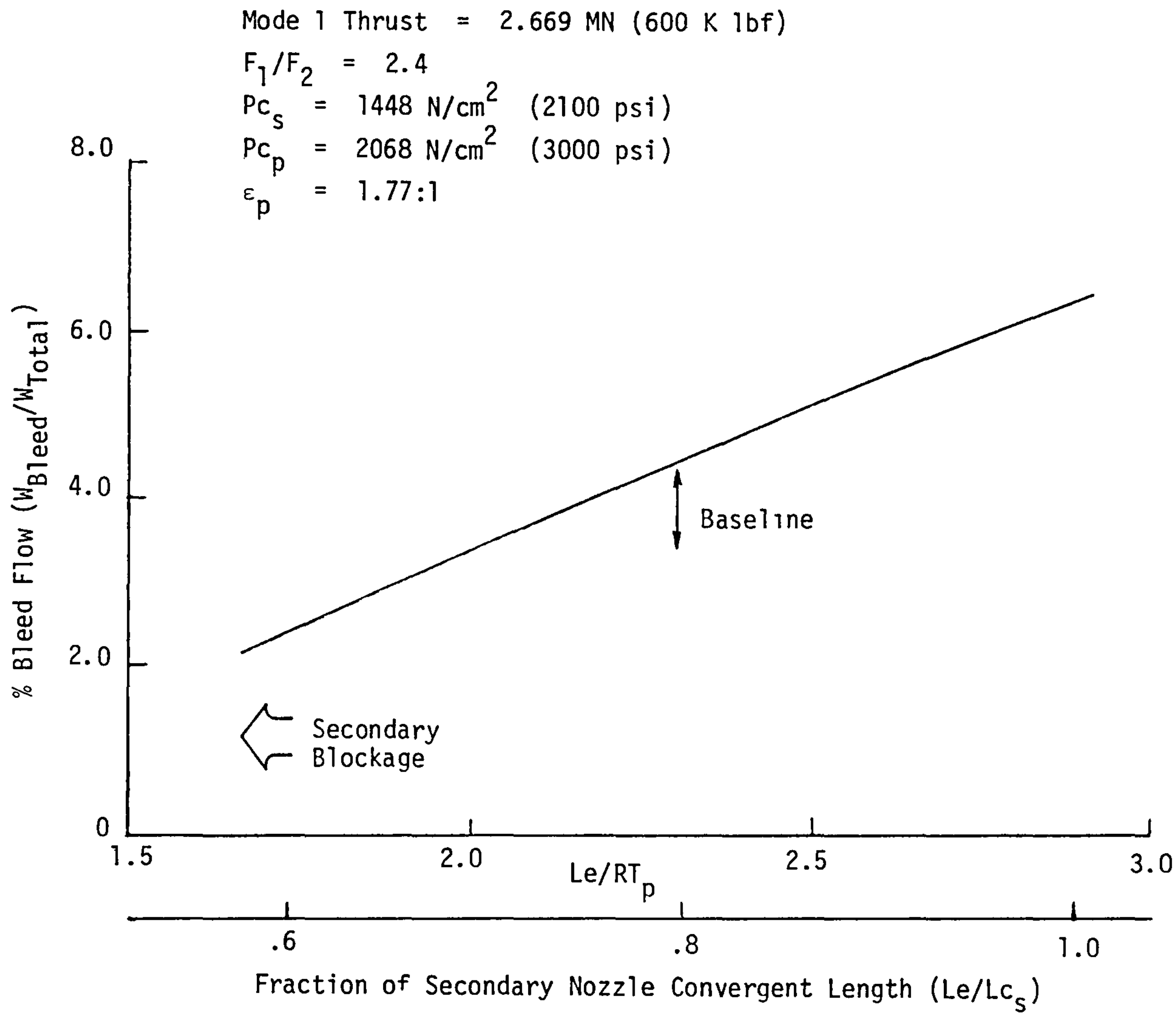

Figure 65. Percent Bleed Flow vs. Nozzle Separation Distance

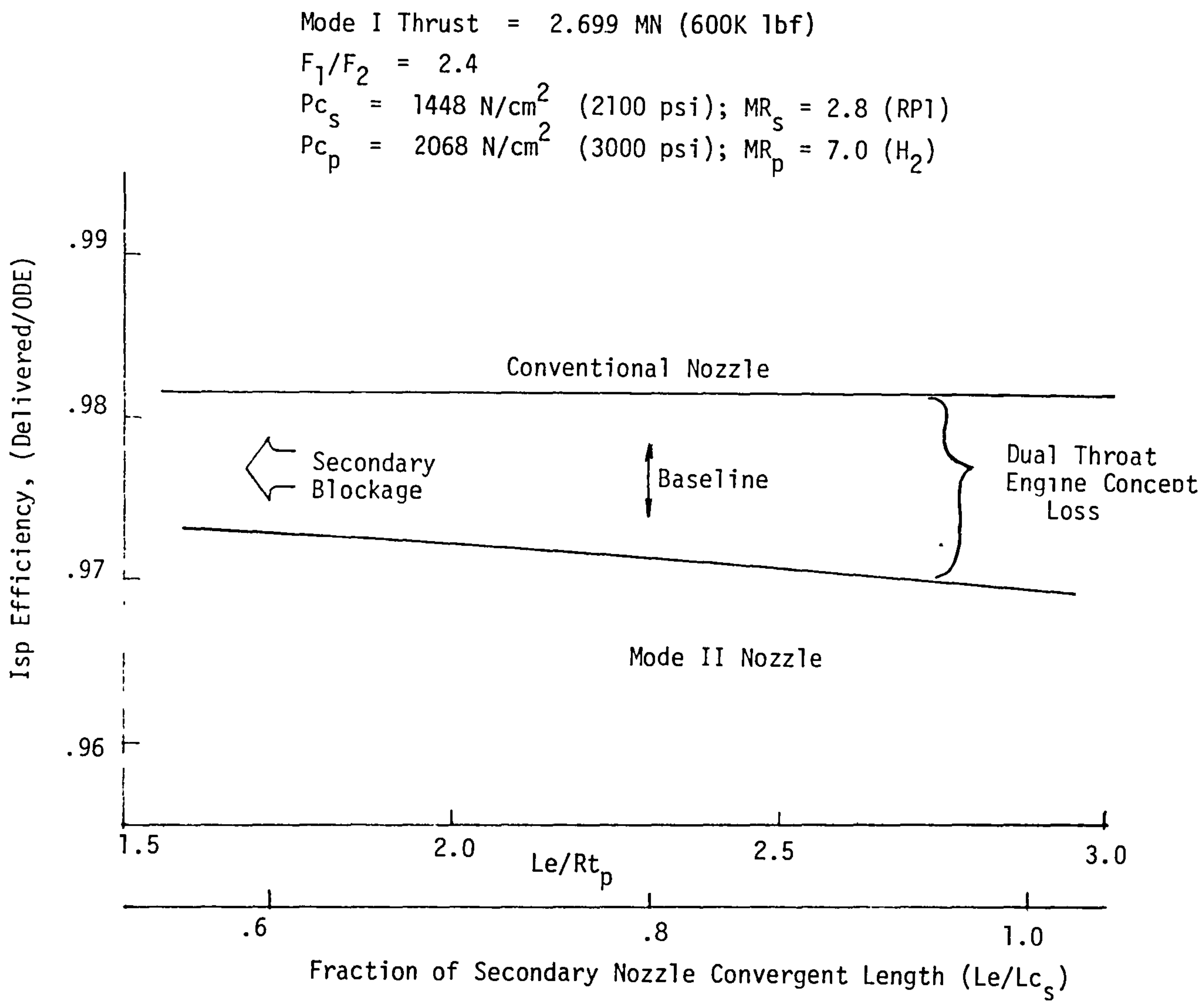

Figure 66. Mode II Isp Efficiency vs. Nozzle Separation Distance

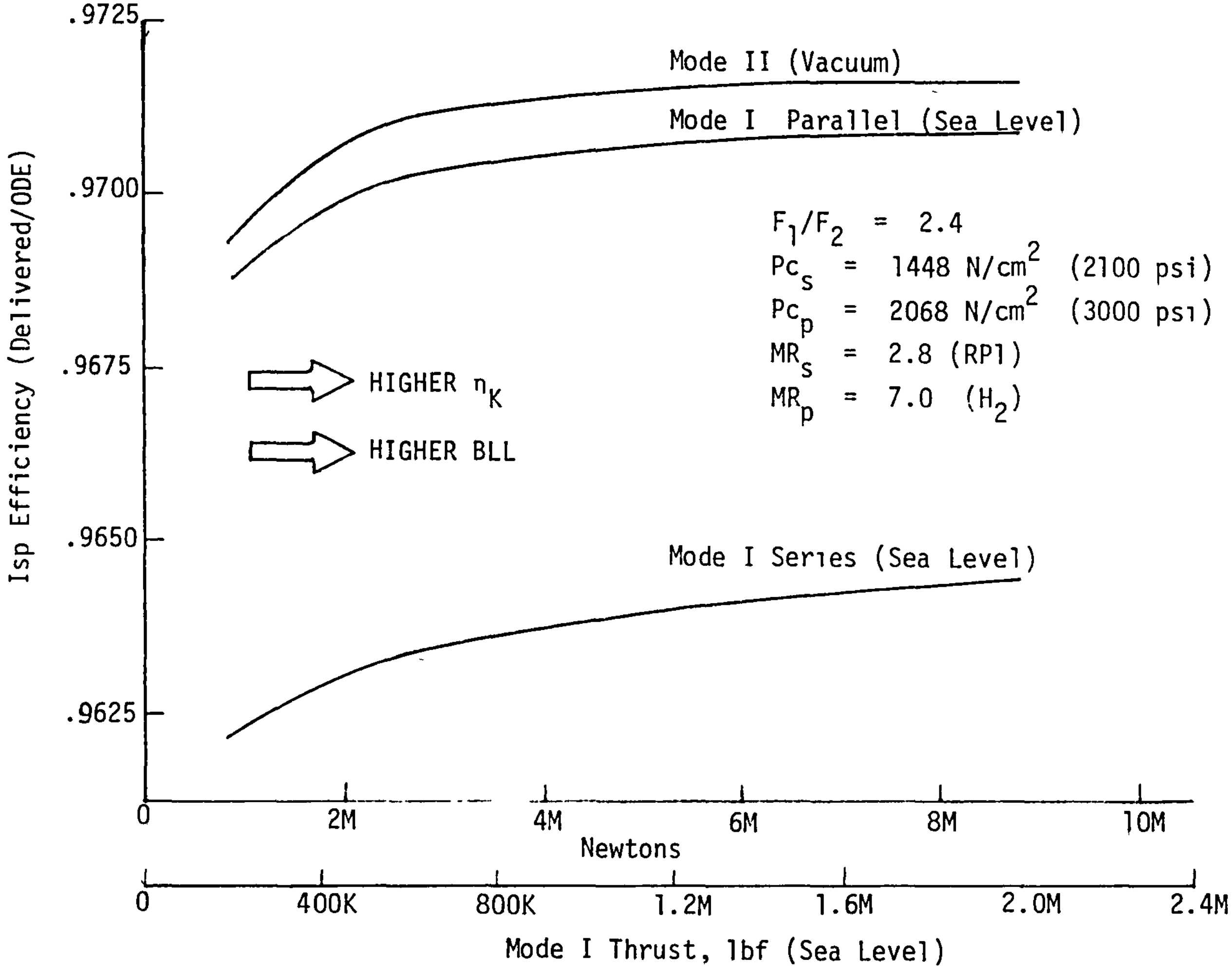

Figure 67. Isp Efficiency vs. Mode I Thrust Level

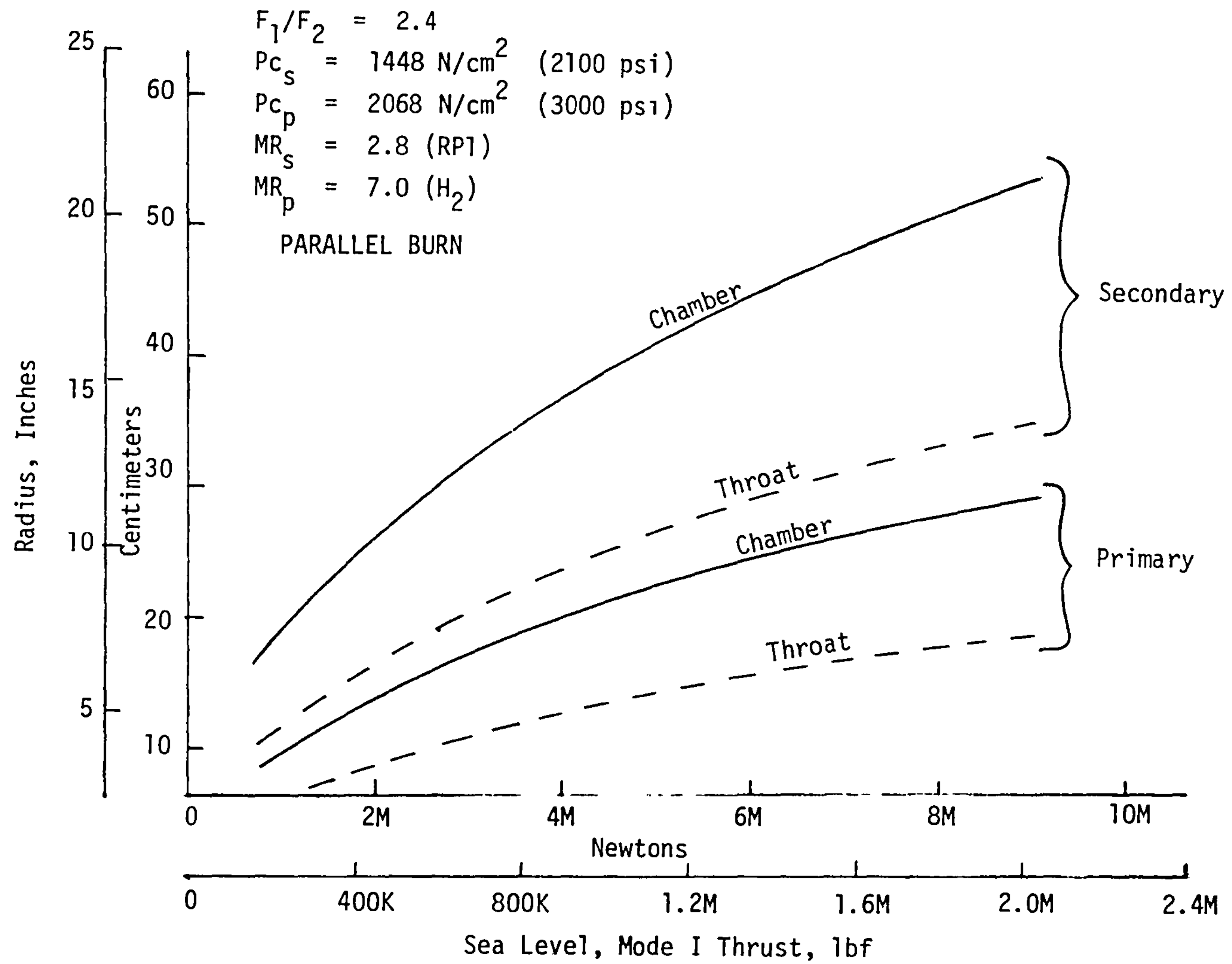

Figure 68. Dual Throat Engine Throat and Chamber Radius as a Function of Mode I Thrust

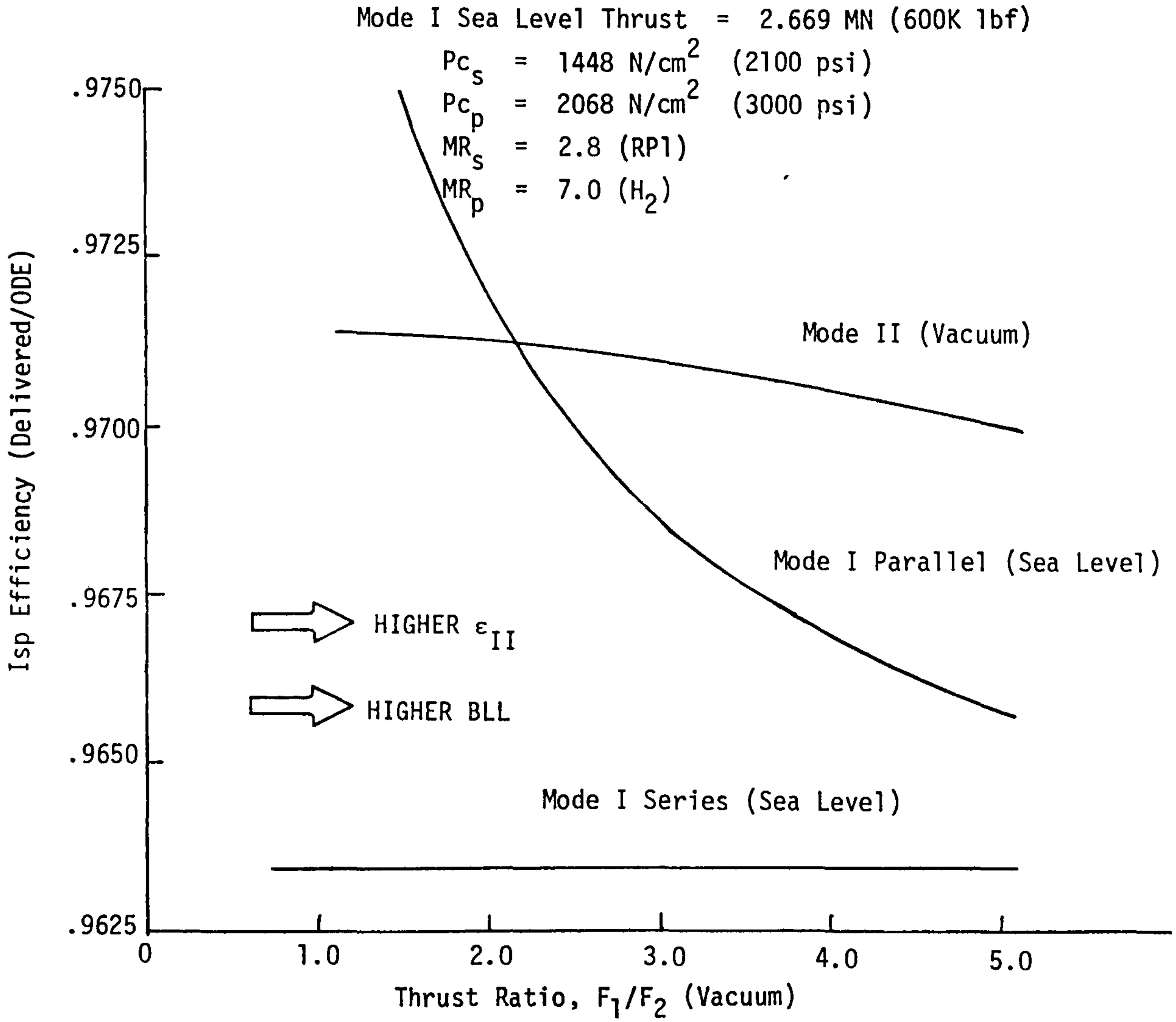

Figure 69. Isp Efficiency vs. Thrust Ratio

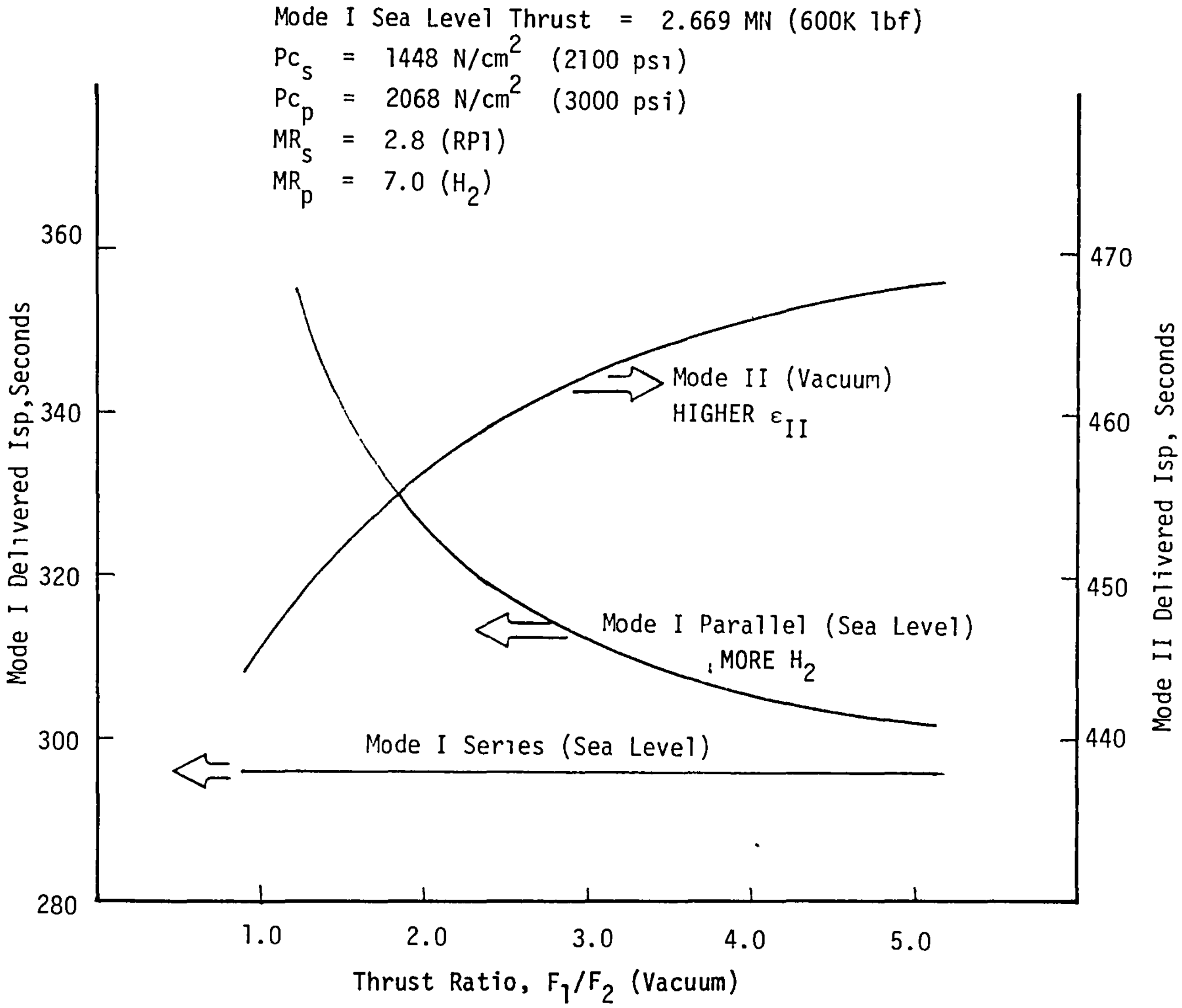

Figure 70. Delivered Isp vs. Thrust Ratio

Mode I Sea Level Thrust = 2.669 MN (600K lbf)

Pc_s = 1448 N/cm^2 (2100 psi)

Pc_p = 2068 N/cm^2 (3000 psi)

MR_s = 2.8 (RP1)

MR_p = 7.0 (H_2)

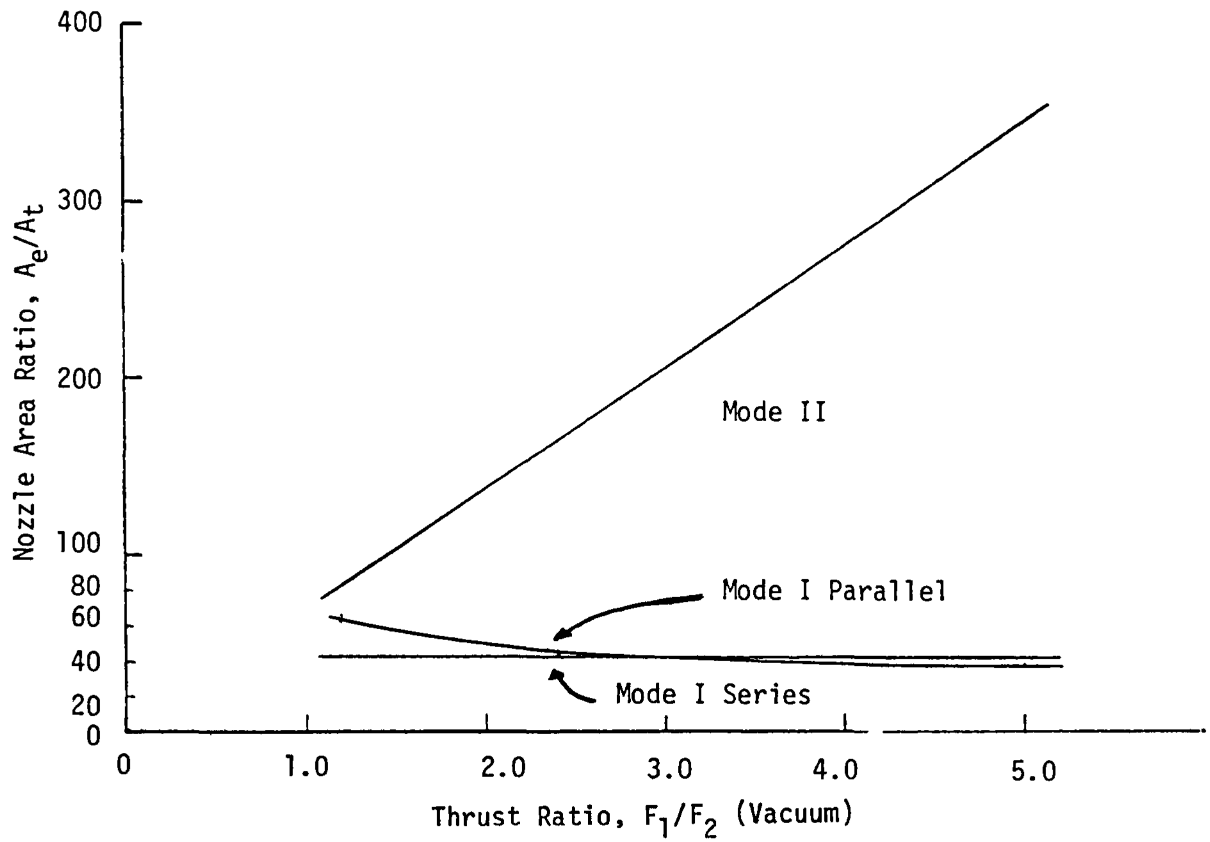

Figure 71. Nozzle Area Ratio vs. Thrust Ratio

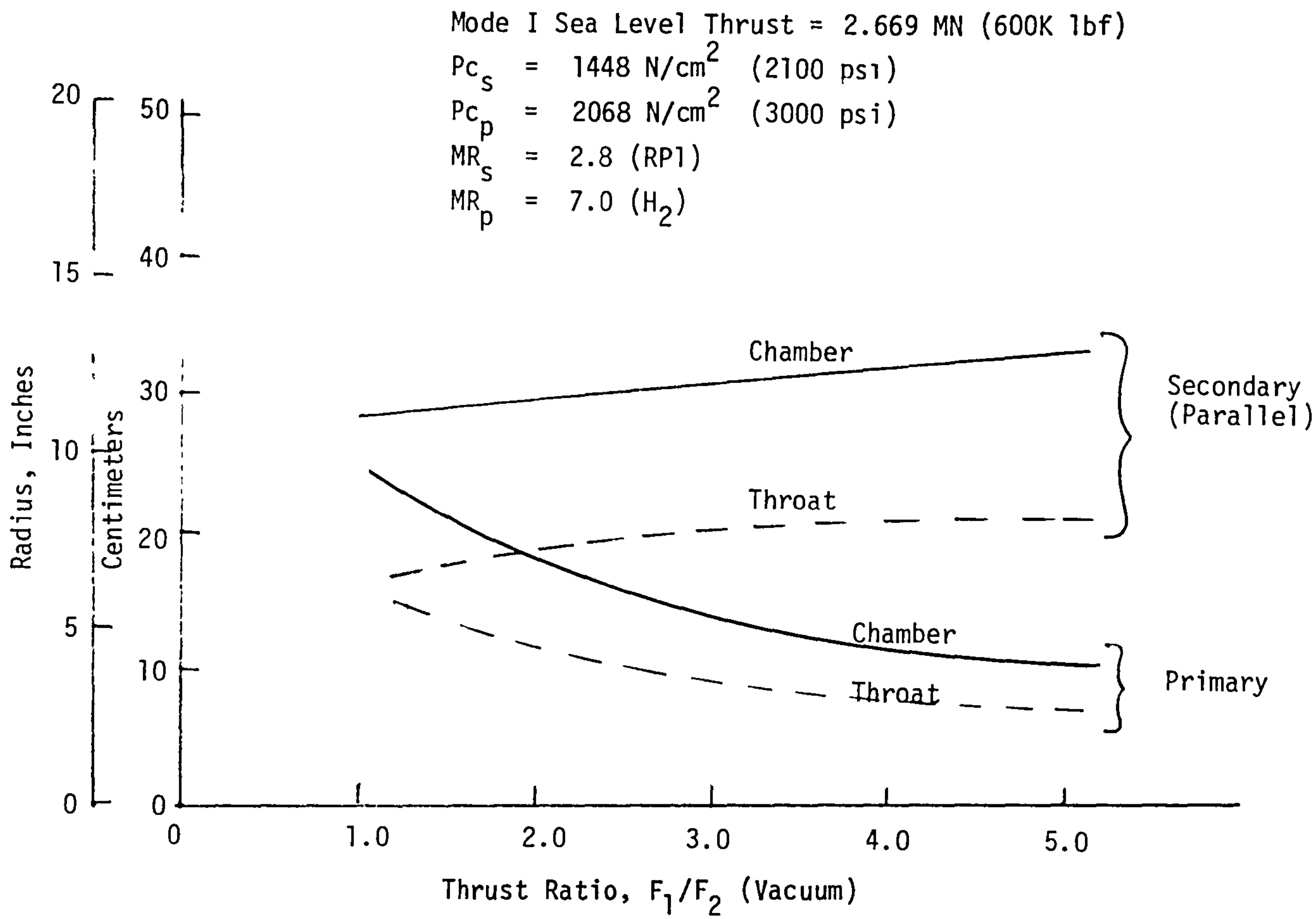

Figure 72. Dual Throat Engine Throat and Chamber Radius as a Function of Thrust Ratio

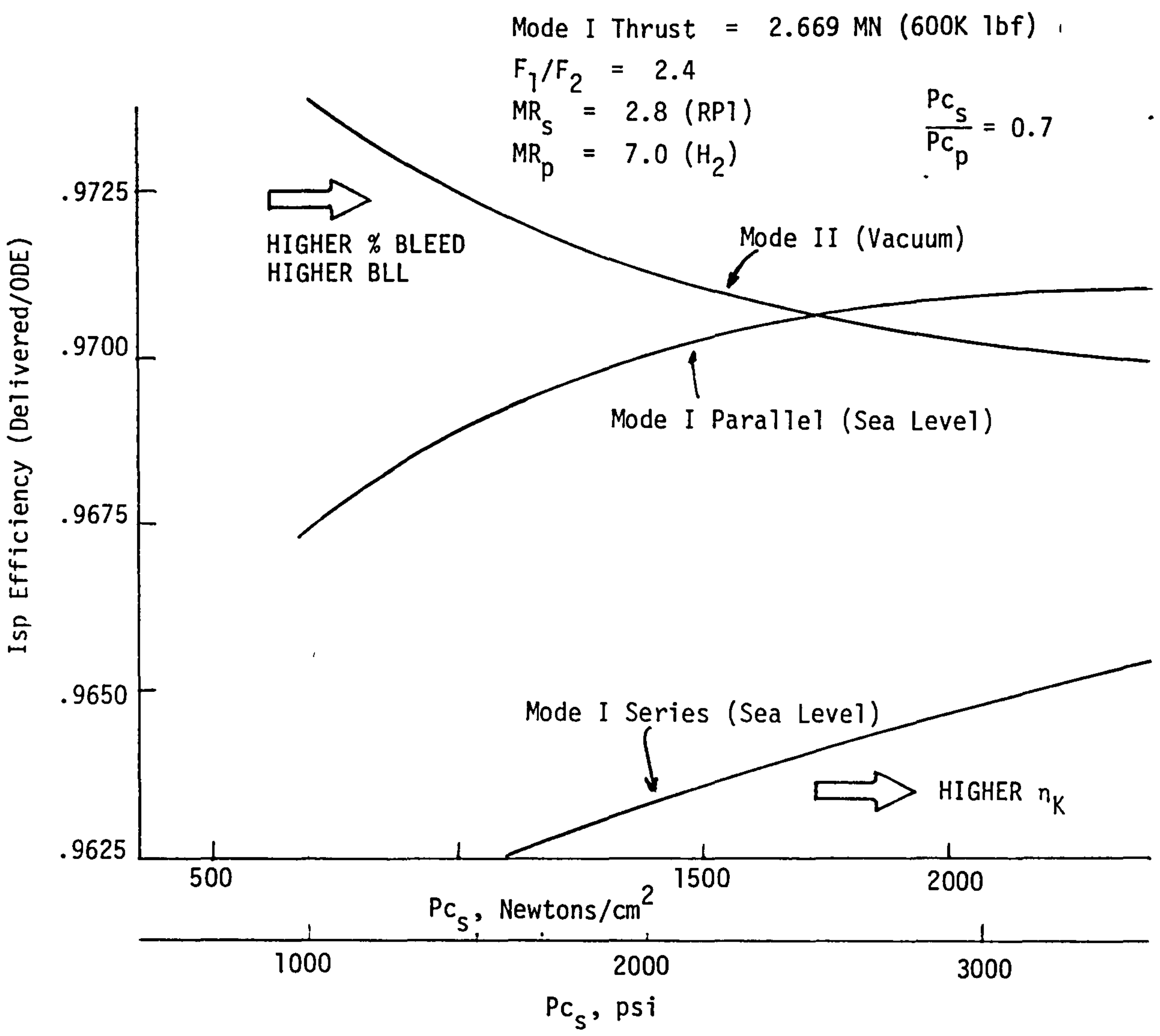

Figure 73. Isp Efficiency vs. Chamber Pressure

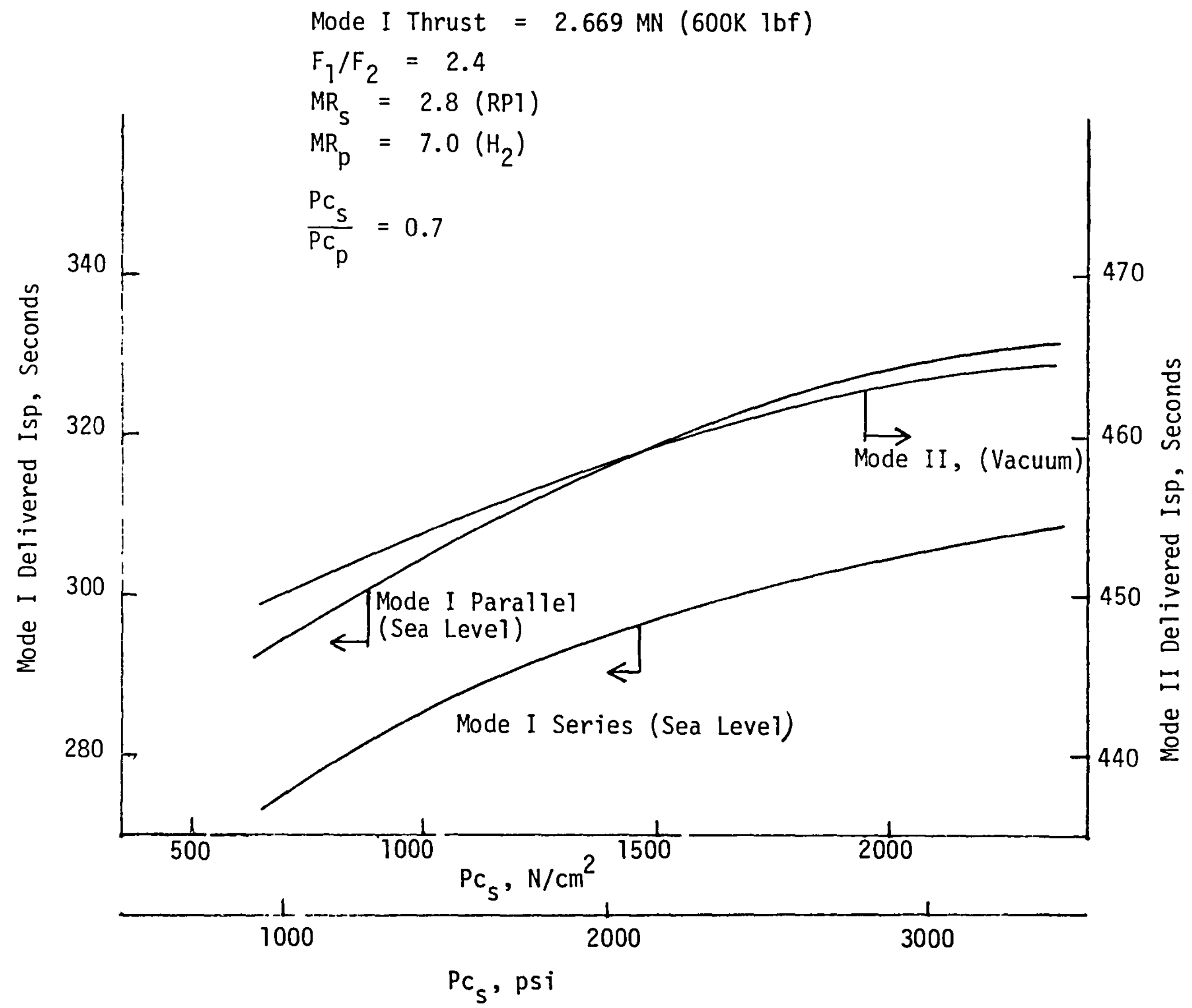

Figure 74. Delivered Isp vs. Chamber Pressure

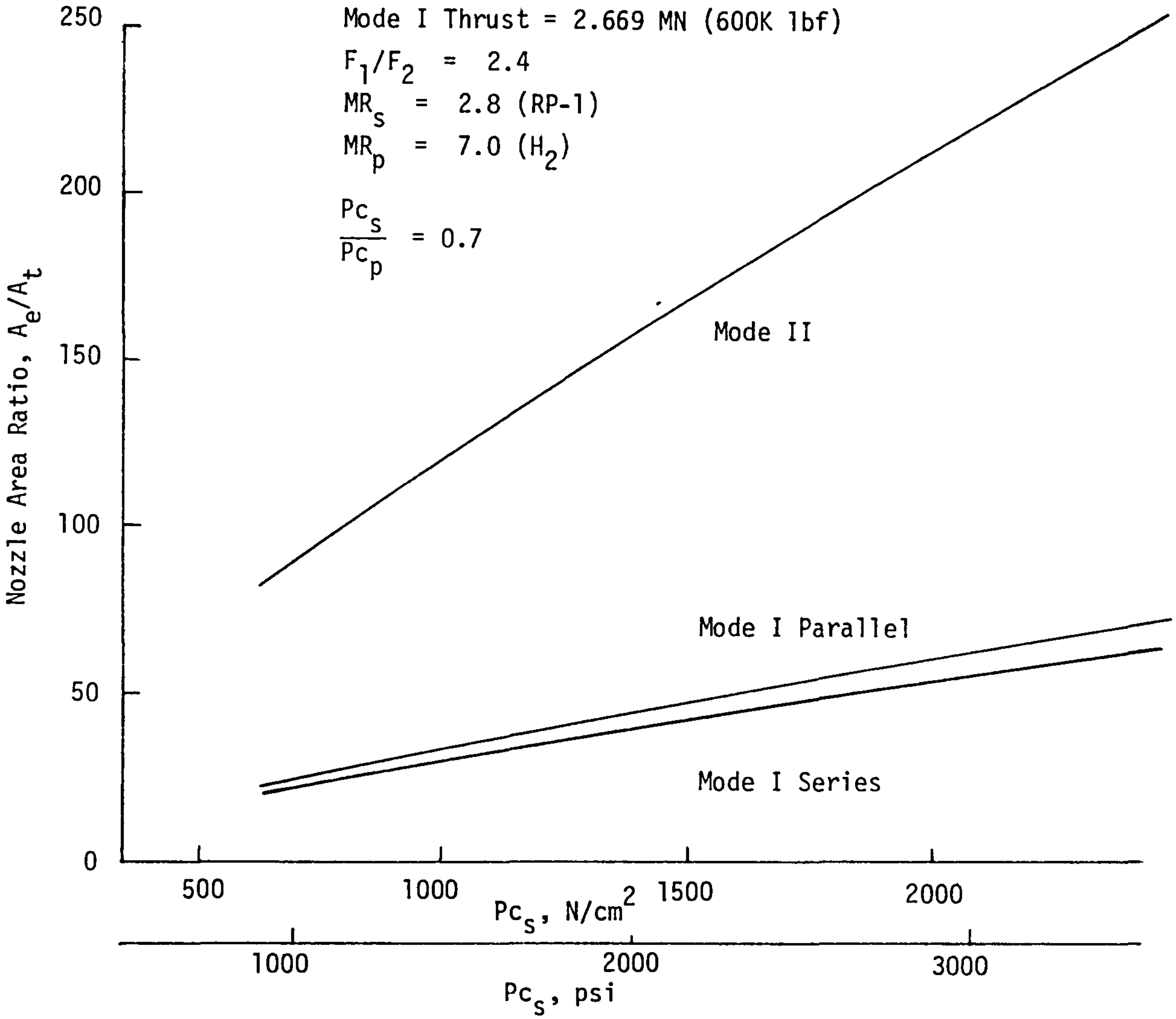

Figure 75. Nozzle Area Ratio vs. Chamber Pressure

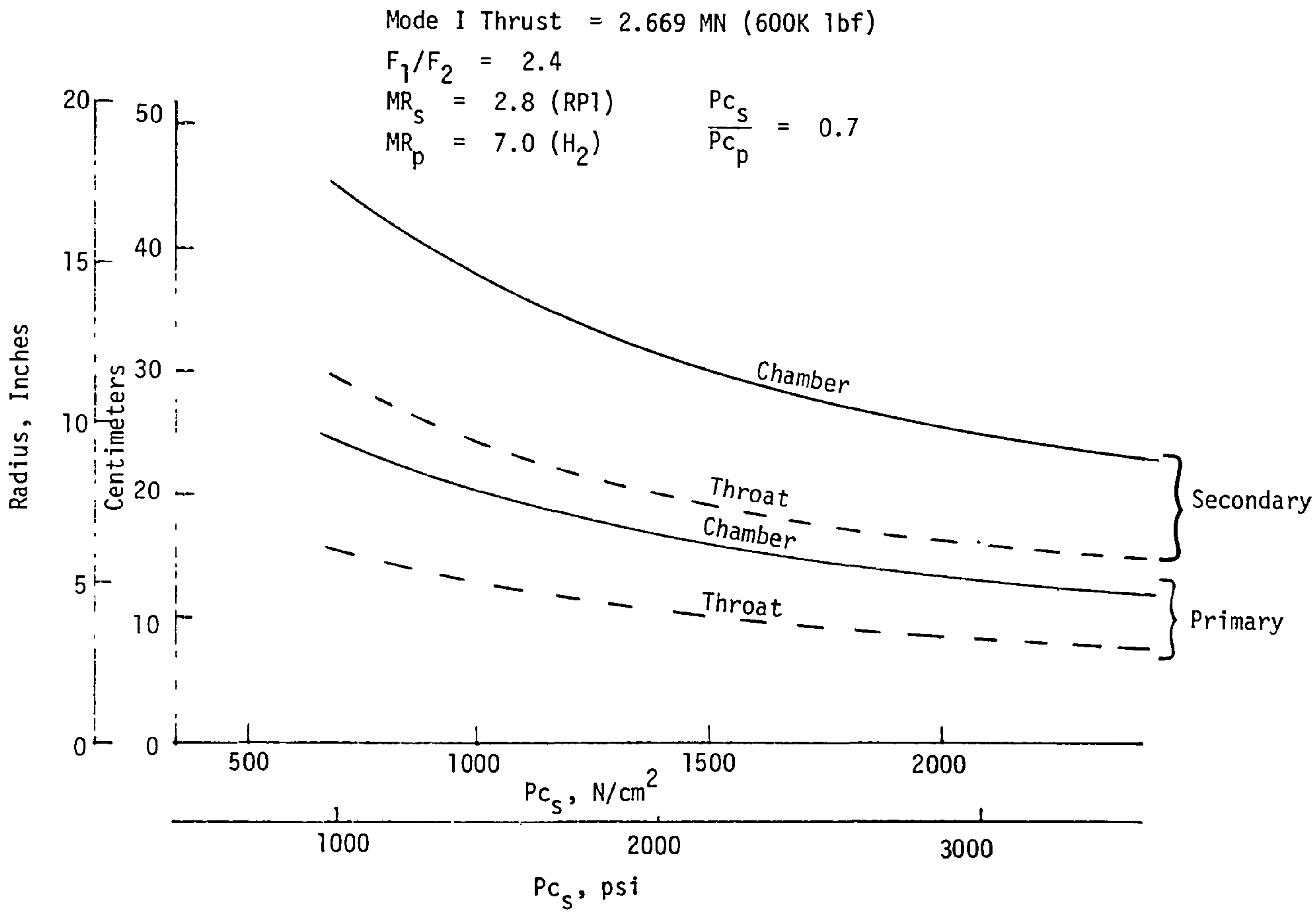

Figure 76. Dual Throat Engine Throat and Chamber Radius vs. Chamber Pressure

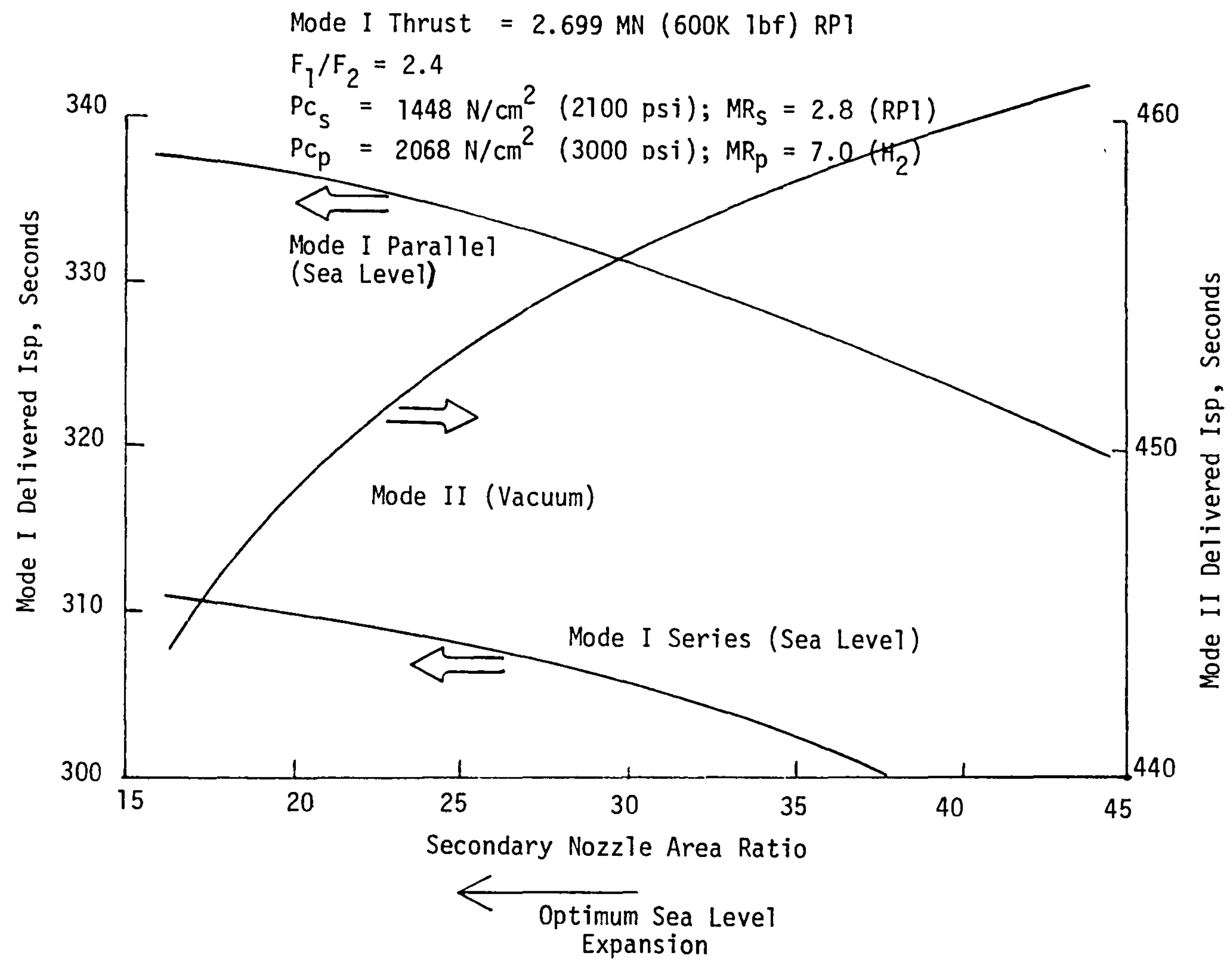

Figure 77. Delivered Isp vs. Mode I Nozzle Area Ratio

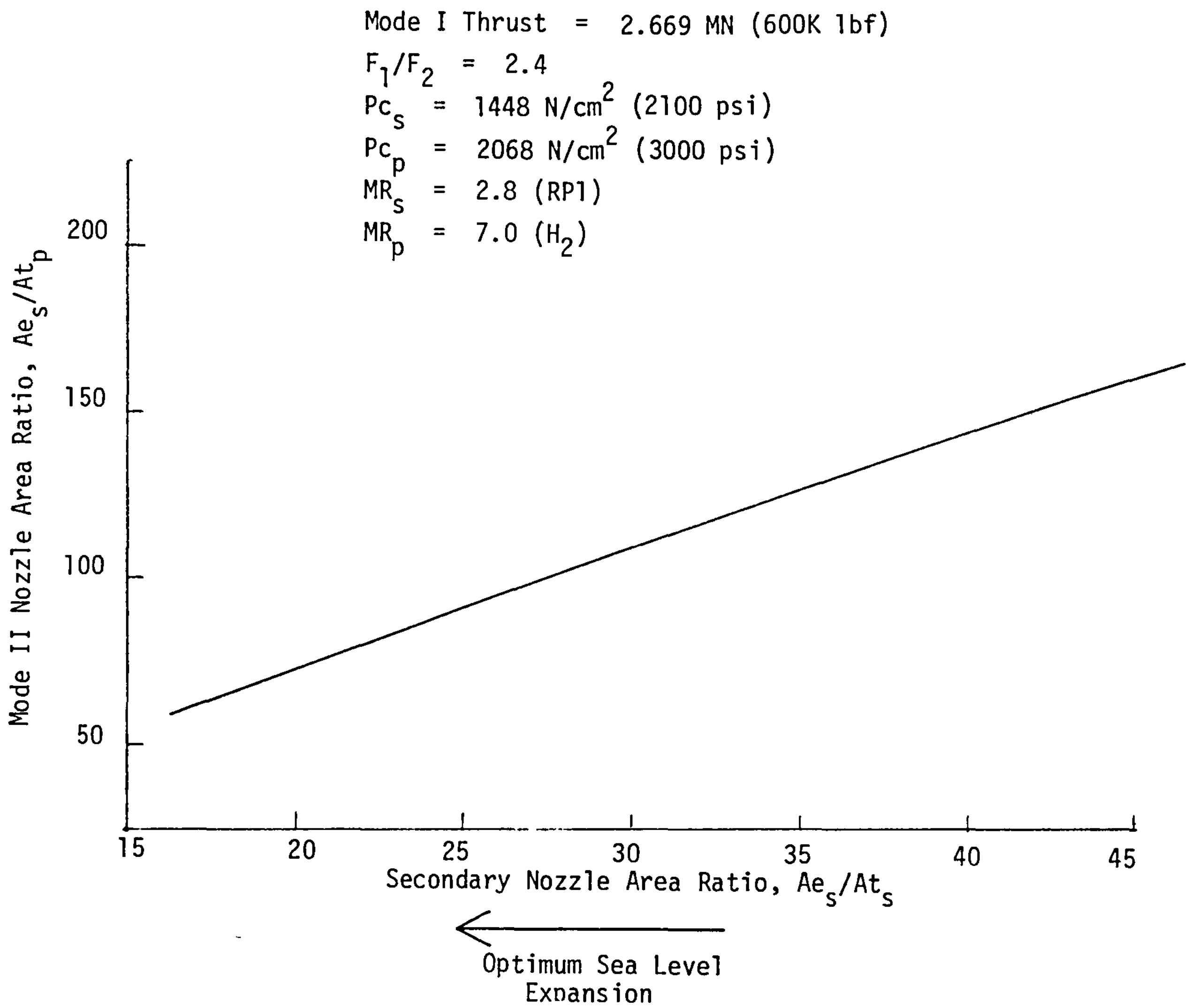

Figure 78. Mode II Area Ratio vs. Mode I Area Ratio

efficiency, Mode I delivered Isp, Mode I and Mode II area ratios and engine size are plotted in Figures 69 through 73. The reduction of the Mode I Isp efficiency as the thrust ratio is increased as shown in Figure 69 is a result of decreasing the mass percent of the LOX/H_2 with respect to the LOX/RP-1. (The LOX/RP-1 energy release efficiency is by definition 98% while the LOX/H_2 is 99%.) Likewise as the mass-percent of the LOX/H_2 decreases the Mode I, parallel burn delivered Isp decreases due to a lower mass-averaged Isp_{ODE} (see Figure 70). The Mode II delivered Isp increases with higher thrust ratios due to the decrease of the primary engine throat area with respect to the secondary nozzle exit. This results in a higher Mode II area ratio (see Figure 71) and in turn produces a higher Isp. As shown in Figure 72 the secondary chamber size is almost constant while the primary chamber gets smaller as the thrust ratio is increased.

Figures 73 through 76 show the effct of chamber pressure on Isp efficiency, delivered Isp, engine size, and nozzle area ratio, respectively. The Mode I Isp efficiency plotted in Figure 73 increases with increasing Pc, a result of higher kinetics and divergence efficiencies. The Mode II efficiency drops slightly due to higher bleed flow requirements which increase the boundary layer losses. The delivered Isp for both modes (see Figure 74) increase with higher Pc because of the corresponding increase in nozzle area (see Figure 75). The Mode I series burn is of course lower because the specific impulse for 100% LOX/RP-1 is less than a mass average of LOX/H_2 and LOX/RP-1. The conventional engine trends of decreasing engine size with higher Pc's is evident also with the dual throat concept as shown in Figure 76.

The effects of varying the secondary nozzle area (optimum sea level and higher) on Mode I Isp and the Mode II area ratio are shown in Figures 77 and 78. The Mode I sea level performance increases as the nozzle area ratio is decreased towards the optimum sea level value for a particular Pc. Conversely, the Mode II vacuum Isp decreases as the Mode I area ratio is optimized for sea level conditions. Obviously tradeoffs incorporating these trends and the vehicle/mission requiements will be necessary to optimize these effects.

The variation of engine mixture ratio produced no significant effects. The differences between LOX/RP-1 and LOX/CH_4 were slight. The trends obtained for LOX/RP-1 were the same for the LOX/CH_4, except that the LOX/CH_4 increased the delivered Isp by approxmately 4-5 seconds.

3. Methodology Improvements

Although the methodology incorporated for this performance analysis reported herein is consistent with the JANNAF simplified procedures, there are several areas which deserve further work and evaluation. The four main areas are:

(1) Because of the many difficulties encountered in obtaining a complete TDK analysis (η_{2D}) for the Mode II nozzle profiles, some uncertainty exists with the TDK results. Further evaluation of methods to obtain the Mode II η_{2D} efficiency is warranted, particularly with the high area ratio expansions.

(2) The thrust decrement within the shear layer should be calculated directly rather than based upon a proportionality of momentum thicknesses. The effects of the reattachment on the downstream boundary layer loss should also be evaluated.

(3) The aerodynamic, base flow program needs to be refined in two areas:

(a) The isoenergetic assumption in treating the plume back pressure and bleed calculation should be modified to accept other types of conditions. The current isoenergetic assumption is satisfactory when the bleed flow is assumed to be of the same composition and conditions of the core flow, but is not correct in analyzing the use of unburned hydrogen gas.

(b) The zero bleed base pressure calculation is currently based upon a correlation developed from the dual throat cold flow data. A direct calculation and/or hot fire test data are necessary to verify or update the cold flow condition.

C. ENGINE WEIGHT

For the purpose of the parametric study, it was necessary to establish the elements of engine weight to be included in the scaling study and to establish baseline engine weight statements. Table XXI lists the engine components included in the parametric analyses. Those items not included are also listed.

1. 1978 State-of-the-Art Engine Weight Parametrics

Engine weight statements for the preliminary baseline LO_2/RP-1 + LH_2 and LO_2/LCH_4 + LH_2 dual throat engines (stream-tube thrust split 60/40) are given in Table XXII. The component weights are based on scaling of historical weights of similar components and/or estimates obtained from conceptual designs such as those given in Ref. (6). Some of the methane engine component weights were derived from a scale factor which accounts for the volumetric flow rate difference between LCH_4 and RP-1 engine components.

With the preliminary baseline engine weight established, engine

TABLE XXI

ENGINE WEIGHT DEFINITION

Included	Not Included
Regeneratively Cooled Combustion Chamber(s)	Gimbal Actuators and Actuation System
Regeneratively Cooled Thrust Chamber Nozzle(s)	Pre-Valves
Thrust Chamber Nozzle Extension	Contingency (a total contingency is normally included in the vehicle weight statement)
Main Injector	
Main Turbopumps	
Boost Pumps	
Preburners (or Gas Generator)	
Propellant Valves and Actuation	
Gimbal	
Hot Gas Manifold (if required)	
Propellant Lines	
Ignition System	
Miscellaneous (Electrical Harness, Instrumentation, Brackets, Auxiliary Lines and Controls)	
Engine Controller	
Tank Pressurant Heat Exchangers and Associated Equipment	

TABLE XXII

ESTIMATION OF DUAL THROAT ENGINE COMPONENT WEIGHTS (STG. COMB CYCLE III)

F = 2700 KN (607 K lb_f) PCP = 2 07 x 10^7 N/M^2 (3000 PSIA)

Component	LOX/RP-1 + LH_2 Dual Throat (60/40) KG	(LB)	LOX/CH_4 + LH_2 Dual Throat (60/40) KG	(LB)
Gimbal	99	219	99	219
Primary Injector (O/H)	106	233	106	233
Secondary Injector (O/HC)	289	638	284	626
Primary Chamber & Nozzle (ε = 5)	107	235	107	235
Sec, Chamber & Nozzle (ε_1 = 14 7)	160	352	154	339
Thrust Chamber Nozzle ($\varepsilon = \varepsilon_1$ to 43)	336	740	329	726
Fuel-Rich Preburner (O/H)	62	137	62	137
Oxidizer-Rich Preburner (O/H)	37	82	37	82
Oxidizer-Rich Preburner (O/HC)	52	114	52	114
Fuel Valves & Actuation (O/H)	50	110	50	110
Fuel Valves & Actuation (O/HC)	15	34	17	38
Oxidizer Valves & Actuation (O/H)	43	95	43	95
Oxidizer Valves & Actuation (O/HC)	23	51	23	51
Low Speed LOX TPA (O/H)	35	77	35	77
Low Speed LOX TPA (O/HC)	59	129	59	129
Low Speed LH_2 TPA	37	81	37	81
Low Speed HC TPA	10	22	15	33
High Speed LOX TPA (O/H)	81	178	81	178
High Speed LOX TPA (O/HC)	136	299	136	299
HIgh Speed LH_2 TPA	168	370	168	370
High Speed HC TPA	51	113	77	170
Low Pressure Lines (O/H)	63	139	63	139
Low Pressure Lines (O/HC)	64	140	74	164
High Pressure Lines (O/H)	122	268	122	268
High Pressure Lines (O/HC)	36	80	43	94
Ignition System(s)	34	76	34	76
Mixcellaneous (O/H)	120	265	120	265
Miscellaneous (O/HC)	134	296	134	296
Engine Controller	59	130	59	130
Pressurization Systems (O/H)	24	53	24	53
Pressurization Systems (O/HC)	40	8	47	104
Hot Gas Manifolds (O/H)	120	264	120	264
Hot Gas Manifolds (O/HC)	27	59	31	69
TOTAL WEIGHT	2,798	6,168	2,841	6,264

*Does not include Gimbal Actuators and Actuation System, Pre-valves, contingency (normally included in vehicle weight statement) component weight scaling relationships were derived as functions of thrust, stream-tube thrust split, thrust chamber pressure and nozzle area ratio. These scaling relationships, used to calculate the weights over the parametric ranges of interest, are given in the Appendix. The scaling equations were established through geometry considerations and empirical data fits of historical data as shown in Figure 79. The engine weights represent 1978 state-of-the-art technology.

Figures 80, 81 and 82 show LO_2/RP-1 + LH_2 dual throat engine weight (staged combustion Cycle III) as a function of sea level thrust and stream-tube thrust split at primary chamber pressures of 0.965, 2.07 and 3.45 x 10^7 N/m^2 (1400, 3000 and 5000 psia), respectively. Figures 83, 84 and 85 show the corresponding data for the LO_2/LCH_4 + LH_2 dual throat engine. The weight comparison between the RP-1 and LCH_4 engines is summarized in Table XXIII.

Parametric weight data for the gas generator/staged combustion mixed cycle engine are given in Figures 86 through 91.

Scaling relationships based on volumetric flow rates and pump discharge pressures were used to obtain an estimate of the variation in engine weight with power cycle. This evaluation primarily involved turbopumps and preburners (gas generators). The resultant variation in engine weight with power cycle is shown in Figure 92. The three preburner staged combustion cycle is seen to be lighter in weight than the two preburner cycle, and the gas generator/staged combustion mixed cycle is seen to weigh approximately 400 pounds less than the staged combustion Cycle III. The pure gas generator cycles are seen to provide the lightest weight engine at the baseline conditions (thrust = 2700 KN (607K), primary chamber pressure = 2.07 x 10^7 N/m^2 (3000 psia).

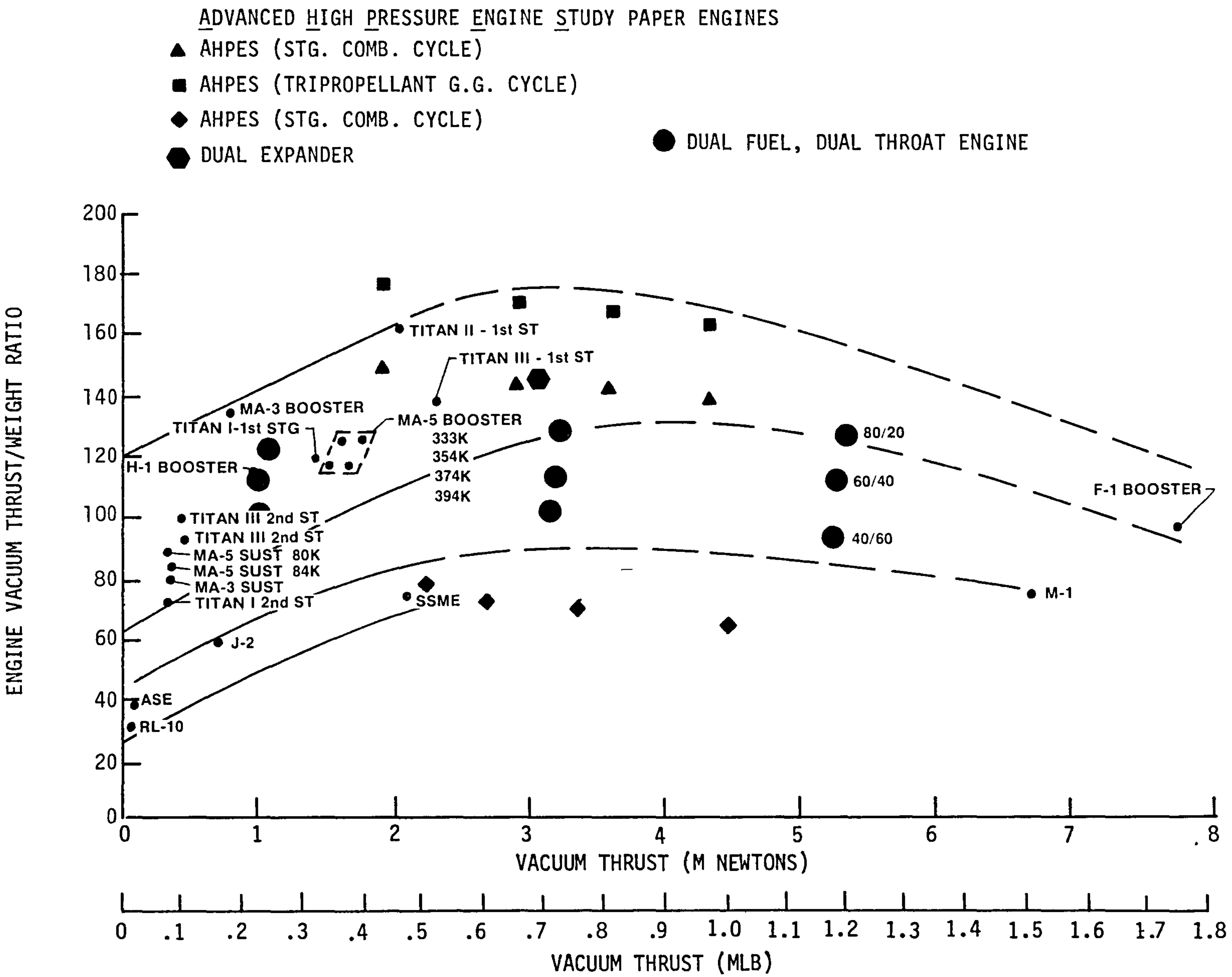

Figure 79. Advanced Technology Engine Design Studies Use Realistic Weights

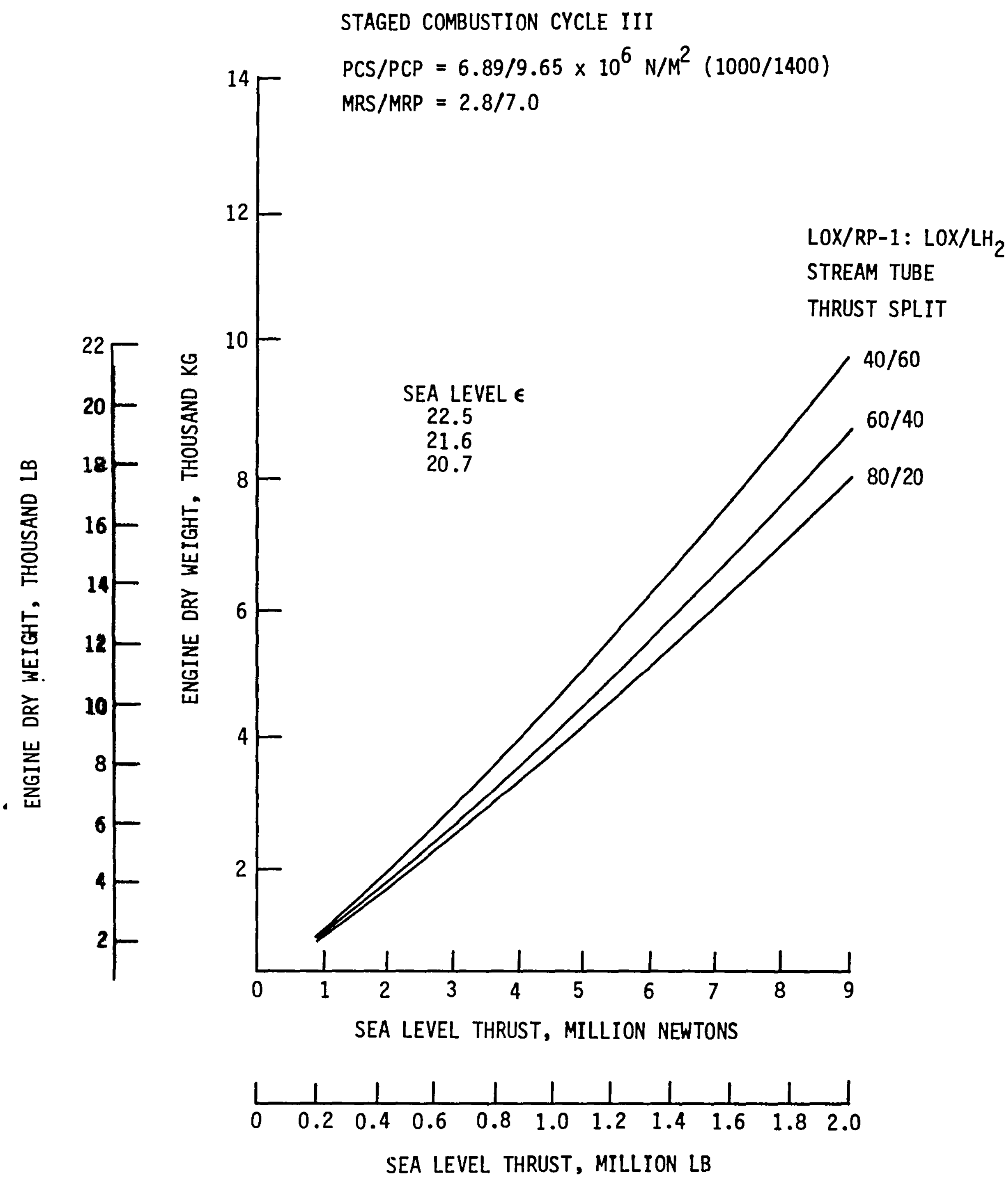

Figure 80. Dual Throat Engine Weight, PCP = 1400 (RP-1)

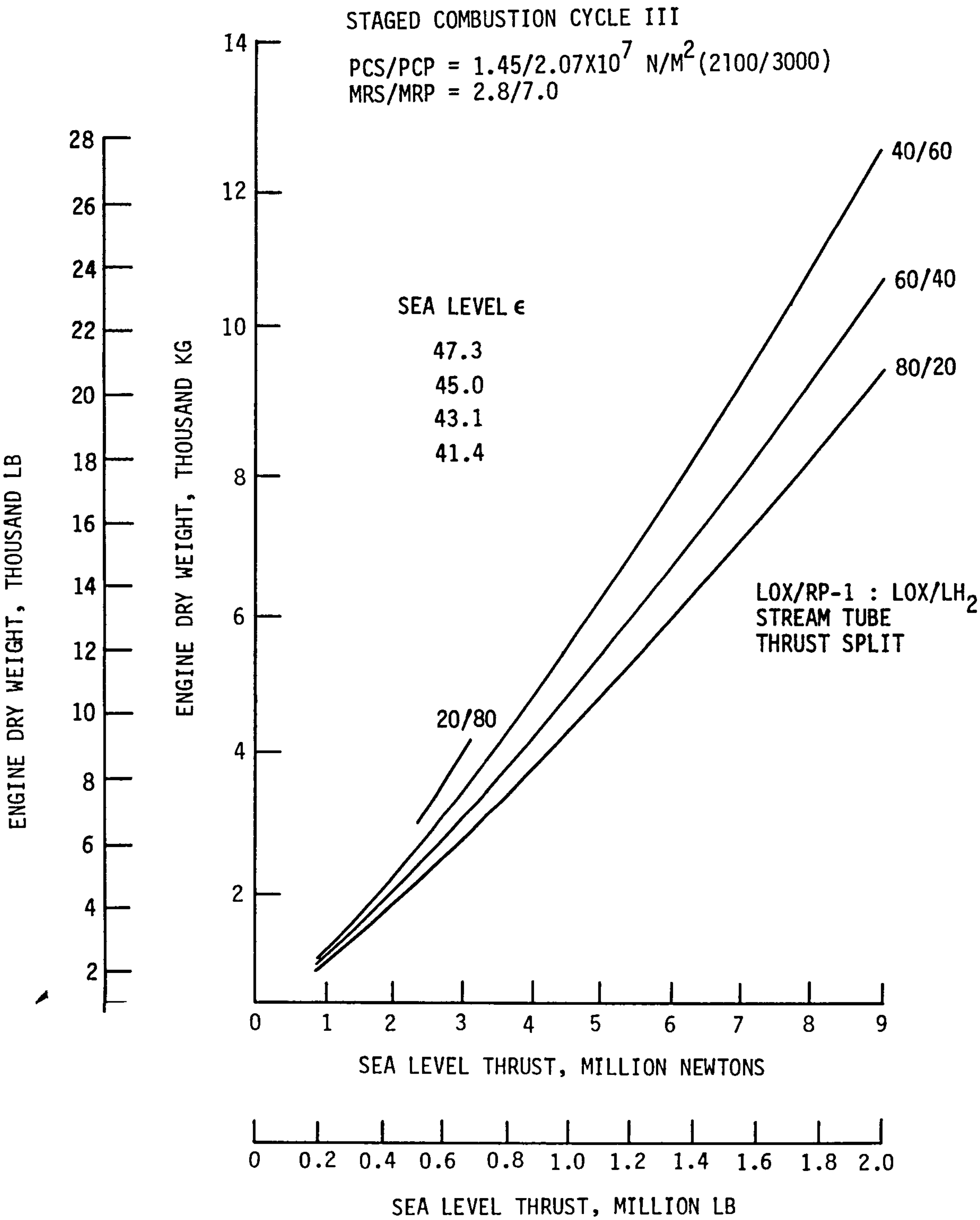

Figure 81. Dual Throat Engine Weight, PCP = 3000 (RP-1)

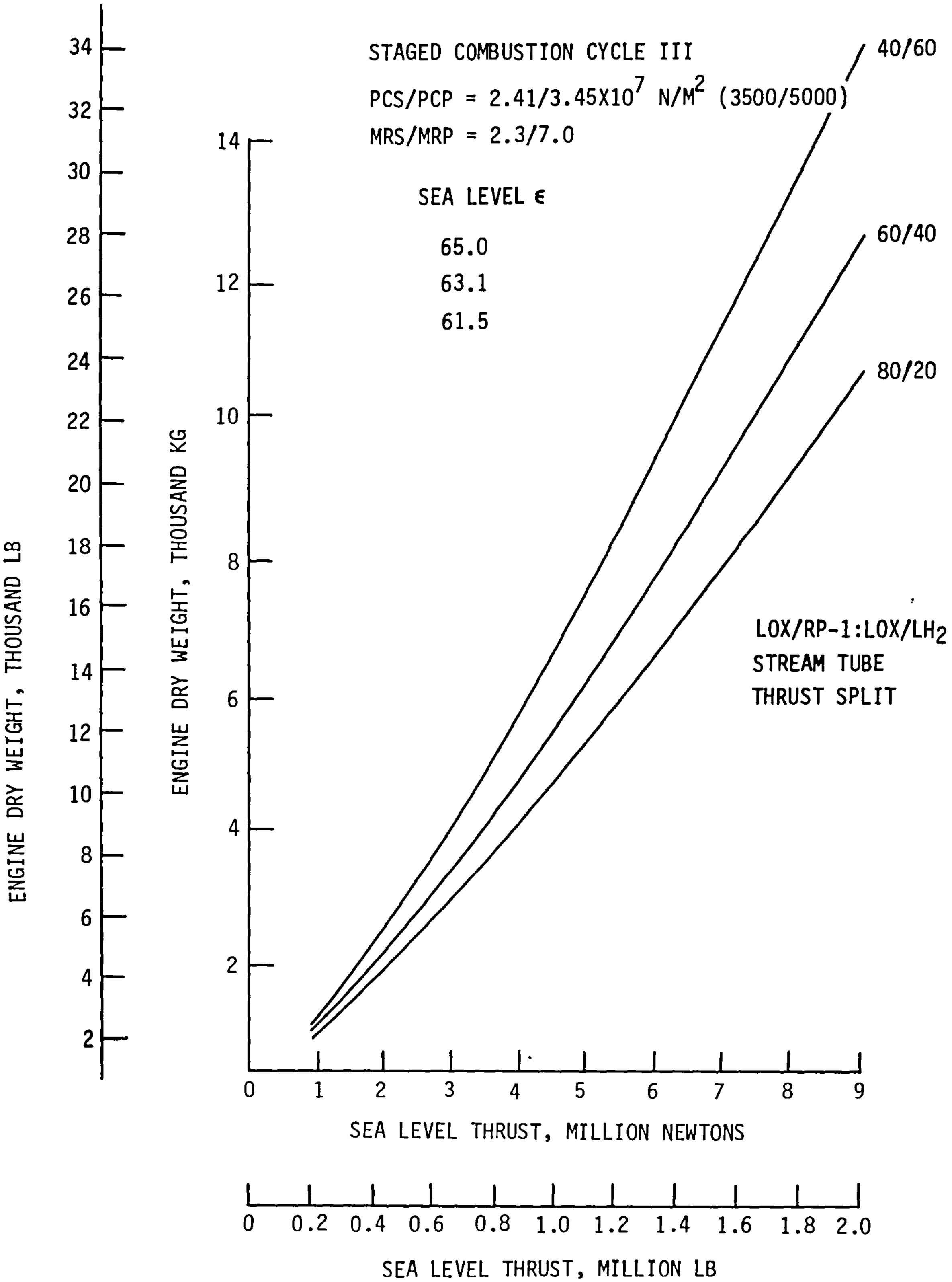

Figure 82. Dual Throat Engine Weight, PCP = 5000 (RP-1)

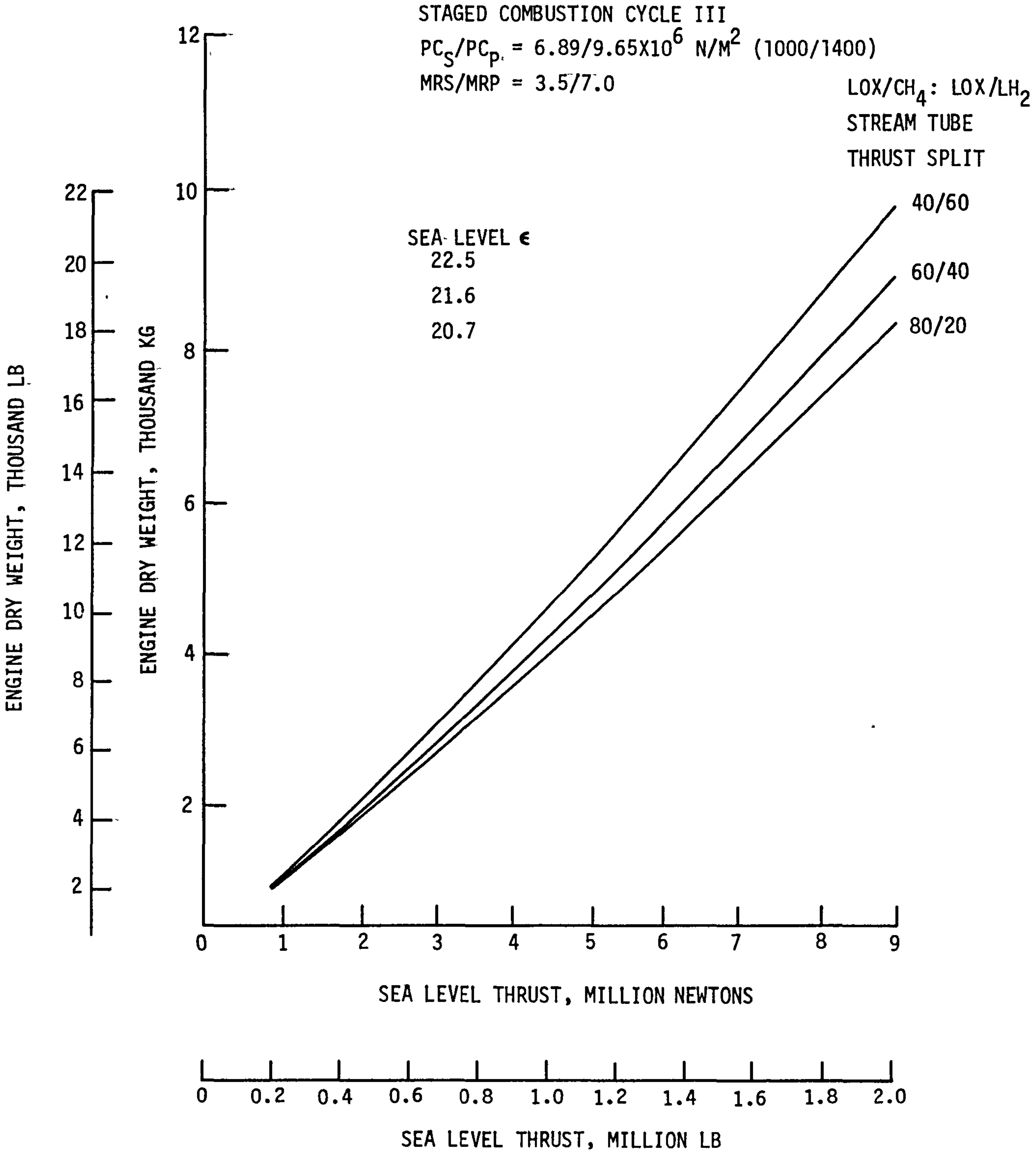

Figure 83. Dual Throat Engine Weight, PCP = 1400 (LCH4)

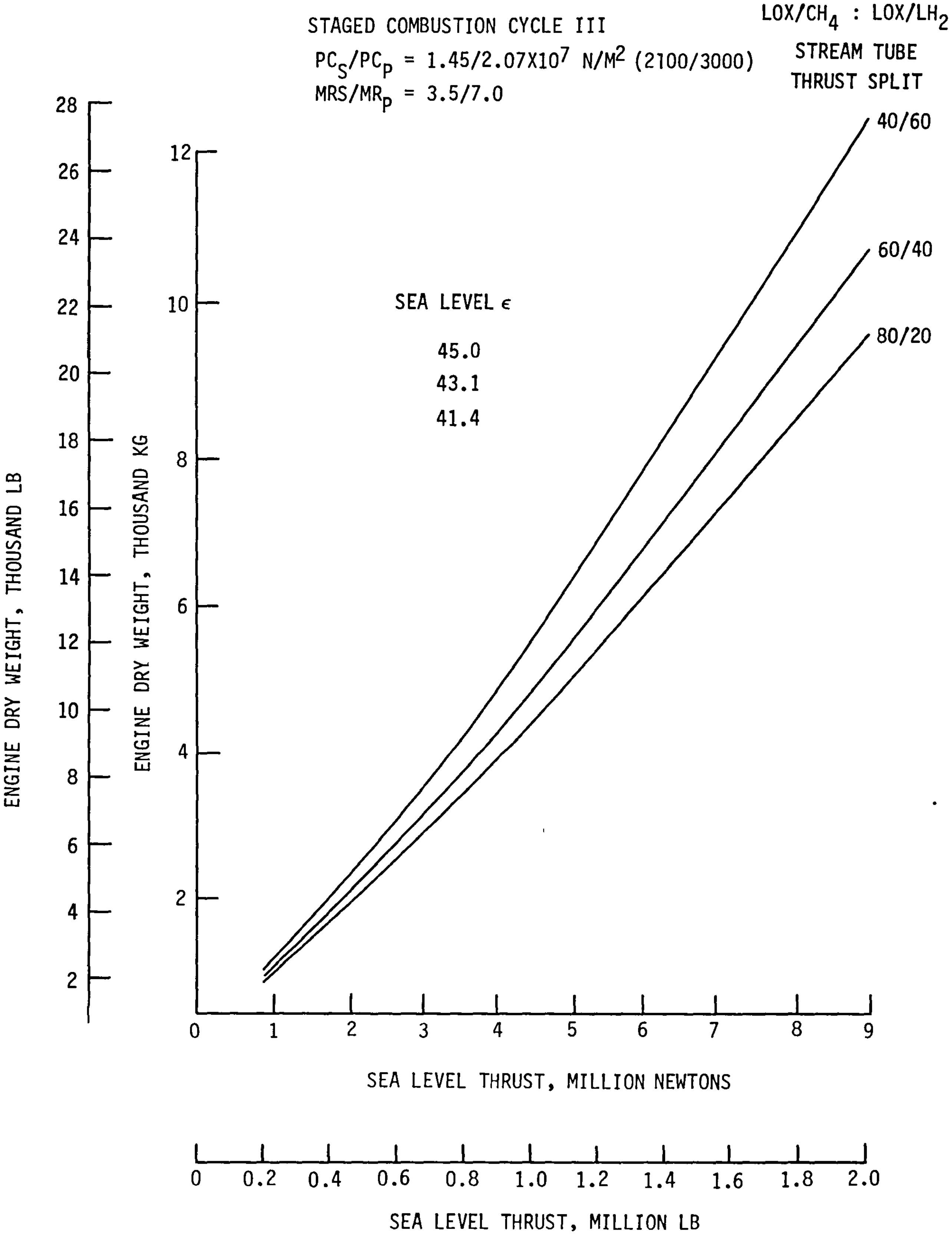

Figure 84. Dual Throat Engine Weight, PCP = 3000 (LCH4)

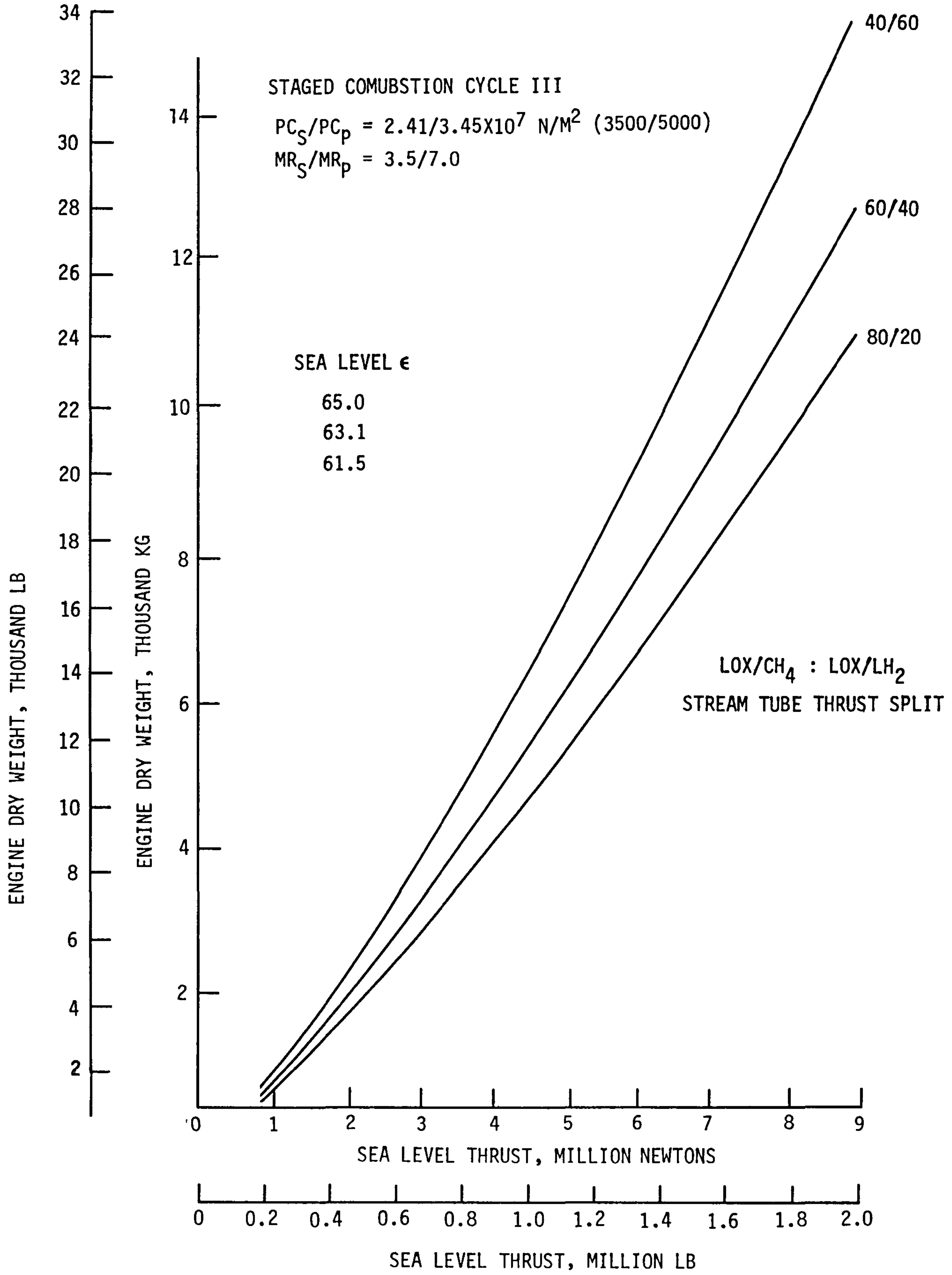

Figure 85. Dual Throat Engine Weight, PCP = 5000 (LCH4)

TABLE XXIII

DUAL THROAT ENGINE WEIGHT COMPARISON

F = 2669 KN (600,000 LB_F)

STAGED COMBUSTION CYCLE III

PCS/PCP 10^7 N/M^2 (PSIA)	STREAM-TUBE THRUST SPLIT HC/H	THRUST RATIO F I/F II	RP-1 WEIGHT KG (LB)	CH_4 WEIGHT KG (LB)
0.69/0.97 (1000/1400)	40/60	1.62	2697 (5946)	2694 (5940)
	60/40	2.38	2492 (5494)	2510 (5534)
	80/20	4.66	2331 (5139)	2372 (5230)
1.45/2.07 (2100/3000)	40/60	1.62	3120 (6878)	3118 (6875)
	60/40	2.41	2765 (6096)	2782 (6134)
	80/20	4.74	2506 (5524)	2544 (5609)
2.41/3.45 (3500/5000)	40/60	1.63	3645 (8035)	3681 (8116)
	60/40	2.43	3110 (6856)	3187 (7026)
	80/20	4.79	2722 (6000)	2844 (6269)

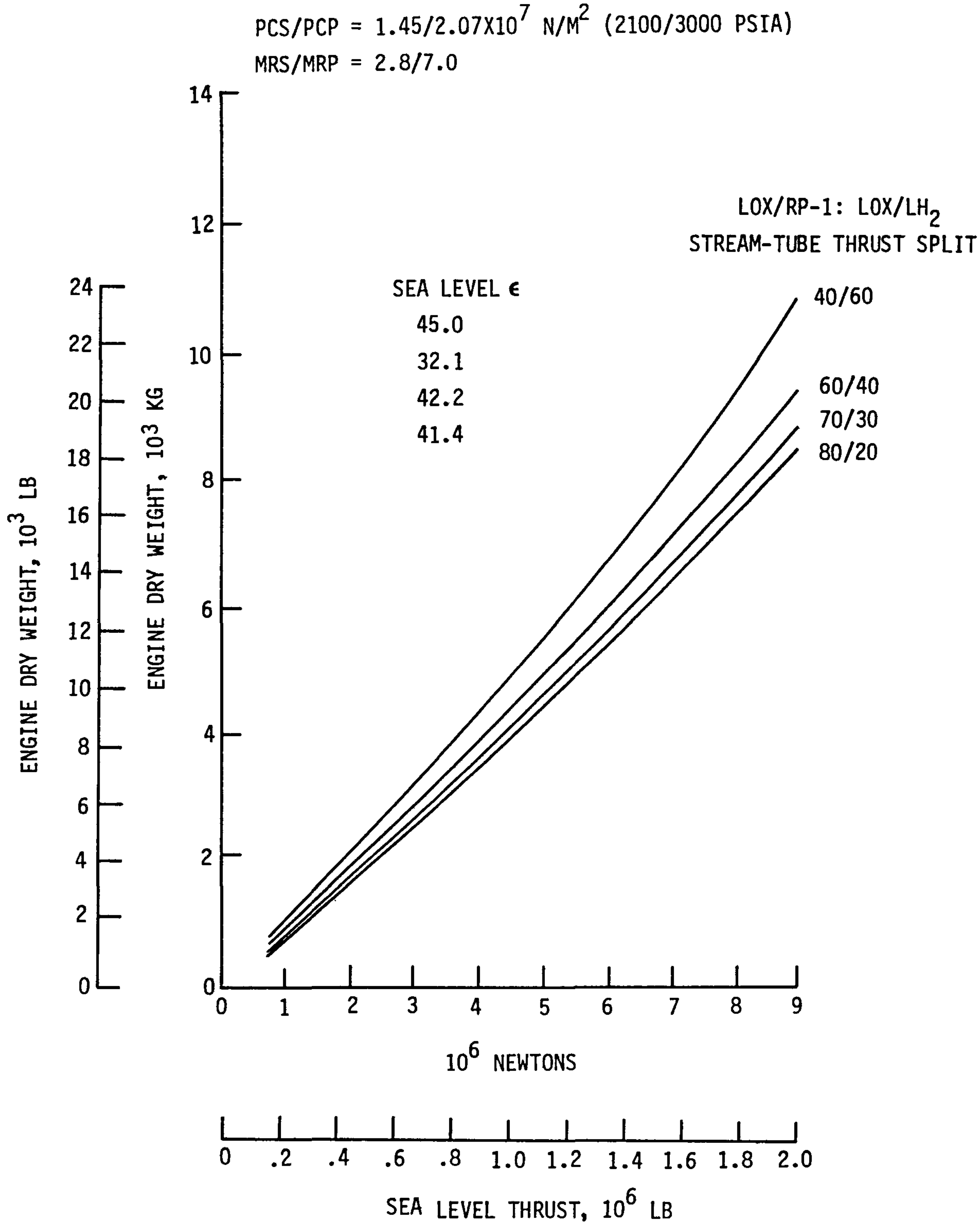

Figure 86. Dual Throat Engine Weight, PCP = 3000, GG/SC Cycle

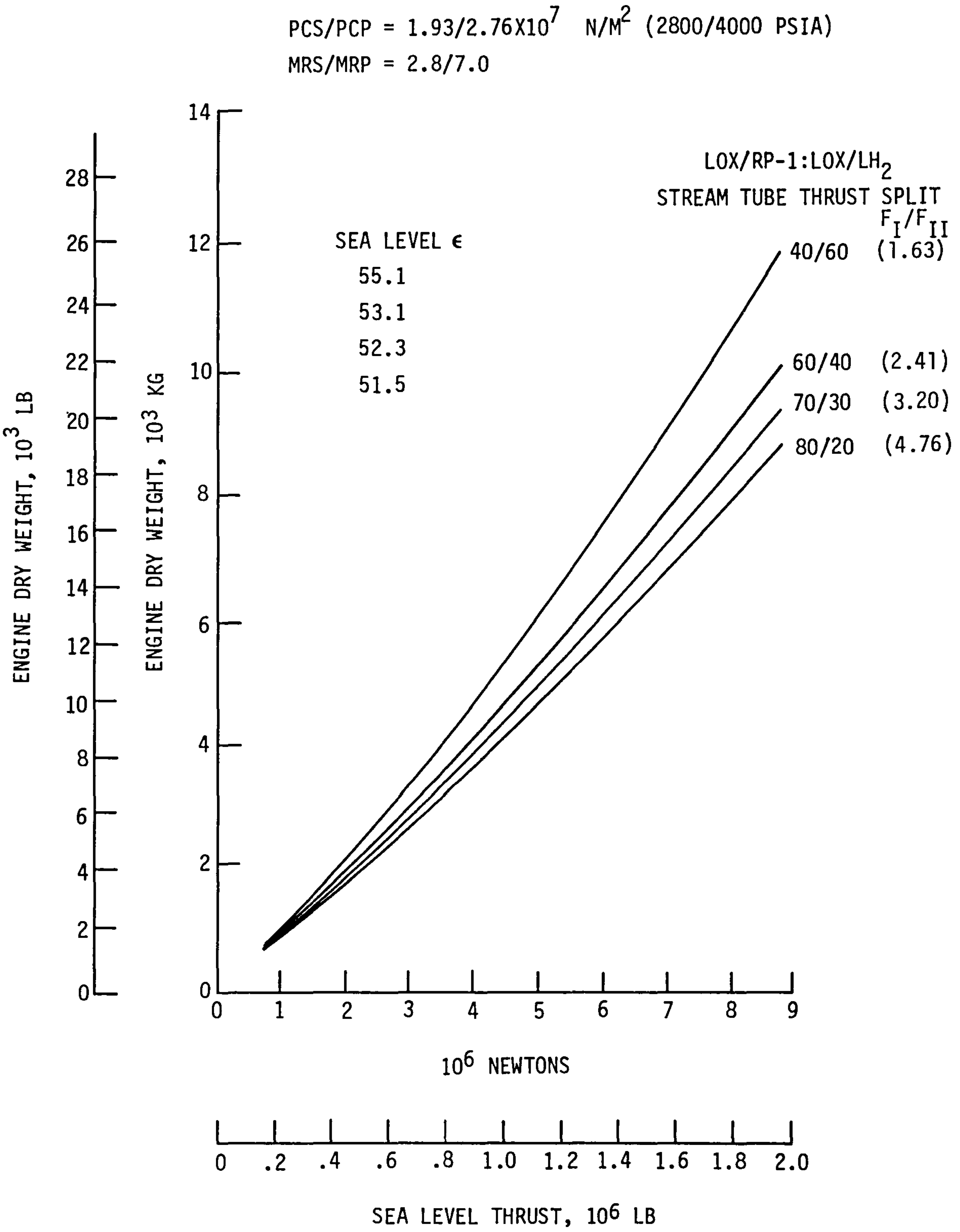

Figure 87. Dual Throat Engine Weight, PCP = 4000, GG/SC Cycle

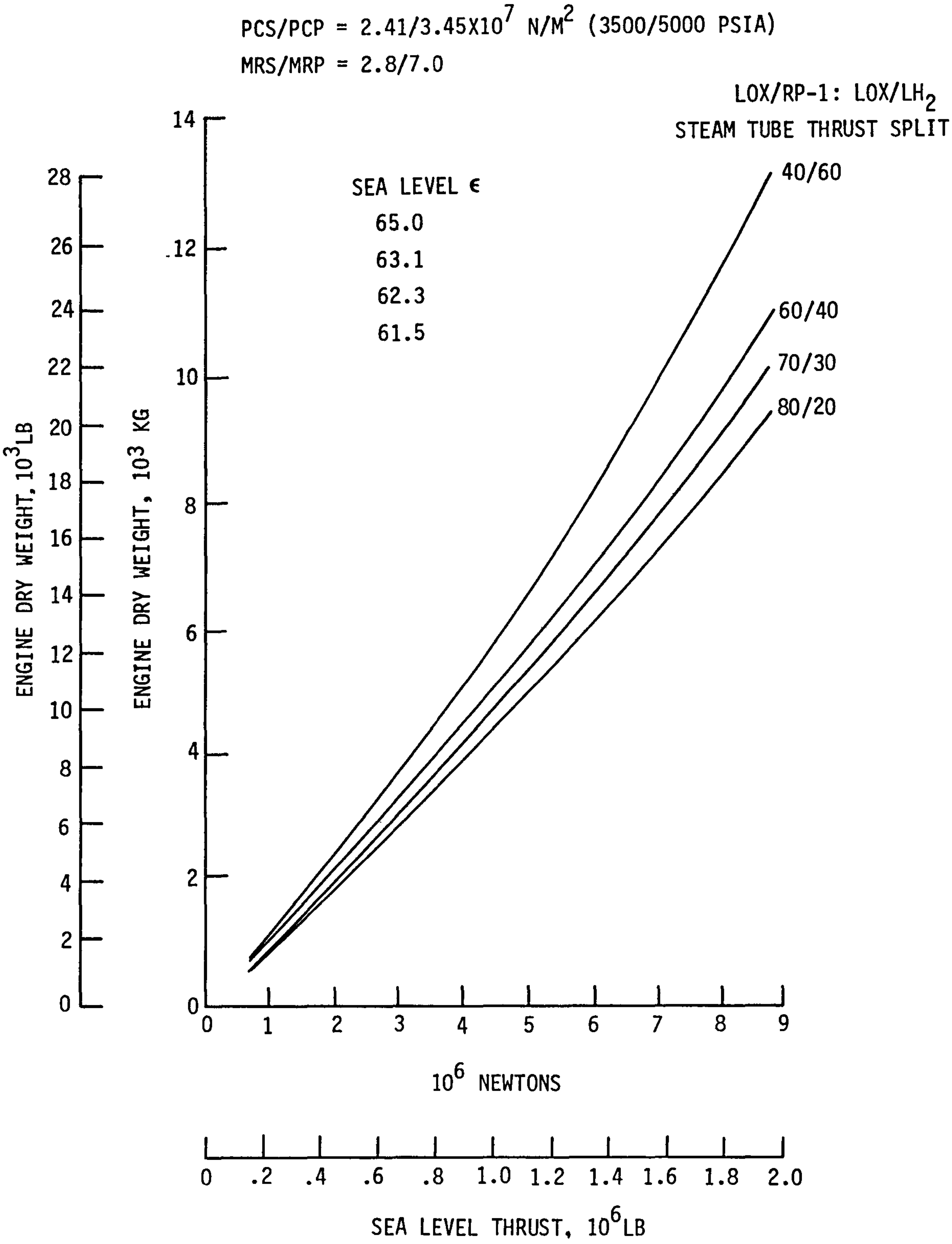

Figure 88. Dual Throat Engine Weight, PCP = 5000, GG/SC Cycle

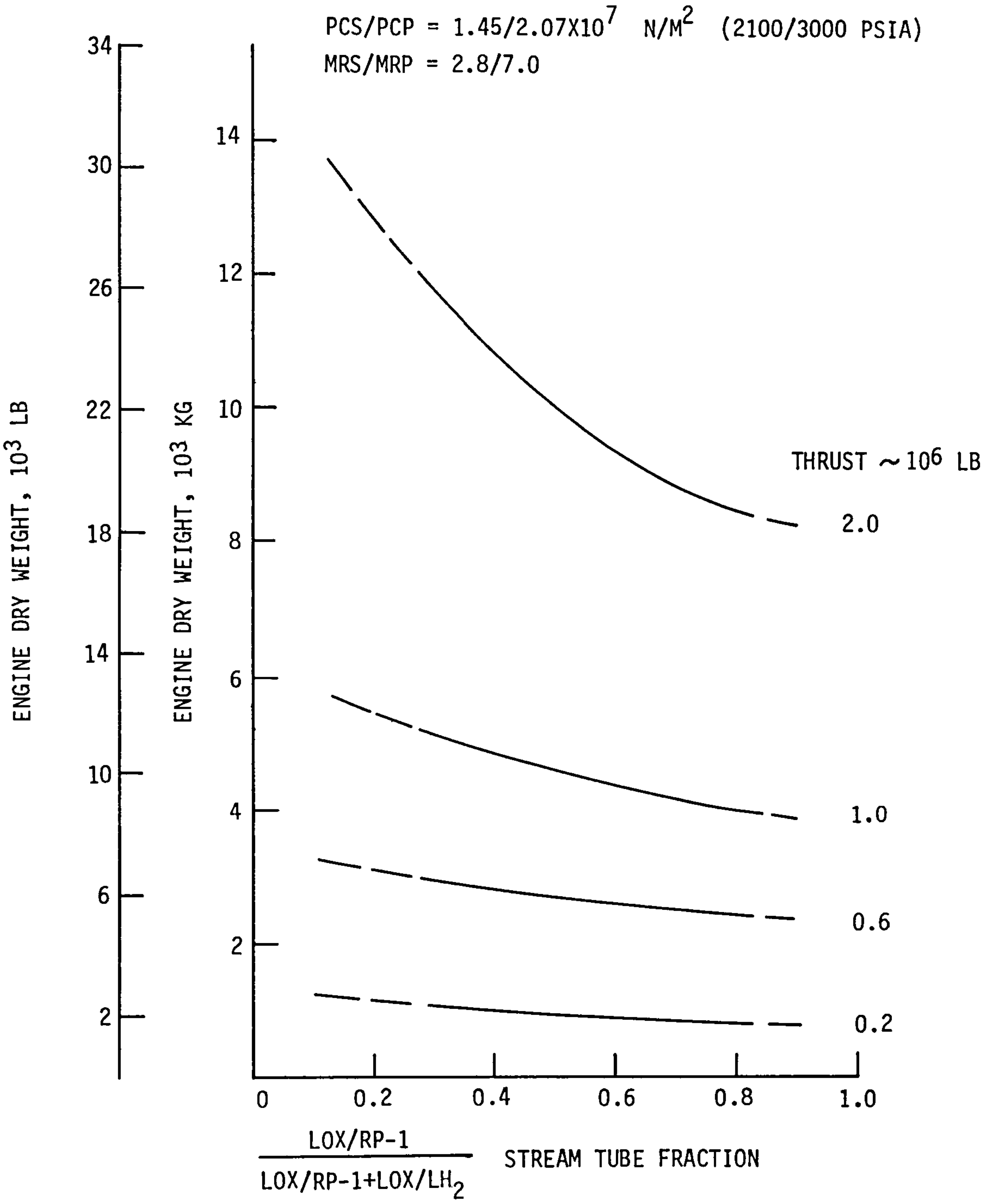

Figure 89. Dual Throat Engine Weight, PCP = 3000 GG/SC Cycle

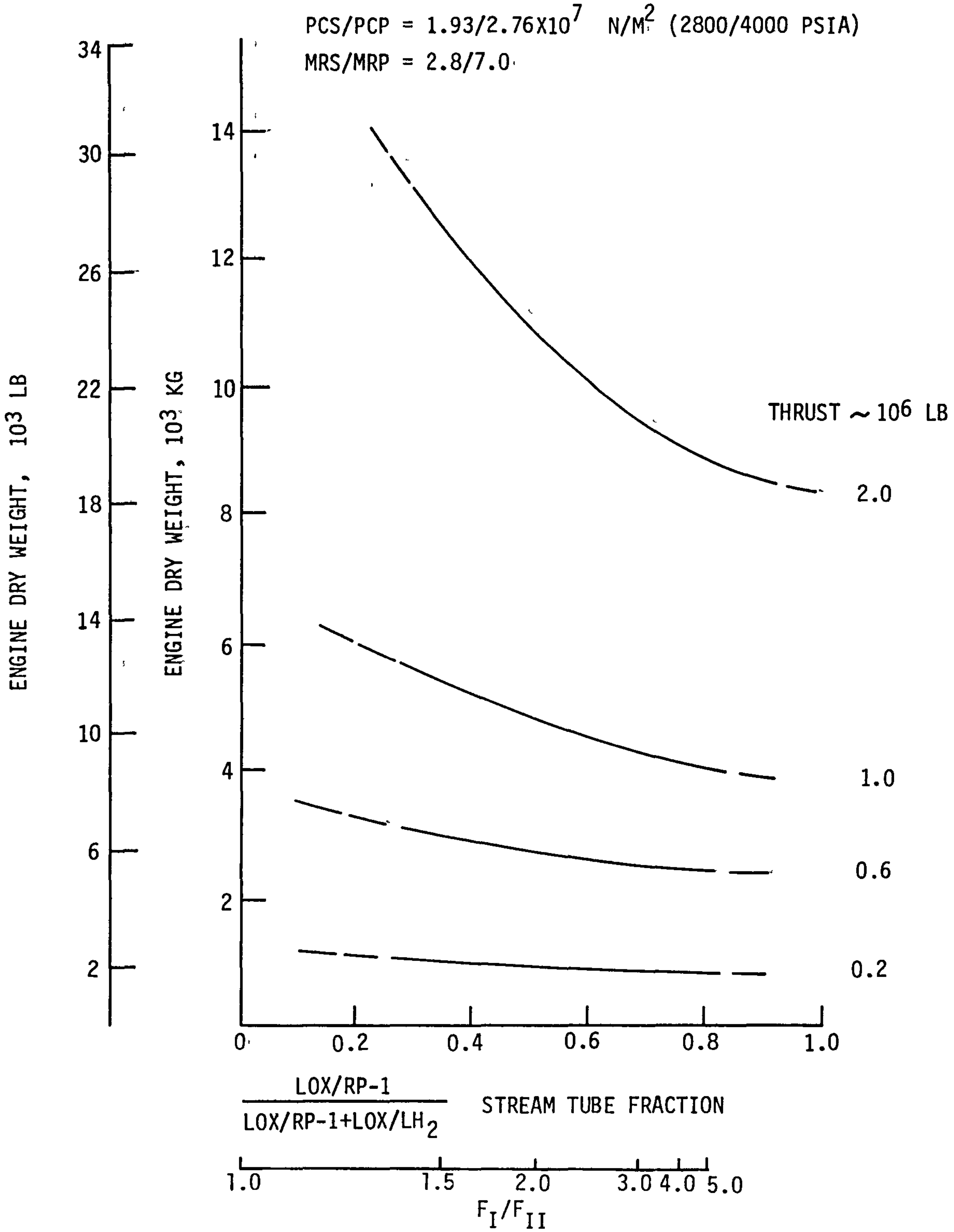

Figure 90. Dual Throat Engine Weight, PCP = 4000 GG/SC Cycle

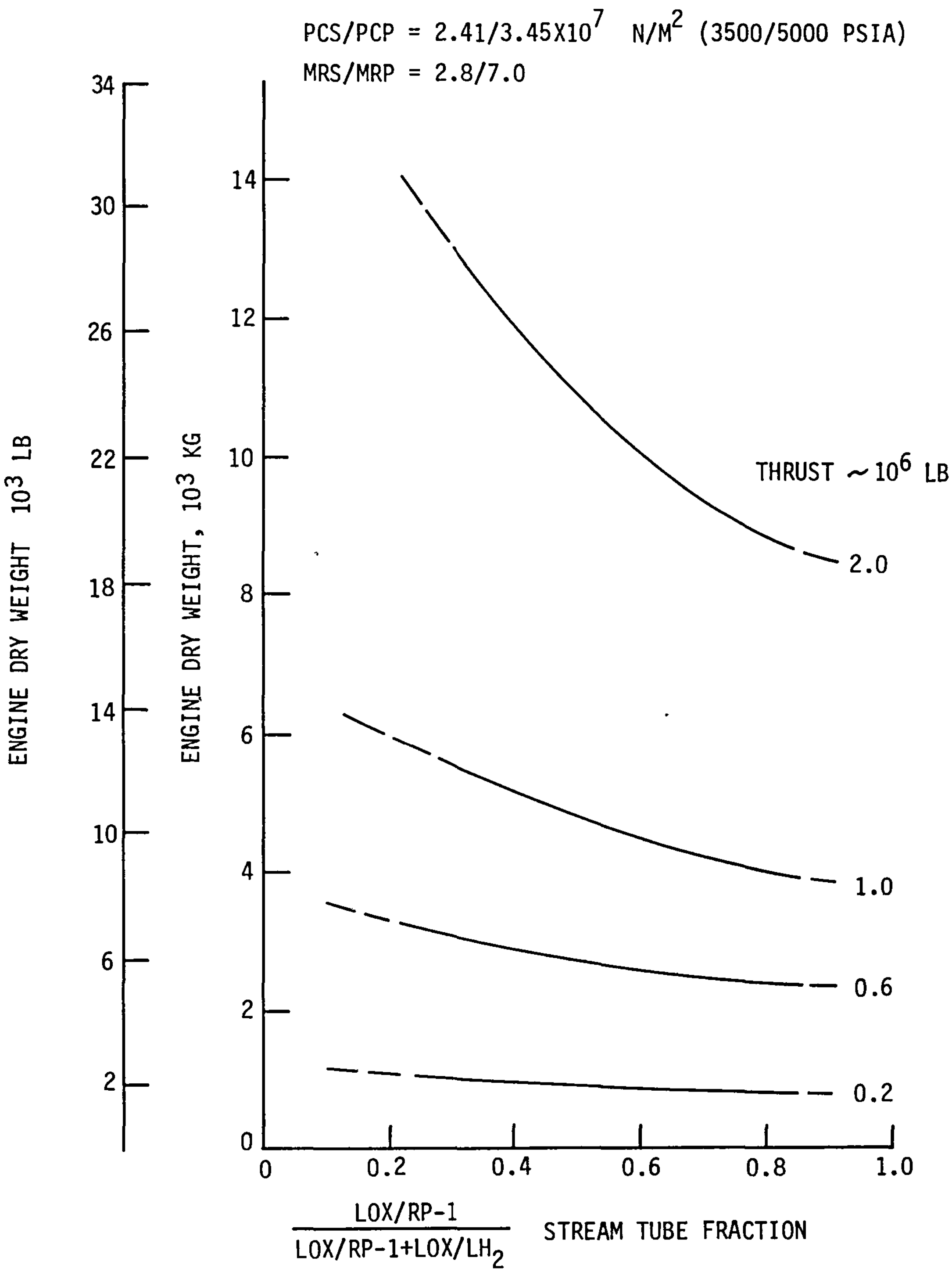

Figure 91. Dual Throat Engine Weight, PCP = 5000 GG/SC Cycle

F = 2700 KN (607K) FI/FII = 2.41 (60/40)

ASSUMPTION: WEIGHT CHANGE DUE TO PREBURNERS & PUMPS

PCS/PCP = 2100/3000

LO_2/RP-1 + LH_2

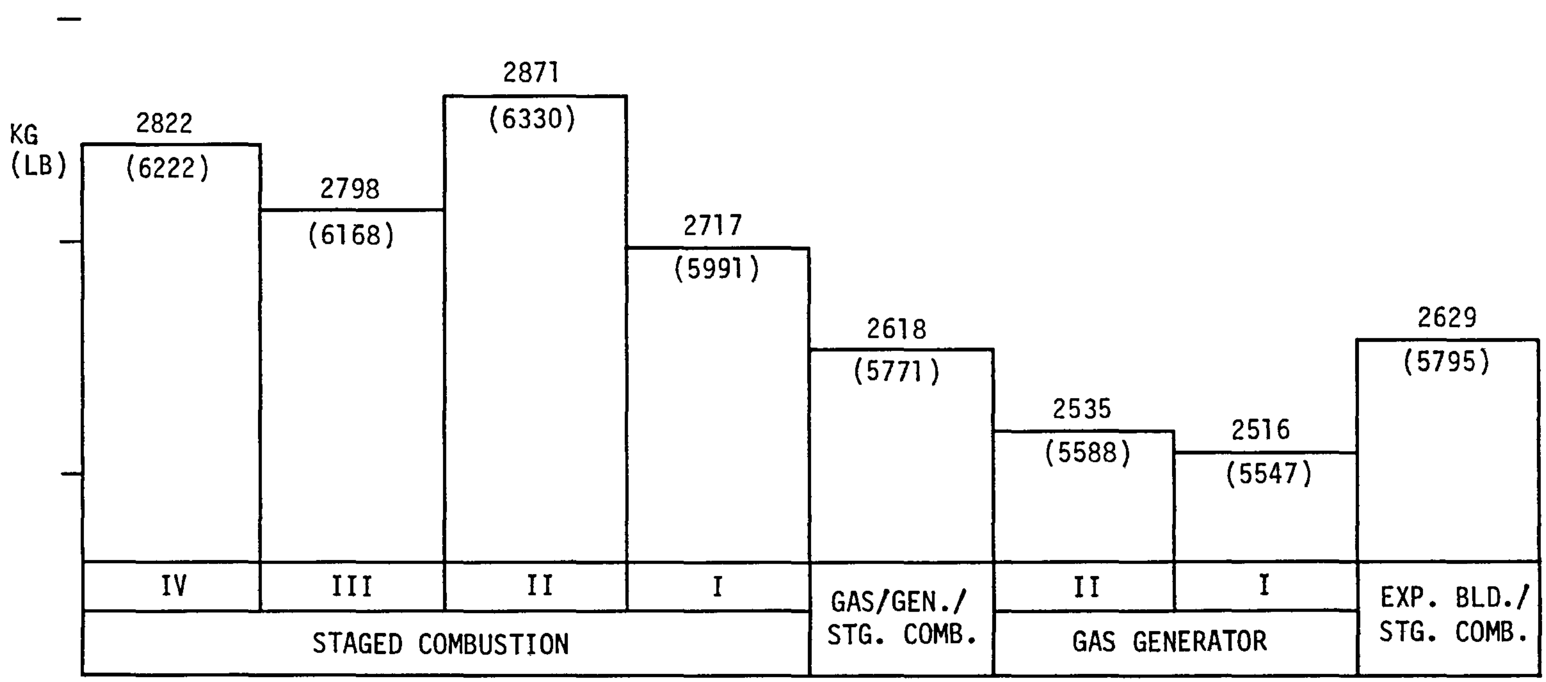

Figure 92. Dual Throat Engine Weight Variation with Power Cycle

2. <u>1995 State-of-the-Art Engine Weight</u>

A thorough study of the materials requirements for high pressure engines was made on Contract NAS 3-19727 (Ref. 6). These data were reviewed and updated in this study (see Section V,F). To estimate yearly improvements in engine weight through 1995, the potential of advanced composite materials (ACM) was evaluated. Typical improved materials and their properties are listed in Table XXIV.

Application of ACM's to rocket engine design promises significant weight reductions. Figure 93 illustrates that with only limited application of ACM's, a 20% weight reduction (over current 1978 technology) by 1995 is entirely plausible.

The weight prediction of Figure 93 is based upon the determination of an equivalent density for the 1995 ACM (1990 bidirectional hybrid composite - Table XXIV) under a prescribed tensile force. This logic guarantees a "fair" comparison of present day materials and ACM's. Since weight is directly proportional to density, the weight of 1995 ACM engines can be derived from the density ratio of 1995 ACM's to 1978 materials. In the absence of a demonstrated correlation, a linear weight relationship was assumed, allowing determination of engine weights between the years 1978 and 1995.

Initially, ACM was applied purely to low temperature engine components such as the turbopump assembly, pressure lines, gimbals, etc. Following this analysis, selected application of ACM to high temperature components were used as parameter limits. The 100% line represents an engine completely constructed out of composite material -- a very optimistic prediction.

TABLE XXIV

IMPROVED MATERIALS FOR REDUCED ENGINE WEIGHT

	MATERIAL	LBS/IN^3	F_{TU}-KSI L	F_{TU}-KSI T	F_{TU}/ρ IN. X 10^6 L	F_{TU}/ρ IN. X 10^6 T	E - psi X 10^6 L	E - psi X 10^6 T	E/ρ IN. X 10^8 L	E/ρ IN. X 10^8 T
CURRENT TITAN III	A356 CAST	0.10	35	35	0.35	0.35	10	10	1.0	1.0
IMPROVED METALS	2219 WROUGHT	0.10	65	65	0.65	0.65	10	10	1.0	1.0
	Ti5Al 2.5 Sn ELI WROUGHT	0.16	125	125	0.78	0.78	16	16	1.0	1.0
	Be38Al WROUGHT	0.075	56	56	0.75	0.75	27	27	3.6	3.6
ADVANCED COMPOSITES	GRAPHITE EPOXY COMPOSITE	0.057	164	6	2.9	0.10	15	1.8	2.6	0.3
	B/Al COMPOSITE	0.089	228	18	2.6	0.20	32	25	3.6	2.8
	BIDIRECTIONAL KEVLAR 49 EPOXY	0.047	70	60	1.5	1.3	4.3	3.5	0.9	0.75
	HYBRID	0.079	125	32	1.7	0.40	18	8.5	2.3	1.1
	1990 BIDIRECTIONAL HYBRID COMPOSITE	0.060	150	90	2.5	1.5	15	9	2.5	1.5

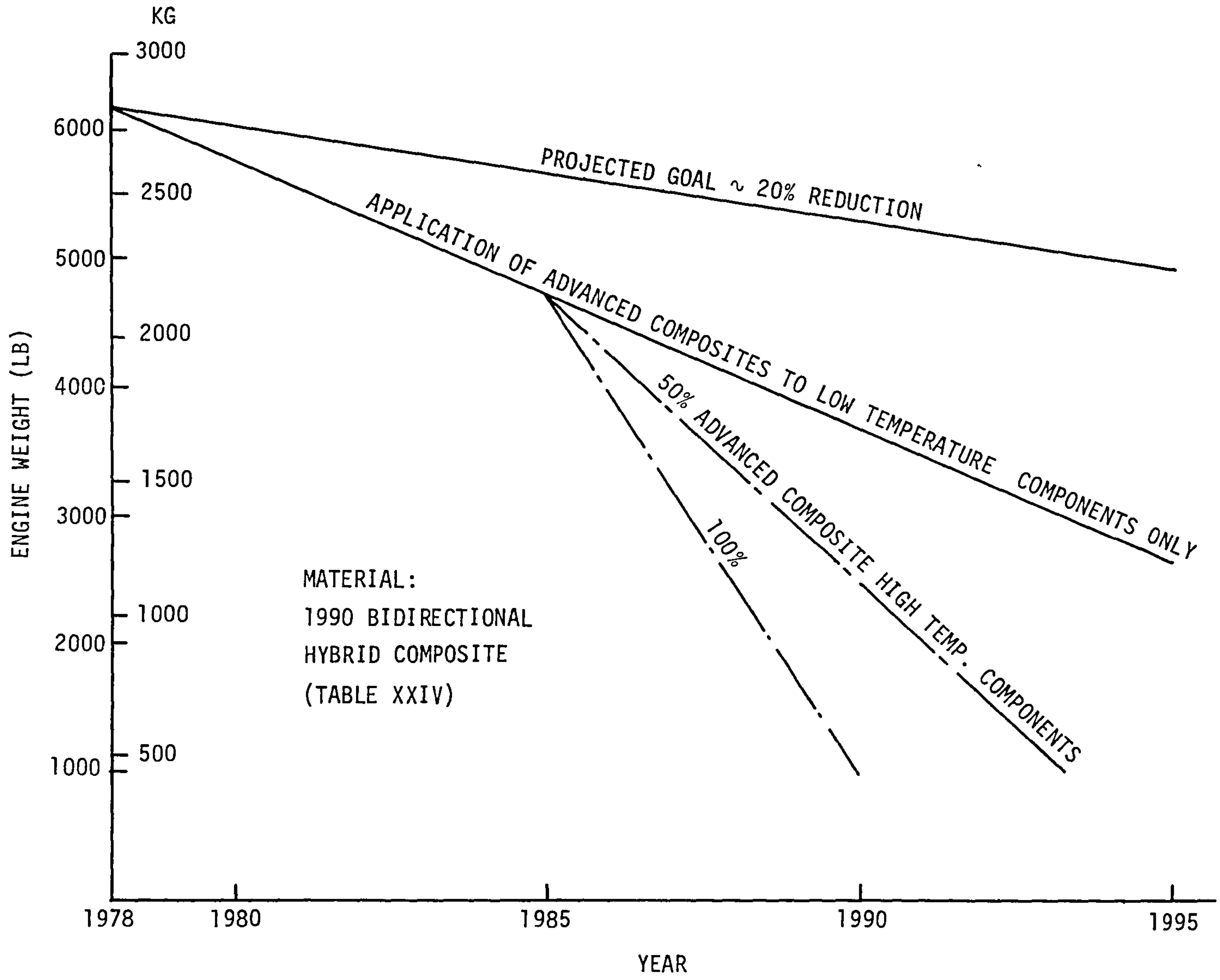

Figure 93, Weight Trends for Tripropellant Dual Throat Engine

It is important to interpret Figure 93 correctly. The figure illustrates the potential of ACM's, but it should be realized that substantial laboratory research and development of these advanced materials is assumed. Therefore, it is important to support laboratory R&D and application studies of promising ACM's at this early stage, if the promised reductions of Figure 93 are to be realized.

D. ENGINE ENVELOPE

Envelope scaling equations based upon geometric considerations were formulated as functions of thrust, stream-tube thrust split, thrust chamber pressure and area ratio. Typical chamber geometry variations with stream-tube thrust split to give maximum engine performance are depicted in Figures 94 through 97.

The diameter and length parametrics for the dual throat engines were calculated using the envelopes established for similar engines in Ref. (6). This assumption proved satisfactory when the dual throat engine layout was prepared (see Section V,B). The parametrics assume a similar engine packaging arrangement for all power cycles. Diameter parametrics include an estimation of the powerhead diameter (pump envelope) to establish whether the nozzle exit or this envelope is greater. In essentially all cases the nozzle exit diameter exceeded the powerhead diameter.

The parametric envelope data for the dual throat engines are given in Figures 98, 99 and 100 at three primary chamber pressures.

E. MISSION APPLICATION

A preliminary assessment of dual throat rocket propulsion was made for

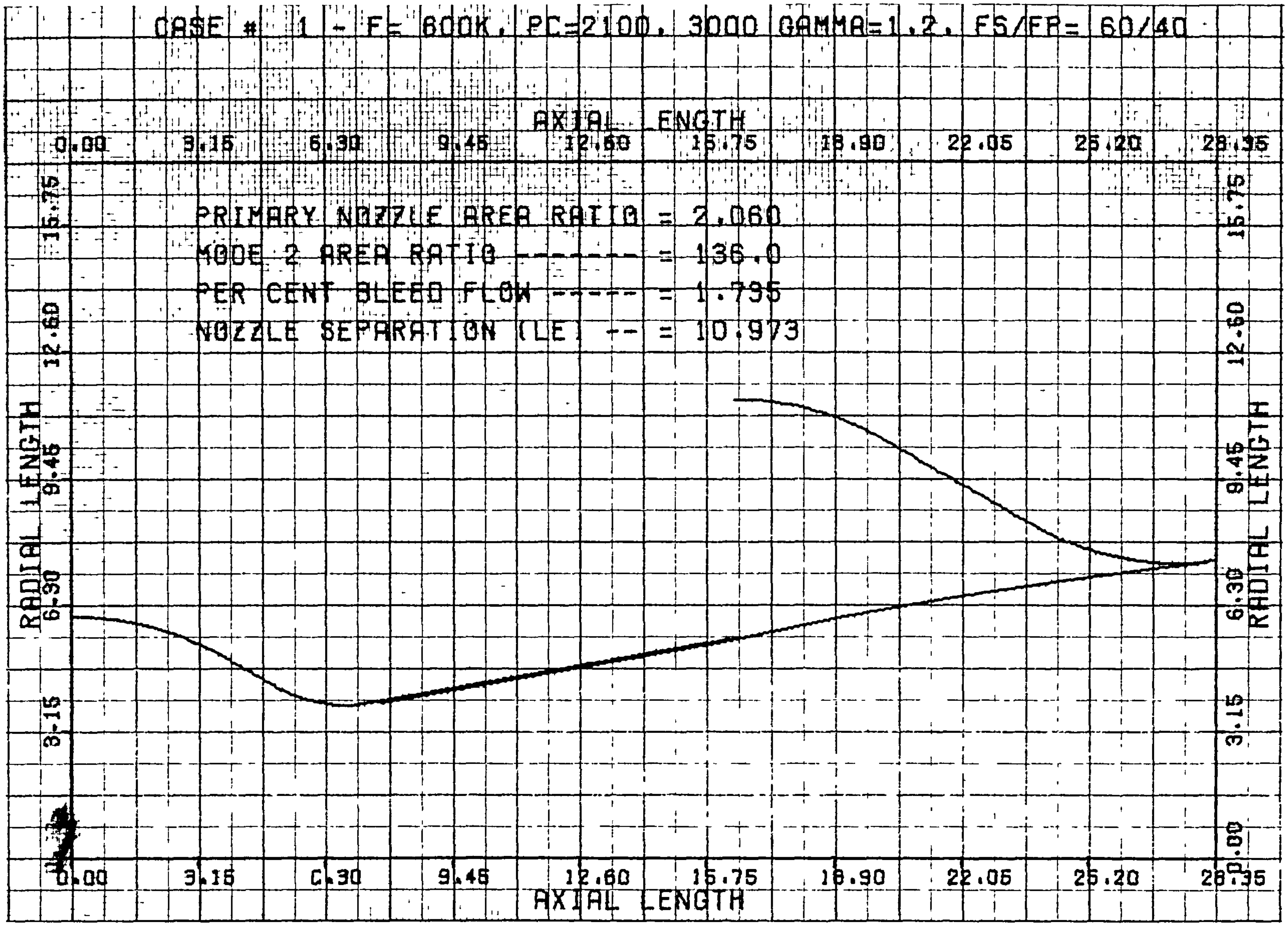

Figure 94. Geometry Determination for Maximum Performance (60/40)

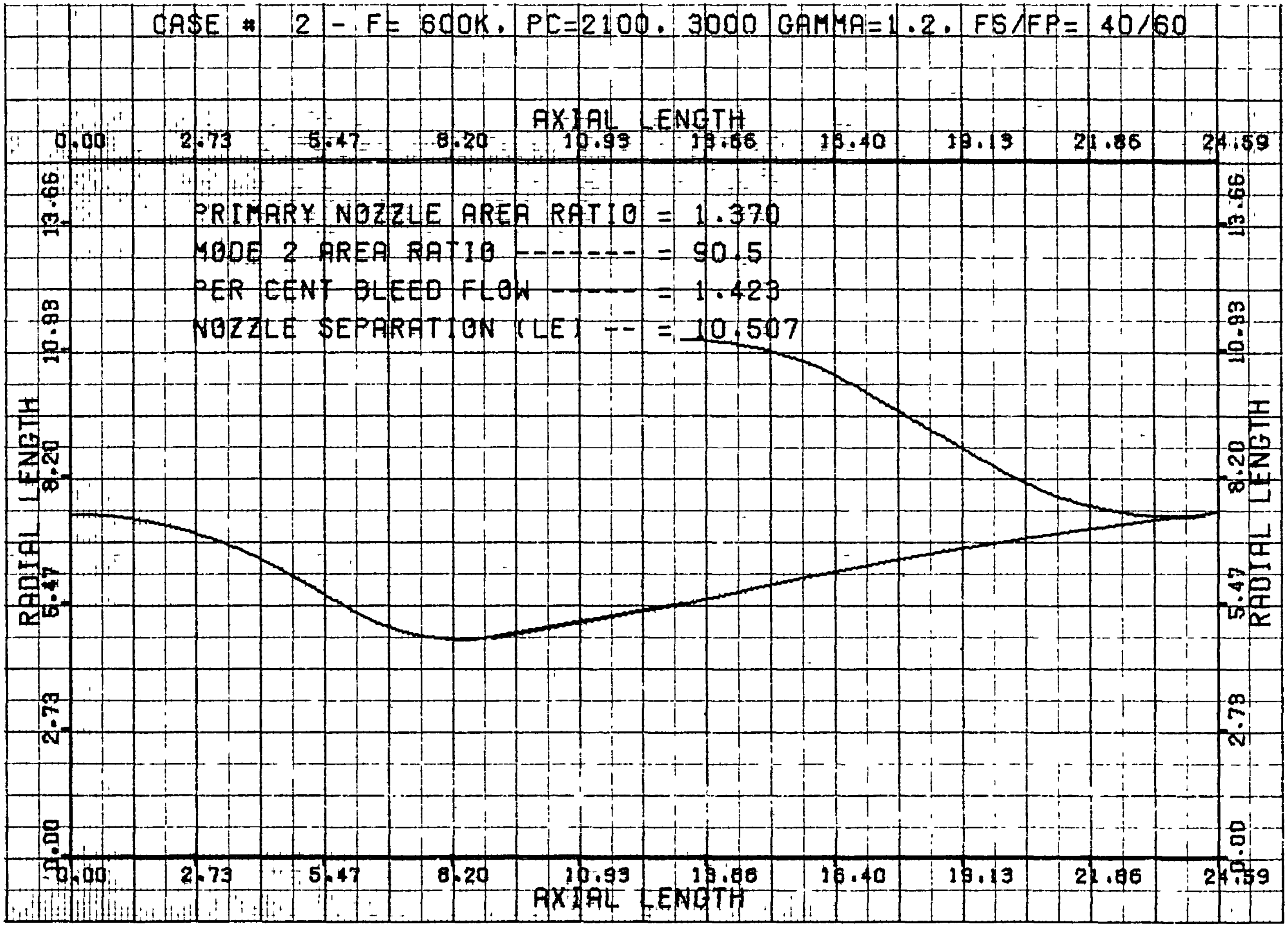

Figure 95. Geometry Determination for Maximum Performance (40/60)

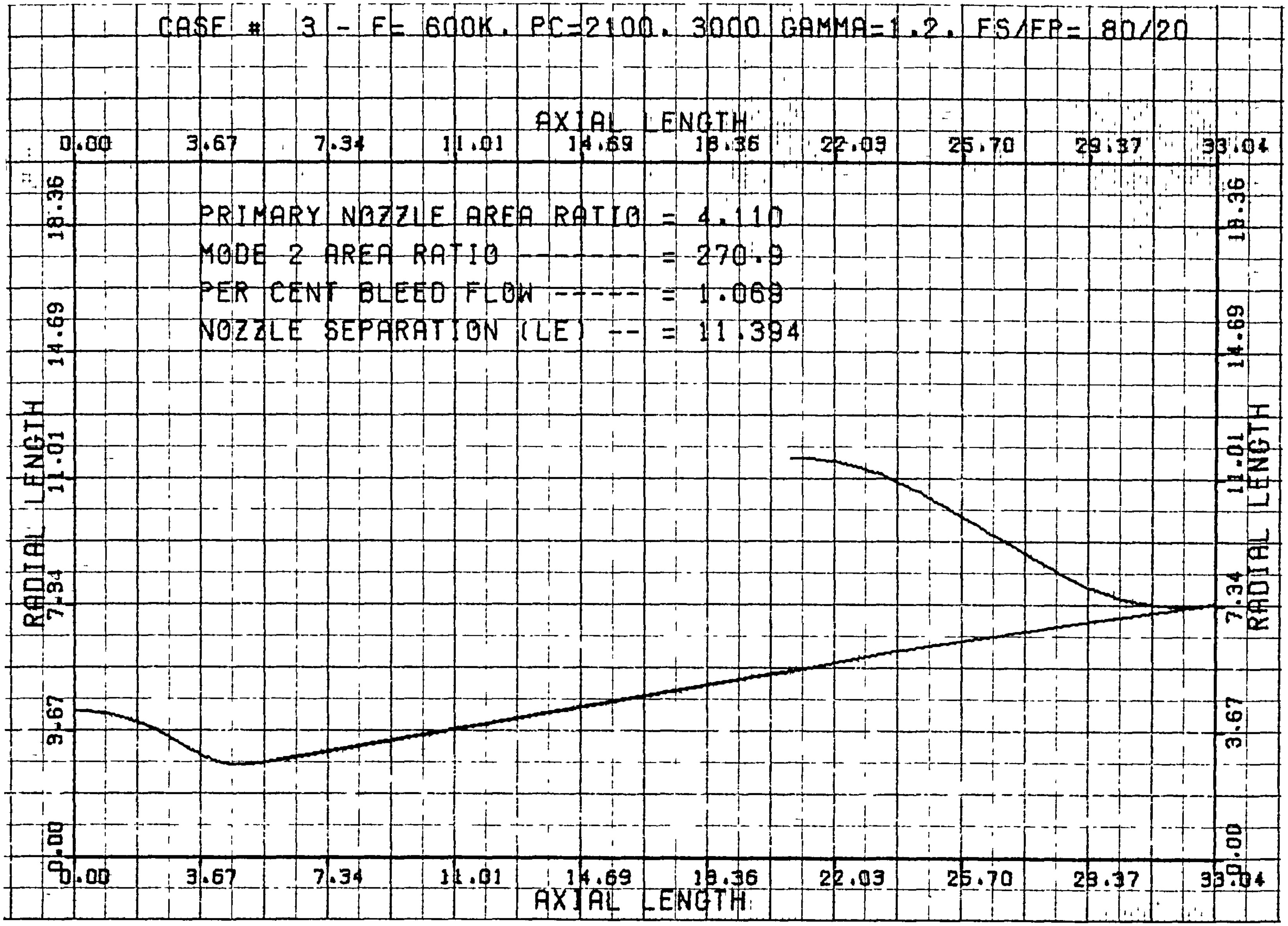

Figure 96. Geometry Determination for Maximum Performance (80/20)

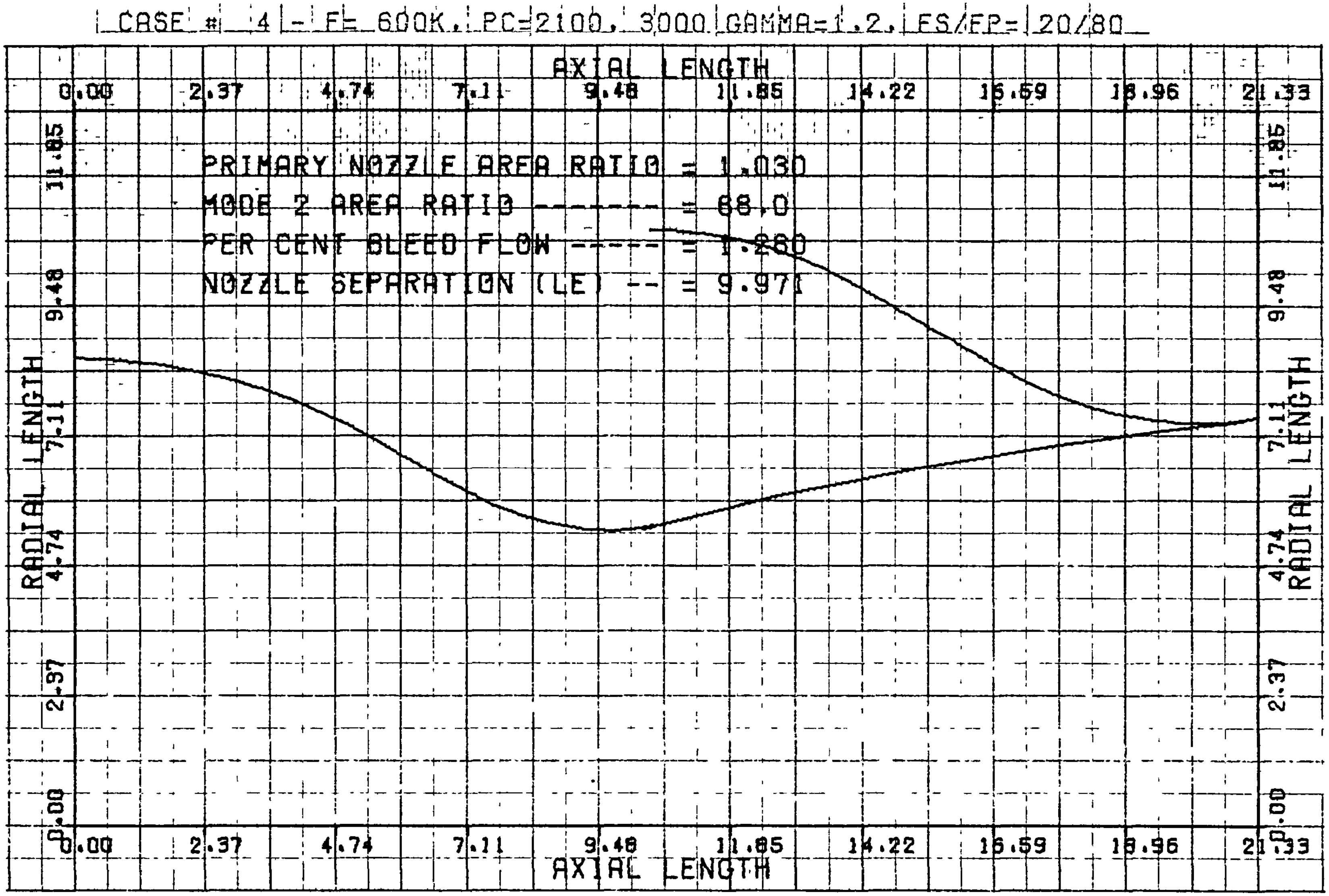

Figure 97. Geometry Determination for Maximum Performance (20/80)

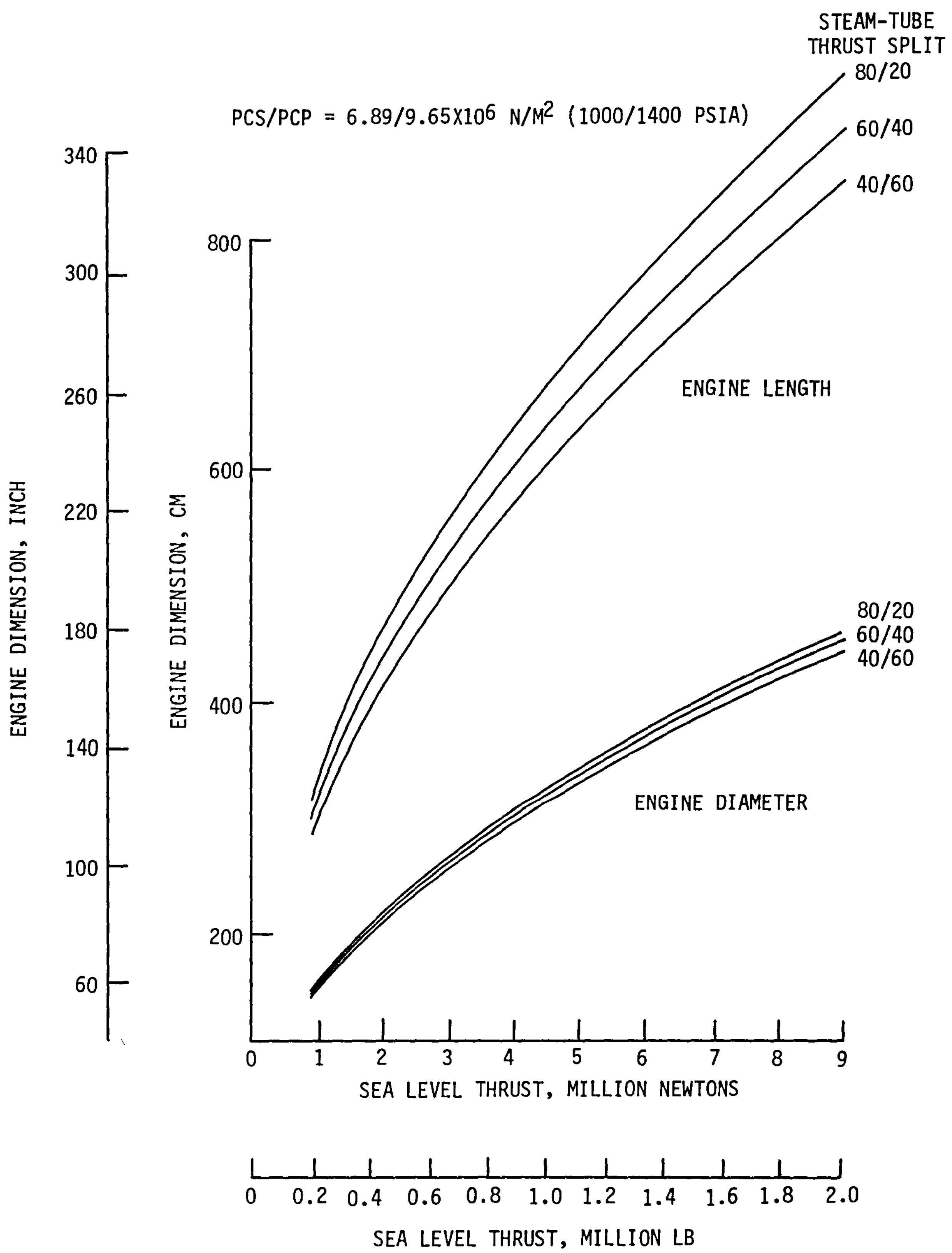

Figure 98. Dual Throat Engine Envelope Parametrics, PcP = 1400

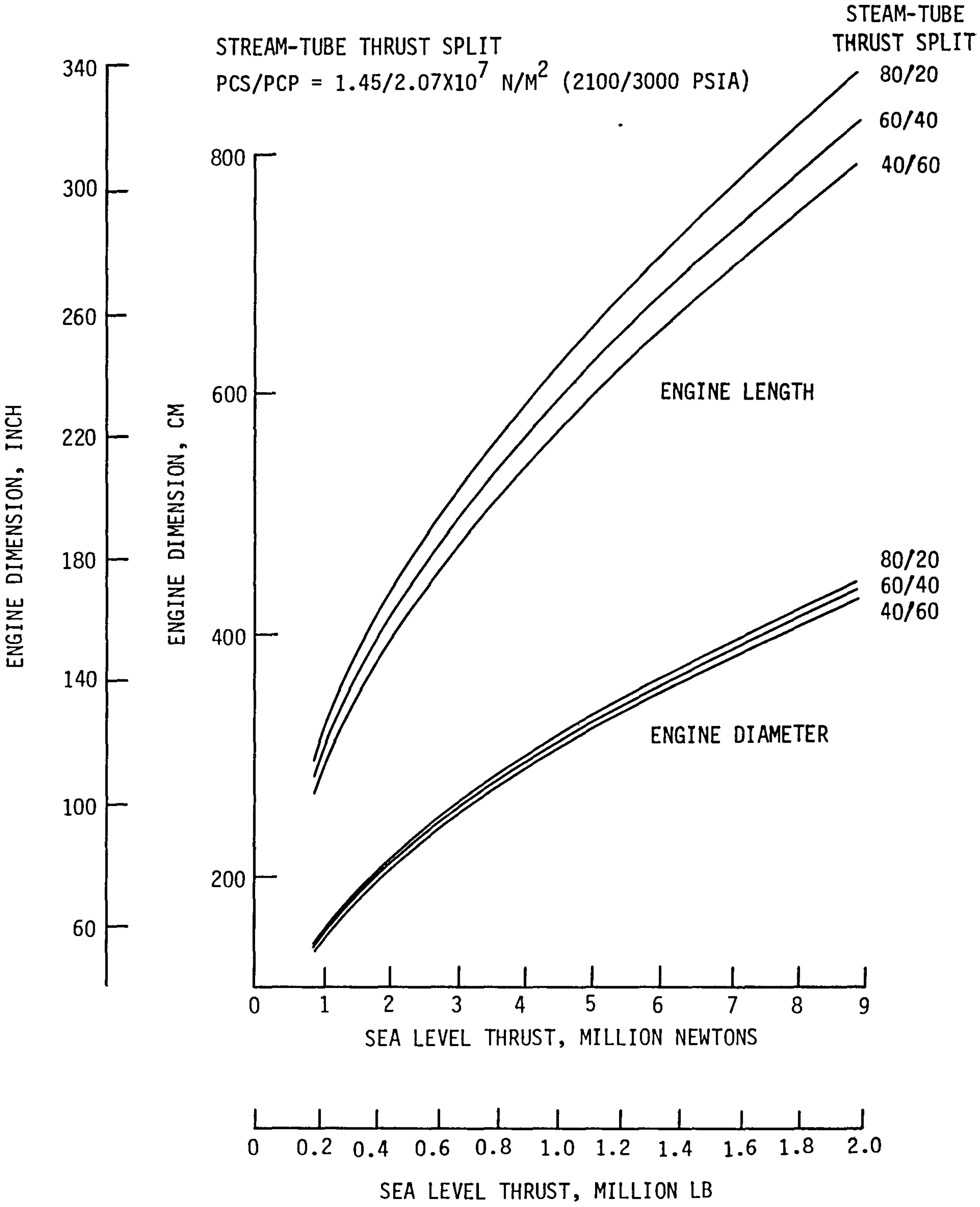

Figure 99. Dual Throat Engine Envelope Parametrics, PCP = 3000

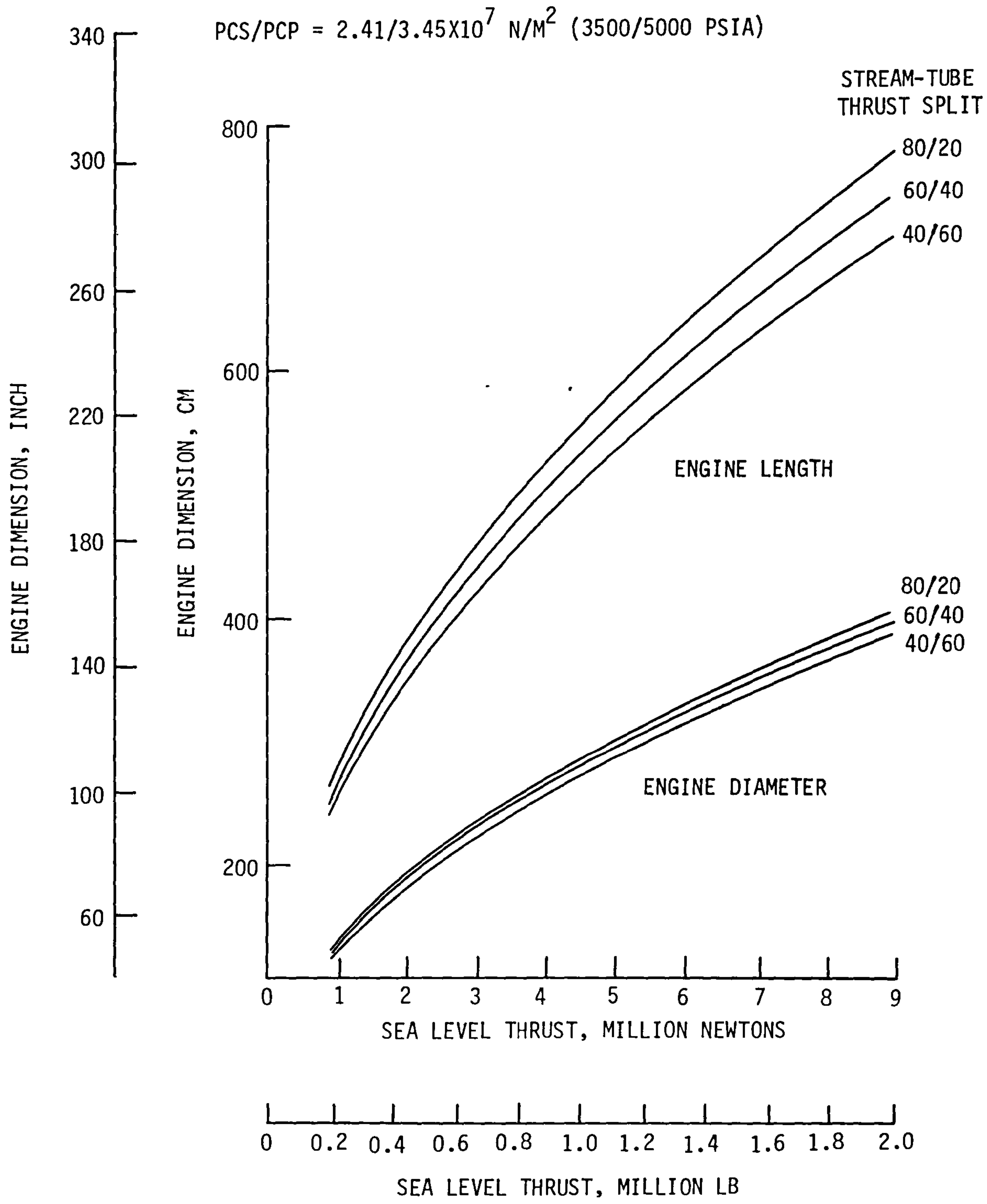

Figure 100. Dual Throat Engine Envelope Parametrics, PCP = 5000

vertical takeoff (VTO) single-stage-to-orbit (SSTO) vehicles in order to: (1) determine the vehicle system performance implications on stream-tube thrust split, and (2) determine the vehicle system performance sensitivity to power cycle selection, primary chamber pressure, and use of LCH_4. This study was performed on ALRC in-house funds, but is included here because the results were beneficial in guiding the power cycle selection.

The assumptions for this analysis are as follows:

- Vehicle weights are scaled from Ref. (1) VTOHL SSTO.
- Ascent propellant volumes constant at 62,900 ft^3.
- Propellant densities are LO_2 = 1307 Kg/m^3 (81.6 lb/ft^3) at NMP; RP-1 = 801 Kg/m^3 (50 lb/ft^3); LH_2 = 72 Kg/m^3 (4.5 lb/ft^3); and LCH_4 = 424 Kg/m^3 (26.5 lb/ft^3).
- LCH_4 is stored in wings and body, similar to RP-1, with no added weight for tanakge modification or insulation.

Weight breakdowns for nine point design vehicles are given in Table XXV. Similar data are provided in Table XXVI for: (1) change in engine cycle to a gas generator/staged combustion cycle, (2) change in primary chamber pressure from 2.07 to 2.76 x 10^7 N/m^2 (3000 to 4000 psia), and (3) change in fuel from RP-1 to LCH_4. The results from this study are summarized in Figures 101, 102 and 103. It can be seen that the analysis indicates a higher stream-tube thrust split is desirable (thrust split > 0.6). Higher stream-tube thrust split values, however, may be limited by other factors, such as g-losses (which accompany reduced Mode II thrust/weight ratios and extended burn times).

The optimum volume split varies between about 0.46 (for a stream-tube thrust split of 0.2) and 0.38 (for a stream-tube thrust split of 0.8). At the Ref. (1) vehicle gross liftoff weight (GLOW = 1.06 x 10^6 Kg or 2339 Klb), the baseline engine provides about six percent less payload (2.8 x 10^4 Kg or 61 Klb). If the stream-tube thrust split of the baseline engine is increased to about 0.72 (72/28) and the volume split, V_I/V, is reduced

TABLE XXV

SOME POINT DESIGN VEHICLES CONSIDERED
(ASCENT PROP. VOL = CONST = 62,900 FT^3) (10^3 LB)

Stream-Tube Thrust Split	0.4			0.6			0.8			REF. 1 NASA CR2968
Volume Split	0.35	0.55	0.75	0.35	0.55	0.75	0.35	0.55	0.75	
Inerts	305	302	331	305	301	325	307	308	327	303
Mode II O_2/H_2	1,062	735	408	1,062	735	408	1,062	735	408	696
Mode I O_2/RP-1/H_2	737	1,158	1,579	972	1,528	2,083	1,206	1,895	2,593	1,340
Payload	37	45	20	56	68	49	78	90	72	65
Glow	2,076	2,175	2,274	2,330	2,567	2,800	2,588	2,963	3,335	2,339

TABLE XXVI

ADDITIONAL POINT DESIGN VEHICLES CONSIDERED

(ASCENT PROP. VOL = CONST. = 62,900 FT^3) (10^3 LB)

Design Option	Preliminary Baseline (RP-1/SC/Pc = 2100/3000)		Cycle Change GG/SC Cycle		Pc Change Pc = 2800/4000		Fuel Change $O_2/CH_4/H_2$		Ref. 1 NASA CR2868
Stream-Tube Thrust Split	60/40	80/20	60/40	80/20	60/40	80/20	60/40	80/20	
Inerts	239	250	233	240	239	250	233	244	303
Mode II O_2/H_4	980	1,013	943	966	980	1,013	980	1,013	696
Mode I O_2/ HC/H_2	1,111	1,325	1,079	1,291	1,111	1,310	1,002	1,128	1,340
Payload	61	82	55	72	67	89	58	72	65
Glow	2,391	2,670	2,310	2,563	2,397	2,662	2,273	2,457	2,339

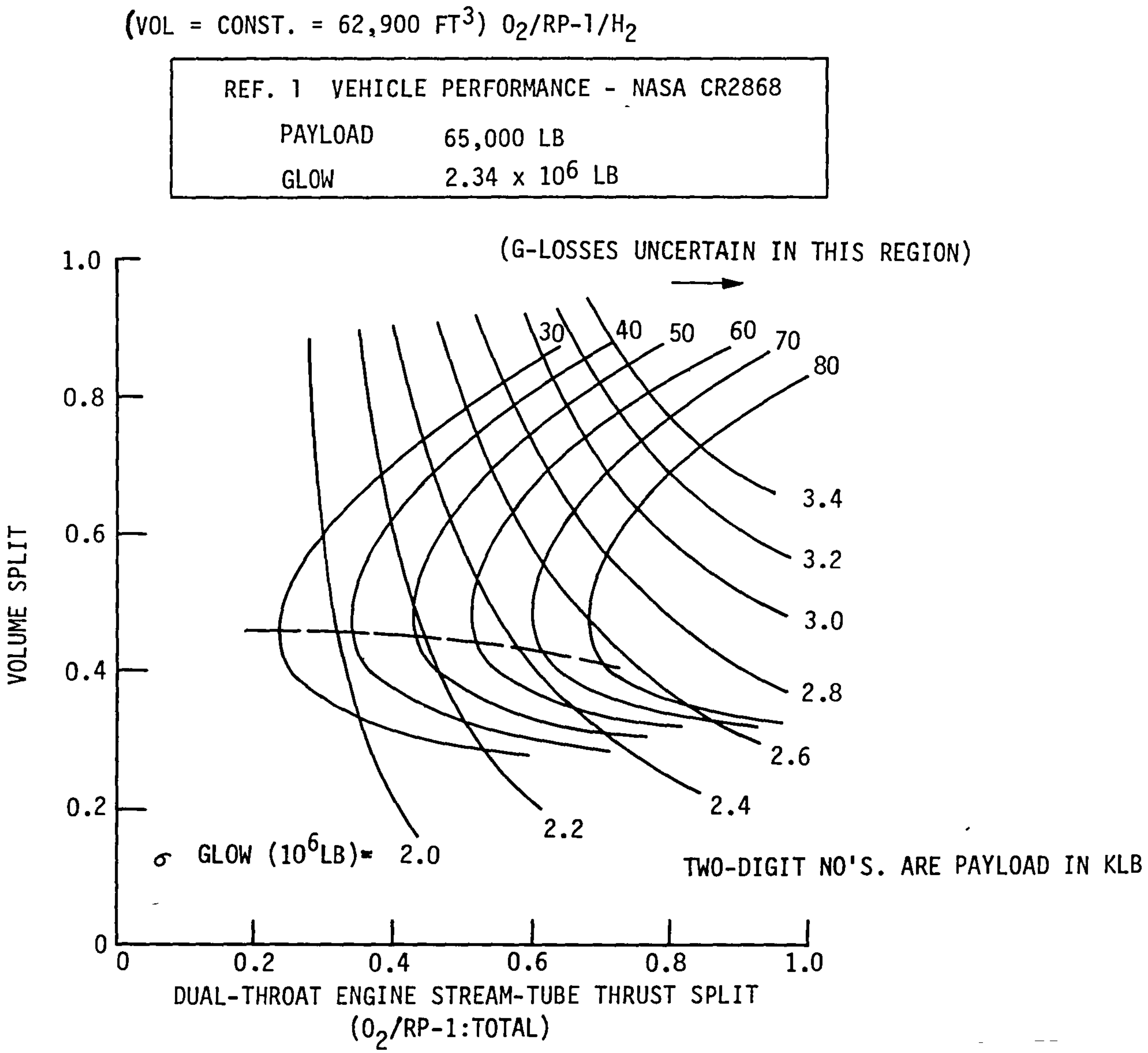

Figure 101. Mixed-Mode Optimization of VTOHL SSTO Shuttle - Payloads

(ASCENT PROPELLANT VOL = CONST. = 62,900 FT^3) O_2/RP-1/H_2

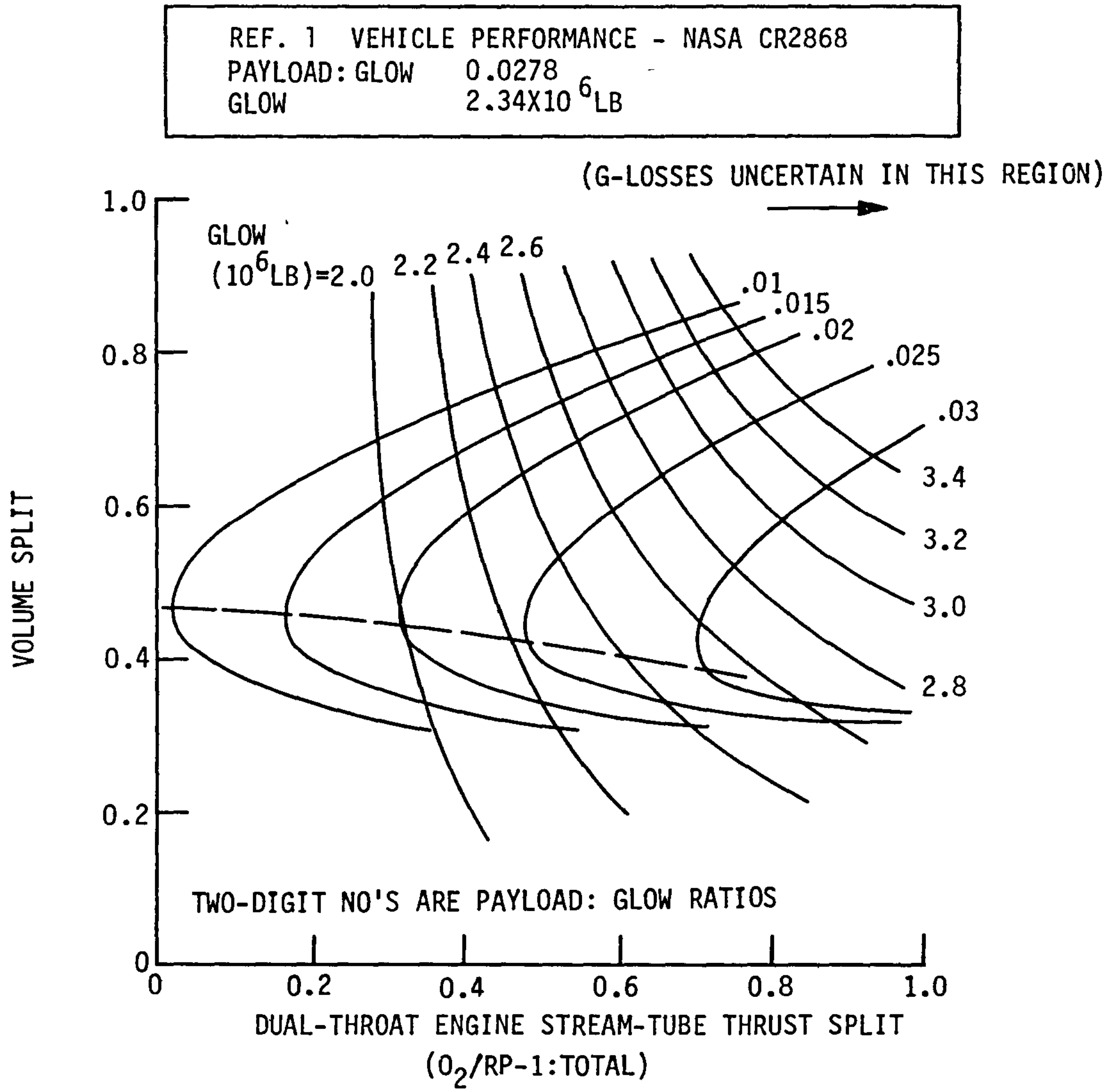

Figure 102. Mixed-Mode Optimization of VTOHL SSTO Shuttle - Payload/GLOW

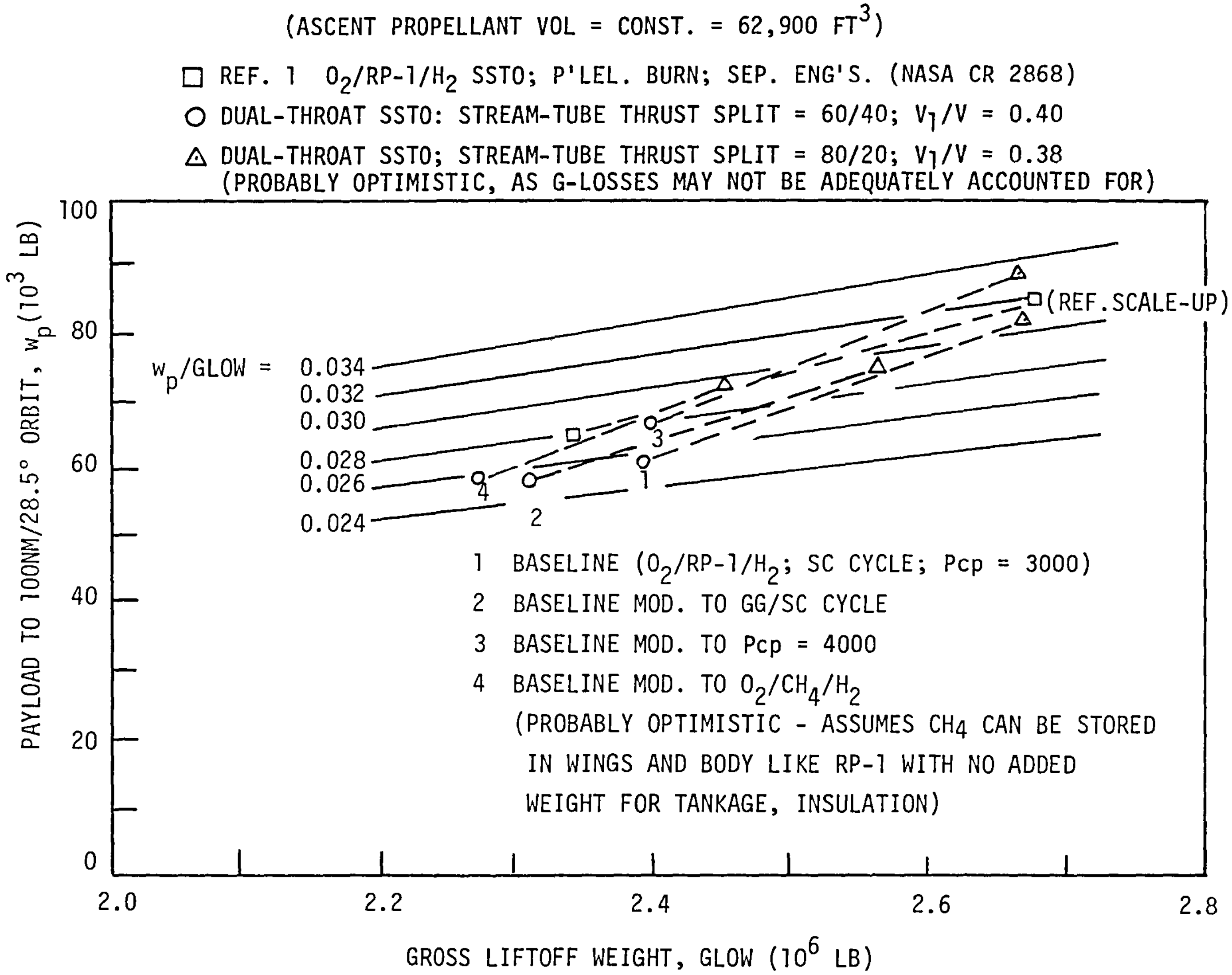

Figure 103. Comparative SSTO Weight and Performance Trends

to about 0.39, the payload/GLOW ratio can be made to exceed the reference vehicle by about eight percent (total gain of about 15%) for a GLOW increase of about eight percent.

The gas generator/staged combustion cycle provides a slight gain in vehicle performance because of its lower engine weight (181 Kg or 400 pounds/engine).

Both higher chamber pressure and the use of LCH_4 fuel appear to provide payload gains of 2,300 to 4,500 Kg (5,000 to 10,000 pounds) at a given GLOW, if there are no tanking/insulation weight penalties for LCH_4 versus RP-1, and if g-losses are not significant at stream-tube thrust splits greater than 60/40 to 70/30.

Compared to the Reference 1 vehicle, which utilized LO_2/RP-1 engines at Pc = 2.76×10^7 N/m^2 (4000 psia) and advanced SSME's at Pc = 2.76×10^7 N/m^2 (4000 psia), an optimized dual-fuel, dual throat engine (PcP = 2.76×10^7 N/m^2 (4000 psia), stream-tube thrust split = 70/30) may provide significant gains in vehicle performance. Additional vehicle performance gains may be realized with LCH_4 fuel if this fuel can be stored in the wings, as assumed in the analysis.

SECTION V

BASELINE ENGINE SYSTEM

A. OBJECTIVES AND GUIDELINES

The preliminary definition of the selected dual throat baseline engine was prepared in this task. This definition includes:

- Overall engine system sketch
- Engine system schematic
- Engine power balance
- Engine and component operating characteristics
- Overall engine envelope
- Weight breakdown by major components
- Predicted performance level
- Start and shutdown sequence.

B. ENGINE CONFIGURATION

The engine cycle selected for the dual throat engine is the gas generator/staged combustion mixed cycle. Selection criteria are summarized in Table IX, Section III,B,7. The engine schematic is shown in Figure 104 including the engine control requirements. The engine utilizes LH_2 cooled chambers and an LO_2 cooled nozzle. The primary chamber uses gaseous propellant main injection and dual preburners in both operating modes. The secondary chamber operates in Mode I only with a gas-liquid main injector. The LO_2 turbopump for the LO_2/RP-1 system is driven by a LOX-rich preburner.

The secondary thrust chamber assembly design incorporates a slotted zirconium copper chamber to a nozzle area ratio of 8:1. An Inconel 718, two pass, tube bundle is utilized from 8:1 to an area ratio of 52:1. The primary chamber assembly utilizes slotted zirconium copper to an area ratio of 1.8:1,

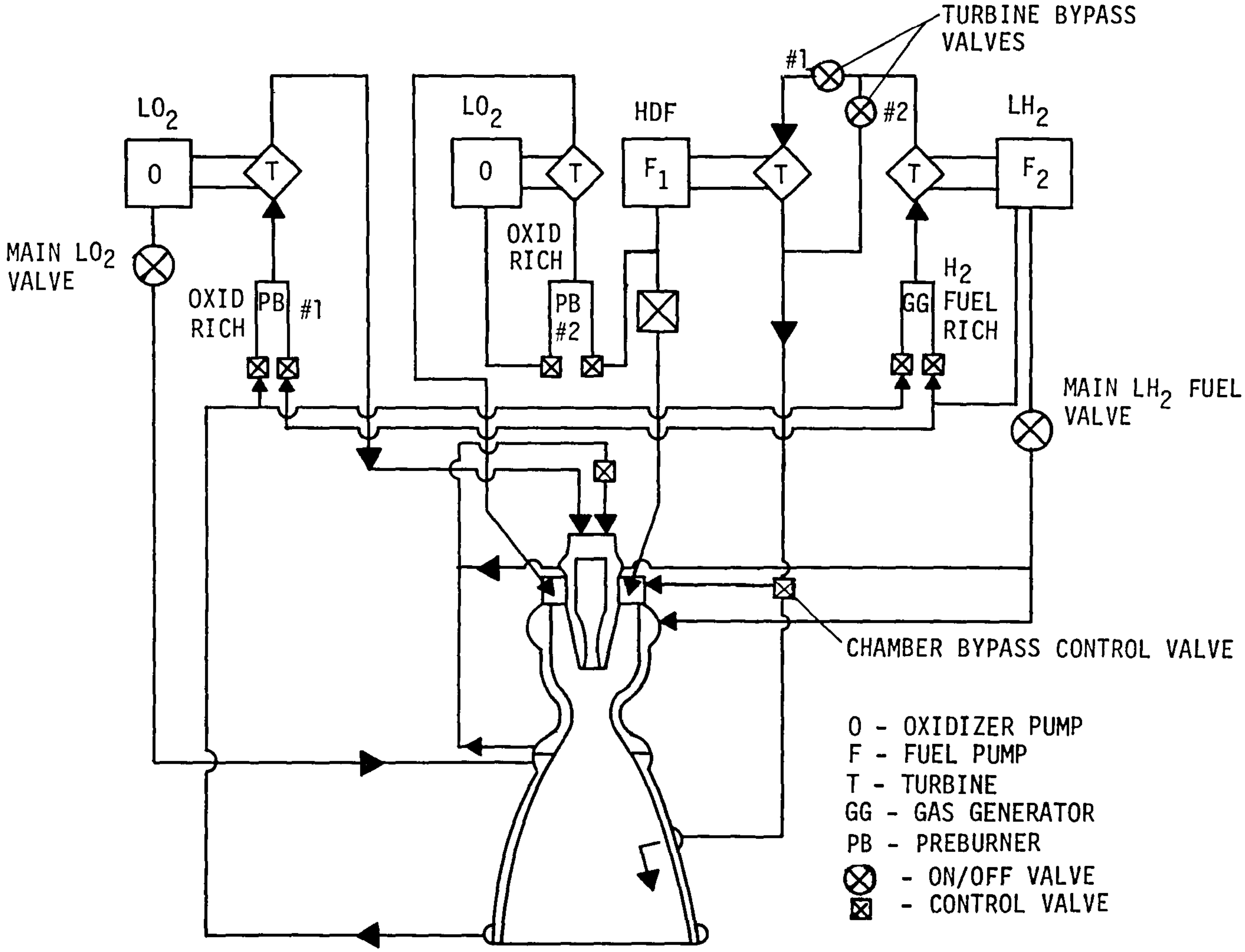

Figure 104. Dual-Fuel, Dual-Throat Engine Gas Generator/Staged Combustion Mixed Cycle

regeneratively cooled on both inner and outer walls with LH_2. Trans-regen cooling will most likely be incorporated into this design in the throat region and primary nozzle exit section.

The preliminary assembly drawing of the baseline engine is shown in Figures 105 and 106. The engine features fixed boost pumps for each propellant circuit clustered around the engine gimbal center. The TPA's are side mounted in order to obtain a favorable center of gravity location.

The engine envelope data are:

Engine Length, cm (in.)	457 (180
Nozzle Exit Diameter, cm (in.)	233 (91.8)

These data are compared in Figure 107 with data generated from the parametric equations used in Section IV,D.

The gimballed envelope was evaluated for a 10° square pattern.

C. NOMINAL OPERATING CONDITIONS

The engine operating conditions for the nominal design point are presented in Table XXVII for both the Mode I and Mode 2 engine operation.

The engine pressure schedules for Mode I and Mode 2 nominal engine operation are given in Table XXVIII.

D. ENGINE OPERATION AND CONTROL

A controls component preliminary evaluation was conducted to determine

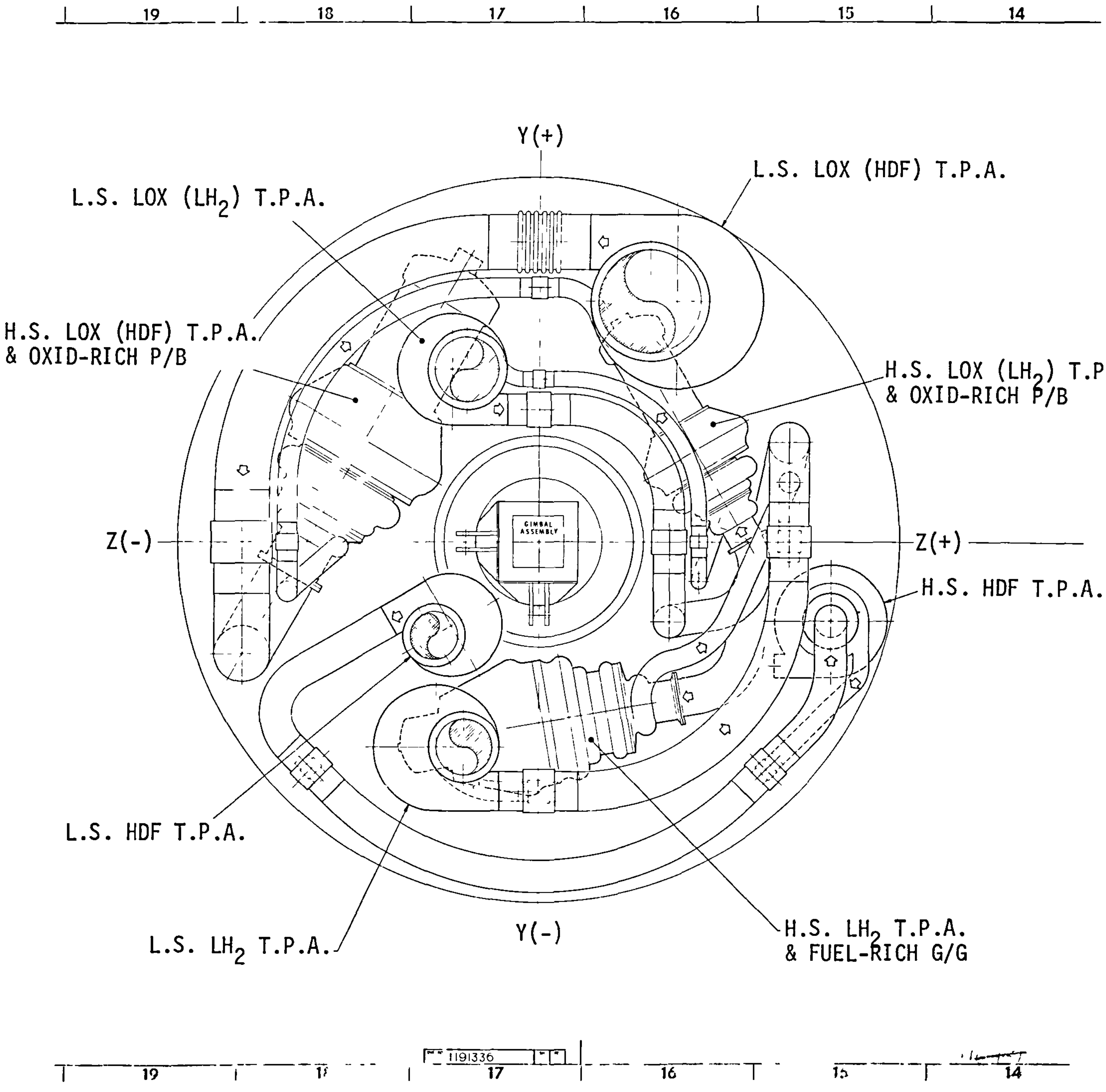

Figure 105. Dual Throat Engine Assembly (Top View)

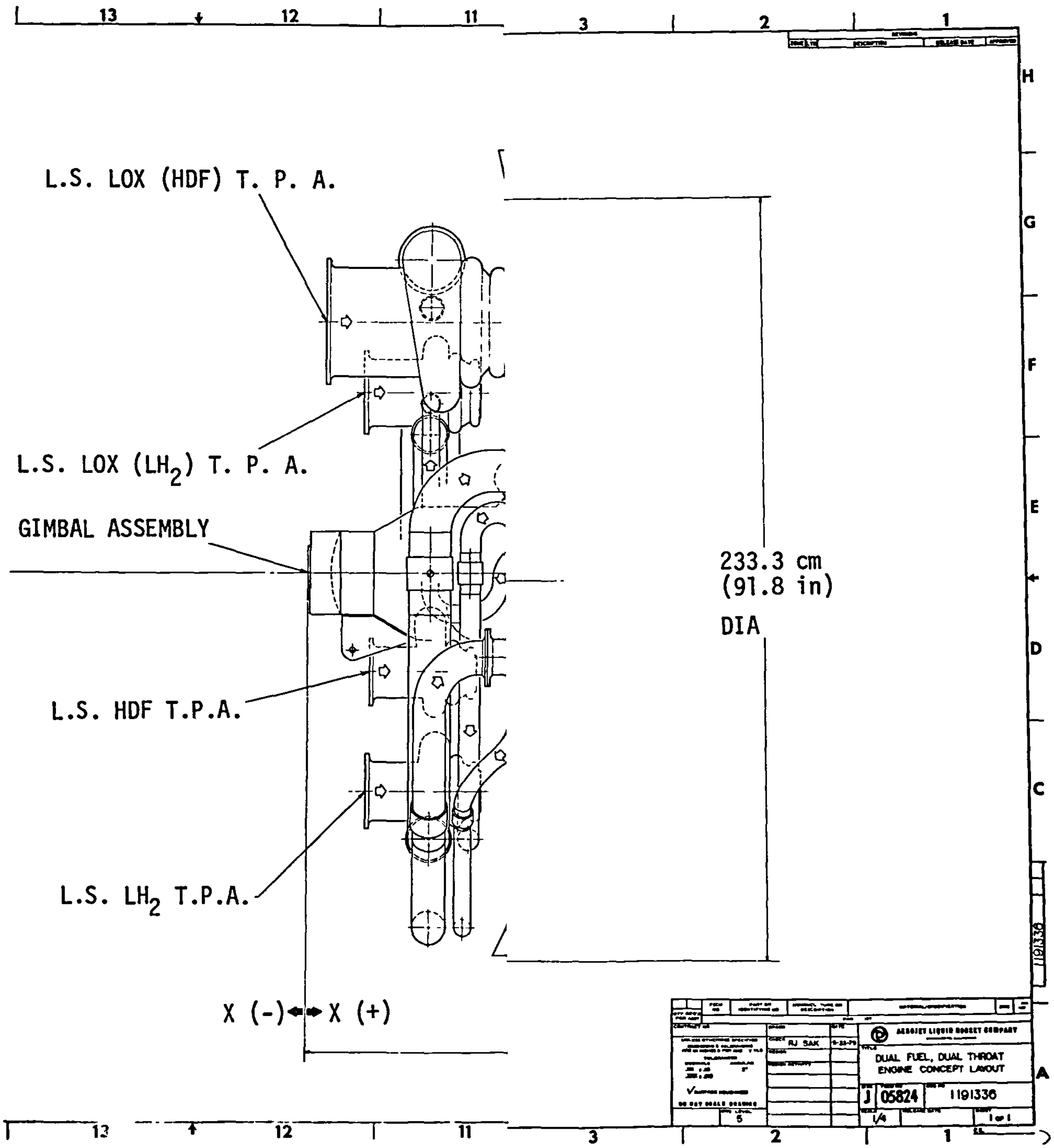

Dual Throat Engine Assembly (Side View)

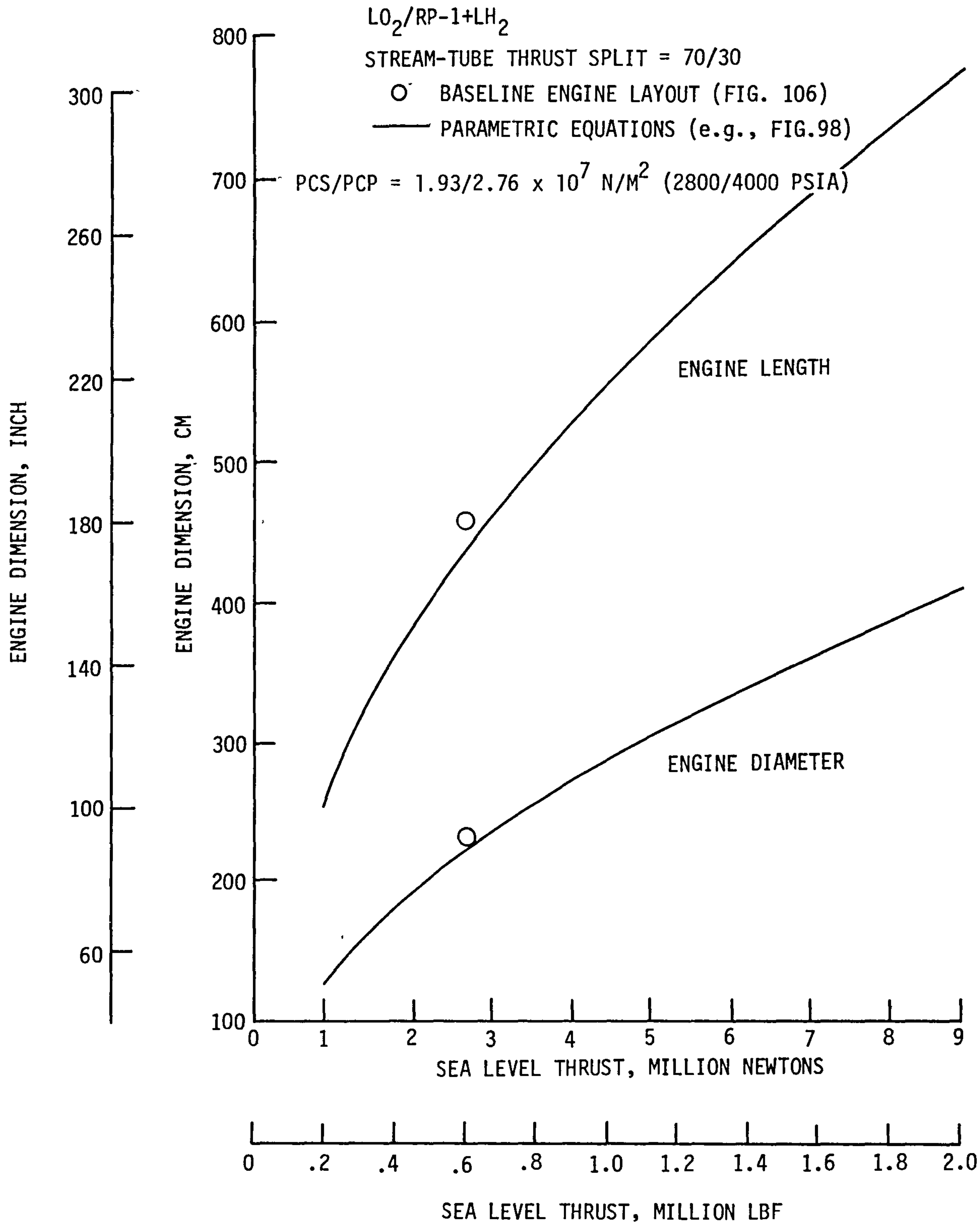

Figure 107. Baseline Dual Throat Engine Envelope Parametrics

TABLE XXVII

OPERATING SPECIFICATION - DUAL-FUEL, DUAL-THROAT ENGINE (GG/SC)

(SI UNITS)

ENGINE	MODE I	MODE II
Sea-Level Thrust (N)	2,684,600	-
Vacuum Thrust (N)	3,080,900	965,400
Mixture Ratio (LOX/RP-1)	2 8	-
Mixture Ratio (LOX/LH_2)	5 81	6 13
Sea-Level Specific Impulse (sec)	327 6	-
Vacuum Specific Impulse (sec)	376 0	463 3
Total Flow Rate (KG/sec)	835 62	212 49
LOX (RP-1) Flow Rate (KG/sec)	456 80	-
RP-1 Flow Rate (KG/sec)	163 14	-
LOX (LH_2) Flow Rate (KG/sec)	179 73	179 73
LH_2 Flow Rate (KG/sec)	25 67	25 67
LOX (GG) Flow Rate (KG/sec)	4 30	2 97
LH_2 (GG) Flow Rate (KG/sec)	5 97	4 12
Chamber Pressure (10^7 N/M^2)	1 93/2 76	2 76
Nozzle Area Ratio	52	232
Throat Diameter (cm)	30 99	14 66
Nozzle Exit Diameter (cm)	223 0	223 0
Coolant Jacket Flow Rate (LH_2) (KG/sec)	24 04	24 04
Coolant Jacket Flow Rate (LO_2) (KG/sec)	184 03	182 70
Coolant Jacket ΔP (LH_2) (10^7 N/M^2)	1 26	1 26
Coolant Jacket ΔP (LOX) (10^6 N/M^2)	1 79	1 79
Coolant Inlet Temp (LH_2) (°K)	61	61
Coolant Inlet Temp (LOX) (°K)	111	111
Coolant Exit Temp (LH_2) (°K)	367	<367
Coolant Exit Temp (LOX) (°K)	283	<283
Chamber Length (cm)	40 1	39 1
Chamber Diameter (cm)	50 0	20 3
Engine Length (cm)	457 2	457 2
Engine Diameter (cm)	233 2	233 2
GAS GENERATOR		
Chamber Pressure (10^7 N/M^2)	4 03	4 03
Combustion Temperature (°K)	1033	1033
Mixture Ratio	0 72	0 72
LOX Flow Rate (KG/sec)	4 30	2 97
LH_2 Flow Rate (KG/sec)	5 97	4 12
TURBINE EXHAUST PERFORMANCE		
Sea-Level Thrust (N)	15,618	-
Vacuum Thrust (N)	28,753	21,836
Sea-Level Specific Impulse (sec)	155 0	-
Vacuum Specific Impulse (sec)	285 4	313 9
Gas Flow Rate (KG/sec)	10 27	7 09
LOX (RP-1) RICH PREBURNER		
Chamber Pressure (10^7 N/M^2)	2 58	-
Combustion Temperature (°K)	9 22	-
Mixture Ratio	45	-
LOX Flow Rate (KG/sec)	456 80	-
RP-1 Flow Rate (KG/sec)	10 15	-
LOX (LH_2) RICH PREBURNER		
Chamber Pressure (10^7 N/M^2)	4 19	4 19
Combustion Temperature (°K)	922	922
Mixture Ratio	110	110
LOX Flow Rate (KG/sec)	179 73	179 73
LH_2 Flow Rate (KG/sec)	1 63	1 63

TABLE XXVII (Con't)

OPERATING SPECIFICATION (Con't)
(SI UNITS)

TURBINES	LOX (RP-1)	LOX (LH_2)	RP-1	LH_2 MODE I	LH_2 MODE II
Inlet Pressure (10^7 N/M^2)	2 58	4 19	0 39	4 03	4 03
Inlet Temperature (°K)	922	922	774	1033	1033
Gas Flow Rate (KG/sec)	467	181	10	10	7
Ratio of Heat Capacities (γ)	1 31	1 312	1 36	1 36	1 36
Molecular Weight, (KG/Mol)	14 5	13 7	1 57	1 57	1 57
Shaft Horsepower (10^7 W)	1 76	1 17	0 90	2 82	2 70
Efficiency (%)	80	80	72	70	70
Speed (RPM)	16,000	16,000	30,000	70,000	70,000
Pressure Ratio	1 19	1 34	2 31	7 75	26 6
Turbine Exit Pressure (10^7 N/M^2)	2 11	3 01	0 17	0 52	0 15
Turbine Exit Temperature (°K)	885	861	621	601	448
MAIN PUMPS					
Outlet Flow Rate (KG/sec)	456 8	184 0	163 2	24 0/7 6	24 0/5 8
Volumetric Flow Rate (LPM)	24,110	9710	12,240	26,940/454	25,360/344
NPSH (M)	96	96	137	261	261
Suction Specific Speed (RPM X $GPM^{1/2}/FT^{3/4}$)	20,000	20,000	20,000	20,000	20,000
Speed (RPM)	16,000	16,000	30,000	70,000	70,000
Discharge Pressure (10^7 N/M^2)	3 16	5 27	3 16	4 34/4 96	4 34/4 96
Number of Stages	2	2	1	3	3
Specific Speed (RPM X $GPM^{1/2}/FT^{3/4}$)	2327/STG	1612/STG	1552	1392/339	1351/295
Total Head Rise (M)	2737	2388	3456	6279	6279
Efficiency (%)	77	76	76	75/42	75/36
LOW SPEED TPA					
NPSH (M)	4 9	4 9	19 8	30 5	30 5
Inlet Flow Rate (KG/sec)	456 8	184 0	163 2	31 7	29 8
Outlet Flow Rate (KG/sec)	581 6	234 4	202 2	37 0	34 8
Discharge Pressure (10^6 N/M^2)	1 24	1 24	1 24	0 32	0 32
Number of Stages	1	1	1	1	1
Efficiency (%)	77	77	77	77	77
HYDRAULIC TURBINE					
Inlet Pressure (10^6 N/M^2)	9 65	9 65	9 65	3 38	3 38
Outlet Pressure (10^6 N/M^2)	1 24	1 24	1 24	0 32	0 32
Flow Rate (KG/sec)	125	50 4	39 1	5 4	5 0
Number of Stages	3	3	3	3	3
Efficiency (%)	70	70	80	80	80

TABLE XXVII (Cont)

OPERATING SPECIFICATION - DUAL-FUEL, DUAL-THROAT ENGINE (GG/SC)

ENGLISH UNITS

ENGINE		MODE I	MODE II
Sea-Level Thrust (lb_f)		603,511	-
Vacuum Thrust (lb_f)		692,624	217,033
Mixture Ratio (LOX/RP-1)		2 8	-
Mixture Ratio (LOX/LH_2)		5 81	6 13
Sea-Level Specific Impulse (sec)		327 6	-
Vacuum Specific Impulse (sec)		376 0	463 3
Total Flow Rate (lb/sec)		1842 22	468 47
LOX (RP-1) Flow Rate (lb/sec)	SECONDARY CHAMBER	1007 07	-
RP-1 Flow Rate (lb/sec)	SECONDARY CHAMBER	359 67	-
LOX (LH_2) Flow Rate (lb/sec)	PRIMARY CHAMBER	396 23	396 23
LH_2 Flow Rate (lb/sec)	PRIMARY CHAMBER	56 60	56 60
LOX (GG) Flow Rate (lb/sec)	GAS GENERATOR	9 48	6 55
LH_2 (GG) Flow Rate (lb/sec)	GAS GENERATOR	13 17	9 09
Chamber Pressure (psia)		2800/4000	4000
Nozzle Area Ratio		52	232
Throat Diameter (in)		12 2	5 77
Nozzle Exit Diameter (in)		97 8	87 8
Coolant Jacket Flow Rate (LH_2) (lb/sec)		53 00	53 00
Coolant Jacket Flow Rate (LO_2) (lb/sec)		405 71	402 78
Coolant Jacket ΔP (LH_2) (psi)		1830	1830
Coolant Jacket ΔP (LOX) (psi)		260	260
Coolant Inlet Temp (LH_2) (°R)		110	110
Coolant Inlet Temp (LOX) (°R)		200	200
Coolant Exit Temp (LH_2) (°R)		660	<660
Coolant Exit Temp (LOX) (°R)		510	<510
Chamber Length (in)		15 8	15 4
Chamber Diameter (in)		19 7	8 0
Engine Length (in)		180 0	180 0
Engine Diameter (in)		91 8	91 8

GAS GENERATOR	MODE I	MODE II
Chamber Pressure (psia)	5843	5843
Combustion Temperature (°R)	1860	1860
Mixture Ratio	0 72	0 72
LOX Flow Rate (lb/sec)	9 48	6 55
LH_2 Flow Rate (lb/sec)	13 17	9 09

TURBINE EXHAUST PERFORMANCE	MODE I	MODE II
Sea-Level Thrust (lb_f)	3511	-
Vacuum Thrust (lb_f)	6464	4909
Sea-Level Specific Impulse (sec)	155 0	-
Vacuum Specific Impulse (sec)	285 4	313 9
Gas Flow Rate (lb/sec)	22 65	15 64

LOX (RP-1) RICH PREBURNER	MODE I	MODE II
Chamber Pressure (psia)	3740	-
Combustion Temperature (°R)	1660	-
Mixture Ratio	45	-
LOX Flow Rate (lb/sec)	1007 07	-
RP-1 Flow Rate (lb/sec)	22 38	-

LOX (LH_2) RICH PREBURNER	MODE I	MODE II
Chamber Pressure (psia)	6071	6071
Combustion Temperature (°R)	1660	1660
Mixture Ratio	110	110
LOX Flow Rate (lb/sec)	396 23	396 23
LH_2 Flow Rate (lb/sec)	3 60	3 60

TABLE XXVII (Cont)

OPERATING SPECIFICATION (Cont)

(ENGLISH UNITS)

TURBINES	LOX (RP-1)	LOX (LH_2)	RP-1	LH_2 MODE I	LH_2 MODE II
Inlet Pressure (psia)	3740	6071	572	5843	5843
Inlet Temperature (°R)	1660	1660	1393	1860	1860
Gas Flow Rate (lb/sec)	1029 5	399 8	22 7	22 7	15 6
Ratio of Heat Capacities (γ)	1 31	1 312	1 36	1 36	1 36
Molecular Weight (lb/mol)	31 9	30 1	3 467	3 467	3 467
Shaft Horsepower (hp)	23,640	15,670	12,070	37,860	36,200
Efficiency (%)	80	80	72	70	70
Speed (rpm)	16,000	16,000	30,000	70,000	70,000
Pressure Ratio	1 19	1 34	2 31	7 75	26 6
Turbine Exit Pressure (psia)	3059	4370	248	754	220
Turbine Exit Temperature (°R)	1593	1549	1117	1082	806
MAIN PUMPS					
Outlet Flow Rate (lb/sec)	1007 1	405 7	359 7	53 0/16 8	53 0/12 7
Volumetric Flow Rate (gpm)	6369	2566	3234	7117/120	6700/91
NPSH (ft)	316	316	450	855	855
Suction Specific Speed (RPM x $GPM^{1/2}/FT^{3/4}$)	20,000	20,000	20,000	20,000	20,000
Speed (rpm)	16,000	16,000	30,000	70,000	70,000
Discharge Pressure (psia)	4584	7646	4584	6294/7200	6294/7200
Number of Stages	2	2	1	3	3
Specific Speed (RPM x $GPM^{1/2}/FT^{3/4}$)	2327/STG	1612/STG	1552	1392/339	1351/295
Total Head Rise (FT)	8,981	7,833	11,337	20,600	20,600
Efficiency (%)	77	76	76	75/42	75/36
LOW SPEED TPA					
NPSH (FT)	16	16	65	100	100
Inlet Flow Rate (lb/sec)	1007 1	405 7	359 7	69 8	65 7
Outlet Flow Rate (lb/sec)	1282 1	516 7	445 8	81 6	76 8
Discharge Pressure (psia)	180	180	180	46	46
Number of Stages	1	1	1	1	1
Efficiency (%)	77	77	77	77	77
HYDRAULIC TURBINE					
Inlet Pressure (psia)	1400	1400	1400	490	490
Outlet Pressure (psia)	180	180	180	46	46
Flow Rate (lb/sec)	275	111	86 1	11 8	11 1
Number of Stages	3	3	3	3	3
Efficiency (%)	70	70	80	80	80

TABLE XXVIII

DUAL THROAT ENGINE PRESSURE SCHEDULE
(SI UNITS)

Propellant Pressure (10^6 N/M^2)	(LOX/RP-1)** (Preburner)	RP-1** (Preburner)	RP-1** (Chamber)	LOX (LH_2) (Preburner)	LH_2 (Preburner)	LOX (LH_2) (Gas Generator)	LH_2 (Gas Generator)	LH_2 (Chamber)
Main Pump Discharge	31 6	31 6	31 6	52 7	49 6	52 7	49 6	43 4
ΔP Shutoff Valve (1%)	-	-	-	0 5	-	0 5	-	0 4
ΔP Line (0 5%)	0 2	0 2	0 2	0 3	0 2	0 3	0 2	0 2
Coolant Jacket Inlet	-	-	-	51 9	-	51 9	-	42 7
ΔP Coolant Jacket	-	-	-	1 8	-	1 8	-	12 6
Coolant Jacket Outlet	-	-	-	50 1	-	50 1	-	30 1
ΔP Line (0 5%)	-	-	-	0 2	-	0 2	-	0 2
ΔP Control Valve (5-10%)	1 9	1 9	1 6	2 5	4 9	2 5	4 9	-
Preburner Inlet	29 6	29 6	-	47 4	44 5	47 4	44 5	-
ΔP Preburner Injector (6-15%)	3 8	3 8	-	5 5	2 7	7 1	2 7	-
Turbine Inlet	25 8 ←	25 8	-	41 9 ←	41 9	40 3 →	40.3	-
Turbine Outlet (1)	21 1	-	-	30 1	-	-	5 2	-
Turbine Outlet (2)	-	-	-	-	-	-	1 7 1 5 (Mode II)	-
ΔP Line (0 5%)	0 1	-	-	0 2	-	-	-	-
Main Injector Inlet	21 0	-	22 7*	30 0	-	-	-	30 0
ΔP Injector (8% & 15%)	1 7	-	3 4	2 4	-	-	-	2 4
Chamber Pressure	19 3	-	19 3	27 6	-	-	-	27 6
Exhaust Dump Pressure	-	-	-	-	-	-	1 7 1 5 (Mode II)	-
Flow Rates (KG/sec)	456 8	10 2	153 0	179 7	1 6	4 3 3 0 (Mode II)	6 0 4 1 (Mode II)	24 0

*Excess pressure available without use of split flow pump
**Operate in Mode I only

TABLE XXVIII (Cont)

DUAL THROAT ENGINE PRESSURE SCHEDULE

(ENGLISH UNITS)

Propellant Pressure (psia)	LOX (RP-1)** (Preburner)	RP-1** (Preburner)	RP-1** (Chamber)	LOX (LH_2) (Preburner)	LH_2 (Preburner)	LOX (LH_2) (Gas Generator)	LH_2 (Gas Generator)	LH_2 (Chamber)
Main Pump Discharge	4584	4584	4584	7646	7200	7646	7200	6294
ΔP Shutoff Valve (1)	-	-	-	76	-	76	-	63
ΔP Line (0 5)	23	23	23	38	36	38	36	31
Coolant Jacket Inlet	-	-	-	7532	-	7532	-	6200
ΔP Coolant Jacket	-	-	-	260	-	260	-	1830
Coolant Jacket Outlet	-	-	-	7272	-	7272	-	4370
ΔP Line (0 5)	-	-	-	36	-	36	-	22
ΔP Control Valve (5-10′)	271	271	228	362	705	362	705	-
Preburner Inlet	4290	4290	-	6874	6459	6874	6459	-
ΔP Preburner Injector (6-15°)	550	550	-	1803	388	1031	388	-
Turbine Inlet	3740 ←	3740	-	6071 ←	6071	5843 →	5843	-
Turbine Outlet (1)	3059	-	-	4370	-	-	754	-
Turbine Outlet (2)	-	-	-	-	-	-	248	-
							220 (Mode II)	-
ΔP Line (0 5)	15	-	-	22	-	-	2	-
Main Injector Inlet	3044	-	3294*	4348	-	-	-	4348
ΔP Injector (8, & 15)	244	-	494	348	-	-	-	348
Chamber Pressure	2800	-	2800	4000	-	-	-	4000
Exhaust Dump Pressure	-	-	-	-	-	-	246	-
							218 (Mode II)	
FLOW RATES (lb/sec)	1007.1	22.4	337 3	396.2	3 6	9 5	13 2	53 0
						6 5 (Mode II)	9 1 (Mode II)	

*Excess pressure available without use of split flow pump

**Operate in Mode I only

basic valve concept selection and sizing for the selected power cycle. The required control functions were identified based on the engine schematic diagram (Figure 104) and the start and shutdown sequence analysis (Table XXIX). A weighted valve configuration trade study was then performed, using the ratings pressented in Figure 108, to aid in the component selection process. Valve configurations were defined and fluid KW requirements were derived based on estimated pressure drop and weight flow requirements. The estimated weights and envelope size for the components were then determined based on historical data, parametric curves and empirical equations developed from other engine programs. A summary of the proposed valve configurations and sizing is presented in Table XXX.

Further study will be necessary to provide for requirements such as engine pre-start chilldown, tank pressurization and instrumentation. In addition, control function transient analysis will be required with respect to concerns such as control of propellant lead-lag during start and shutdown transients, control of thrust level overshoot, mixture ratio, and propellant utilization at steady state conditions.

1. Main Fuel and Oxidizer and RP-1 Pump Turbine Bypass Shutoff Valves

For parallel burn both the LO_2/LH_2 engine circuits will be started and operated to an altitude where the LO_2/RP-1 engine will be shutdown. The LO_2/LH_2 engine will then continue burning until command shutdown prior to orbit insertion. Therefore, based on the start and shutdown sequence it was determined that the main fuel and oxidizer and the RP-1 pump turbine bypass valves would be on/off valves.

The primary function of the main fuel and oxidizer valves is to initiate propellant flow during the engine start squence and shutoff flow

TABLE XXIX

SEQUENCE OF OPERATION - DUAL FUEL DUAL THROAT ENGINE

START

The primary (LOX/LH_2) circuit will be started slightly ahead of the secondary (LOX/RP-1) circuit The primary circuit will utilize a fuel-lead start while the secondary circuit will involve an oxidizer-lead start of from 1 to 3 milliseconds The oxidizer lead procedure is consistent with Titan I and F-1 experience and avoids contamination of the LOX circuit with hydrocarbon fuel [More recent experience (Contract NAS 3-21030) with both oxidizer and fuel lead starts for a LOX/RP-1 igniter showed that smoother starts were achieved with a 1 to 3 millisecond(s) fuel lead This result is attributed to the hydraulics of the system, and the main combustor on that program will utilize a LOX lead to prevent accumulation of fuel during startup]

Oxidizer-rich preburners will incorporate oxidizer-lead starts and oxidizer-lag shutdowns

SEQUENCE

1 Purge all fuel and oxidizer lines and manifolds
2 Chill all cryogenic circuits
3 Energize spark igniters on
4 Open main LH_2 fuel valve
5 Open igniter valves on #1 oxidizer-rich preburner and H_2 fuel-rich gas generator
6 Open main LO_2 valve
7 Open H_2 control valves on #1 oxidizer-rich preburner and H_2 fuel-rich gas generator
8 Open oxidizer control valves on #1 oxidizer-rich preburner and H_2 fuel-rich gas generator
9 Ramp open H_2 control valve to primary (O/H) combustion chamber

[It is assumed that there will be a purge into the secondary (O/RP-1) injector just prior to combustion in the primary chamber to limit the backflow of recirculated gases during the start transient This should eliminate the need for check valves in the lines to the secondary injector] Timing should allow for a fuel-rich start in the primary chamber, but an accidental oxidizer-rich (O/H) start with preburner gas and LH_2 is not a problem for the MR = 7 combustion chamber design, as the combustion temperature is very close to that for stoichiometric (MR=8) conditions

10 Open igniter valves on #2 oxidizer-rich preburner
11 Open LOX and RP-1 control valves on #2 oxidizer-rich preburner
12 Open RP-1 pump turbine bypass valve #1, close RP-1 pump turbine bypass valve #2, and ramp open the RP-1 control valve

TRANSITION (MODE I TO MODE II)

1 Close the oxidizer and RP-1 control valves and igniter valves on #2 oxidizer-rich preburner to provide a LOX-rich shutdown of the preburner
2 Initiate LOX system purge
3 Open RP-1 pump turbine bypass valve #2, close pump turbine bypass valve #1, and ramp close the RP-1 control valve to provide a fuel-rich secondary chamber shutdown
4 Open chamber bypass control valve to secondary chamber
5 Cutoff igniter spark energy to LOX/RP-1 circuit

SHUTDOWN

1 Close control valves on #1 oxidizer-rich preburner and H_2 fuel-rich gas generator
2 Close main LOX valve and initiate oxidizer purge
3 Ramp close H_2 control valve
4 Close main LH_2 fuel valve
5 Close igniter valves on #1 oxidizer-rich preburner and H_2 fuel-rich gas generator
6 Cutoff igniter spark energy to LOX/LH_2 circuit
7 Open chamber bypass valve to nozzle

PARAMETER	REQUIREMENT	MAXIMUM POSSIBLE RATING	ANGLE POPPET	ANGLE SLEEVE	BUTTERFLY	ROTATING BALL	WEDGE GATE	COAXIAL POPPET
			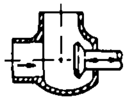 CLOSURE IS ACCOMPLISHED BY A DISK OF A PLUG NESTING IN A CIRCULAR SEAT MOTION AWAY FROM THE SEAT ALONG ITS CENTER AXIS OPENS THE VALVE	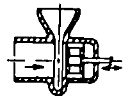 SIMILAR TO THE POPPET VALVE WITH A SLEEVE TAKING THE PLACE OF THE POPPET	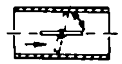 THE GATE IS CIRCULAR OR ELIPTICAL IN THE FLOW STREAM. THE VALVE IS OPENED OR CLOSED BY ROTATING THE GATE WITH A SHAFT WHICH EXTENDS ACROSS THE BORE TRANSVERSELY WHEN A SEAL RING IS USED THE SHAFT IS CANTED WITH RESPECT TO THE GATE AND THE BORE TO MOVE THE SHAFT OUT OF THE WAY OF THE SEAL RING	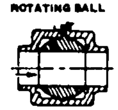 A BALL SHAPED GATE WITH TRANSVERSE FLOW PASSAGE FITS BETWEEN TWO SEAL RINGS THESE PARTS ARE ASSEMBLED INTO THE VALVE BODY WITH ZERO CLEARANCE FIT BETWEEN SEALS AND BALL IN MANY DESIGNS THE SEALS ARE SPRING LOADED TO MAINTAIN SEAL CONTACT	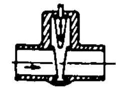 GATE TRAVELS PERPENDICULAR TO FLOW STREAM SANDWICHED BETWEEN TWO CIRCULAR SEATS THE GATE IS USUALLY WEDGE SHAPED WITH FLEXIBLE OR HINGED FACES TO ENHANCE SEALING THE GATE IS WITHDRAWN INTO A SEALED CHAMBER AT ONE SIDE OF THE VALVE THE VALVE OPENING STROKE IS A MINIMUM OF ONE SEAT DIAMETER	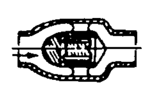 POPPET AND POPPET GLIDE ARE HOUSED IN A CENTER BODY IN THE FLOW STREAM
ENVELOPE	LEAST	4	ONE OF THE LARGER VALVES CONSIDERED BUT EFFECTIVE IF CHANGE IN THE FLOW DIRECTION IS REQUIRED RATING = 2	ABOUT THE SAME SIZE AS THE ANGLE POPPET RATING = 2	SMALLEST SIZE OF VALVES CONSIDERED RATING = 4	SMALL BUT LARGER THAN THE BUTTERFLY VALVE RATING = 3	BODY IS LARGE BECAUSE OF SPACE NEEDED TO ENCLOSE GATE. RATING = 2	BODY IS LONG BUT DIAMETER IS COMPARATIVELY SMALL RATING = 3
WEIGHT	LEAST	4	ONE OF THE HEAVIER VALVES CONSIDERED RATING = 2	APPROXIMATELY THE SAME WEIGHT AS THE ANGLE POPPET RATING = 2	SHORT LENGTH ALLOWS LIGHT BODY, BUT HEAVY GATE, SHAFT AND BEARINGS ESPECIALLY IN HIGH PRESSURE APPLICATIONS RATING = 2	SMALL FLOW PASSAGES BUT HEAVY BODY SHAFT AND BEARINGS RATING = 3	BODY NEEDED TO ENCLOSE GATE IS HEAVY RATING = 1	SHELL TYPE CONSTRUCTION RESULTS IN LIGHTEST VALVE RATING = 4
FLOW COEFFICIENT	HIGHEST	4	CONFIGURATION FACTOR 0 96 RATING = 2	CONFIGURATION FACTOR 0 96 RATING = 2	CONFIGURATION FACTOR 1 30 RATING = 3	CONFIGURATION FACTOR 1 60 RATING = 4	CONFIGURATION FACTOR 1 60 RATING = 4	CONFIGURATION FACTOR 1 40 RATING = 3
COMPLEXITY	LEAST	5	PARTS REQUIRED TO BALANCE VALVE ARE COMPLICATED RATING = 3	RETAINERS AND EXTRA SEAL COMPLICATE VALVE RATING = 3	RETAINERS FOR HIGH PRESSURE SEAL ADD SOME COMPLEXITY, (BUT IT IS LEAST COMPLEX OF VALVES RATING = 5	MECHANISM TO ELIMINATE SEAL RUBBING COMPLICATES VALVE RATING = 2	TOLERANCES NEEDED FOR GATE COMPLICATE VALVE RATING = 2	ACTUATOR LINKAGE VALVE RATING = 3
EXPERIENCE	MOST	5	MOST COMMONLY USED OF ALL VALVE TYPES RATING = 5	SOME SUCCESS AT MEDIUM PRESSURES (1200 PSI) ON M-1 PROGRAM RATING = 3	WIDE EXPERIENCE ON ROCKET ENGINES RATING = 4	WIDE EXPERIENCE ON ROCKET ENGINES BUT NOT AT HIGH PRESSURES RATING = 4	WIDE COMMERCIAL EXPERIENCE BUT NOT ON ROCKET ENGINES RATING = 2	HAS BEEN USED AS LOW PRESSURE PRE VALVES RATING = 3
SEALING CAPABILITY	HIGHEST	5	CAN ACHIEVE BUBBLE TIGHT SEALING AND LONG LIFE RATING = 5	LARGE SLEEVE SEAL CREATES EXTRA LEAK PATH WHICH IS DIFFICULT TO SEAL DUE TO THERMAL CONDITIONS AND RUBBING ACTION RATING - 3	RUBBING MOTION AS GATE CLOSES PRODUCES LEAKAGE AND WEAR RATING = 3	RUBBING SEALS AGGRAVATE SEAL WEAR & LEAKAGE RATING = 2	HIGH LOADING AND RUBBING DURING LAST PART OF STROKE AGGRAVATES SEAL WEAR & LEAKAGE RATING = 2	SEALING CAPABILITY AS GOOD AS ANGLE POPPET VALVE RATING = 5
CONTAMINATION SUSCEPTABILITY	LEAST	4	POSSIBLE TO TRAP PARTICLES UNDER POPPET SHUTOFF SEAL RATING = 3	LARGE DYNAMIC SLEEVE SEAL AREA SUBJECT TO DAMAGE FROM TRAPPED CONTAMINANTS RATING = 2	WIPING ACTION BEST FOR CON TAMINATION RATING = 4	WIPING ACTION GOOD BUT BODY CAVITY COULD TRAP CON TAMINATION RATING = 3	WEDGE CLOSING ON SEAT COULD TRAP PARTICLES RATING = 3	SAME REMARKS AS FOR ANGLE POPPET RATING = 3
CYCLE LIFE	HIGHEST	4	LONG SHUTOFF SEAL LIFE 0 0 RUBBING MOTION RATING = 4	LARGE SLEEVE SEAL HAS RUBBING ACTION AND IS SUBJECT TO WEAR RATING = 3	HIGH LOADING ON SEAL AND RUBBING ACTION LIMITS MAIN SEAL LIFE RATING = 2	REMARKS THE SAME AS FOR BUTTERFLY VALVE RATING = 2	REMARKS THE SAME AS FOR BUTTERFLY AND BALL VALVE RATING = 2	SAME REMARKS AS FOR ANGLE POPPET RATING = 4
STORAGE LIFE	LONGEST	3	SHUTOFF SEAL CAN BE EN TRAPPED TO MINIMIZED COLD FLOW RATING = 3	LARGE SLEEVE SEAL SUBJECT TO COLD FLOW RATING = 2	SHUTOFF SEAL DIFFICULT TO ENTRAP RATING = 1	SAME REMARK AS FOR BUTTERFLY RATING 1	MAIN SHUTOFF SEAL EASY TO ENTRAP RATING = 3	SAME REMARKS AS FOR THE ANGLE POPPET RATING = 3
RESPONSE	FASTEST	4	SHORTEST POSSIBLE STROKE CAN BE 0.25 OF OUTLET DIAMETER RATING = 4	SHORT STROKE & SLEEVE PROVIDES GOOD HYDRAULIC BALANCE RATING = 3	NOT BALANCED & LONG STROKE RATING = 2	SAME REMARKS AS FOR BUTTERFLY. RATING = 3	VERY LONG STROKE & NOT BALANCED HEAVY GATE RATING = 1	SHORT STROKE VERY EASY TO BALANCE RATING = 4
POWER REQUIREMENT	LONG	4	LARGE POWER REQUIREMENT CAN BE REDUCED BY HYDRAULIC BALANCING RATING = 3	LOW POWER BECAUSE OF HYDRAULIC BALANCE RATING = 3	HIGH POWER BECAUSE OF UN BALANCED CONDITION AND HEAVY GATE RATING = 2	SAME REMARK AS BUTTERFLY RATING 2	HIGH POWER BECAUSE OF LONG STROKE & UNBALANCED CONDITION RATING = 2	LOW POWER BECAUSE OF LIGHT PARTS AND BALANCED CONDITION RATING = 4
ADAPTABILITY	HIGHEST	3	GOOD ADAPTABILITY FOR SMALL & MEDIUM SIZE VALVES BUT VERY BULKY IN LARGE SIZES 2 INCHES AND LARGER RATING = 2	GOOD ADAPTABILITY EXCEPT FOR LARGE SIZES RATING = 2	DIFFICULT TO USE FOR THROT TLING VALVES AND HIGH PRESSURES RATING = 2	SAME REMARK AS FOR BUTTERFLY RATING 2	DIFFICULT TO USE FOR THROT TLING VALVE RATING = 2	GOOD ADAPTABILITY FOR LARGE & SMALL SIZES RATING = 3
PRODUCIABILITY	HIGHEST	3	IRREGULAR SHAPED BODY DIFFICULT TO MAKE RATING = 2	SAME REMARK AS ANGLE POPPET RATING = 2	SMALL SYMMETRICAL SHAPE BODY EASY TO MAKE RATING = 3	CLOSE TOLERANCE BALL SEAL UNLOADING MECHANISM COMPLICATE FABRICATION RATING = 1	CLOSE TOLERANCES NEEDED TO ALIGN GATE, COMPLICATE MANUFACTURE RATING = 2	RIGHT ANGLE LINKAGE COMPLI CATES FABRICATION RATING = 2
FABRICATION COST & TIME	LEAST	4	IRREGULAR SHAPED BODY COSTLY TO MAKE EXTRA MACHINING TAKES TIME RATING = 2	SAME REMARK AS ANGLE POPPET RATING = 2	SMALL SYMMETRICAL BODY & GATE EASY TO MAKE RATING = 4	SYPHERICAL BALL TOLERANCES COSTLY & TIME CONSUMING TO MACHINE RATING = 2	GATE ALIGNMENT TOLERANCES COSTLY AND TIME CONSUMING TO MACHINE RATING = 2	LINKAGE CONSTRUCTION COSTLY & TIME CONSUMING RATING = 3
MAINTAINABILITY	HIGHEST	4	LOCATION OF SHUTOFF SEAL RE QUIRES REMOVAL OF AT LEAST ONE FLANGE RATING = 3	EXTRA LARGE SLEEVE SEAL COMPLICATES RATING = 3	LOCATION OF SHUTOFF SEAL COMPLICATES RATING = 2	SAME REMARK AS BUTTERFLY VALVE RATING = 2	SEALS AND SEATS WOULD BE EASY TO REPLACE WITHOUT UNBOLTING FLANGES RATING = 4	ONE FLANGE MUST BE UNBOLTED TO REPLACE SEAT & SEALS RATING = 3
SAFETY	FAIL OPEN		CAN BE MADE TO FAIL OPEN OR CLOSED RATING = 5	FAILS OPEN RATING = 5	DEPENDS ON STROKE POSITION MAX. TORQUE AT 75° OF 90° STROKE RATING = 2	DEPENDS ON STROKE POSITION MAX TORQUE IS REACHED BETWEEN 60 & 90 DEGREES RATING = 2	WILL NOT FAIL OPEN ON LAST PART OF STROKE BECAUSE OF PRESSURE BALANCE RATING = 3	CAN BE MADE TO FAIL OPEN OR CLOSED RATING = 5
RELIABILITY	HIGHEST	5	LARGE FORCE NEEDED TO ACTUATE COMPROMISES RELIABILITY RATING = 4	LARGE GATE SEAL COMPROMISES RELIABILITY RATING = 3	SEAL LOADING & RUBBING COMPROMISES RELIABILITY RATING = 3	SAME REMARK AS BUTTERFLY VALVE APPLIES RATING = 2	SEAL RUBBING COMPROMISES RELIABILITY RATING = 3	LINKAGE REQUIREMENTS MAY COMPROMISE RELIABILITY RATING = 4
	TOTAL	70	54	45	47	40	40	59

Figure 108. Typical Shutoff Valve Trade Study

TABLE XXX

VALVE CONFIGURATION AND SIZING

Valve	Type	Configuration	Fluid Kw Requirement	Approx Valve Line Dia cm (in)	Approx Valve & Actuator Wt Kg (lb)	Approx. Vlv & Actuator Envelope Dimensions Diameter cm (in)	Approx. Vlv & Actuator Envelope Dimensions Length cm (in)
Main LO_2 Valve	On-Off (N C)	Co-Axial Poppet	43 3	7 6 (3 0)	22 (48)	30 (12)	46 (18)
Main LH_2 Valve	On-Off (N C.)	Co-Axial Poppet	27 8	6 4 (2 5)	15 (34)	25 (10)	43 (17)
RP-1 Pump Turbine GH_2 Bypass Valve	On-Off (N O.)	Angle Poppet	5 7	3 8 (1 5)	7 (15)	15 (6)	51 (20)
RP-1 Pump Turbine GH_2 Bypass Valve	On-Off (N C)	Angle Poppet	7 7	5 1 (2 0)	10 (23)	20 (8)	51 (20)
Oxid Rich Pre-Burner #1 - O_2 Control Valve	Control	Angle Poppet	16 1	6 4 (2 5)	15 (33)	23 (9)	61 (24)
- H_2 Control Valve	Control	Angle Poppet	1 0	1 9 (0 75)	4 (8)	10 (4)	38 (15)
Oxid Rich Pre-Burner #2 - O_2 Control Valve	Control	Angle Poppet	49 2	10 8 (4 25)	39 (85)	25 (10)	71 (28)
- RP-1 Control Valve	Control	Angle Poppet	1 3	2 5 (1 0)	4 (9)	13 (5)	41 (16)
H_2 Fuel Rich Gas Generator							
- O_2 Control Valve	Control	Angle Poppet	0 3	1 0 (0 375)	3 (6)	8 (3)	30 (12)
- H_2 Control Valve	Control	Angle Poppet	2 5	2 5 (1 0)	4 (9 5)	13 (5)	43 (17)
RP-1 Thrust Chamber Control Valve	Control	Angle Poppet	19 7	7 0 (2 75)	18 (40)	25 (10)	61 (24)
H_2 Thrust Chamber Control Valve	Control	Angle Poppet	14 4	6 4 (2 5)	14 (31)	23 (9)	61 (24)
Chamber By-Pass Control Valve	Control	Angle Poppet (Diversion Valve)	195	14 6 (5 75)	16 (35)	30 (12)	64 (25)

from the LH_2 and the LO_2 pump in the LO_2/LH_2 circuit. To minimize flow resistance, actuation forces and resultant valve weight, the coaxial balanced poppet configuration was selected for both the main LO_2 and LH_2 valves. The shell type construction of these valves will also aid in attainment of minimum weight.

The angle poppet configuration was chosen for the RP-1 pump turbine bypass shutoff valves. This configuration is readily adaptable to this valve size range without being bulky and can be balanced to minimize actuation forces. Also, the angle configuration is effective when changes in flow direction are required as will probably be the case in this part of the engine system line configuration.

2. Preburner, Gas Generator and Thrust Chamber Control Valves

The function of the oxidizer-rich preburner and fuel-rich gas generator valves is to initiate and control flow and mixture ratio to the oxidizer rich preburners and the fuel rich gas generator after the main LO_2 and LH_2 valves have been opened during the engine start transient. Since these valves will most likely be mounted directly on the preburner and gas generator injectors, an angle poppet configuration would provide the necessary change in flow direction to keep the engine compact and at the same time provide a flow control element that can be shaped for proper mixture control as well as having the required shutoff feature to terminate flow during engine shutdown.

The function of the thrust chamber control valves will be to initiate, control, and terminate RP-1 and H_2 flow to the main thrust chamber injectors during engine start, operation and shutdown. These valves will either be angle poppet or coaxial poppet type valves depending on the final engine line configuration.

The chamber bypass control valve will divert turbine exhaust gas to the LO_2/RP-1 chamber, following LO_2/RP-1 engine shutdown, to control the shape of the LO_2/LH_2 engine exhaust plume. This valve will be in the form of a single inlet-dual outlet poppet type valve which translates to divert flow from one outlet port to the other when actuated. A valve of this configuration was designed and developed by Aerojet and used on the Titan I engine system.

3. Igniter Valves

Although the igniter valves were not shown on the engine schematic or included on Table XXX a summary of the proposed general configuration is as follows:

Type:	Poppet-Solenoid Operated
Line Size:	9.5 mm (.375 inch) diameter
Weight:	0.77 Kg (1.7 lbs) each

It is anticipated that a total of eight igniter valves will be required for the engine system. This includes two igniter valves for each oxidizer-rich preburner, two valves for the fuel-rich gas generator, and two valves for the O_2/H_2 combustion chamber. It is postulated that igniter valves will not be required for the O_2/RP-1 chamber since the O_2/H_2 engine circuit is started first and will supply the ignition source for the O_2/RP-1 circuit.

4. Valve Actuation

During valve actuation the operating forces to be considered include forces due to flow and pressure, friction of the seals, bearings, and gears, and inertial forces of the moving parts.

For this preliminary study electromechanical actuation was selected based on consideration of the tradeoffs examined during the more detailed space shuttle main engine (AJ-550) study where similar valve operating presures, propellants, line sizes and response times were evaluated. During the SSME program study, electrical, hydraulic and pneumatic systems were evaluated on the basis of seventeen design considerations; the primary factors being weight, contamination susceptibility, power requirements, fabrication cost and lead time, maintainability, reliability and safety. Although the results of the SSME study indicated the three systems were relatively equal in their ability to satisfy the overall design requirements of the engine evaluated, there are other factors that must also be considered to assure accurate position control of the preburner, gas generator and thrust chamber control valves. For instance, pneumatic systems pose a control problem in terms of gas compressibility and cryogenic collapse factors. The same problem occurs when using propellant pressure actuated systems unless the propellant used for actuation can be maintained in a liquid state by continuous bleed techniques. When using hydraulic oil systems, weight and envelope become a problem due to thermal barrier requirements to prevent excessive childown of the hydraulic oil. One exception is that propellant or hydraulic pressure actuation could be used for the RP-1 preburner and thrust chamber control valves; however, use of electromechanical actuation for all of the engine valves provides the potential advantage of component commonality.

With respect to electrical power required it is obvious that the electrical system requires more electrical power than the hydraulic or pneumatic systems, however, the total energy from the vehicle power source is not expected to be significantly different. Based on the SSME study the estimated operating power requirements will range from 200 to 300 watts for the main LO_2 and LH_2 valves and the preburner No. 2 oxidizer control valve down to 50 to 75 watts for the other control valves.

5. Materials

The materials selected for the proposed valve configurations are based on engine operating conditions and the propellants utilized. Primary consideration was given to material qualities such as corrosion resistance, hydrogen embrittlement, LO_2 impact sensitivity, high strength to weight ratio and adequate toughness and fatigue life at operating temperatures. A list of materials under consideration for the major valve subcomponents is included in Table XXXI.

E. ENGINE PERFORMANCE

The performance of the selected dual throat engine is given in Table XXVII as 327.6 seconds at sea level (376.0 seconds in vacuum) for Mode I and 463.3 seconds for Mode II. These values represent an engine efficiency of 97.3% in Mode I and of 97% in Mode II. Parametric representation of these data for various secondary nozzle area ratios is depicted in Figure 109. The baseline stream-tube analysis for a staged combustion type cycle is given in Table XXXII for comparison.

F. ENGINE MASS PROPERTIES DATA

The weight breakdown for the baseline dual throat engine is shown in Table XXXIII. Parametric engine weight data are given in Figures 87 and 90.

TABLE XXXI

VALVE MATERIALS

COMPONENT	MATERIALS
Valve Bodies	A-286 CRES 6061-T6 Aluminum
Shafts	A-286 CRES
Shutoff Seals	Phosphor Bronze Seal on CRES 347 (Electrolized) Seat Gold Plated CRES 347 Seal on Electrolized 347 CRES Seat Encapsulated Teflon Poppet on 347 CRES Seat
Dynamic Shaft Seals	15% Graphite Filled Teflon (Delta Seal)
Guide Bushings	Filled Teflon
Valve Springs	Inconel 750
Electric Motor Housings	356 -T6 Alum. Alloy

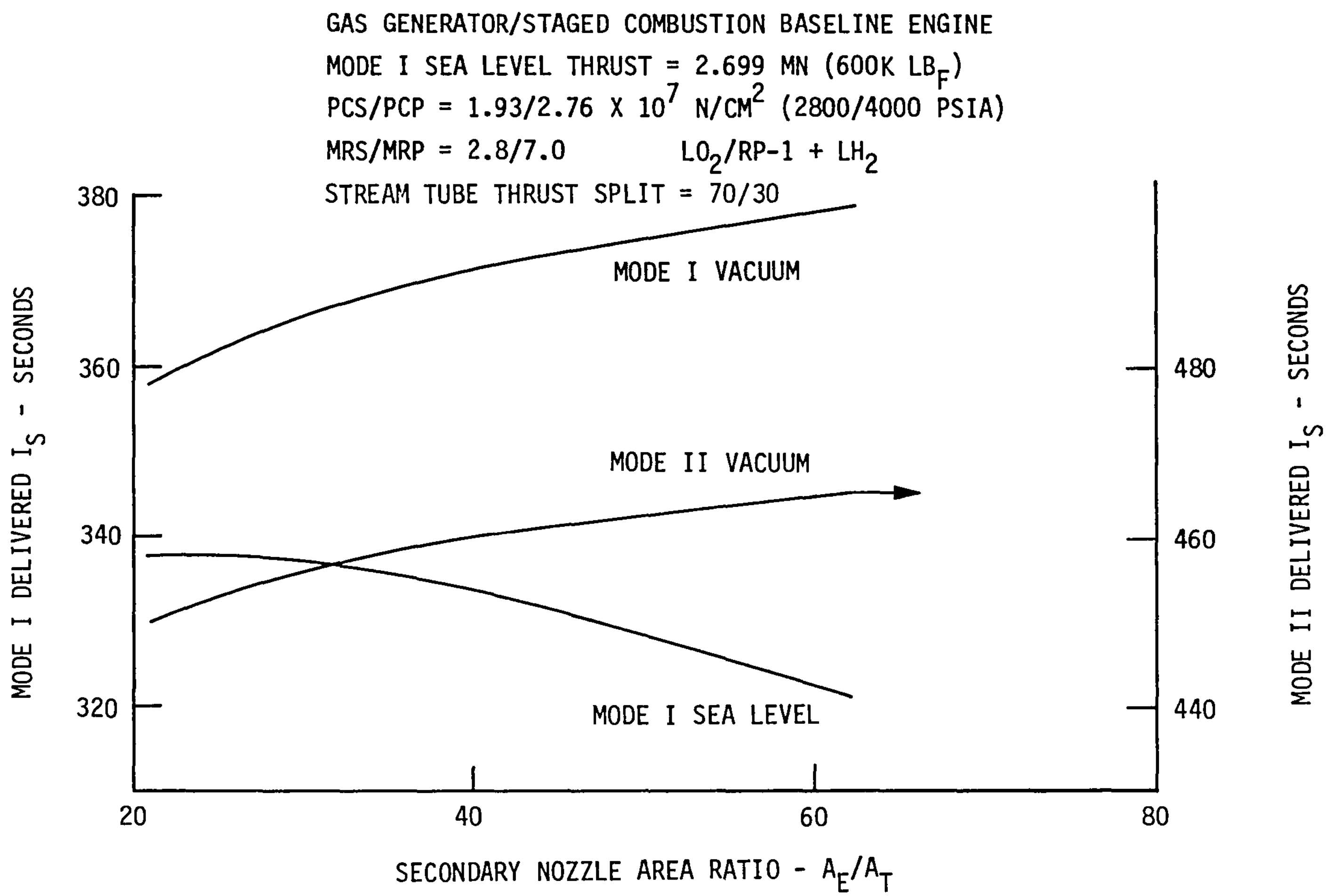

Figure 109. Delivered Performance vs Mode I Area Ratio

TABLE XXXII

DUAL-FUEL DUAL-THROAT ENGINE STREAM-TUBE ANALYSIS

STAGED COMBUSTION CYCLE III

(SI UNITS) F_1/F_2 = 3.20

	70% x 1 LO_2/RP-1	30% x 1 LO_2/LH_2	MODE 1 LO_2/RP-1 & LH_2	MODE 2 LO_2/LH_2
Thrust, SL, KN	1868	801	2669	-
Thrust, VAC, KN	2151	901	3052	953
Mixture Ratio	2.8	7.0	3.37	7.0 (TCA)
Chamber Pressure 10^7 N/M^2	1.93	2.76	-	2.76
Area Ratio	(50)	(60)	52.3	232
ODE Is, SL, sec	316.8	405.6	(338.9)	-
ODE Is, VAC, sec	364.7	456.4	(387.5)	478.0)
Is Efficiency, %	97	98	97.3	97**
Is, SL, Delivered, sec	307.3	397.5	329.8	-
Is, VAC, Delivered, sec	353.8	447.3	377.1	463.7
Total Flow Rate, Kg/s	619.94	205.40	825.34	209.51**
Fuel Flow Rate, Kg/s	163.14	25.67	188.82	29.78**
Oxidizer Flow Rate, Kg/s	456.80	179.73	636.52	179.73
c*,m/s	1804	2261	-	2261
Throat Area, cm^2	579	168	748	168
Throat Diameter, cm	-	14.7	30.9	14.7
Exit Area, cm^2	28,970	10,104	39,077	39,077
Exit Diameter, cm	-	-	223	223
Exit Pressure, 10^4 N/M^2	3.7	3.9	3.8	0.7

*Optimum LO_2/LH_2 ε_{SL} = 28 LO_2/RP-1 ε_{SL} = 23

**Assumed 1% Is loss and 2% bleed flow

TABLE XXXII (Cont)

STAGED COMBUSTION CYCLE III

(ENGLISH UNITS)

$F_1/F_2 = 3.20$

	70% x 1 LO_2/RP-1	30% x 1 LO_2/LH_2	MODE 1 LO_2/RP-1 & LH_2	MODE 2 LO_2/LH_2
Thrust, SL, lb	420,000	180,000	600,000	-
Thrust, VAC, lb	483,554	202,551	686,104	214,160
Mixture Ratio	2.8	7.0	3.37	7.0 (TCA)
Chamber Pressure, psia	2800	4000	-	4000
Area Ratio	(50)	(60)	52.3	232
ODE Is, SL, sec	316 8	405 6	(338.9)	-
ODE Is, VAC, sec	364.7	456 4	(387.5)	478.0
Is Efficiency, %	97	98	97.3	97**
Is, SL, Delivered, sec	307.3	397.5	329.8	-
Is, VAC, Delivered, sec	353.8	447 3	377.1	463 7
Total Flow Rate, lb/sec	1366.74	452.83	1819.57	461.89**
Fuel Flow Rate, lb/sec	359.67	56.60	416.27	65.66**
Oxidizer Flow Rate, lb/sec	1007.07	396.23	1403.30	396.23
c*, ft/s	5920	7419	-	7419
Throat Area, in.^{2}	89 81	26 10	115.92	26.10
Throat Diameter, in.	-	5.77	12.15	5.77
Exit Area, in.^{2}	4490.7	1566.27	6056.98	6056.98
Exit Diameter, in.	-	-	87.82	87.82
Exit Pressure, psia	5.4	5.6	5.5	1.0

*Optimum LO_2/LH_2 $\varepsilon_{SL} = 28$ LO_2/RP-1 $\varepsilon_{SL} = 23$

**Assumed 1% Is loss and 2% bleed flow

TABLE XXXIII

BASELINE ENGINE COMPONENT WEIGHT BREAKDOWN

INPUT

VARIABLES

F (LB)(N)	600000.	2668932.
F SPLIT	.7	.7
PC PRIMARY (PSI)(ATM)	4000.	272,18
PC SEC (PSI)(ATM)	2800.	190,53
AREA RATIO	52,3	52,3

OUTPUT

COMPONENT WEIGHTS

WG	WMISCS	WMISCP	WINJS	WINJP	WPBOS	WPBOP	WPBFP	WVOS	WVFS	WVOP
(LB)	(LB)	(LB)	(LB)	(LB)	(LB)	(LB)	(LB)	(LB)	(LB)	(LB)
215,22	329,97	213,09	612,62	147,90	110,35	47,39	14,16	69,38	46,25	73,91
(KG)	(KG)	(KG)	(KG)	(KG)	(KG)	(KG)	(KG)	(KG)	(KG)	(KG)
97,623	149,672	96,655	277,881	67,087	50,053	21,495	6,423	31,471	20,981	33,527

WVFP	WBPOS	WBPFS	WBPOP	WBPFP	WMPOS	WMPFS	WMPOP	WMPFP	WLPLS	WLPLP
(LB)	(LB)	(LB)	(LB)	(LB)	(LB)	(LB)	(LB)	(LB)	(LB)	(LB)
85,58	168,87	28,80	57,65	60,64	284,13	127,29	73,62	140,22	152,21	104,13
(KG)	(KG)	(KG)	(KG)	(KG)	(KG)	(KG)	(KG)	(KG)	(KG)	(KG)
38,821	76,598	13,063	26,149	27,507	128,878	57,739	33,392	63,601	69,043	47,231

WHPLS	WHPLP	WPSS	WPSP	WHGMS	WHGMP	WTCN	WCCS	WCCP	WIGN	WCONTR	ENGINE WEIGHT WE
(LB)	(LB)	(LB)	(LB)	(LB)	(LB)	(LB)	(LB)	(LB)	(LB)	(LB)	(LB)
121,49	228,00	97,67	38,45	90,44	217,50	771,10	320,88	182,61	76,00	130,00	5437,52
(KG)	(KG)	(KG)	(KG)	(KG)	(KG)	(KG)	(KG)	(KG)	(KG)	(KG)	(KG)
55,107	103,417	44,302	17,440	41,021	98,656	349,766	145,548	82,831	34,473	58,967	2466,416

ENGINE THRUST WEIGHT RATIO 110,3

SEE APPENDIX FOR NOMENCLATURE

The materials for the engine component weights are of 1978 state-of-the-art, and are essentially the same as utilized in Ref. (6). The selected materials for the major engine components are listed in Table XXXIV. These materials were selected to achieve lightweight engines with consideration of the design and long life requirements and the environmental and propellant compatibility aspects.

1. Advanced Materials Review

An estimate of the yearly improvements in engine weight through 1995 was provided in Section IV,C,2. As part of the materials selection process for the baseline dual throat engine, a review was made of potential advanced materials. This review is included in the following.

Of the various advanced materials (metals, nonmetallics, composites and ceramics), the modulus enhanced, metal matrix filamentary composites have demonstrated the most promise for improved performance. These composites have been applied in commercial and military aircraft as structural reinforcement panels. Weight savings to 37% have been obtained over conventional panels in honeycomb structures utilizing aluminum alloy cores with titanium 6Aℓ-4V, boron/epoxy reinforced face sheets. Further improvements may be obtained with sheets fabricated from titanium or aluminum material/ceramic filament composites. Composites of this type are directly applicable to rocket engine structural components which are not subjected to the environmental restraints of propellant and hot gas systems. The use of these materials at moderately elevated and cryogenic temperatures are questionable, however, due to the differential expansion of the composite constituents. Their application is also dependent on additional development of: (1) fabrication techniques to produce the configurations such as integral tube-flange structures, (2) develoment of mechanical properties

TABLE XXXIV

MATERIALS SELECTION

Component		
1.	Low Speed LOX TPA	
	a. Shaft	Inconel 718
	b. Impeller & Turbine	7075 T-37 Aluminum Alloy
	c. Housing	A356T-6 Al Alloy
	d. Bolts	A-286
	e. Housing Liner	FEP Teflon Fused Coating
	f. Bearings	CRES 440C; Alternate Haynes Star Alloy PM
2.	Low Speed RP-1 TPA	All materials the same as low speed LOX TPA except Teflon Coating is not required.
3.	Low Speed LH_2 TPA	All materials the same as low speed LOX TPA except Teflon Coating is not required.
4.	High Speed LOX TPA	
	a. Shaft	A-286
	b. Impeller	Inconel 718
	c. High Pressure Pump & Turbine Housing	ARMCO Nitronic-50
	d. Inducer Housing	Inconel 718
	e. Turbines	Inconel 718 and UDIMET 630
	f. Bolts (pump)	A-286
	g. Bolts (turbine)	Waspaloy
	h. Bearings	CRES 440C or Alternate

TABLE XXXIV (cont)

	Component	Material
5.	High Speed RP-1 TPA	
	a. Inducer Housing	5AL-2.5 SnEli Titanium Alloy
		All other material the same as High Speed LOX TPA
6.	High Speed LH_2 TPA	
	a. Inducer Housing	5AL-2.5 SnEli Titanium Alloy
	b. High Pressure Pump Housing	5AL-2.5 SnEli Titanium Alloy
	c. Turbine	UDIMET 630
	d. Impeller	A-286
	e. Turbine Housing	ARMCO Nitronic-50
	f. Shaft	A-286
	g. Bolts (pump)	A-286
	h. Bolts (turbine)	Waspaloy
	i. Bearings	CRES 440C
7.	LOX/RP-1 Ox-Rich Preburner	
	a. Injector Body	ARMCO Nitronic-50
	b. Chamber	ARMCO Nitronic-50
8.	LOX/LH_2 Ox-Rich Preburner	
	a. Injector Body	ARMCO Nitronic-50
	b. Chamber	ARMCO Nitronic-50

TABLE XXXIV (cont.

Component		
9.	LOX/LH_2 Fuel-Rich Preburner or Gas Generator	
	a. Injector Body & Chamber	ARMCO Nitronic-50
10.	Thrust Chamber Injector	
	a. Body	Inconel 625 or ARMCO Nitronic-50
	b. Manifolds	CRES 347 or ARMCO Nitronic-50
	c. Injector Face	Inconel 625
11.	Combustion Chamber	ZR Cu
12.	Tubes	Inconel 718 or A-286
13.	Nozzle Extension	Columbium
14.	Hot Gas Manifold	ARMCO Nitronic-50

including fracture toughness, and (3) the development of NDE techniques for complex fabricated parts.

High temperature resistant composite materials offer a key to improved engine efficiency. The potential for materials in applications above 2000°F in turbine sections is promising. Tungsten-hafnium carbide/superalloy composites offer a potential improvement of 167°K (300°F) for an equivalent strength to density ratio of nickel base superalloys. The fracture mechanics analysis of silicon nitride for gas turbine applications indicates that high purity silicon nitride has a potential life operating stress of 9.65×10^6 N/m^2 (1400 psi) at 1672°K (2550°F). Directionally solidified refractory oxide eutectics offer an experimental material with exceptional high temperature strength in excess of that obtained with silicon nitride. A bend strength of 5.1×10^8 N/m^2 (74,000 psi) at 1811°K (2800°F) was exhibited by a eutectic of aluminum oxide and yttria stabilized zirconia directionally solidified to form oriented zirconia whiskers in an aluminum oxide matrix.

Improvements in turbomachinery performance may be realized with improved bearing materials such as powder metallurgy composites which offer improved lubricity, and with ceramics which offer improved life at higher loads than steel bearings. Use of ceramic bearings is highly dependent on fabrication details to produce defect free parts.

The development of carbon-carbon composites for solid rocket nozzle and re-entry vehicle applications provides a basis for the improved performance of rocket engine thrust chambers and nozzles at service temperatures in excess of 1922°K (3000°F). However, their use in some applications may be dependent on the development of thermodynamically stable coating compounds such as the refractory platinates and the processes for their application.

V, F, Engine Mass Properties Data (cont.)

Other challenges to advanced materials in rocket engine design are applications which are governed by low temperature ductility, propellant compatibility or high strength with attendant high thermal conductivity. These requirements have not been addressed in either composite research and development, or in alloy development in recent times. Currently, the advanced materials are experimental with few being adequately characterized to establish their feasibility or to allow detailed design analysis.

SECTION VI

CONCLUSIONS AND RECOMMENDATIONS

A. CONCLUSIONS

The conclusions which have been derived from the results of the Dual-Fuel, Dual-Throat Engine Preliminary Analysis study are presented in Table XXXV for easy reference.

The overall conclusion is that the dual throat engine is a viable concept for SSTO applications from a propulsion system viewpoint and from a preliminary vehicle system evaluation.

B. RECOMMENDATIONS

The recommendations for further study fall into two categories: (1) vehicle system analysis, and (2) technology development of the dual throat engine.

Vehicle applications analyses should be conducted similar to those performed by NASA/Langley (Ref. 8 and 15-17) to determine the comparative merit of the dual throat configuration for several NASA missions.

Technology development of the dual throat concept should continue to accurately define the performance of the engine in both modes of operation and to determine the maximum chamber pressure possible when trans-regen cooling is applied.

TABLE XXXV

CONCLUSIONS

o	Cycle Selection	The gas generator/staged combustion mixed cycle proved to be the most promising candidate when primary chamber pressures greater than 2.07×10^7 N/m^2 (3000 psia) are considered.
o	Chamber Pressure Selection	The PCS/PCP = $1.93/2.76 \times 10^7$ N/m^2 (2800/4000 psia) dual throat engine provides a more attractive SSTO payload than lower pressure versions. Improvements in TPA state-of-the-art will allow even higher Pc selection.
o	Performance	Dual throat engine performance should exceed the conservative values utilized in this study.
o	Cooling	Trans-regen cooling will allow higher dual throat chamber pressures with a small performance degradation.
o	Stream-Tube Thrust Split	A practical stream-tube thrust split of 70/30 was selected to provide good performance and cooling capability.
o	Propellants	The LO_2/RP-1 propellant combination was selected instead of the LO_2/LCH_4 combination, but a detailed cost analysis and a vehicle system analysis is required before a final selection can be made.
o	Vehicle Application	Simplified trajectory analyses indicate the dual-fuel, dual-throat engine as a viable SSTO candidate.

APPENDIX

ENGINE WEIGHT SCALING EQUATIONS

APPENDIX

Weight scaling equations used in Ref. (6) were modified for the dual throat configuration, and were used to generate the engine parametric weights given in Section IV,C. The equations assume similarity in configuration, and may not be applicable to engine concepts with differing power cycles. The equations appear to give too optimistic an engine weight at 200K pounds thrust, but appear valid at engine thrust values from 1779 through 8896 KN (400K through 2M).

The constants for the equations are included for both the LO_2/RP-1 and LO_2/LCH_4 dual throat engines.

WEIGHT SCALING EQUATIONS - DUAL THROAT ENGINE

Gimbal

$$WG = WGB\left(\frac{FSL_E}{FSLB_E}\right)^{1.5}$$

Injectors

$$WINJ_P = WINJB_P\left[\frac{AT_P}{ATB_P}\right]\left(.5 + .5\,\frac{PC_P}{PCB_P}\right)$$

$$WINJ_S = WINJB_S\left[\frac{AT_S}{ATB_S}\right]\left(.5 + .5\,\frac{PC_S}{PCB_S}\right)$$

Combustion Chambers

$$WCC_P = WCCB_P\left[\frac{AT_P}{ATB_P}\right]^{.5}\left(.8 + .2\,\frac{PC_P}{PCB_P}\right)\left[\frac{4350\left(\frac{\dot{W}_P}{AC_P\ PC_P}\right)}{LCB_P}\right].$$

$$WCC_S = WCCB_S\left[\frac{AT_E}{ATB_E}\right]^{.5}\left(.8 + .2\,\frac{PC_S}{PCB_S}\right)\left[\frac{4350\left(\frac{\dot{W}_S}{AC_S\ PC_S}\right)}{LCB_S}\right]$$

Thrust Chamber Nozzle

$$WTCN = WTCNB\left[\frac{AT_E}{ATB_E}\right]\left(\frac{\varepsilon_E - \varepsilon_1}{\varepsilon_{EB} - \varepsilon_1}\right)\left[.8 + .2\,\frac{PC_S}{PCB_S}\right]$$

Preburners

$$WPBF_P = WPBFB_P\left[\frac{AT_P}{ATB_P}\ \frac{PC_P}{PCB_P}\right]\left(.5 + .5\,\frac{PC_P}{PCB_P}\right) \qquad \text{Fuel-Rich}$$

$$WPBO_P = WPBOB_P\left[\frac{AT_P}{ATB_P}\ \frac{PC_P}{PCB_P}\right]\left(.5 + .5\,\frac{PC_P}{PCB_P}\right) \qquad \text{Ox-Rich}$$

$$WPBO_S = WPBOB_S\left[\frac{AT_S}{ATB_S}\ \frac{PC_S}{PCB_S}\right]\left(.5 + .5\,\frac{PC_S}{PCB_S}\right) \qquad \text{Ox-Rich}$$

Valves

$$WVF_P = WVFB_P \left[\frac{AT_P}{ATB_P} \frac{PC_P}{PCB_P}\right]^{1.35} \left(.4 + .6 \frac{PC_P}{PCB_P}\right)$$ Fuel Valves

$$WVO_P = WVOB_P \left[\frac{AT_P}{ATB_P} \frac{PC_P}{PCB_P}\right]^{1.35} \left(.4 + .6 \frac{PC_P}{PCB_P}\right)$$ Ox Valves

$$WVF_S = WVFB_S \left[\frac{AT_S}{ATB_S} \frac{PC_S}{PCB_S}\right]^{1.35} \left(.4 + .6 \frac{PC_S}{PCB_S}\right)$$ Fuel Valves

$$WVO_S = WVOB_S \left[\frac{AT_S}{ATB_S} \frac{PC_S}{PCB_S}\right]^{1.35} \left(.4 + .6 \frac{PC_S}{PCB_S}\right)$$ Ox Valves

Low Speed Pumps

$$WLSPF_P = WLSPFB_P \left[\frac{AT_P}{ATB_P} \frac{PC_P}{PCB_P}\right]^{1.35} \left(\frac{PC_P}{PCB_P}\right)^{.5}$$ Fuel

$$WLSPO_P = WLSPOB_P \left[\frac{AT_P}{ATB_P} \frac{PC_P}{PCB_P}\right]^{1.35} \left(\frac{PC_P}{PCB_P}\right)^{.5}$$ Ox

$$WLSPF_S = WLSPFB_S \left[\frac{AT_S}{ATB_S} \frac{PC_S}{PCB_S}\right]^{1.35} \left(\frac{PC_S}{PCB_S}\right)^{.5}$$ Fuel

$$WLSPO_S = WLSPOB_S \left[\frac{AT_S}{ATB_S} \frac{PC_S}{PCB_S}\right]^{1.35} \left(\frac{PC_S}{PCB_S}\right)^{.5}$$ Ox

High Speed Pumps

$$WHSPF_P = WHSPFB_P \left[\frac{AT_P}{ATB_P} \frac{PC_P}{PCB_P}\right]^{1.35} \left(\frac{PC_P}{PCB_P}\right)^{.8}$$

$$WHSPO_P = WHSPOB_P \left[\frac{AT_P}{ATB_P} \quad \frac{PC_P}{PCB_P}\right]^{1.35} \left(\frac{PC_P}{PCB_P}\right)^{.8}$$

$$WHSPF_S = WHSPFB_S \left[\frac{AT_S}{ATB_S} \quad \frac{PC_S}{PCB_S}\right]^{1.35} \left(\frac{PC_S}{PCB_S}\right)^{.8}$$

$$WHSPO_S = WHSPOB_S \left[\frac{AT_S}{ATB_S} \quad \frac{PC_S}{PCB_S}\right]^{1.35} \left(\frac{PC_S}{PCB_S}\right)^{.8}$$

Low Pressure Lines

$$WLPL_P = WLPLB_P \left[\frac{AT_P}{ATB_P} \quad \frac{PC_P}{PCB_P}\right]^{.9}$$

$$WLPL_S = WLPLB_S \left[\frac{AT_S}{ATB_S} \quad \frac{PC_S}{PCB_S}\right]^{.9}$$

High Pressure Lines

$$WHPL_P = WHPLB_P \left[\frac{AT_P}{ATB_P} \quad \frac{PC_P}{PCB_P}\right]^{1.4} \left(\frac{PC_P}{PCB_P}\right)$$

$$WHPL_S = WHPLB_S \left[\frac{AT_S}{ATB_S} \quad \frac{PC_S}{PCB_S}\right]^{1.4} \left(\frac{PC_S}{PCB_S}\right)$$

Ignition System

$$WIGN_P = 16$$

$$WIGN_S = 60$$

Miscellaneous

$$WMISC_P = 169\left[\frac{FSL_P}{FSLB_P}\right] + 59\left[\frac{FSL_P}{FSLP_P}\right]^{.5} + 37$$

$$WMISC_S = 187\left[\frac{FSL_S}{FSLB_S}\right] + 72\left[\frac{FSL_S}{FSLB_S}\right]^{.5} + 37$$

Controller

$$WCTRL = 130$$

Pressurization System

$$WPS_P + WPSB_P\left[\frac{AT_P}{ATB_P}\ \frac{PC_P}{PCB_P}\right]$$

$$WPS_S = WPSB_S\left[\frac{AT_S}{ATB_S}\ \frac{PC_S}{PCB_S}\right]$$

Hot Gas Manifold

$$WHGM_P = WHGMB_P\left[\frac{AT_P}{ATB_P}\ \frac{PC_P}{PCB_P}\right]^{1.5}\left(\frac{PC_P}{PCB_P}\right)$$

$$WHGM_S = WHGMB_S\left[\frac{AT_S}{ATB_S}\ \frac{PC_S}{PCB_S}\right]^{1.5}\left(\frac{PC_S}{PCB_S}\right)$$

WEIGHT SCALING CONSTANTS
STREAM-TUBE THRUST SPLIT = 60/40

Symbol	Nomenclature	LO_2/RP-1 + LH_2	LO_2/LCH_4 + LH_2
WGB	Gimbal	219	219
$WINJB_P$	Primary Injector	233	233
$WINJB_S$	Secondary Injector	638	626
$WCCB_P$	Primary Combustion Chamber	235	235
$WCCB_S$	Secondary Combustion Chamber	352	339
$WTCN_B$	Thrust Chamber Nozzle	740	726
$WPBFB_P$	Primary Fuel-Rich Preburner	137	137
$WPBOB_P$	Primary Ox-Rich Preburner	82	82
$WPBOB_S$	Secondary Ox-Rich Preburner	114	114
$WVFB_P$	Primary Fuel Valves	110	110
$WVOB_P$	Primary Ox Valves	95	95
$WVFB_S$	Secondary Fuel Valves	34	38
$WVOB_S$	Secondary Ox Valves	51	51
$WLSPFB_P$	Primary Low-Speed Fuel Pump	81	81
$WLSPOB_P$	Primary Low-Speed Ox Pump	77	77
$WLSPFB_S$	Secondary Low-Speed Fuel Pump	22	33
$WLSPOB_S$	Secondary Low-Speed Ox Pump	129	129
$WHSPFB_P$	Primary Fuel Pump	370	370
$WHSPOB_P$	Primary Ox Pump	178	178
$WHSPFB_S$	Secondary Fuel Pump	113	170
$WHSPOB_S$	Secondary Ox Pump	299	299
$WLPLB_P$	Primary Low-Pressure Lines	139	139
$WLPLB_S$	Secondary Low-Pressure Lines	140	164
$WHPLB_P$	Primary High-Pressure Lines	268	268
$WHPLB_S$	Secondary High-Pressure Lines	80	94
$WIGN_P$	Primary Ignition System	16	16
$WIGN_S$	Secondary Ignition System	60	60
WCTRL	Engine Controller	130	130
$WPSB_P$	Primary Pressurization System	53	53
$WPSB_S$	Secondary Pressurization System	89	104
$WHGMB_P$	Primary Hot-Gas Manifold	264	264
$WHGMB_S$	Secondary Hot-Gas Manifold	59	69

Symbol	Nomenclature	Units	LO_2/RP-1 + LH_2	LO_2/LCH_4 + LH_2
$FSLB_E$	Engine Sea Level Thrust	lbF	607,000	607,000
$FSLB_P$	Primary Stream-Tube Sea Level Thrust	lbF	242,800	242,800
$FSLB_S$	Secondary Stream-Tube Sea Level Thrust	lbf	364,200	364,200
ATB_E	Engine Throat Area	in^2	157 11	154 14
ATB_P	Primary Stream-Tube Throat Area	in^2	47 97	47 97
ATB_S	Secondary Stream-Tube Throat Area	in^2	109 14	106 17
LCB_P	Primary Chamber Length	in	9 91	9 91
LCB_S	Secondary Chamber Length	in	10 15	12 18
PCB_P	Primary Chamber Pressure	psia	3,000	3,000
PCB_S	Secondary Chamber Pressure	psia	2,100	2,100
W_P	Primary Chamber Flow Rate	lb/s	625 80	625 80
W_S	Secondary Chamber Flow Rate	lb/s	1,249 88	1,182 56
AC_P	Primary Chamber Area	in^2	91 61	91 61
AC_S	Secondary Stream-Tube Chamber Area	in^2	255 1	241.34
ϵ_{EB}	Engine Area Ratio	--	43 1	43 1
ϵ_1	Tube Bundle Nozzle Attach Area Ratio	--	14 7	14 7

REFERENCES

1. Haefeli, R.C., Littler, E.G., Hurley, J.B., and Winger, M.G., "Technology for Advanced Earth-Orbital Transportation Systems, Dual-Mode Propulsion", Martin Marietta Corp. Report NASA-CR-2868, Contrct NAS 1-13916, October 1977.

2. Salkeld, R., "Mixed-Mode Propulsion for the Space Shuttle, Astronautics and Aeronautics, Vol. 9, No. 8, August 1971, pp. 52-58.

3. Hepler, A.K. and Bangsund, E.L., "Technology Requirements for Advanced Earth Orbital Transportation Systems - Dual Mode Propulsion", Boeing Aerospace Co., Report NASA -CR-3037, Contrct NAS 1-13944, July 1978.

4. "Systems Concepts for STS-Derived Heavy-Lift Launch Vehicles Study", Boeing Aerospace Co. Final Briefing, Contract NAS 9-14710, June 1976.

5. Dod, R.E., "Systems Concepts for STS-Derived Heavy Lift Launch Vehicle Study-Extension", Boeing Aerospace Co. Report D180-20505-2, Contract NAS 8-32169, February 1977.

6. Luscher, W.P. and Mellish, J.A., "Advanced High Presure Engine Study for Mixed-Mode Vehicle Applications", Aerojet Liquid Rocket Co. Report NASA-CR-135141, Contract NAS 3-19727, January 1977.

7. Lundgreen, R.B., Nickerson, G.R. and O'Brien, C.J., "Dual Throat Thruster Cold Flow Analysis", Aerojet Liquid Rocket Co. Report 32666F, Contract NAS 8-32666, August 1978.

8. Henry, B.Z. and Eldred, C.H., "Advanced Technology and Future Earth-to-Orbit Transportation Systems", AIAA Paper No. 77-530, presented at the Third Princeton/AIAA Conference on Space Manufacturing Facilities, May 1977.

9. Hess, H.L. and Kunz, H.R., "A Study of Forced Convection Heat Transfer to Supercritical Hydrogen", ASME Paper No. 63-WA-205, November 1963.

10. Spencer, R.G. and Rousar, D.C., "Supercritical Oxygen Heat Transfer", Aerojet Liquid Rocket Co. Report NASA CR-135339, November 1977.

11. Powell, W.B., "Simplified Procedures for Correlation of Experimental Measured and Predicted Thrust Chamber Performance", NASA TM 33-548, April 1973.

12. Nickerson, G.R., et al., "The Two-Dimensional Kinetic (TDK) Rocket Nozzle Analysis Reference Computer Program", December 1973.

13. Rao, G.V.R., "Exhaust Nozzle Contour for Optimum Thrust", Jet Propulsion, June 1958, pp. 377-382.

14. Pieper, J.L., ICRPG Liquid Propellant Thrust Chamber Performance Evaluation Manual, CPIA 178, September 1968.

15. Martin, J.A., "Econometric Comparisons of Liquid Rocket Engines for Dual-Fuel Advanced Earth-to-Orbit Shuttles", AIAA Paper No. 78-971, presented at the AIAA/SAE 14th Joint Propulsion Conference, July 25-27, 1978.

16. Wilhite, A.W., "Propulsion--A Key Technology for Advanced Space Transportation", AIAA Paper No. 79-1219, presented at the AIAA/SAE/ASME 15th Joint Propulsion Conference, June 18-20, 1979.

17. Martin, J.A., "Dual-Fuel Propulsion: Why It Works, Possible Engines, and Results of Vehicle Studies", AIAA Paper No. 79-879, presented at the Conference on Advanced Technology for Future Space Systems, May 8-11, 1979.

End of Document